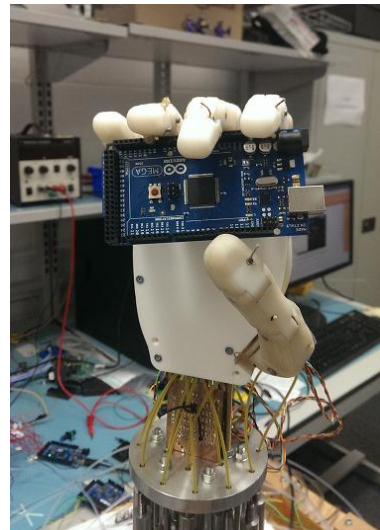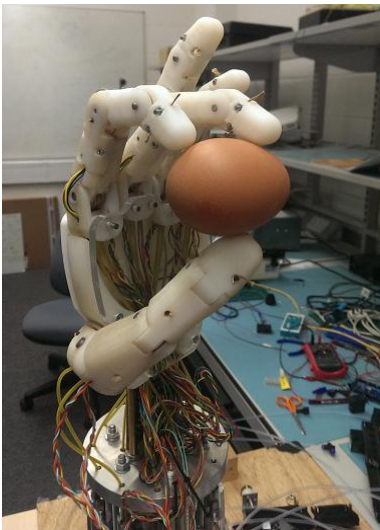# Remote-Controlled Ambidextrous Robot Hand
Actuated by Pneumatic Muscles:
from Feasibility Study
to Design and Control Algorithms

A thesis submitted for the Degree of

Doctor of Philosophy

By

Emre Akyürek

Department of Electronic and Computer Engineering

School of Engineering and Design

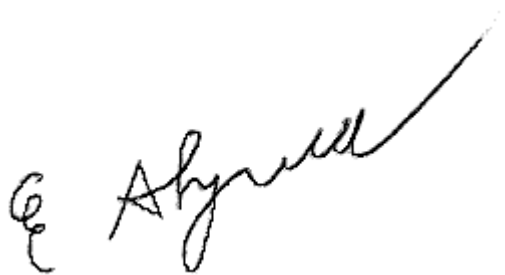Brunel University

June 2015

Declaration of Authorship

I, Emre Akyürek, certify that the work introduced in this thesis entitled "Remote-Controlled Ambidextrous Robot Hand Actuated by Pneumatic Muscles: from Feasibility Study to Design and Control" is my own. I confirm that:

-This work was entirely achieved while in candidature for a Doctor of Philosophy degree at Brunel University.

-The works done by my colleagues or achieved as teamwork are clearly defined and specified.

-The articles I have consulted for my research are referenced.

Signed:

Date: 10/06/2015

To my ex-brothers in arms Kim-Hwa Khoo, Michaël Rouart and Daniel Truong

By the sides of whom I fought these evil monsters called exams and assignments.

To those by the sides of whom I bled and suffered,

Learning the true meanings of distress and agony.

To those who were always at my side

To heal my wounds and to repair my weapons,

Teaching me the true meanings of friendship and solidarity.

To my dear friends Kim-Hwa, Michaël and Daniel,

Who were my only family on the battlefield.

To my ex-brothers in arms,

By the sides of whom I have become the warrior I am.

Abstract

This thesis relates to the development of the Ambidextrous Robot Hand engineered in Brunel University.

Assigned to a robotic hand, the ambidextrous feature means that two different behaviours are accessible from a single robot hand, because of its fingers architecture which permits them to bend in both ways. On one hand, the robotic device can therefore behave as a right hand whereas, on another hand, it can behave as a left hand. The main contribution of this project is its ambidextrous feature, totally unique in robotics area. Moreover, the Ambidextrous Robot Hand is actuated by pneumatic artificial muscles (PAMs), which are not commonly used to drive robot hands. The type of the actuators consequently adds more originality to the project.

The primary challenge is to reach an ambidextrous behaviour using PAMs designed to actuate non-ambidextrous robot hands. Thus, a feasibility study is carried out for this purpose. Investigating a number of mechanical possibilities, an ambidextrous design is reached with features almost identical for its right and left sides. A testbench is thereafter designed to investigate this possibility even further to design ambidextrous fingers using 3D printing and an asymmetrical tendons routing engineered to reduce the number of actuators. The Ambidextrous Robot Hand is connected to a remote control interface accessible from its website, which provides video streaming as feedback, to be eventually used as an online rehabilitation device.

The secondary main challenge is to implement control algorithms on a robot hand with a range twice larger than others, with an asymmetrical tendons routing and actuated by nonlinear actuators. A number of control algorithms are therefore investigated to interact with the angular displacement of the fingers and the grasping abilities of the hand. Several solutions are found out, notably the implementations of a phasing plane switch control and a sliding-mode control, both specific to the architecture of the Ambidextrous Robot Hand. The implementation of these two algorithms on a robotic hand actuated by PAMs is almost as innovative as the ambidextrous design of the mechanical structure itself.

Acknowledgements

First and foremost, I wish to express my acknowledgments to everybody who worked at my side or who provided me assistance on the Ambidextrous Robot Hand project.

Firstly, I thank my parents for the funding of my PhD and their support over these three years I spent in United Kingdom.

Secondly, I thank my supervisors. Dr Tatiana Kalganova, for having proposed me to carry on my engineering internship as a PhD study and for having gathered teams of students every year to work on the different parts of the project. Dr Roger Powell, for his approval and his support about the control methods I used during the third year of my project. Dr Peter Turner, for his advices in electronics and for having guided me on my first steps in control theory during my first year, but who sadly passed away in the middle of my second year. May he rest in peace. Finally, my unofficial supervisor Prof Stelarc, who had the idea of a robotic hand with an ambidextrous design, and without whom the project would not exist. I acknowledge him for his enthusiasm and for having funded a number of pneumatic and electronic devices, without which the Ambidextrous Hand could not be actuated.

I am very grateful to Shadow Robot Company, which also played an important role in the project. They provided a number of pneumatic materials, electronic devices and hardware coding at an early stage of the project. On these points, I mainly thank Mr Richard Walker for his advices and his help about computer and software parts, Mr Armando De La Rosa Thames and Mr Matthew Godden for their knowledge in pneumatic equipment, as well as Mr Agust Johannson for his knowledge in analog electronics. During the second and third years of my PhD, Shadow Robot carried on provided help by finding and selling very specific devices, using their relationships with professional suppliers.

I also thank Festo, for having sold a large amount of pneumatic muscles at half price and for having received me for free at a training session about modern industrial pneumatic in the beginning of my second year of PhD.

Then I wish to sincerely acknowledge each of my colleagues, who joined the Ambidextrous Robot Hand in partial fulfilment for their Bachelor or Master degrees, either as half-time researchers through an academic year or as research visitors during short

internships. None of them were paid but each contributed to the project in one way or another.

Mashood Mukhtar, the only PhD student but me, who joined the project in the beginning of my third year. His analog and research skills were helpful to complete my work. Mashood is the one who will keep cohesion in the project and who will guide the incomers after my departure. I wish him the best of luck.

Nicolas Lesne, who worked on the project in summer 2014. His solid practical knowledge allowed him to implement a new type of sensors and additional electronic devices on the hardware system. Nicolas also upgraded this hardware system and computed very fast the grasping algorithms that I engineered.

Paul Bazin, who joined the project during the academic year 2013/2014, Marina Honoré, Frédéric Giang and Anthony Tran, who were at my side in summer 2013. Paul and Marina worked on the signal acquisition of electromyography, Frédéric considerably improved a hand gesture recognition application and Anthony developed a server connected to the software frameworks Robotic Operating System. Although none of the works achieved by these four students directly interfere with my research, I appreciated their company and their contribution to the project.

The mechanical team of the academic year 2012/2013: Luke Steele, Michal Simko, Luke Kavanagh and Alisdair Nimmo, for having designed the mechanical structure of the Ambidextrous Robot Hand I have worked on during my third year. In addition to have all contributed to the design of ambidextrous fingers, each of them worked on specific parts as well. Luke S. designed Hall effect sensors and implemented them in the hand. Michal modified the design of a number of mechanical structures in record time, to make them compatible with other versions of pneumatic muscles received very late. Luke K. worked on the thumb, the palm, the routing and fixation of tendons. Alisdair also worked on the thumb and the palm, as well as on the implementation of load cells.

A special acknowledgment to Anthony Huynh, for the excellent work he did on the hardware part during the academic year 2012/2013, making microcontroller units compatible with a full robot hand. Anthony worked with me on many parts, such as analog and pneumatic interfaces, sensors' calibrations, control algorithms, remote experiments, electronic and mechanical testing. A number of sleepless nights were spent on some of these

tasks during my second year. Other kinds of sleepless nights were spent together during my third year, this time playing video games and watching horror movies. Thank you for being such an excellent friend, Anthony!

I would like to emphasise that Luke S., Michal, Luke K. and Anthony carried on working on the project for one month and half after their deadline (Alisdair could not continue as he was recruited for a job), even though they had already submitted their report long ago, without expecting any rewards but own satisfaction.

My high school friend Michel Heinrich, who came in Brunel in autumn 2012, to design the project's website and to debug issues with the remote control system. Michel being a professional web designer, working with him allowed me to acquire knowledge about web development very fast.

The remote control team of summer 2012: Alexandre Dilly, Fabrice Jourdan and Zhu Liu, who made the robot hand prototype move from internet with a video feedback for the first time, through a number of applications. A special acknowledgement to Alexandre for having worked very efficiently and produced so much in a very short time. Designing a server-client interface including an embedded webcam, Alexandre reached all his requirements at half of his internship. He was then asked to work on a plugin for hand gesture recognition using a webcam, adding even more originality to the project. His knowledge in software and programming were very useful to the project and he guided me to design my part of the remote control interface. Fabrice and Zhu respectively worked on a Facebook application and on client software, connecting the computer processes of Alexandre and myself to their remote systems.

Souraneel Chattoraj, who worked with me on early prototypes and control theory through the academic year 2011/2012. Not reaching ambidextrous movements after months was frustrating and discouraging. Seeing Souraneel having the same difficulties as mine helped me to feel more confident. And at the end of the day, we finally succeeded to have an ambidextrous finger working.

A special thought to my very first colleague, Itziar Berruezo Juandeaburre, with whom I did my internship in Brunel in summer 2011. Learning about microcontrollers, software, pneumatic and mechanics, we succeeded to make something moving at the end of our three months. Without her company, starting the project from nothing and without any

robotic knowledge would have been a big issue. I probably would have never asked to carry on my work placement as a PhD project if I had been on my own.

I acknowledge all of them for the work they did and the time we spent together.

I thank the electronic and mechanical departments of Brunel University, as well as the College Stores, the Information technology, the Research Office, the wood shop and the Computer Support for providing me assistance and the material I needed. I particularly acknowledge Mr Michael Lateo for his savoir-faire in analog electronics and the help he provided me for a number of electronic interfaces. I also thank Mr Simon Hodkinson for having helped me finding appropriate pneumatic devices.

I acknowledge Dr Nina Sellars for having enthusiastically introduced me to a prototype of her PhD project "Lucida" and who permitted me to discover some outcomes reached by the merging of art and science.

Last but not least, I thank a lot my amazing girlfriend, my close brother and once again my parents, thanks to whom I spent excellent holidays and could come back to Brunel in excellent shape.

Abbreviations

3D	Three-dimensional space
ADC	Analog-to-digital converter
AI	Artificial intelligence
BSC	Backstepping control
CPU	Central processing unit
DAC	Digital-to-analog converter
DC	Direct current
DIP	Distal interphalangeal
DOF	Degree of freedom
EMG	Electromyography
FPAM	Pneumatic artificial muscle manufactured by Festo
FPGA	Field-programmable gate array
GA	Genetic algorithm
GUI	Graphical user interface
HCI	Human-computer interaction
HGR	Hand gesture recognition
HTML	HyperText Markup Language
HTTP	Hypertext Transfer Protocol
ID	Inside diameter
IDE	Integrated development environment

IP	Internet Protocol
IR	Infrared
I/O	Inputs/outputs
LED	Light emitting diodes
MCP	Metacarpophalangeal
MCU	Microcontroller unit
MOSFET	Metal-oxide-semiconductor field-effect transistor
N/A	Not available
NN	Neural network
OD	Outside diameter
PAM	Pneumatic artificial muscle
PD	Proportional derivative
PI	Proportional integrative
PIC	Peripheral Interface Controller
PID	Proportional integrative derivative
PIP	Proximal interphalangeal
PLP	Phantom limb pain
PPSC	Phasing plane switch control
PSI	Pounds per square inch
PSO	Particle swarm optimisation
PWM	Pulse-width modulation
RCI	Remote control interface

RF	Radio frequency
SDCC	Small Device C Compiler
SPAM	Pneumatic artificial muscle manufactured by Shadow Robot
SPCU	Shadow Pneumatic Control Unit
SMC	Sliding-mode control
TCP/IP	Internet protocol suite
UDP	User Datagram Protocol
VR	Virtual reality
XML	Extensible Markup Language

Table of Contents

List of Figures

List of Tables

Chapter 1: Introduction

Robotic systems are generally engineered to imitate the behaviours of limbs or animals, which is why their architecture is close to the one responsible of movements for animate beings. Indeed, robotic systems are generally made of four main parts which are the mechanical architecture, the actuators, the electronic interface and the computer program. An analogy can be done between mechanical architecture and body, actuators and muscles, electronic interface and nervous system, computer program and brain. The computer program generates sequences of instructions executable by the electronic interface which interacts with the actuators. The actuators are linked to the mechanical interface that achieves the tasks for which the robot is designed. Robots can therefore be qualified of automatic electromechanical devices. As for living beings, each type of robots has its own characteristics and specificities.

In case of robot hands driven by PAMs, a number of parameters related to anthropomorphism have to be taken into account, such as the shape of the device, the tendon routing and the mechanical behaviour. The connections between the different parts of such a structure are illustrated in Figure 1.1. Tendons are connected between strategic points of the mechanical architecture and air muscles, the length of which varying according to compressed air flowing in or out. The air flow is controlled by valves connected both to a pneumatic circuit and an electronic interface. According to the command inputs, the delivered voltages turn the valves on or off for specific amounts of times, controlling the contraction rates of muscles and therefore the finger gestures. Response time, accuracy and stability depend on control algorithms implemented on microcontrollers, which receive data feedback provided by sensors (although sensors are embedded on the hand in Figure 1.1, they can also be connected to devices close to the mechanical architecture, such as the air muscles or the tendons).
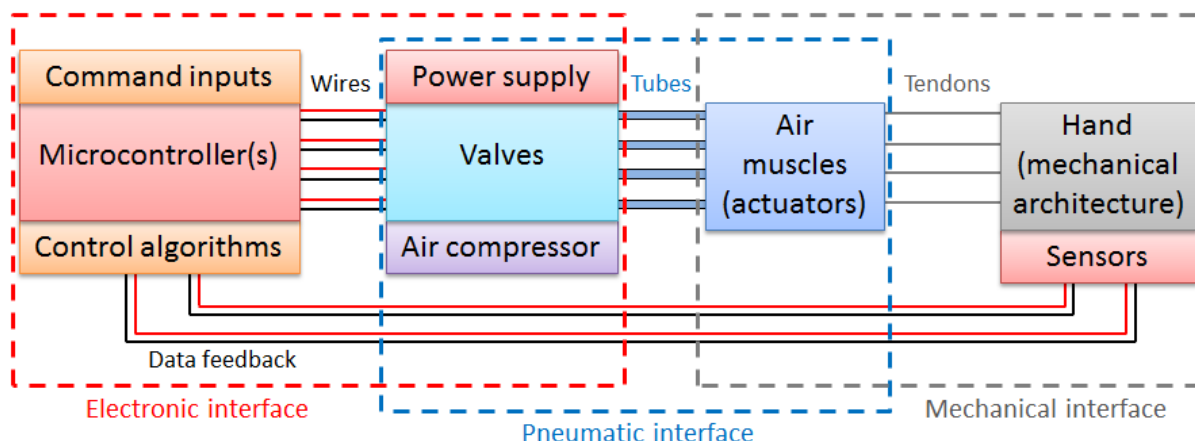
Figure 1.1: Connection of the different devices to actuate a robot hand driven by air muscles

1.1.   Purposes of an ambidextrous robot hand

The design of an ambidextrous hand implies a range about twice larger as the one of human hands, as fingers can curve in both ways. On one hand, the robotic device can consequently behave as a right hand whereas, on another hand, the robotic device can behave as a left hand. Combining the two different behaviours, the Ambidextrous Hand can therefore produce gestures impossible to achieve by humans. The first purpose of such a device is consequently to increase the mechanical possibilities of anthropomorphic hands. This is the reason why the Ambidextrous Hand can be conceived both as an artistic and a scientific project.

1.1.1. Ambidextrous hand as an artistic project

The definition of art significantly evolved through the ages. Indeed, in Antiquity, Plato was referring to art as an ability to create based on human intelligence [1], whereas Aristotle estimated that art was a representation of the human instinct for harmony or balance [2]. Despite the disagreement concerning the definition of arts, both Plato and Aristotle agreed that art mainly aims at representing beauty. Art was still relying on this standard in the eighteenth century, as I. Kant investigated the subjectivity of aesthetic judgements that were related to it [3]. However, as explained in [4], art aimed at reaching new criteria at the end of the nineteenth century, and L.N. Tolstoy defined art as a concept referring to original creations relying on technical skills [5]. Therefore, modern and contemporary arts do not

focus on beauty anymore but rather on epistemological rupture [6]. Thus, some works explore the boundaries of the human body and investigate alternate anatomical architecture, such as in [7] where an artificial ear is surgically attached to the arm of Stelarc. The concept of art-science therefore emerged, as merging the two cultures permits to create original works impossible to design without the use of recent technologies [8], [9]. The notion matches with the artistic ideology of L.N. Tolstoy [5], even though some works can prompt discussions about biomedical ethics [8]. Besides, art-science's pieces of work can be associated to the human anatomy without involving any surgical operations, or even without any interactions with a human body. This is for instance the case of N. Sellars' project "Lucida", a light installation that projects shadows representing the interior of fictional bodies [10]. Lucida is described as a poetic exploration of light in relation to the microscopic study of cells and aims at changing the perception of the anatomical body [10].

Based on these definitions and these examples, the Ambidextrous Hand can consequently be defined as an artistic project as it allows overreaching the limits defined by mother nature and performing movements unrealisable by any other organisms or structures.

1.1.2. Ambidextrous hand as a scientific project

In addition to its artistic purpose, the Ambidextrous Robot Hand can also be used in the same way as classic designs of robot hands, as being used in situations dangerous for human beings. These situations may include, for examples, the defusing of bombs, the manipulation of objects in aerospace or in radioactive environments. However, the ambidextrous design may have an advantage to other models in another field, which is biomedical area. Even though the need of an air compressor prevents the Ambidextrous Hand to be used as a prosthetis, the design of a remote control interface (RCI) through internet could allow an instantaneous access to the robotic device and possibly ease the phantom limb pain (PLP) felt by amputees.

As explained in [11], PLP is a chronic experience of pain in the residual impression of a limb persisting after amputation. The feeling results from cortical maps which organises the sensory information perceived by brains [12]. When a cortical map is affected by stimuli, a new cortical map is created. The process is defined as cortical remapping and occurs for brain disorders such as cerebral palsy or embryonic abnormalities [13]. However, in case of

amputations, it is argued that the cortical maps remain intact even though the inter-regional connectivity is disrupted [14]. Experimental results show that a strong relationship exists between the amount of cortical reorganisation and the magnitude of PLP experienced after arm amputation [15]. PLP is consequently related to plastic changes in primary somatosensory cortex [15]. This cortical plasticity can be modified by behavioural interventions that provide feedback to the brain areas that were altered by pain memories [16]. Thus, neurological rehabilitation is used to guide the neural reorganisation and facilitate the recovery of cortical maps [17]. Among these neurological rehabilitations, it has already been proved that different kinds of physiotherapy contribute to PLP relief, such as the use of mirror boxes which proved to be efficient in many cases, as observed in [18], [19] or [20]. The prevailing explanation about the ease provided by mirror boxes is that observing mirrored movements causes additional neural activity in motor areas located in the affected hemisphere, leading to cortical reorganisation and improved function [21]. According to [22], the mirror box phenomenon eases PLP because the estimated position of a limb is not only based on sensory information, but also on the stream of motor commands issued to the limb muscles. Thus, the normal experience of the limb can be based on the predicted state provided by the mirror box, rather than an actual state. However, the mirror boxes have restrictions as they operate within a narrow spatial dimension, requiring the patient to remain in a restricted and fixed position [23] and only suit for unilateral amputees [24]. Thus, environments based on virtual reality (VR) have been developed, such as in [11] or [25], to overcome these limitations.

Based on these facts and these assumptions, the control of the Ambidextrous Robot Hand through internet can provide a new type of physiotherapy and a new interface close to VR. It would therefore ease the PLP as well, permitting the control of a real robot hand displayed by video feedback showing a scene filmed in a real environment. By combining the RCI with electromyography (EMG) or hand gesture recognition (HGR) by webcam, the movements of the robotic hand displayed by video feedback may be interpreted as the one of the missing limb by the brain, which would guide the neural reorganisation [17] and ease the PLP. Similar cases of studies have been done in the past. Amputees or people suffering from neurological disorder have indeed been provided assistance by connecting robot limbs to a human-computer interface (HCI) [26], [27] and robotic hands have also been used as rehabilitation devices for recovering patients [28], [29]. However, most of rehabilitation devices are expensive or difficult to access in short delays and none of them propose a free

therapy treatment instantly accessible online, from home or from workspace. To increase this ease of accessibility, the ambidextrous hand can imitate the movements either of a right hand or a left hand, permitting assistance to injuries of both sides with only one robotic device.

The summary of the project is shown in Figure 1.2, with images from [30], [31], [32], [33], [34] and [35]. A user can interact with the Ambidextrous Robot Hand using either HGR or EMG. The control commands are sent through internet to the robotic device, the movements or which being visible on the user's computer because of a video feedback.
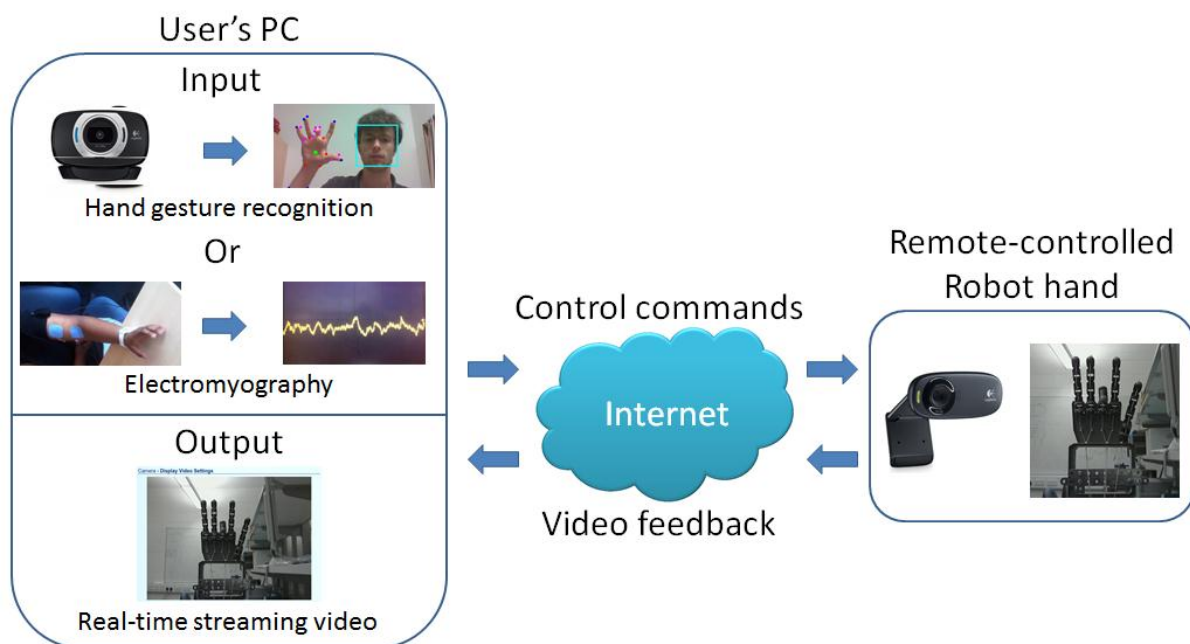
Figure 1.2: Summary of the telerehabilitation part of the project, with images from [30], [31], [32], [33], [34] and [35]

1.2. Aim and objectives of the thesis

The aim of the project is to develop a remote-controlled ambidextrous robot hand actuated by PAMs. The work introduced in this thesis consequently has to reach several objectives.

First, pneumatic and electronic devices necessary to actuate a robot hand are introduced, as well as the way they are connected together and interact with the mechanical structure. Next, the overall architecture of the system has to be designed.

Then, prototypes of single fingers are designed until reaching an ambidextrous range, to prove the feasibility of the project. The mechanical structure of the prototypes can be duplicated afterwards to design the fingers of a whole hand. The possibility to reduce the number of actuators is also investigated. The feasibility study includes the implementation of feedback control algorithms as well, to prove that both angular position and force applied by the fingertip can be driven successfully.

Furthermore, the overall design of ambidextrous hand has to be finalised. To establish design from a single finger to a whole hand implies the choice of suitable material, which is why mechanical structures are further investigated, this time designing a testbench that is connected to a number of electronic devices to collect experimental data.

Besides, the remote control feature of the project also has to be exploited. The robotic structure must therefore be connected to a RCI, itself connected to the website of the project. The way to use this RCI and interact with it from the website is also explained in this thesis.

Finally, control algorithms appropriate to the unique architecture of the ambidextrous hand must be considered, implemented and tested. Control algorithms implemented on such a structure concern both the angular displacement of fingers and the grasping features of the hand. In case of an ambidextrous design, the hand must be able to grab objects both on right and left sides.

1.3. Project achievements and contribution to science

This thesis relates the successful development of a robot hand with an ambidextrous design, which is a unique feature in the realm of robotics. The originality of the project goes even further as the Ambidextrous Robot Hand is driven by PAMs, which are not commonly used to actuate humanoid robots [36]. Moreover, an asymmetrical tendon routing is engineered to reduce the number of PAMs necessary to actuate such a structure, as discussed in [37] and [38]. The Ambidextrous Robot Hand is consequently driven by a minimised ratio between its number of degrees of freedom (DOFs) and its number of PAMs.

In addition to the mechanical contribution, the project also includes a RCI allowing an online access to the robot hand [39]. The software embedded on the server system provides a

video streaming as feedback. It therefore permits an instantaneous access to the robot hand through internet.

Last but not least, this thesis relates to the development of control algorithms specific to the Ambidextrous Robot Hand, taking its range, its asymmetrical tendon routing and the nonlinearity of its PAMs into account. Furthermore, most of these algorithms have never been implemented on robot hands driven by PAMs before. This is the case of the unique phasing plane switch control designed for this purpose, or of the first sliding-mode control implemented to grab objects with such a device [40]. In addition to control algorithms engineered from angular and pressure feedbacks, other ones were engineered from force feedback. Unique implementations are realised with bang-bang and backstepping controls, but the best results obtained from force feedback control are achieved with proportional-integrative-derivative loops, which are commonly used in robotics [41]. These three force control algorithms are connected to a neural network used a safety mechanism, to prevent the fingers tightening in case the objects are not in contact with the force sensors.

The ways these achievements are reached are discussed in this thesis.

1.4.   Outline of the thesis

Chapter 1 introduces the topic, discussing the research motivations and objectives.

Chapter 2 starts providing a literature review about mechanical designs of a number of dexterous robotic hands, giving a particular attention to robot hands controlled by PAMs. Over a second phase, devices and software necessary to implement electronic and remote control interfaces are considered as well. Finally, a number of papers concerning control algorithms implemented on robotic structures driven by PAMs are analysed. The part of the literature review concerning the mechanical structures of robot hands is summarised in [38], whereas the part concerning the control algorithms are summarised in [40] and [41].

Chapter 3 first describes the functioning of pneumatic devices and the way they are connected to each other, to the electronic interface and to tendons which actuate robotic limbs. Secondly, it explores the structure of dexterous robot hands to make them ambidextrous. This investigation is used to proceed to the feasibility study of the project. Tests are done on a single finger until reaching an ambidextrous range and enough force on

the fingertips to proceed to angular and force controls. The system is then integrated to a remote control interface accessible via the website of the project. The achievements of Chapter 3 are summarised in [39] whereas the part about force control is more deeply discussed in [41].

Chapter 4 presents the implementation of a testbench to evaluate the behaviour of more advanced designs. It first deals with the architecture of the testbench and the implementation of the electronic hardware used to proceed to the data collection. This second part includes the choice of sensors, their calibration and their implementation in the whole system. Experimental data of ambidextrous fingers is then analysed and the mechanical architecture is taken into consideration prior to investigating the control algorithms introduced in Chapter 5. The research achievements resulting from the work introduced in Chapter 4 are summarised in [37] and [38].

Chapter 5 selects some of the algorithms analysed in Chapter 2. The selected algorithms are designed to be compatible with the specific features of the Ambidextrous Robot Hand and to reach new kind of behaviours. Both angular displacements and grasping features are investigated. These grasping features are considered using two kinds of feedbacks, which are the pressure from PAMs and the force from the fingers architecture. The content of Chapter 5 is summarised in [40] and [41].

Chapter 6 summarises the overall findings and suggests recommendations for future works.

Chapter 2: Literature review

This chapter introduces reviews analysis of the five main points necessary to engineer a remote-controlled ambidextrous robot hand.

The first of these five points is the mechanical design of robot hands. The ways they are actuated permit to classify them into four main different categories. Indeed, robot hands can be actuated by human body, motors, artificial muscles (which include PAMs) and pneumatic cylinders. The way the mechanical features vary according to the kind of actuation is going to be discussed.

The second point concerns the electronic microcontrollers, necessary to control such structures. The research is less specific in this area, as every project belonging to embedded systems requires microcontrollers. However, some characteristics and features are relevant to robot hands controlled by PAMs.

The third point is the remote control interface. As for microcontrollers, the literature review is not as specific in this area, because a high number of engineering projects includes such an interface. Nevertheless, different possible ways to actuate an embedded system remotely are going to be explored as well.

The fourth point is the use of pneumatic technology in robotic area. In addition to robot hands, it is observed that PAMs are mainly used to actuate robot arms and that they can also be used as power assist wears. As robot hands actuated by PAMs are not very numerous, this research will be useful prior to investigating the last point of this Chapter, which concerns the different types of algorithms applicable to PAMs.

The last point is an analysis of control algorithms applicable on pneumatic technology, so algorithms can be selected and implemented to control both the angular displacement and the grasping force of the Ambidextrous Hand.

2.1.   Robotic hands' mechanical features

Robot hands can be divided into four main categories according to the way they are actuated: body-powered, controlled by motors, driven by pneumatic cylinders or by artificial muscles. Artificial muscles include a number of different materials. The most commonly used

to actuate robot hands are made of rubber, from which PAMs are made from [36], but the structure of human muscles can also be imitated by other materials, such as shape memory alloys or electroactive polymers. As robot hands driven by PAMs are few in number, an overview of all these categories permits to familiarise more with both mechanical structures and development of robot hands through history.

Body-powered hands can mainly be divided into prosthetic or bionic hands. In the first case, they do not include any electronic devices and cannot be classified as robot hands. In the second case, they include mechanisms totally different from the ones of hands actuated by artificial muscles. Consequently, the analysis of body-powered hands will be quite succinct as it does not really match the subject of this thesis. The mechanisms of hands driven by motors or pneumatic cylinders, however, are much closer to the ones of hands driven by artificial muscles.

2.1.1. Body-powered hands

In case robot hands are body-powered, their main aim is to replace missing limbs and they are thus referred as prosthetic hands, such the feasibility study described in [42], where the motor actuating the fingers can be replaced by a physical human interaction. For other models, it is possible to transplant the mechanical structure on forearms and to link tendons to the patient's shoulder [43]. Both of these designs aim at reducing a maximum the weight and the mechanical routings of robotic architectures, with the possibility to actuate them without any electronic interfaces. Consequently, fingers' movements are not independent and they all close when the motor or the shoulder interact with the tendons routing. These models have the advantages of allowing convenient grasping features and interactions with objects, as well as being relatively cheap, as the bigger cost comes from surgery operation. The Natural Dexterous Hand [43], for example, costs about £600 including the whole operation in 2011. More advanced prosthetic hands aim at increasing the number of degrees of freedom (DOFs) to extend the possible interactions between the user and the fingers. This kind of technology requires the implementation of electromyography (EMG) that measures the electronic activities of human muscles to convert them into signals that actuate prosthetic hands, which are then referred as bionic hands. Bionic hands include a number of models, such as the modular prosthetic limb funded by the Defense Advanced Research Projects Agency [44], the

bebionic3 designed by RSLSteeper [45] and the i-limb ultra revolution developed by Touch Bionics [46]. However, given the technology used to achieve this goal, the costs are much more substantial. According to Singularity University, the prices of such devices in 2010 were about £6.5 k for the Bebionic hand and £10.2 k for the i-Limb Hand [47]. The high cost of such devices is explained because of the implementation of electronic interfaces and actuators which, in this case, are motors. It can consequently be said that bionic hands belong to hybrid systems, controlled by human bodies but actuated by motors.

2.1.2. Motorised robot hands

Robotic structures driven by motors constitute the second and the widest category belonging to robot hands. A considerable amount of literature has indeed been published in this area, ones of the earliest and most famous being the Robonaut hand in 1999 [48] and the Gifu hand in 2001 [49]. Contrary to prosthetic or bionic hands, motorised hands are mainly dedicated to research, or can aim at replacing human beings in dangerous situations, such as the defusing of bombs or interactions with objects in aerospace or radioactive environments. The Robonaut hand [48], for example, was specifically designed by the Dextrous Robotics Laboratory at NASA's Johnson Space Center to work in similar environments as astronauts. However, a number of robot hands engineered around the year 2000 present some physical limitations compared to the ones developed nowadays. For instances, a robotic structure developed in Ritsumeikan University [50], in 2000, was wired to move inside a cube, whereas a multi-fingered robotic hand developed in Kyushu University [51] had three fingers and a circular structure to facilitate the interaction with objects. Besides, reducing the number of fingers is a solution often opted by designers to limit the number of actuators, as it can be seen for the four fingered teleoperation system published in 2005 [52], the testing of a three-fingered hand in 2006 [53], the robot application published in 2007 [54] conceived to be applied to prosthetics or the development of the four-fingered Meka H2 Compliant Hand in 2009 [55].

In addition to the number of fingers, a feature characteristic to robot hands is their number of DOFs. Indeed, an important number of DOFs increase the quantity of movements achievable by robot hands, and consequently allows behaviour closer to human hands, which have a total of 27 DOFs [56] (or 21 DOFs without taking the wrist into account). A number of motorised robot hands are summarised in Table 2.1, in which the numbers of fingers,

DOFs and actuators are indicated for each of them. It can be seen that some designers find a compromise between the number of DOFs and the number of motors to have an appropriate control of the hand with fewer resources, such as the Southampton remedy hand that has six DOFs for six motors [57]. Other robot hands opt for a higher number of DOFs that cannot be controlled independently, such as the hand conceived by N. Fukaya et al. that has 20 DOFs for one motor [58], the model developed by L. Zollo et al. which has ten DOFs for three motors [54] or the one designed by G. Stellin et al. [59] with 20 DOFs for nine motors. It is also noticed that some designers develop robot hands dedicated to very specific tasks. For instances, the three-fingered Ishikawa Watanabe Laboratory's high-speed robot hand [60] is specialised in the manipulation of objects at very high-speed and can reproduce a human gesture in 1 µs, whereas a two-fingered hand developed by D. Gunji et al. [61] is controlled by a single motor and only aims at grasping objects. In addition to their limited number of fingers, none of these two hands have an anthropomorphic shape; the fingers of [60] are arranged in triangle whereas the two fingers of [61] are totally opposite. Even though not having an anthropomorphic shape is not an inconvenience in robotics, this feature may become problematic if the aim of the project is to ease PLP, as the patient would not be able to assimilate his missing limb to the robotic device [11].

Despite these previous examples, most of robot hands have a ratio close to 1 ± 0.2 by comparing the number of DOFs with the number of motors. This is indeed the case for the hands described in [48], [49], [50], [52], [57], [61], [62], [63], [64] and [65]. However, it is also noticed that, in some cases, robot hands include more actuators than necessary to reach new kind of behaviours, such as compliancy for the ACT hand [66] or robustness for the DLR hand [67]. Finally, it can be noted that most of the robot hands developed over the last five years opt for a five fingers design, as it is observed for [68], [70], [69], [67], [72], [62], [65] and [66].

Table 2.1: Mechanical features of a number of motorised robot hands

Robotic Hands	# fingers	# DOFs	# motors	Ratio # DOFs / # motors	# and type of sensors
Robonaut hand [48], 1999	5	14	14	1.00	43 position sensors
N. Fukaya et al. [58], 2000	5	20[a]	1	Irrelevant[a]	None
S. Kawamura et al. [50], 2000	3	6	7	0.86	~5[b] laser sensors
The Southampton remedy hand [57], 2001	5	6	6	1.00	~5[b] tactile sensors
The Gifu hand III [49], 2002	5	16	19	0.84	6 axes force and 1 distributed tactile sensors
H. Hu et al. [52], 2005	4	13	13	1.00	13 Hall effect and more than 100 dimensional torque sensors
I. Yamano and T. Maeno [63], 2005	5	20	~20[b]	~1.00[b]	N/A angle sensors
S. Takamuku et al. [71], 2007	5	18	13	1.38	N/A torque, angle and haptic sensors
L. Zollo et al. [54], 2007	3	10[a]	3	Irrelevant[a]	2 force and 8 Hall effect sensors
D. Gunji et al. [61], 2008	2	1	1	1.00	1 laser displacement and 2 pressure tactile sensors
C. Chivu et al. [64], 2008	5	5	5	1.00	N/A
The iCub hand [59], 2008	5	20[a]	9	Irrelevant[a]	12 Hall effect, 2 optical proximity, 5 cable tension and 3 torque sensory systems
High-speed hand [60], 2009	3	8	N/A	N/A	N/A tactile and pressure conductive sensors
H2 Compliant hand [55], 2009	4	12[a]	5	Irrelevant[a]	N/A
C.H. Kuo and C. Chen [68], 2010	5	16	12	1.33	Tactile and pressure sensors
Elu2 Hand [70], 2010	5	9	N/A	N/A	N/A pads tactile sensing
EH1 Milano hand [69], 2010	5	16	12	1.33	5 force, 6 position, 6 current and 12 limit switch sensors
DLR hand [67], 2011	5	19	42	0.45	N/A torque and position sensors
OCU Hand II [72], 2011	5	19[a]	13	Irrelevant[a]	16 force and 4 tactile sensors

Robotic Hands	# fingers	# DOFs	# motors	Ratio # DOFs / # motors	# and type of sensors
Shadow Dexterous hand E1M3R, E1M3L [62], 2013	5	20	20	1.00	N/A Position, tactile, force, temperature, current and voltage sensors, total ≥ 37
DEXMART Hand [65], 2013	5	20	20	1.00	N/A tactile sensors
ACT Hand [66], 2013	5	23	36	0.64	36 photosensors

[a] A number of DOFs cannot be controlled independently
[b] Estimations are done from pictures or videos of the robot hands

Regarding the sensors, Table 2.1 shows that the most popular are tactile, angular, torque and Hall effect sensors. As explained in [73], Hall effect sensors are transducers for which the output voltage varies according to magnetic fields. Magnets can be fixed either on fingers joints as for the iCub Hand [59] or on motors as for the teleoperation system developed by H. Hu et al. [52]. Thus, as their magnetic fields vary when the magnets rotate, they can be used either to measure the angles of the fingers or the pulling ratio of the motors. A large number of sensors can be necessary when designers include accurate interactive features to their robot hands, such as the over 100 sensors included in the model of H. Hu et al. [52]. Otherwise, a large variety of different sensors can be explained by the addition of security systems to robot hands, as for the Shadow Hand [74] that includes temperature and current sensors. Some other dexterous hands reduce the number of different kind of sensors implementing only angular feedbacks. This is the case of the hand engineered by I. Yamano and T. Maeno [63], for which the force is calculated from the angular deformation of elastic elements, or the ACT hand [66] that uses an arm manipulator developed by Barret Technologies [75] for which the specific motors allow the control of both position and force. Research institute can also develop their own sensors, such as Dainichi Co. Ltd. that designed a distributed tactile sensor for the Gifu hand III [49] which, besides, is one of the main modifications compared to the previous models of the hand [76]. Ishikawa Watanabe Laboratory also uses a very specific kind of sensory system for their high-speed hand [60] as tactile sensors are connected to conductive films and pressure conductive rubber, which provides an overall data feedback for each the displacement of each finger.

Contrary to bionic hands, as motorised robot hands mainly belong to research area, their prices are most often not specified. However, when it is indicated, it is noticed it is much higher than the ones accessible to public. Indeed, it is indicated on their respective

stores that the Gifu Hand III costs about £30 k in 2002 [49] and the Shadow Hand costs about £71 k in 2013 [62].

2.1.3. Robot hands driven by artificial muscles

This Section provides an overview of robot hands driven by three different kinds of artificial muscles, the advantages and inconveniences of which interacting in some ways or others with the mechanical specificities of the robotic devices.

Robot hands actuated by artificial muscles are less current than motorised models [36], as motorised models have the advantage to combine power and accuracy [77]. However, artificial muscles permit reducing the joints stiffness and adding softness to the system [77], which is why they were firstly designed to reduce the danger level in case robotic systems work in public environment [36].

Different types of artificial muscles exist. They can for instance be hydraulic, pneumatic, piezoelectric, made of shape memory alloys or of electroactive polymers [78]. Each type of artificial muscles has specific criteria, such as contraction rate, reaction speed or fracture toughness [79]. Because of their properties, a number of types of artificial muscles are not suitable to actuate robot hands properly. The three main types of artificial muscles used for this purpose are PAMs, shape memory alloys (SMAs) and electroactive polymers (EAPs) [36]. In addition to their respective low weights, their main features that are investigated are generally their diameter, on which depends the size of the robotic system, their contraction rate, on which depends the range of mechanical movements, their actuation stress, on which depends the force they provide, and their reaction speed, on which depends the speed of the system [79]. These criteria are summarised in Table 2.2, for PAMs, SMAs and EAPs, based on [36], [78] and [79]. The actuation stress and reaction speed depend on the artificial muscles' diameters or thickness; the ones indicated in Table 2.2 are the values obtained with standard sizes of materials implemented on robotic systems. Possible diameters and thicknesses of artificial muscles available on market are indicated as well, based on [80], [81], [82] and [83].

Table 2.2: Comparison of mechanical properties between PAMs, SMAs and EAPs

Artificial muscles	Contraction rate (%)	Actuation stress (MPa)	Reaction speed	Diameter or thickness
PAMs [36], [78], [80], [81]	25 to 37	16	µs	10 mm to 40 mm
SMAs [36], [78], [79], [82]	8	700	sec to min	25 µm to 500 µm
EAPs [36], [79], [82], [83]	10 to 32	0.1-3	µs	1 µm to 2 mm

Table 2.2 shows that PAMs have the highest contraction rate and reaction speed, as well as a strong actuation stress, but that their diameter is the largest one. SMAs have the highest ratio between actuation stress and diameter, but are limited by their reaction speed and their contraction rate. EAPs have a contraction rate and a reaction speed close to the ones of PAMs, but also have the smallest actuation rate among these three artificial muscles.

A number of robot hands actuated by PAMs, SMAs and EAPs are then considered in details.

2.1.3.1.   *Robot hands actuated by PAMs*

PAMs contract and extend according to the pressure of air they are filled with. Their contraction rate usually varies from 25% to 37% ([81] and [80]) which is close to the 40% of human muscles [36]. Because of PAMs' operating mode, robot hands actuated by such actuators require a high level of air pressure to interact with robotic limbs [84], which implies the use of an air compressor. Moreover, as explained in [85], the size of PAMs makes the design of a human-sized robot hand difficult. These two disadvantages complicate the use of robot hands actuated by PAMs as prosthetic applications. Furthermore, the non-linearity existing between the air pressure of the contracted PAM and the force it provides [86], [87] makes the robot hands more difficult to control properly. It also creates a delay between the control signals and the effective joints movements as the pressure inside PAMs increases over time [88]. On another hand, it is also noticed that PAMs allow adding flexibility to the overall behaviour of the systems [89], [90]. In addition to their compliance, they have a low mass, an excellent ratio between strength and weight and can as well be used for safe human-machine interactions [91]. Because of these advantages, some designers prefer using PAMs to actuate robot hands.

One of the very first model of robot hands using PAMs' technology is a skeletal framework developed in the University of Tokyo in 1999 [92], with fifteen DOFs for sixteen

PAMs. As the hands [54], [58] and [59] previously mentioned in Section 2.1.2, some of the DOFs of the artificial hand of the University of Tokyo cannot be controlled independently as the distal interphalngeal (DIP) and proximal interphalangeal (PIP) joints of the fingers move synchronously with the metacarpophalangeal (MCP) joint. Despite this first step achieved before 2000, robot hands using PAMs are barely developed before 2008. One of the exceptions is a previous model of the Shadow Dexterous Hand, designed by Shadow Robot Company in 2005 [93] and which became the model described in [94] in 2013. Other exceptions are the Humanoid Hand developed in Curtin University of Technology in 2006 [95] or the model engineered in Doshisha University in 2006 [96], but such robot hands are more often designed after 2009. Indeed, the models introduced in [90], [97], [98], [99], [100], [94] and [101] were all designed between 2010 and 2013. The features of these robot hands are summarised in Table 2.3. A noteworthy difference with motorised robot hands is the number of actuators which is much higher, even though the number of DOFs does not increase for all that. The reason why such a number of PAMs is necessary is because the most common way to connect them to joints is similar to the way human muscles are connected to bones. Connection diagrams are illustrated, for examples, in the works [102], [103], [104] or [105], one of them being copied as Figure 2.1. It is observed that PAMs work in an antagonistic way, which is why the actuation of a single DOF often requires two PAMs.
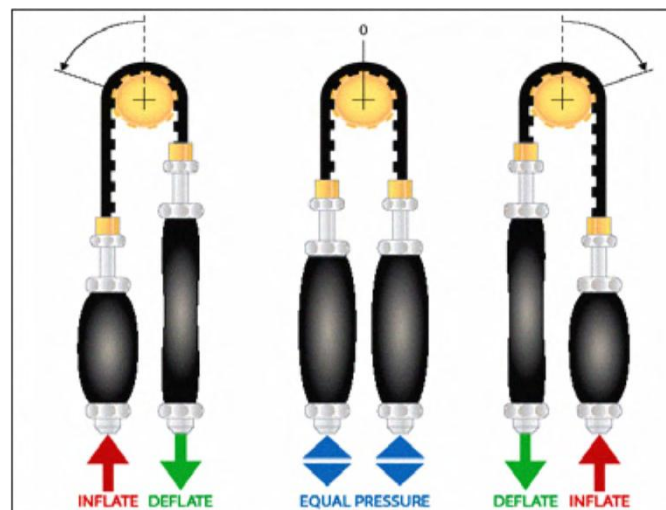
Figure 2.1: Working principles of a joint [102]

This joint actuation explains why the models described in [94], [95], [101], [100] have twice more PAMs than DOFs. However, some methods can be engineered to reduce this ratio. Automatic return mechanisms can indeed be implemented, such as springs for the hand

17

of Swinburne University of Technology [99], the hand designed by P.Y. Chua et al. [106] or the hand engineered by J.Y. Nagase et al. [98]. Elastic gums are used in an identical way for the model of S. Nishino et al. [96] or for an early design of [99] observable in [107]. On another hand, the model of Osaka University [90] reduces this ratio by implementing the PAMs directly inside the finger's architectures. Also, even though robot hands actuated by PAMs with less than five fingers are not common, the three-fingered model engineered by T. Nuchkrua et al. [101] can be assimilated to the two-fingered motorised design of D. Gunji et al. [61], as they are both designed for specific grasping applications.

Table 2.3: Mechanical features of a number of pneumatically actuated robot hands

Robotic Hands	# fingers	# DOFs	# PAMs	Ratio # DOFs / # PAMs	# and type of sensors
Y.K. Lee and I. Shimoyama [92], 1999	5	15[a]	16	Irrelevant[a]	N/A micro-pressure sensors
P. Scarfe and E. Lindsay [95], 2006	5	10	20	0.50	N/A
P.Y. Chua et al. [106], 2006	5	21	~20[b]	1.05[b]	N/A tactile and pressure sensors
S. Nishino et al. [96], 2007	5	~13[b]	~16[bc]	~0.81[bc]	~10[b] position, 1[b] force and 16[b] pressure sensors
Y. Honda et al. [90], 2010	5	17	25	0.68	N/A angle sensors
The Festo Hand [97], 2010	5	~15[b]	~25[b]	0.60[b]	N/A
J.Y. Nagase et al. [98], 2011	4	4	4[c]	1.00[c]	4 force sensors
C.Y. Lau and A. Chai [99], 2012	5	16	14	1.14	14 linear potentiometers
A. Uribe et al. [100], 2012	5	14	28	0.50	N/A
The Shadow Dexterous Hand E1P1R, E1P1L [94], 2013	5	20	40	0.50	N/A Position, tactile and pressure sensors, total ≥ 56
T. Nuchkrua et al. [101], 2013	3	3	6	0.50	N/A

[a] A number of DOFs cannot be controlled independently
[b] Estimations are made from pictures, videos or descriptions of the robot hands
[c] Actuators are referred as pneumatic ballons instead of PAMs; both function in identical ways

Regarding the sensors, Table 2.3 shows that the dominant ones are pressure sensors, as seen for [92], [106], [96] and [94]. Concerning the fingers' displacements, they can either be provided by angle sensors such as [90] or by position sensors such as in [96], [94] or [99]. Although it is not specified, it is possible that the hand developed by T. Nuchkrua et al. [101]

uses no sensors, the same way as the hand [58] previously introduced in Section 2.1.2, given that both of the models are designed for very specific tasks.

In average, it is however noticed that hands actuated by PAMs use fewer sensors than motorised models because of PAMs' flexibility, as explained in [92]. Indeed, PAMs' flexibility makes systems safer, which is why S. Nishino et al. were interested in developing pneumatic actuators in [96].

2.1.3.2.   *Robot hands actuated by shape memory alloys*

Shape-memory alloys (SMAs) are alloys for which the shape varies according to the temperature and that have the propriety to memorise their original shape. They can be deformed at low-temperature and recover their original shape when they are heated [108], the heating being generally obtained from an electric current.

Artificial muscles made of SMAs have the strongest ratio between force and diameter [78]. Indeed, SMAs with a diameter of 150 μm has an actuation stress of 700 MPa whereas standard PAMs only have an actuation stress of 16 MPa, which is more than 40 times lower than SMAs [78]. However, the use of SMAs is made difficult because of their contraction mode, the heating of the alloys implying the investigation of adapted cooling systems [109]. It is also seen in [79] that, contrary to other actuation materials for which the reaction speed is measured in μs, the one of SMAs goes from sec to min. This lack of reaction speed prevents the SMAs to have diameters as big as the ones of PAMs, as it would make the heating and cooling times even longer. Indeed, it can for instance be observed that the introduced wire bundle actuated by SMAs introduced in [110] can lift 445 N but requires the parallel contraction of 48 SMA wires. These wires have a diameter of 150 μm and can individually lift a weight of 9 N. It is specified the system needs a delay of 2 sec to cycle again and that this delay would increase to 8 sec with diameters of 300 μm. SMA actuators also have a contraction rate of 8% [79], which is about four times lower than the one of PAMs [36], and must therefore be accurately implemented in the mechanisms to achieve large motions [111]. Despite the need of a cooling system, their slow reaction speed, their low frequency and their small contraction rate, SMAs also have a small size, volume, weight, are low cost and have a high force to weight ratio [110], which is why they are integrated in a number of robot hands.

The finger of four DOFs introduced in [112] in 2000 is one of the first robotic structures actuated by SMAs. Three SMAs are attached to the distal joint; one actuates the flexion whereas the two other ones deal with the recovery force needed to reposition the finger to its original configuration. Abduction and adduction are provided by passive movements of the ball rod end. The system is improved in 2004 [113], as Hall effect sensors are integrated in each revolute joint to control the rotational movements. A similar finger is developed in 2009 in [114], with four DOFs driven by as many SMAs. A force sensor is embedded on its fingertip, a bend sensor on its PIP joint and two potentiometers control the abduction/adduction. Concerning the actuation of several fingers, the SMA robot hand [115] and the robot gripper introduced in [116] are ones of the first robot hands driven by SMAs. Both of the papers were published in 2002 and both hands have three fingers. The robot gripper [116] has a single DOF actuated by a single SMA and its fingers are made of flexible rods, so the device can adapt itself to the shape of light objects without requiring any sensors feedback. Concerning the SMA robot hand [115], it is specified that the device can fully open itself in 3 sec with a specific cooling system. The model is redesigned as the ITU robot hand in 2004 [117] to check the compatibility of the system to clear mines. The ITU robot hand still includes three fingers and its full gripping position is obtained in 3.76 sec. Neither the number of DOFs nor the number of SMAs are specified in [115] or [117], but it can be deduced from the unique pressure sensor of the system [115] that it has probably only one DOF for one SMA, as for [116].

More anthropomorphic models of robot hands actuated by SMAs are developed after 2004, such as in [118], where a five fingered anthropomorphic robot hand driven by ten SMA wires for which the hysteretic behaviour is prevented by the use of a segmented binary control. The behavior of the model is improved in 2007 [119], as the device is driven by 32 SMAs for a total of sixteen DOFs and a weight lower than 800 grams. Besides, the low volume and weight of SMAs permit the actuators to be investigated for the designs of prosthetic hands, such as the ones introduced in [120] and [121]. The model discussed in [120] has seven DOFs for as many SMAs, the antagonistic motion of which being accomplished by the contraction of springs during the cooling phase. The prosthetic model of [121] also uses the implementation of springs to reduce the number of SMAs. It has ten DOFs for as many SMAs, and the experiment illustrated in [122] shows that it has a grasping time of 6 sec. The slow reaction speed of SMAs is compensated in other researches, such as in [123], where the miniature robot hand that is introduced is about one third of human hands,

which consequently reduces the required contraction rate and increases the SMAs' reactivity. Indeed, its SMAs only have a diameter of 50 μm, which is thrice smaller than the SMAs of [110]. Thus, it makes the fingers' movement have a time constant of about 0.2 sec, which is much faster than the times previously indicated in [117] and [122], respectively of 3.76 and 6 sec. The miniature hand introduced in [123] also have among the best abilities of the robot hands driven by SMAs, as it has a total of twenty DOFs for forty SMA wires. It also contains fourteen strain gauges, one in each joint, which are used as angular sensors. The inconveniences of SMAs actuator can also be compensated by the design of hybrid robotic models, driven both by SMAs and DC motors. This is for instance the case of the finger discussed in [124], for which DC motors are integrated in proximal and medial phalanges to control the rotation around PIP and DIP joints. Another example is the four-fingered hand introduced in [125], for which both the SMAs and the two DC motors are embedded in the palm.

The mechanical characteristics of these robotic devices driven by SMAs are summarised in Table 2.4, hybrid models being not included. As for motorised hands analysed in Section 2.1.2, the number of DOFs is often equal to the number of SMAs, as for [116], [117], [120], [114] and [121]. Only [123] and [119] have a ratio of 0.50. It is also noticed that [123] and [119] are the only robot hands of Table 2.4 for which the number of DOFs exceeds twelve, whereas most of the hands driven by motors and PAMs, respectively summarised in Table 2.1 and Table 2.3, had more than twelve DOFs.

Table 2.4: Mechanical features of selected robot hands or fingers driven by SMAs

Robotic Hands	# fingers	# DOFs	# SMAs	Ratio # DOFs / # SMAs	# and type of sensors
K. Yang and C.L. Gu [116], 2002	3	1	1	1.00	None
ITU Hand [117], 2004	3	1[a]	1[a]	1.00[a]	1 pressure sensor
K.J. De Laurentis and C. Mavroidis [113], 2004	1	4	3	1.33	3[a] Hall effect sensors
Miniature five-fingered robot hand [123], 2006	5	20	40	0.50	14[a] strain gauges
SBC Hand [119], 2007	5	16	32	0.50	32 displacement sensors[b]
K. Andrianesis and A. Tses [120], 2008	5	7	7	1.00	N/A
V. Bundhoo et al. [114], 2009	1	4	4	1.00	1 force, 1 bend and 2 angular sensors
S. Matsubara et al. [121], 2012	5	10	10	1.00	N/A

[a] Estimations are done from pictures of the robot hand or of the actuation mechanism
[b] If setup mechanism is the same as previous work [118]

Regarding the sensors, Table 2.4 indicates that the most recurrent ones permit controlling the joints' angles or the tendons' displacement, such as for [113], [123], [119] and [114]. The obtained feedbacks are consequently closer to the ones of hands actuated by PAMs than actuated by motors, as these ones often include tactile sensors (see Table 2.1). As for PAMs that can be connected to pressure sensors ([106] and [94]), the force obtained in the fingertips of robot hands driven by SMAs is currently defined because of feedback due to the material's properties and deformation, such as in [123], [118] or [119], which can prevent the implementation of force sensors to interact with objects.

2.1.3.3.   Robot hands actuated by electroactive polymers

Electroactive polymers (EAPs) have the ability to change their shape or size in response to electrical stimuli [83]. Some EAPs reach a contraction rate of 32% [79], which is four times higher than the one of SMAs. As for PAMs, the reaction speed of EAPs is also measured to be about 30 000 times faster than the one of SMAs whereas the force they produce is about 450 times lower [126]. Despite of EAPs' advantages, their lack of actuation stress is the reason why the main use of EAPs for the imitation of human behaviours is the actuation of facial expressions [127] that require light weight and volume, such as in [128], [129] or [130].

Nevertheless, EAPs can also be used to actuate heavier architectures. In [131], for instance, EAPs are wrinkled to increase according to a particular geometry to increase their force and their contraction rate. According to the theoretical model which is developed, it would permit the EAP technology to control an octopus-like arm without exceeding a force of 0.35 N. Another robot arm introduced in [132] can defeat a human at a wrestling match. Although the number of EAPs is not indicated, it is probable many of them are required to actuate the robotic structure as a second arm wrestling robot, discussed in [133], is driven by more than 250 rolled dielectric elastomers, which are a specific type of EAPs. Even though a hand is included to both of these arms, none of them is designed to execute tasks different from arm wrestling. Their number of DOFs is therefore not mentioned and it is possible the fingers are motionless.

Robot hands actuated by EAPs are indeed very rare. Only three have been identified in this literature review. The numbers of DOFs being indicated for none of them, the estimations are done according to pictures and videos. The first hand has four fingers and is linked to a robotic arm described in [126]. Both the arm and the hand act as a gripper. Lifting tests are done with a weight of 10.3 grams. According to the gripper function of the robotic structure, the hand probably has a single DOF. It is also noticed that, contrary to the other robot hands introduced in Section 2.1, the fingers are not constituted of different phalanges but by a single one, made of a flexible material. The same structure is used for the five fingers' of the robot hand illustrated in [134], which has probably five DOFs. The third and last hand [135], however, has four fingers made of two phalanges each whereas the thumb seems to have a single moveable phalange. The number of DOFs is consequently estimated to nine. The EAPs have then been replaced by motors to carry on the development of the hand [135].

2.1.4. Robot hands driven by pneumatic cylinders

Pneumatic cylinders have features similar to PAMs'. They indeed have a high power for a small size [137] and are both compact and light [138]. They also have unstable output characteristics [138], which complicate the control of the robotic devices. According to [78], pneumatic cylinders have the same reaction speed than PAMs (measurable in µs) but only have an actuation stress of 0.9 MPa, whereas PAMs can have one of 16 MPa. However,

contrary to PAMs that were barely implemented on robot hands before the year 2000, air cylinders were implemented much earlier, such as on the Utah/M.I.T. Dextrous Hand that was designed in 1986 [139].

In average, the ratio between the number of DOFs and the number of PAMs for robot hands actuated by pneumatic cylinders is also close to the one of robot hands actuated by PAMs. As shown in Table 2.5, the Utah/M.I.T. Hand [139] uses 32 air cylinders to actuate about sixteen DOFs, the anatomical robot hand discussed in [140] uses 31 air cylinders to actuate about 20 DOFs, the anthropomorphic skin-covered hand described in [141] uses 22 air cylinders to actuate sixteen DOFs and the anthropomorphic robotic hand introduced in [142] uses 40 air cylinders to actuate 20 DOFs. The ExoHand developed by Festo [143] implements double-acting cylinders, permitting antagonistic movements to be driven by a single actuator and consequently allowing the DOFs to be controlled by a reduced number of air cylinders.

Table 2.5: Mechanical features of some robot hands actuated by air cylinders

Robotic Hands	# fingers	# DOFs	# air cylinders	Ratio # DOFs / # actuators	# and type of sensors
Utah/M.I.T. Hand [139], 1986	4	~16[a]	32	0.50[a]	32 tendon tension and ~8[a] angle sensors
D.D. Wilkinson et al. [140], 2003	5	~20[a]	31	0.64[a]	N/A
S. Takamuku et al. [141], 2008	5	16	22	0.73	26 polyvinylidene fluoride films, 21 strain gauges and N/A pressure sensors
ExoHand [143], 2012	5	~10[a]	8[b]	1.25[ab]	8 position, 16 pressure, N/A force and angle sensors
Z. Xu et al. [142], 2013	5	20	40	0.50	20 tactile, N/A valve and length sensors

[a] Estimations are made from pictures or videos of the robot hands
[b] Actuators are specified to be "double-acting"

Table 2.5 shows that hands actuated by pneumatic cylinders implement, in average, more sensors than hands actuated by PAMs. As for other robot hands models, sensors can be implemented to provide angular feedback such as for [139] or [143]. Sensors can also be connected to the tendon tension, the tendon length or to air the pressure to estimate the force provided by the actuators, such as in [139], [141], [143] or [142]. These four models also discuss the implementation of force feedback mechanisms at the level of the palm or at the

level of fingers. Tactile sensors are indeed implemented in [143] or [142], whereas the implementation of tactile sensors is also discussed for the future steps of the project [139] to increase the stiffness of joints when they are in contact with objects. The force of the hand [141] is controlled by 26 polyvinylidene fluoride films, which detect the velocities of strain. Joint sensors are also planned to be implemented on future versions of [142] to explore different manipulation tasks.

2.2.   Microcontroller boards

Microcontrollers are highly used in the development of embedded systems. Thus, research concerning microcontrollers was necessary to implement the electronic interface of the Ambidextrous Hand.

A microcontroller unit (MCU) is an integrated circuit constituted of one Central Processing Unit (CPU), memory and programmable inputs/outputs (I/O) [145]. It was previously noticed in Section 2.1 that one of robot hands' main features was their number of DOFs. These DOFs are controlled by the actuators, which are connected to the I/O of MCUs. MCUs therefore have also a very important part in the actuation of robot hands, one of their main features being their number of I/O.

As MCUs are not manufactured by the designers of robot hands, these MCUs are barely mentioned in research papers because they are designed by firms independent to robot hands' projects. A number of exceptions can however be found in the papers quoted in Section 2.1. Concerning the motorised robot hands, it is said in [146] that R. Van Ham et al. use Motorola 68HC916Y3 MCU for their research, as it includes ADC and incremental encoder readout, with enough processing power and internal memory. It is indicated that the forefinger developed by C. Chivu et al. is connected to a PIC16F628, the electronic layout of which includes two IR LEDs and two phototransistors [64]. Nevertheless, the paper does not indicate if the MCU have enough I/O to control the four other fingers in addition to the forefinger. According to the layout of electronic circuit designed around the PIC16F628, it is estimated that at least two of them would be necessary to actuate the 5 DOFs of the robot hand. Even though the DLR hand does not precise which MCU is used, some information about its electronic platform is mentioned in [67]. It is indeed mentioned that two Virtex FPGA provide connection to the masters system, the communication, the router and the

signal routing at a maximum operating frequency of 550 MHz, whereas the communication is set up with Xilinx Spartan 3e XC3S500EP132. A hybrid example is the Shadow Hand, which uses PIC18Fxx80 micro-controllers for the main part of their system and a PIC32 for the palm, both for their motorised and pneumatic versions [62]. It proves that the kind of actuators does not interfere with MCUs, except for the number of I/O (as a robot hand usually requires more PAMs than motors to actuate the same number of DOFs).

Concerning the pneumatic systems, indications are provided for some robotic hands and arms. The hand discussed in [106] is driven by a 100Hz PWM signal generated by an Atmega128 microcontroller. The arm introduced by P. Pomiers in [104] uses a control system implementation MPC555 MCU with a 40 MHz frequency for a Linux/RTAI interface, whereas the arm discussed by I. Boblan et al. in [103] is driven by two PIC 18F458 controllers, that have a clock speed of 10 MHz [147], communicating with Controller Area Network bus and executing control loops.

Through these examples, it has been seen that different kind of MCUs can be embedded to control robotic hands. Consequently, a number of MCUs is listed in Table 2.6, with an emphasis on the number of I/O, directly related to the number of potential DOFs of the Ambidextrous Hand. Digital I/O are meant to be connected as outputs of the MCU. As it will be explained in Section 3.2, it is possible to actuate PAMs without analog I/O. However, most of sensors use a digital feedback, necessary to implement control algorithms of robot hands. Analog I/O would then be connected as inputs of the MCU. It is consequently possible to use MCUs without any analog I/O but, as shown in [95] or [148], it would require the design of ADCs between the robotic interface and the MCU.

Table 2.6: Technical features of a number of MCUs

MCUs	Processor	# digital I/O	# analog I/O	Clock speed (MHz)
Arduino Uno [149]	ATmega328	14	6	16
Arduino Mega 2560 [150]	ATmega2560	54	16	16
Arduino Ethernet [151]	ATmega328	14	6	16
Axon [152]	ATmega640 64kb flash	55	16	16
Ether IO24 R [153]	Ubicom SXS280/PQ	24	0	8
Ether IO72 TCP [154]	N/A	72	0	8
Module ec555 [155]	MPC555 (Motorola)	22	10	40
Orangutan SVP-1284 [156]	ATmega1284P 32 kb flash	17	12	20
PIC18F458 Controller [147]	PIC18F458	32	0	10
PIC32-PINGOUINO [157]	PIC32	16	6	80
Pololu Micro Serial Servo Controller (assembled) [158]	PIC16M2BA	8	0	2
USBIO24 DIP R [159]	N/A	24	0	50

Table 2.6 shows that almost half of the MCUs which are listed do not include digital I/O: [147], [153], [154], [158] and [159], even though this last one, the Ether IO72 TCP, has the highest number of digital I/O. Therefore, the most suitable of these MCUs for the Ambidextrous Hand project would be one of the Arduino boards, especially the model Mega 2560 which has 54 digital I/O and sixteen analog I/O [150].

2.3.   Remote control interfaces of robotic applications

The design of a remote control interface (RCI) is necessary to make the Ambidextrous Robot Hand accessible for telerehabilitation process. Different ways to implement an RCI are consequently investigated. Some robotic applications previously mentioned in Section 2.1 are compatible with such applications. The OCU Hand II [72], for instance, can be controlled from the signals sent since a glove including six bending sensors. The Shadow hand can be connected to a 22 sensors CyberGlove for remote applications [62]. The arm designed by T. Kato et al. [148] includes a teleoperation feature through internet using UDP and a webcam.

In addition to the literature review investigated in Section 2.1, some robotic applications for which the main aim is precisely the implementation of an RCI include more

technical details in research papers. The Wi-Fi-based control of the robot arm designed by G.S. Gupta et al. [160], implements RF transceivers. A webcam is mounted on the robot arm and transmits the images to the control station using TCP/IP. Thus, the user can access to the server entering the IP address of the system. The rescue robot designed by S.S. Yeh et al. [161] includes a wireless sensor network using the ZigBee network which has a transmitting rate of 115200 kbps. An IR ranging sensor is also embedded on the robot so it can detect obstacles, as well as a camera to provide vision feedback. The remote-controlled car introduced by H. Rissanen et al. in [162] is driven through Bluetooth, with a client-server implemented with LabVIEW. The robot car includes a personal data assistant that directly deals with data feedback from sensors, without exchanging these signals with remote PCs or MCUs. In [163], Z. Zhang controls a robot vehicle by sending text messages from Skype. Two Xbee modules provide connection between the remote MCU and the remote PC. The remote PC needs a local Wi-Fi network and a Wi-Fi wireless webcam is mounted on the robot to provide vision. The robot vehicle can move within the maximum range of the Wi-Fi network. Another remote robot vehicle is designed in [164]. Its teleoperation system includes an on-board IR camera, for which the output is transmitted to a server by a RF transmitter. A multi-touch device allows the operator to send several commands. This multi-touch device is connected to the server via a wireless channel.

For the early stages of development of the Ambidextrous Robot Hand, starting with a RCI similar to the one introduced in [160] seems to be the most suitable option. Indeed, the system can be controlled using only TCP/IP, meaning the development of the RCI would not include any additional costs. Using Ethernet access instead of Wi-Fi, additional devices such as RF transceivers would not need to be embedded on the Ambidextrous Hand. In future stages of the project, the implementation of data gloves may be considered, as it would constitute an interacting interface easy to use for the operators.

2.4.   Pneumatic muscles in robotic area

In addition to actuate artificial hands, PAMs can be used for a number of other robotic applications. As the literature review did not reveal a high number of hands actuated by PAMs, gathering information about other devices using such a technology is useful for future steps of the project, as it increases the database of control algorithms applicable to PAMs.

Because of the strong ratio between their length and the force they provide [165], PAMs are often used to control robot arms. Contrary to pneumatically actuated robot hands, a number of pneumatically actuated robot arms were designed before 2005. Among them, there are for examples the model designed by P. Pomiers in 2003 for workers' safety [104], the one engineered by K. Kawashima et al. in 2004 for restoration work from disasters [166], or the one designed by S. Laksanacharoen in 2004 to be used as an arm prosthesis [167]. Similar robot arms carry on being developed later, such as the 9-DOFs model designed by X. Jiang in 2010 for rehabilitation purposes [28] or the AMO arm developed in 2011 that can be referred as being a bionic arm [26]. It is noticed that most of these robot arms are driven by PID controllers, but a more detailed analyse of control algorithms will be discussed in Section 2.5.

Still because of the high force PAMs provide, another one of their use is the actuation of legged robots. An example is the robot developed by Vrije Universiteit Brussel. In a paper published in 2000, it is specified the single legged robot can carry a load up to 10 kg on a one-dimensional set-up [168]. This robotic structure became a bipedal walking robot called Lucy some years later, as indicated by a paper published in 2004 [169]. As for the robot arms, the control algorithms used to actuate Lucy are going to be discussed in Section 2.5. Other examples of robot legs can be seen for the quadruped robot dog designed by Biorobotics Laboratory for which the two legs can lift 13.5 kg in 2006 [170] or, more recently, the quadruped robot PIGORASS designed by ISI Lab introduced at the International Conference on Intelligent Robots and Systems (IROS) in 2011 [171].

In addition to robotic limbs, PAMS can also be used as power assist wears. Such devices consist in detecting users' movements before being duplicated by the pneumatic device, providing more force to the user. Some examples of such applications can be found before 2006, with for instance the arm designed by H. Hu et al. in 2005 [52]. Indeed, the project consists in a wearable exoskeleton for upper limb that can be used for rehabilitation. Nevertheless, similar examples become much more common after 2007 and can even be adapted to the shape of a hand. Thus, the model developed by K. Xing et al. [172] in 2009 used two PAMs to control two DOFs and ease the extension of two fingers. Another example is a power assist glove developed by T. Noritsugu et al. in [173] and [174] between 2008 and 2009 to assist elderly and disabled people. The Exo-hand designed in 2012 [143] can also be worn as a glove to help with the rehabilitation of stroke patients, in addition to being a robotic structure.

2.5.   Control algorithms related to pneumatic muscles

This Section gathers and analyses a number of papers concerning control algorithms implemented on pneumatic structures. These algorithms are divided into four main categories, which are feedback, feedforward, nonlinear and AI-based controls. Based on these four categories, different systems can be combined to create hybrid algorithms.

The evolution of these algorithms through the years is also investigated.

2.5.1.   Feedback and feedforward based algorithms

Feedback loops are control algorithms taking the output of systems into account to adjust the process variable until it reaches the target put as input. The two feedback controls analysed in this section are PID and bang-bang controls.

Feedforward control requires the implementation of a second control loop, connected to an environment external to the system, such as a data collection or nonlinear algorithms. This outer loop regulates the setpoint of the inner loop, this one being usually based on feedback control. The feedforward loops analysed in this section are cascade controls.

2.5.1.1.   *PID control*

PID control is a feedback algorithm that combines proportional, integrative and derivative controls to bring a system to its setpoint.

PID control is widely used in robotics, either for motorised structures, such as for the ACT hand [175] or the Shadow hand [74], as well as for structures driven by PAMs.

The mechanical joint introduced in [176] and the rehabilitation robotic arm described in [28], for instance, use PID controllers to regulate both the position of the system and the pressure of its muscles. Similar control loops can be applied to robot hands, as it can be seen for [96] and [85], where the system is connected to pressure, angle and force sensors. Both of these papers describe the same type of master-slave system which can be driven either with a single PID controller or with two PID loops used as a cascade control. The same kind of cascade control is used to drive the modular robot arm introduced in [104]. Other hands

driven by PAMs use PID loops as control algorithms, as the Shadow Hand [94], for which the control interface is the same for the motorised version [74]. PID loops are also implemented in the hand engineered by Y. Honda et al. [90], taking the ratios of the antagonistic PAMs into account in [177] and [178].

A number of robot arms driven by PAMs combine PID loops with AI-based algorithms, such as neural networks (NNs), as the ones used in [179] or [180]. The PAM joint introduced in [181] uses a similar control system, as its PID controller is self-tuned by a particle swarm optimisation (PSO) algorithm. In addition to NNs and PSOs, PID loops can also be combined to fuzzy logic, as for the robot arm described in [182] or the wearable rehabilitation hand discussed in [183]. Another approach is performed in [184], where the positioning of PAMs is driven by PID loops combined to nonlinear coefficients.

PID control is also implemented to actuate the bipedal walking robot called "Lucy", previously introduced in Section 2.4. The control strategy of the walking robot is discussed in [146], [185], [186] and [187]. In addition to PID control, these four papers are also the only ones describing the implementation of a bang-bang control on robotic systems driven by PAMs, which is why their analysis is done in section 2.5.1.2.

2.5.1.2.   *Bang-bang control*

Bang-bang control is a feedback control consisting in switching brusquely between two states, which is why it is also referred as on-off controller.

Bang-bang control is not commonly used in robotics because, as explained in [188] or as mentioned in [189], its shooting function is not smooth enough and requires to be regularised. This is the reason why bang-bang control is often combined with other control methods, such as fuzzy logic which adds more flexibility in the rotation of a single-axis pneumatic actuator in [190]. On another hand, PI or PID loops can be implemented to calculate the switching time of the bang-bang inputs. This kind of cascade control is used to activate a DC motor in [191].

Concerning pneumatic technologies, bang-bang control is used to actuate the bipedal walking robot called "Lucy", as discussed in [146], [185] and [186]. These three articles use a cascade control similar to the one introduced in [191], PI or PID loops calculating the switching time of the bang-bang inputs. However, another control architecture introduced in

[187] shows that the valves of the bipedal walking robot can be efficiently activated without connecting the bang-bang controller to any PI loops. Nevertheless, PID feedback loops are used to calculate the joint trajectory torques, whereas bang-bang control is triggered by a delta-p control which estimates the required pressure of each joint.

2.5.1.3.   Cascade control

Cascade control is a feedforward control made of two distinct control loops, the setpoint of one being controlled by the second one. The inner controller deals with feedback received from the system whereas the outer controller anticipates the evolution of the system through the evolution of the inner controller.

As explained in [105], cascade control can be used to deal with uncertainties and ensure high precision positioning. The rotation of the joint introduced in this paper is driven by the two PAMs controlled by an outer position predictive controller is connected to an inner torque controller. In [104], P. Pomiers implements the inner loop of the system connecting it to pressure control whereas the outer loop calculates angular position based on pressure control. Both of these loops are based on PID control. A robot with two DOFs and driven by four PAMs discussed in [192] reaches its setpoints because of a torque controller linked to the centre point of the system. In [193], an inner loop is implemented as a force controller whereas the outer loop deals with a position control implemented as a linear tracking controller, which means the system is similar to the one introduced in [104] by P. Pomiers in 2003. A slightly different approach is engineered in [194], where a PAM is controlled by implementing a PID controller in its inner loop to deal with the pressure nonlinearity, whereas the outer loop implements a hysteresis compensation to compensate the dynamic nonlinearity of the PAM itself.

The nonlinear cascade control described in [195] by H. Aschemann and E.P. Hofer in 2006 combines an inner flatness-based pressure control loop with an outer, also flatness-based, control loop. This outer loop decouples carriage position and provides reference pressures to the inner loop. The same parallel robot discussed in [196] uses the same kind of inner loop, whereas the outer loop is a sliding-mode control dealing with decoupling control of an end-effector position. In [197], the inner loop of the parallel robot still focuses on pressure whereas adaptive backstepping control loops deals with the carriage position.

Finally, the literature review revealed two cascade controls implemented on robotic hands driven by PAMs. The first one is introduced in [96], where PID control is compared with cascade control for force control. The cascade control is made of two PID controllers, the first one receiving pressure feedback and the second one being connected to an electro pneumatic regulator. The angular control, however, is driven by a single PID controller. The second of these cascade controls is discussed in [198], where the inner loop also receives feedback from pressure sensors. As the joint torque is directly affected by pressure, the outer loop calculates the position from the inner loop.

2.5.2. Nonlinear control algorithms

Nonlinear control algorithms are designed to stabilise nonlinear systems around a specific state or a specific target. The dynamics of the nonlinear systems are taken into account to reach a behaviour defined as target.

The two nonlinear control algorithms analysed in this section are sliding-mode control and backstepping control.

2.5.2.1. *Sliding-mode control*

Sliding-mode control (SMC) makes system slide along a line made of predefined values to reach a specific behaviour.

In [199], SMC is compared to backstepping control to stabilise the behaviour of a PAM tracking the errors caused by its nonlinearity. It is shown that both algorithms reach similar achievements. M. Van Damme et al. combines PID control with SMC to stabilise a planar manipulator of two DOFs in [200], where the PID deals with the local dynamics (such as small positional errors) whereas the SMC deals with global dynamics (which are classified as large positional errors). Both systems are controlled by PAMs, but SMC has been chosen instead of bang-bang to control the planar manipulator.

A number of papers about SMC related to PAM technology has also be written by H. Aschemann and D. Schindele. For instance, a linear axis driven by a pair of PAMs has its carriage driven by flatness and SMC in [201]. Flatness-based control is used as an inner loop

on pressure feedback whereas SMC is used as an outer control loop to decouple angles according to internal pressure of both PAMs. Flatness-based control, SMC and backstepping control are separately implemented on the same parallel robot in [202]. The results obtained for each of them are then investigated and compared to each other. It is revealed that the most accurate achievements are reached with SMC, which is the reason why SMC is the main algorithm considered in their next paper, [196], published in 2010. The internal pressure of PAMs is controlled by a fast underlying control loop whereas the outer loop of the cascade control consists in a SMC.

As for the research introduced by H. Aschemann et al., SMC is mainly used to control single robot joints, such as arms. For instance, the sliding variables of the robot arm discussed in [203] are defined to allow a SMC dealing with discontinuous terms. A second robot arm introduced in [102] is controlled based on an SMC for which the uncertainties are dealt by a neural network before the final outputs are regulated by PID controllers. A third robot arm engineered in [204] uses a similar system, but also implementing fuzzy logic in addition to neural networks and without implementing PID loops. A high-order SMC is defined in [205] to drive a joint model. A similar approach is investigated in [206], as a delta operator system is defined to fix conditions to the SMC of a robotic joint model.

2.5.2.2.   *Backstepping control*

Backstepping control (BSC) consists in stabilising nonlinear systems with a recursive structure based on derivative control.

As mentioned in Section 2.5.2.1, BSC was compared to SMC in [199] written by P. Carbonell et al. Even though the results are similar, it is shown show that the BSC is slightly more appropriate to control the PAM actuator, as the SMC is limited by a chattered signal. This is the reason why BSC is the chosen algorithm to be coupled with fuzzy logic in another paper written by P. Carbonell et al. [207], which discusses about a further step of the project. The performances of BSC are again compared with the ones of the SMC to actuate the parallel robot discussed in [202] by H. Aschemann et al. This time, it is revealed that more accurate achievements are reached with SMC. However, the last paper published about this parallel robot project comes back to BSC and shows that the experimented models compensate the hysteresis of PAMs in a very accurate way as feedforward controls in [197].

2.5.3. Artificial intelligence-based algorithms

AI-based algorithms aim at imitating intelligence by making the system reason by themselves, according to the data feedback.

Four main AI-based algorithms are distinguished in the area of control of pneumatic systems. These ones are neural networks, particle swarm optimisation, genetic algorithms and fuzzy logic.

2.5.3.1.   Neural networks

Neural networks (NNs) are used to implement pattern recognition and can make a system react differently according to the way it evolves.

The ratio between the pressure and the force of PAMs is depicted in [208] before being connected to a NN that defines input vectors according to the evolution of the PAM. A similar system is designed in [209], the PAM not being connected to any robotic architecture. A third similar system is engineered in [210], as the hysteresis nonlinearity is taken into account by NN, except that the controlled structure is a parallel manipulator driven by two PAMs instead of a single PAM.

Combining NNs with fuzzy logic, a learning process is designed for the two-links PAM manipulator discussed in [179] by K.K. Ahn et al., allowing the manipulator to have an adaptive and dynamic self-organising structure in 2006. K.K. Ahn and H.P.H. Anh connect a NN to PID loops in 2007, creating an intelligent phasing plane switch control (PPSC) to overcome the nonlinearities of PAMs' pressure feedback [211] (more details concerning the results obtained with the PPSC are provided in [212]). Additional NNs are combined with particle swarm optimisation to increase the accuracy of the system in [213].

2.5.3.2.   Particle swarm optimisation

Particle swarm optimisation (PSO) maintains a swarm of particles moving around a search space, the particles being influenced by the improvements discovered by the other particles [214]. PSO therefore aims at optimising a system by selecting an appropriate behaviour among a number of candidate solutions.

Two models of PSO were found for PAM technology, both of them published in 2010. The parameters of the PAMs nonlinearity which control the robot arm discussed in [213] are identified and overcome because of a PSO. In [181], the second robot arm is controlled by PID loops combined with PSO. The aim of the PSO is to make the PID controller self-tunes itself. Both angles and pressure are considered in these two papers.

2.5.3.3.   *Genetic algorithms*

Genetic algorithms (GAs) imitate the process of natural selection by investigating the behaviour of populations in a search space of candidate solutions [215]. Populations are successively replaced by others, the behaviour of each being analysed by GAs to generate solutions to solve the problems.

The only papers found concerning the development of GAs over PAM technology are written by K.K. Ahn and H.P.H. Anh. In [216], published in 2006, the errors of the joint angle of the robot manipulator of University of Ulsan are tracked by a GA which analyses the current parameters of the system according to a predefined model. Two papers are published in 2007. In [217], a system similar to the one introduced in [216] is described, as GAs allow the joint angle position to tune itself using a minimum variance control. In [218], the system discussed in [217] is optimised modifying the equations of the predefined model on which are based the GAs. In 2008, GAs are combined with fuzzy logic to deal with the nonlinearities of the system in [219]. This system is further improved in 2011, as GAs interact both with a fuzzy model and a PID controller in [182].

2.5.3.4.   *Fuzzy logic*

Fuzzy logic is an approach that deals with reasoning and approximations instead of fixed states and values.

Fuzzy logic was already mentioned in most of the subsections of Section 2.5. Indeed, as fuzzy logic approximates data, it is most often combined with another type of algorithms to reach a specific behaviour, which is why most of the papers discussed in this section were already mentioned in previous ones. In [207], the PAMs' dynamic nonlinearity is compensated combining fuzzy sets with BSCs. The authors from Univeristy of Ulsan combine fuzzy logic with NNs in [179], published in 2006, so the torque of the system can

adapt itself to angular positions in real time. In 2008, the same research team and Y.J. Il publish [219]. As said in section 2.5.3.3, the engineered system deals with the PAMs' nonlinearity combining a fuzzy model with GAs whereas the system is improved in [182] in 2011, adding a PID controller to the fuzzy model on which the GAs interact on. In 2012, a paper written by A. Rezoug et al. [204] introduces a robot arm controlled by a SMC driven both by fuzzy logic and NNs.

Some other papers deal with the implementation of fuzzy logic without any other control algorithm. It is for example the case of the PAM introduced in [220] in 2006, for which the fuzzy logic is designed to be self-organised. Also, the fuzzy logic implemented on the four fingered robot hand discussed in [98] permits the mechanical structure to grasp soft objects (even though the structure is not actuated by PAMs, but by pneumatic balloons). The algorithm is compared with PI loops and it is shown that fuzzy logic is more effective, as higher overshoots are obtained with PI loops. This behaviour obtained with PI loops is normal because, as explained in section 3.4.1, one of the main aims of the derivative term, missing here, is precisely to reduce the overshoot. A second robot hand driven by fuzzy logic is discussed in [183], where the fuzzy mode is combined to PID control to actuate a wearable rehabilitation device, providing assistive forces for grasping and finger extension.

Contrary to other AI-based algorithms, it is noticed that two papers discussing the implementation of fuzzy logic actually refer to robot hands ([98] and [183]) instead of any other pneumatic devices.

2.5.4. Evolution of control algorithms through the years

In order to analyse the frequency of control algorithms considered in Section 2.5, the control methods will be investigated in chronological order.

As previously indicated in Section 2.1.3, robotic systems actuated by PAMs barely existed in the past century, which is why the first papers related to the control of such structures were published in 2001, [199] and [207]. It is however noticed that most of the papers are related to the control of robot arms, such as [219], [104], [217] and [102] or robot manipulators such as [221] and [222]. Concerning the control of robot hands driven by PAMs, the first papers that describe appropriate robust control strategies are published after

2006, such as [96] in 2007. It actually matches with the literature review of Section 2.1.3 as, except the work of Y. K. Lee and I. Shimoyama in 1999 [92], the first publications concerning robot hands actuated by PAMs released in 2006, with the work of P. Scarfe and E. Lindsay [95] or the one of P.Y. Chua et al. [106].

To investigate further among control strategies, the algorithms are gathered into the major groups described in Section 2.5.1, Section 2.5.2 and Section 2.5.3, as well as hybrid systems, which combine a number of the control systems previously mentioned. These control algorithms are summarised in Figure 2.2, which takes the classifications into account. Even though flatness-based control has never been implemented on its own in the previous literature review, it is included in the diagrams for its recursive uses in [195], [201] and [202].
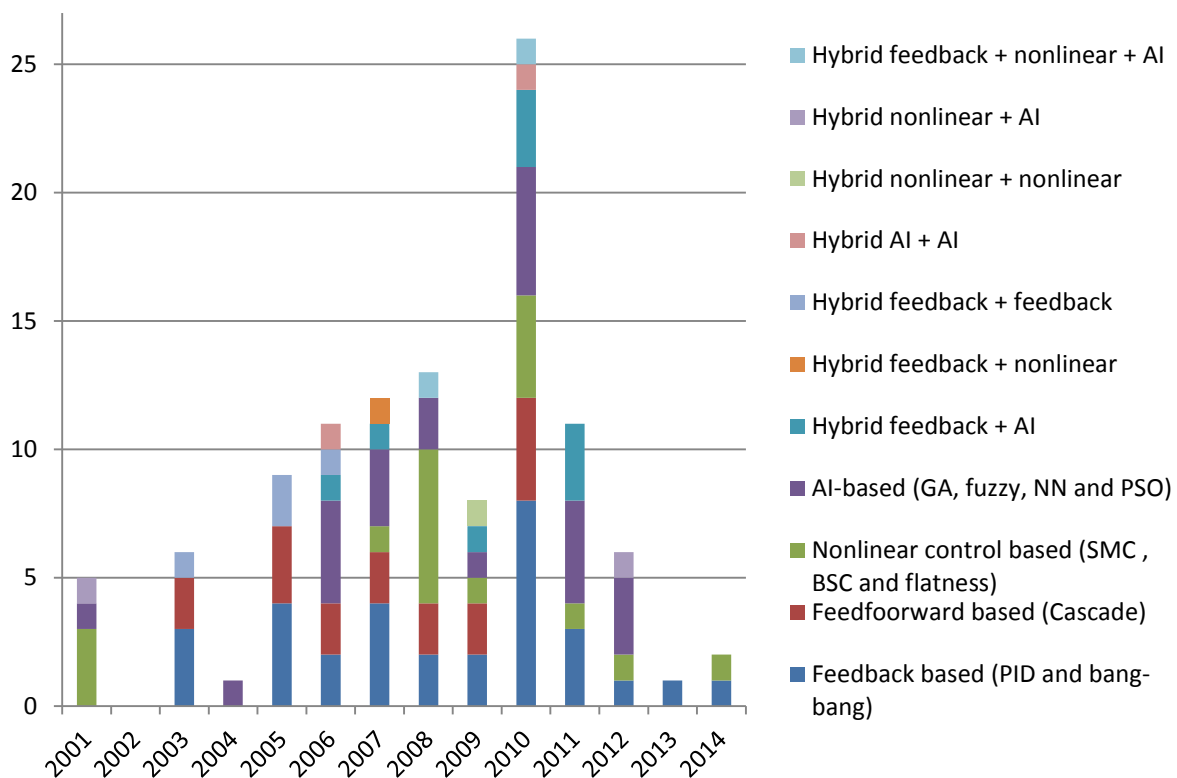
Figure 2.2: Evolution of control algorithms discussed in Section 2.5

Figure 2.2 shows that nonlinear control algorithms were almost non-existent in the early years, with only [199] and [207] written in 2001. Between 2003 and 2007, the main algorithms used to control structure driven by PAMs are mainly feedback and feedforward based controls, with a high use of PID control, as it can be seen in [146], [104], [185], [186],

[187], [211] or [96] and cascade control that is used in [96], [192] and [195]. However, it is noticed that cascade control is very often a combination of two different PID controllers, the output of the second PID controller being connected to the set point of the first one. As observed in Section 2.5.1.1, PID control is not that common when it is not cascaded or combined with AI-based systems. Bang-bang control also becomes more common, as four papers related to this control architecture were published during these same years [146], [185], [186], [187].

Between 2004 and 2008, AI-based systems are more often implemented in the control of pneumatic structures. GAs are introduced in the five papers [218], [219], [216], [217] and [182]. In addition to GAs, fuzzy logic is introduced twice in the same years, in the papers [220] and [179]. As many papers are published about NNs, with the articles [208] and [179]. It is noted that [179] is quoted both for fuzzy logic and NN here, as the two control methods are coupled to create a hybrid system, which later became the GA engineered in [217] by the University of Ulsan.

From 2008, the implementation of nonlinear control algorithms becomes more important as well. Indeed, SMC is discussed in the eight following papers: [201], [202], [205], [102], [196], [204], [203] and [206], even though three of them are written by H. Aschemann and D. Schindele, from University of Rostock. Besides, these two researchers also published works about BSC between 2008 and 2014. The first one, [202], compares the tracking errors of the driven parallel robot obtained with SMC, BSC and flatness-based control. The second one, [197], uses BSC as a control loop included in a cascade control to investigate three different models concerning the hysteresis of PAMs.

In addition to SMC and BSC, PID and cascade controls are still widely used after 2008, as it is proved by the papers [176], [177], [183], [180], [181], [182], [178] and [184] concerning the PID control. Concerning cascade control, the system is discussed in a number of articles published after 2009: [198], [105], [193], [196] and [197].

AI-based algorithms are still investigated past 2009. For instance, two research studies including PSO, which are [181] and [213], were both published in 2010. PSO is combined to the learning process of NNs in [213], written by H.P.H. Anh and N.H. Phuc, previously mentioned for having developed AI-based algorithms related to PAMs' technology between 2004 and 2008. Then, H.P.H. Anh investigates on a process based on GAs [182] in 2011. NNs are also used to deal with PAMs' nonlinearity in [209], published in

2012. Fuzzy logic systems are still recurrent after 2008 as well, as they are investigated in [183] in 2009, in [182] and [98] both published in 2011, as well as in the article [204] published in 2012.

The first hybrid algorithm of this literature review is [207], that combines an AI process with a nonlinear control method, which are respectively fuzzy logic and BSC. Without taking cascade control into account, it is seen that combining different types of algorithms is not very common before 2007, as next occurrence appears in 2006, when K.K. Ahn and H.P.H. Anh [179] combine two AI processes, which are fuzzy logic and NN. In the same year, the two authors also investigate GAs [216]. Even though this paper does not introduce a hybrid controller, it is seen that a GA can be based on nonlinear control methods to drive pneumatic structures. Then, K.K. Ahn combines a feedback PID control with NN in [211] in 2007.

Some other hybrid methods are obtained by combining two AI-based algorithms. Indeed, fuzzy models are combined with GAs in [219] and [182], respectively published in 2008 and 2011. It is noted that AI-based algorithms are also combined with feedback control after 2008, as in [183], published in 2009, where PID control is combined with fuzzy logic. Nevertheless, it is noticed that nonlinear control are not often combined with others. Some exceptions still exist, such as [204] in which SMC is combined with fuzzy logic.

This literature review has revealed that, in average, the most frequently used algorithms to control pneumatic structures are feedback and feedforward algorithms, mainly with PID and cascade control. SMC, NN and fuzzy logic are respectively the third, fourth and fifth algorithms with the most occurrences in the area. However, the most important point concerns the few numbers of algorithms implemented on robot hands, mainly for nonlinear controls. Even though SMC and BSC have been implemented on a number of pneumatic systems, this literature review reveals that none of these systems were robot hands. As illustrated in Figure 2.3, these nonlinear controls can consequently be explored to add more originality to the Ambidextrous Robot Hand project. In addition to SMC and BSC, PID, PPS, bang-bang and cascade controls will be investigated as well. Although PID and cascade controls have already been implemented on robot hands driven by PAMs, the implementations of PPS and bang-bang controls will also be unique.
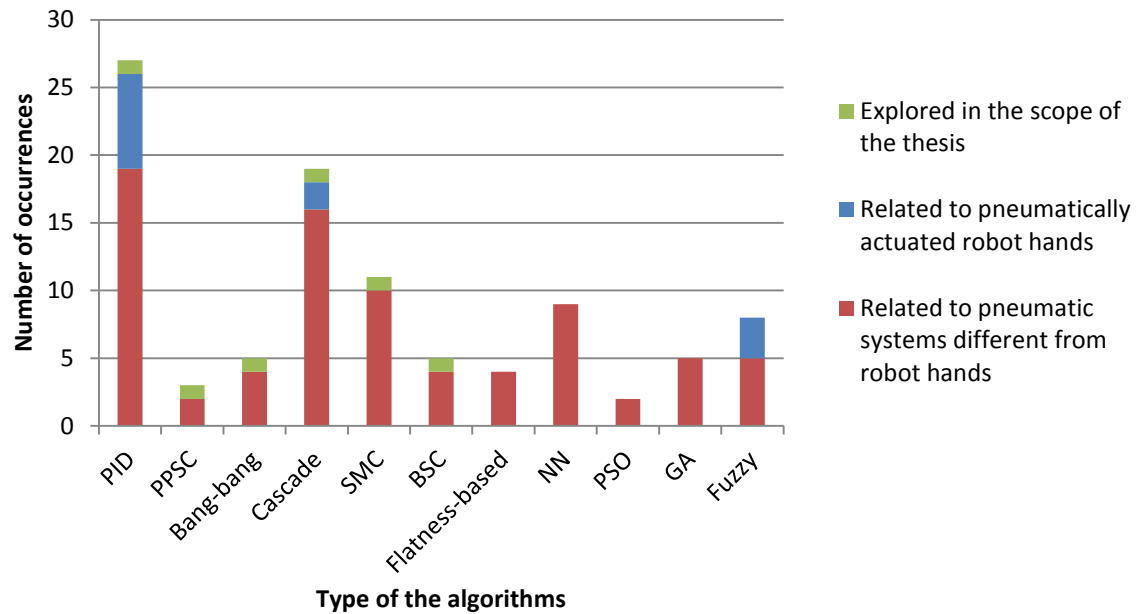
Figure 2.3: Control algorithms explored in the scope of the thesis against control algorithms related to the pneumatic systems discussed in Section 2.5

2.6. Chapter summary

This Chapter has given an overview about the main mechanical features of robot hands, the technologies used to actuate them and the types of sensors commonly used. It was revealed that robot hands are much more often actuated by motors than by PAMs, even though the implementation of PAMs has increased over the last five years. The advantages of PAMs are an excellent ratio between strength and weight and a short reaction speed. However, it was also observed that robotic structures driven by PAMs often have about twice more actuators than DOFs, contrary to other actuators, such as motors or SMAs, which can control one DOF each. Most importantly, no robot hands with an ambidextrous design occurred in the literature review, which proves the originality of the project.

Prior to be implemented on any robotic systems, PAMs must be connected to MCUs, which is why MCUs and their different features were also investigated. As controlling a high number of DOFs requires a high number of digital and analog I/O, the MCUs were chosen on these main features. The Arduino Mega 2560 [150], seems to be a suitable option, as it has 54 digital I/O and sixteen analog I/O. RCIs were also explored, to allow a remote access to the Ambidextrous Hand. An RCI based on TCP/IP appears to be the most appropriate option, as

it would not include any costs in material and would make the Ambidextrous Hand accessible from a website. Thus, the access to the robotic structure would be fast and convenient.

Given that robot hands driven by PAMs are not very numerous, this chapter also provided an overview about PAMs' other robotic applications, and so their control algorithms can be explored. The investigations showed that control algorithms related to robotic structures driven by PAMs can be classified into four main categories which are feedback and feedforward, nonlinear, AI-based and hybrid algorithms (hybrid algorithms combining algorithms from the three first categories). Even though nonlinear algorithms have been widely implemented on robotic structures driven by PAMs, the literature review revealed that none of these structures are robot hands. The originality of the project can consequently increase by implementing an SMC or a BSC on the Ambidextrous Robot Hand.

Chapter 3: Feasibility study of a remote ambidextrous device

This chapter discusses the feasibility study of the Ambidextrous Robot Hand project. The aim of this study is to identify the restrictions and boundaries when attempting to design and to implement the ambidextrous behaviour of a finger.

Prior to achieving this aim, the pneumatically actuated robot architecture will be introduced. Therefore, the devices necessary to implement a robotic structure driven by PAMs are discussed in detail. The discussion includes both the electronic and the pneumatic interfaces It includes both the electronic and pneumatic interfaces and explains how the interfaces and explains how the interfaces are connected to each other.

Further, a number of finger prototypes designed to test the ambidextrous behaviour are introduced. The limitations of each prototype are discussed, and the origins of the problems are identified before designing the next models. Mechanical features are compared to each other and the classification reveals that some models can be used for more advanced testing using control theory with sensors' feedback.

As the literature review of Section 2.5.4 revealed that PID controllers are the most commonly implemented algorithms to drive pneumatic structures (and particularly robot fingers), PID loops are connected to sensors embedded on the prototypes to control both the angular position and the force applied by the fingertip.

Finally, the control functions are connected to an RCI, which make them accessible from the website of the project.

3.1.   Introduction to pneumatic devices

The feasibility study is done using a number of pneumatic devices, for which the functioning must be understood prior to working on the first steps of the project. Therefore, this chapter introduces the devices used to design a robotic structure driven by PAMs and the way they are connected to each other. These devices are an air compressor, pneumatic tubing and fittings, manual valves and PAMs.

3.1.1. Air compressor

The air compressor is a device that uses power from electric motors to pressurise air. The air compressor is necessary to supply pneumatic systems, as it provides compressed air to the actuators. The model at disposal is a EURO-TEC 20A [223] and can supply a maximum pressure of 6 bars. The EURO-TEC 20A has a tank content of 1.5 L and a maximum air flow of 20 L/min. The number of PAMs it can supply in compressed air depends on PAMs' mechanical features. In case PAMs' lengths and diameters do not exceed respectively 200 mm and 20 mm, for a maximum pressure that do not exceed 3.5 bars, the EURO-TEC 20A can then actuate a robotic structure driven by about 40 PAMs, such as the Shadow Hand [94]. However, the tank and the air flow of the EURO-TEC 20A would not fit as well with the actuation of a robot arm. Arms are indeed actuated by PAMs that can have a volume about fifteen times higher than the PAMs that drive robot hands hands [97]. The capacities of the actuator would then need to be higher to avoid any delays between movements. The EURO-TEC 20A is shown in Figure 3.1. Its weight of 14 kg does not allow it to be embedded on a light robotic limb; this is one of the reasons why the design of a RCI will be investigated.

Figure 3.1: Air compressor EURO-TEC 20A

Figure 3.1 also shows that the air compressor's output is connected to pneumatic tubing, used to drive the pressurised air from one point to another and to a manual valve. A zoom on this manual valve is shown in Figure 3.2.

Figure 3.2: Manual valve

As indicated by its name, the manual valve can be opened or closed manually, to let the air cross it or, on the contrary, to block it. It is noted that the mechanism allows an air evacuation from its output side when the valve is closed, whereas the air pressure is always maintained from its input side. In addition to block the air, this mechanism consequently allows interacting with the output and can be used in case of emergency or as safety equipment.

3.1.2. Pneumatic artificial muscles

PAMs are pneumatic structures that contract and extend according to the pressure of air they receive. Their functioning is illustrated in Figure 3.3, where a PAM is connected to the air compressor and the manual valve is alternatively turned ON and OFF. The air compressor's output is adjusted to have an output of 2 bars. The recommended maximum pressure to actuate a PAM manufactured by Shadow Robot is 3.5 bars [80]. The higher the pressure, the stronger the contraction and the provided force.

(a)   (b)

Figure 3.3: PAM's behaviour
The manual valve is OFF in (a) and is ON in (b)

The experiment illustrated in Figure 3.3 is done connecting the PAM directly to the air compressor's output. As the PAMs' length reduces when it is supplied with pressurised air, the device is theoretically able to interact with an object if both of them are tied with a string. This functioning is schematised in Figure 3.4, where the arrival of compressed air causes a reduction of the muscle's length, which pulls on a tendon tied to an object. Replacing this random object by some key points of mechanical architectures, PAMs can be used the same way as human muscles.
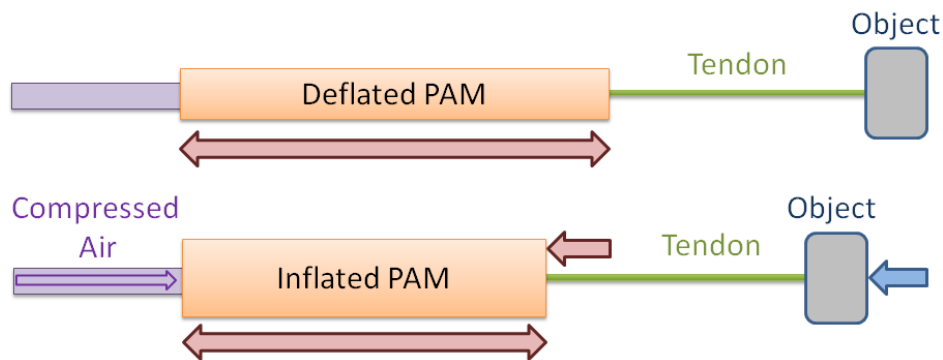
Figure 3.4: Functioning of PAMs

PAMs are currently manufactured by two businesses, which are Shadow Robot Company and Festo Corporation [224]. The pulling force of each of them depends on the length and the diameter of PAMs. However, some characteristics such as the maximum operating pressures and contraction rates do not depend of the size of the PAMs. These characteristics are summarised in Table 3.1. The ranges are indicated in %, according to the

PAMs' nominal lengths. Active range refers to the maximum permissible contraction at the maximum operating pressure and passive range refers to the maximum permissible extension for a pressure of 0 bars.

Table 3.1: Maximum operating pressures and ranges of PAMs

PAMs' Manufacturer	Maximum operating pressure (bars)	Active range	Passive range	Total range
Shadow Robot Company [80]	3.5	N/A	N/A	37%
Festo Corporation [81]	6 or 8[a]	25%	3% to 5%[a]	28% to 30%[a]

[a] Depending on the models

In addition to the features summarised in Table 3.1, it is indicated that PAMs manufactured by Festo can lift up to 1500 N for a diameter of 20 mm [81], whereas none of the measures and values of [80] indicate that the PAMs manufactured by Shadow Robot can lift more than 700 N for a diameter of 30 mm. It can therefore be estimated that, despite their shorter range, PAMs designed by Festo have a much higher lifting force than PAMs designed by Shadow Robot. From this point of the thesis, PAMs manufactured by Shadow Robot will be referred as SPAMs whereas PAMs manufactured by Festo Corporation will be referred as FPAMs.

Among the four SPAMs delivered with metallic connectors, two of them have a length of about 125 mm whereas the two other ones are about 150 mm, without taking the connectors into account. The difference of their length when they are totally stretched or totally contracted at 3.5 bars is about 30 mm for the short PAMs and 40 mm for the longer ones. However, as they must be used in an antagonistic way, the contraction of a first PAM causes the stretching of a second one, which is why the PAMs cannot be completely stretched when at their initial position. Therefore, to anticipate the stretching of the antagonistic PAM, only half of the range is taken into account to actuate an ambidextrous finger.

3.1.3. Pneumatic push in fittings

In order to control several muscles with the same air compressor, the air flow must be divided in several outputs, so the same air supply can be transferred to several PAMs. For this are used Y or tee tube-to-tube adapters, which are pneumatic push in fittings. As shown in

Figure 3.5, such names are attributed because of their shapes. Each of them has three I/O, in which it is possible to insert pneumatic tubing that allows the compressed air to take several paths.

(a)   (b)

Figure 3.5: Pneumatic fittings.
(a) is a Y adapter and (b) a tee adapter

Tubes can be removed from the fittings by pushing the buttons in same time as pulling on the tube.

3.2.   Electronic devices and controller

The air flowing from one pneumatic material to another is regulated using electronic devices.

As the airflow from the compressor is divided into several paths, a system is required to provide or to block the airflow at the level of the different outputs. This system is based on valves that are electronically actuated, the voltage of which being provided by a MCU. This Section explains the functioning of these electronic devices and how they are connected to the pneumatic interface.

3.2.1. Solenoid valves

Solenoid valves are devices that can be electronically actuated. As shown in Figure 3.6, the Isonic model designed by Mead Fluid Dynamics [225] can be supplied with 24 V DC and can endure until 8.3 bars. Pneumatic tubing with a 4mm OD can be inserted in their two

I/O called "IN" and "OUT". When the solenoid device receives 24 V DC, an internal mechanism opens the valve, which means the pressurised air inserted in "IN" is transferred to "OUT". The valve closes itself when it is not provided by appropriate voltage anymore.

Figure 3.6: Solenoid valve manufactured by Mead Fluid Dynamics

Consequently, it means these valves are used as I/O for each PAM. As shown in Figure 3.7, a first valve must be used as an input, to let the air goes in and contract the PAM, whereas a second valve is used as output, to let the air goes out and extend the PAM. It also means that the pneumatic system is going to include twice more solenoid valves than PAMs.
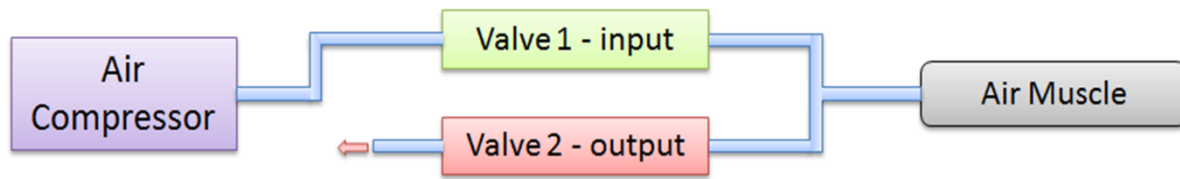
(a)
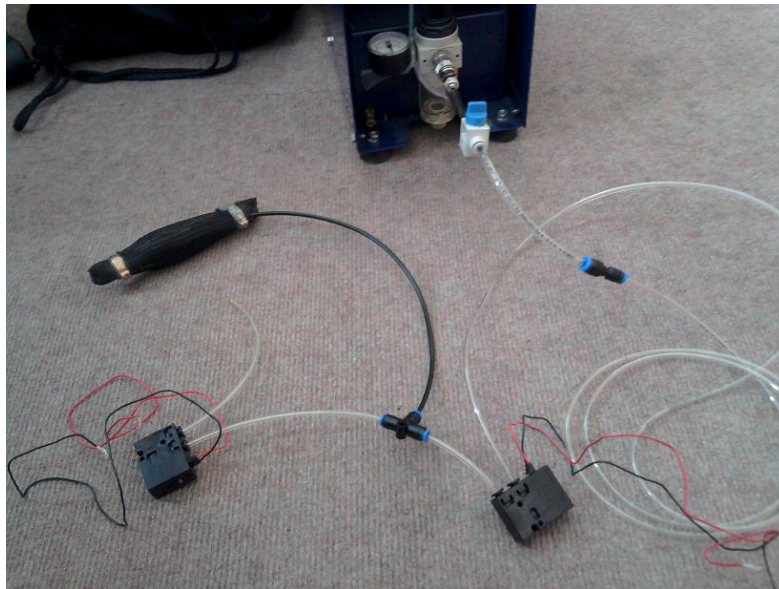
(b)

Figure 3.7: Connection between two valves and one air muscle.
(a) a scheme an (b) actual devices.

The automation of the voltage's switching is done connecting the wires to an MCU, which computes and regulates the voltages sent to each of its outputs.

3.2.2. The Shadow Pneumatic Control Unit

The Shadow Pneumatic Control Unit (SPCU) [226] is a controller board designed by Shadow Robot Company Ltd. The SPCU includes all electronic systems necessary to experiment a small pneumatic system. Its block diagram is showed in Figure 3.8. As it can be observed, the SPCU is designed around a CPU (which is a PIC18F2580 –I/SP [227]). The power input is fed by a 24V DC, which is the voltage used to turn on the valves. These valves are connected to a driver that switches ON or OFF the delivered voltage according to the commands received from the CPU. The CPU is powered from the same power input, which

also provides 5V DC on the sensor inputs. The values received from sensors are read by the ADC before being processed by the CPU.

The SPCU also includes a reset button, a LED and a serial port to be connected to a host computer. The code contained in the CPU can be modified and uploaded using Piklab [228] and Small Device C Compiler (SDCC) [229]. Piklab is an IDE for PIC microcontrollers and SDCC is a C compiler suite that targets the Intel MCS51 based microprocessors.
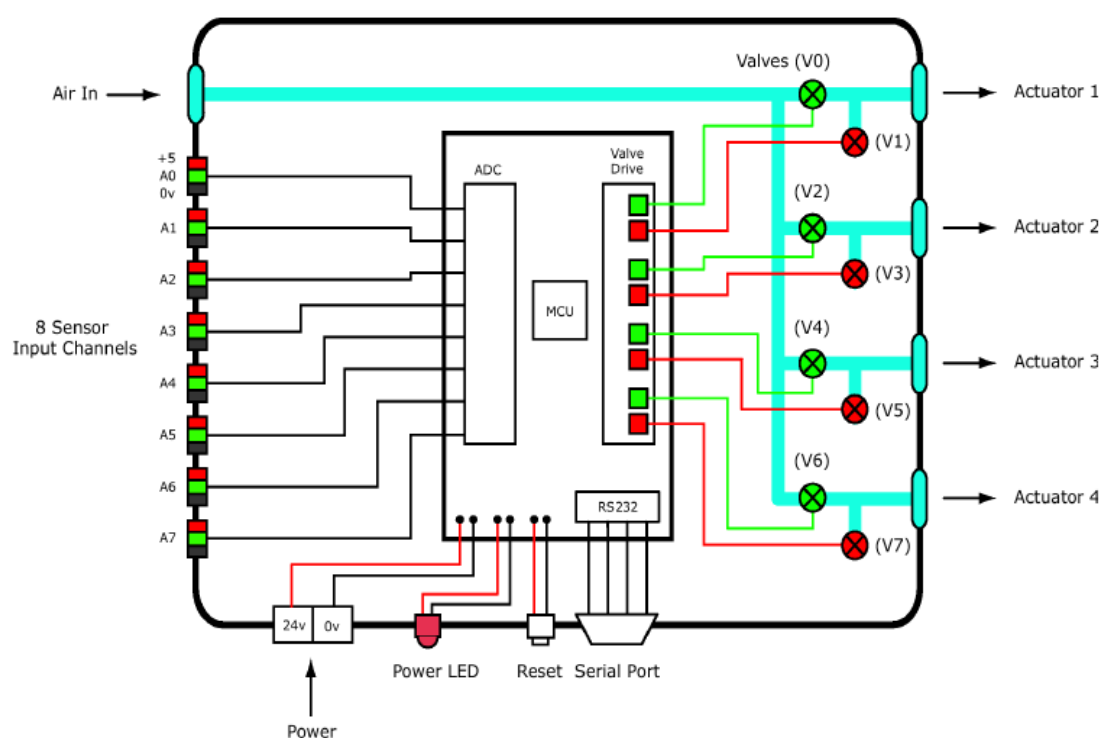
Figure 3.8: Block diagram of the SPCU designed by Shadow Robot Company [226]

Although the pneumatic income is included in the block diagram of the SPCU for more clarity, the air circuit is in fact designed apart from the MCU. As it will be illustrated in Figure 3.7, the airflow received from the air compressor is equally divided into four different inputs, which avoids any pressure drop in case of several valves being opened in same time.

Even though the SPCU includes all necessary devices, it is limited by its number of I/O. Indeed, it is seen on Figure 3.8 that the valve drive has only eight outputs. It means eight valves can be connected to the SPCU, which consequently can actuate a maximum number of four PAMs, whereas it has been seen in 2.1.3 that pneumatically actuated robot hands usually include more than 20 PAMs. The same restriction can be seen on the sensors' side. Despite its limitations, the SPCU still allows to experiment ambidextrous designs on single fingers.

51

The connections between the valves, the air compressor and the PAMs are shown in Figure 3.7 (a), whereas the connections between the SPCU and eight solenoid valves are shown in Figure 3.7 (b).
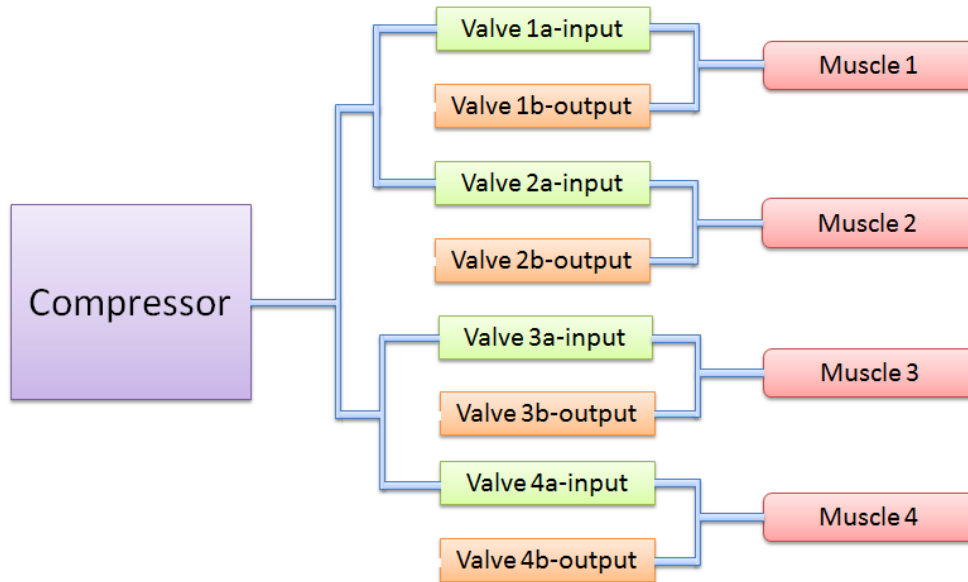
(a)
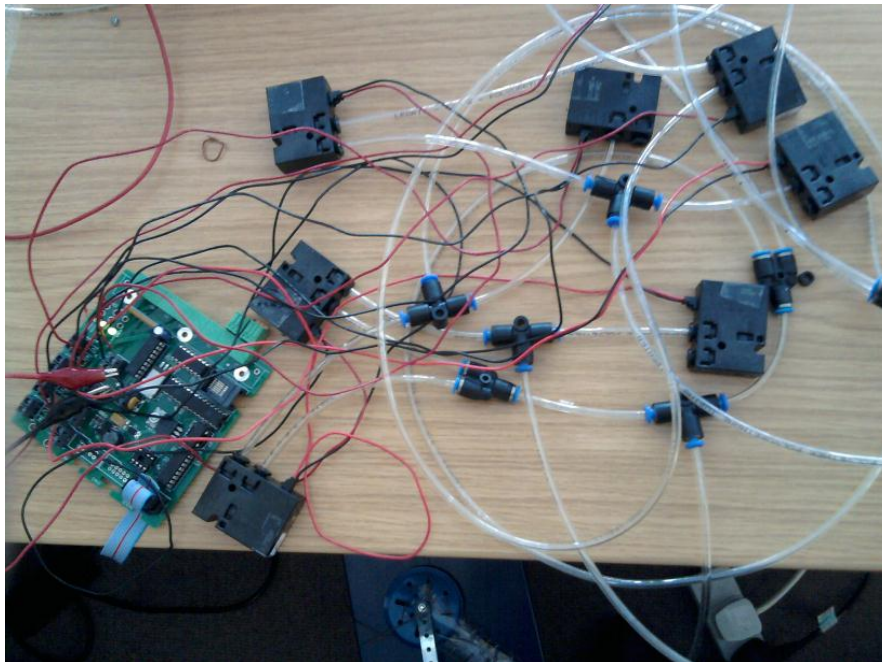
(b)

Figure 3.9: Connection between the SPCU, the valves and pneumatic devices. (a) a scheme showing the connections between the eight valves and the pneumatic devices and (b) the actual setup of the valves and the SPCU.

If muscles 1 and 2 are connected to the same part of a finger, it means they work in antagonistic way. In other words, the muscle 1 contracts when the muscle 2 extends. It means that the valve 1a is opened to let the air in whereas the valve 1b is closed so the muscle 1 contract. It also means that the valve 2a is closed whereas the valve 2b is opened so the muscle 2 extend. A simple command consequently causes reactions for the whole system, which is why the commands sent to the SPCU must be synchronised.

3.3.   Prototypes of ambidextrous fingers

Prototypes of ambidextrous fingers are designed, connected to PAMs and tested to prove the feasibility of an ambidextrous robot hand.

Thus, an analysis about the implications of an ambidextrous behaviour is firstly discussed.

Next, a number of prototypes of ambidextrous fingers are designed using kits of Meccanos. The prototypes are linked to PAMs and tested to reach the range of an ambidextrous finger. Their limitations are discussed and solutions are found to go from one prototype to another. The figures that illustrate the tendon routings of Designs D, G and H are achieved using the Matlab software introduced in [38].

Finally, the best obtained design is compared to robotic fingers of other robot hands.

3.3.1. Analysis of ambidextrous implications

In order to imitate a finger's behaviour, a maximum of its DOFs must be reproduced. Human fingers can make two kinds of antagonist movements: flexion and extension, or abduction and adduction. Flexion and extension control the angular displacement of the three phalanges of a finger, which means as many DOFs. Abduction and adduction imply lateral rotations of a whole finger and constitute another DOF, which makes a total of four distinct DOFs per finger [230]. As abduction and adduction are not essential for a number of applications, a number of dexterous hands have been developed without taking them into account, such as [70], [55] and [57]. Indeed, it allows both easing the control of the structure

and reducing the number of needed actuators. As only four PAMs can be controlled by the SPCU, this feasibility study does not take abduction and adduction into account either.

Moreover, as the movement of both distal and medial phalanges is coupled together in case of the human hand, these DOFs are often controlled by a single actuator [65]. In these cases, the flexion/extension of the proximal phalange is driven by a second actuator while the finger's abduction/adduction is controlled by a third one. The same mechanism is going to be investigated for an ambidextrous design.

According to [231], the fingers' ranges of motion are 90° for the proximal phalange, 100° for the medial phalange and 80° for the distal phalange. It means that an ambidextrous design would aim at reaching 180°, 200° and 160° respectively for the proximal, medial and distal phalanges.

The previous literature review also revealed that robot fingers are usually built as a succession of three phalanges, with sockets preventing them to reach non-natural angles [63], [232]. These sockets must be ignored for ambidextrous fingers, for which the range aims at being twice as the one of other fingers. The succession of the three phalanges is however compatible with an ambidextrous design, which is why the models can be inspired from others.

Concerning the tendons' routing, some clear illustrations were published by the University of Bologna. In [233], for example, it is explained that a single pulling of tendon bends a joint in opposition to the stiffness and the concentrated elastic joints along the finger's structure. The finger's pattern is shown in Figure 3.10. The linear motion is controlled by double-acting actuators for which position and force control can be provided.
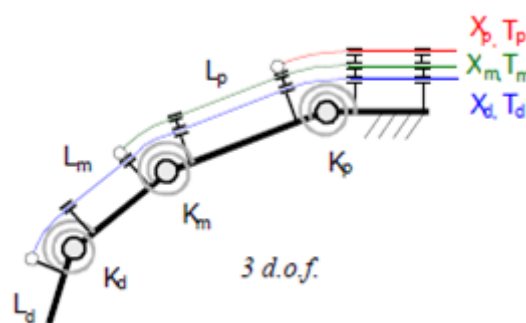
Figure 3.10: 3 DOFs actuation pattern, coloured version of [233]

Another example of a three joints' finger is illustrated in [232]. A pattern is provided in Figure 3.11. It is seen that the design has evolved. Indeed, even though three tendons are still necessary to drive the structure, it is noted that only two of them are connected to actuators. It is then said that the design includes two active and one passive tendons. This kind of mechanism is also going to be investigated for the design of ambidextrous fingers.
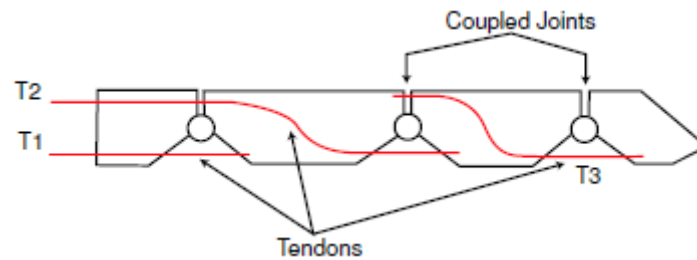
Figure 3.11: Structural scheme of a finger's endoskeleton, coloured version of [232]

Besides, as the ambidextrous fingers are controlled by PAMs, the main challenge of the research is to reach their two extreme positions. Indeed, the two main kinematic features to be taken into account are the stretching force of the antagonist PAM, which provides a huge force cancellation when the first PAM contracts, and the limitation of the PAM extension. Consequently, mechanical designs have to be optimised according to the PAMs' elasticity, taking into account their active and passive ranges. As the PAMs at disposal are designed to actuate either a right hand or a left hand, their range is limited.

Another issue to be considered is the number of PAMs necessary to control one finger. As said in section 2.1.3, the antagonist movements are often simulated with PAMs used by pairs, such as [90], [102] and [211], meaning that the system would require twice more PAMs as DOFs, even though a minimum number of $n+1$ actuators is necessary to control a number of n DOFs [50]. The first design consequently focuses on a single DOF controlled by two PAMs, whereas most of the others investigate the control of two DOFs by four PAMs.

3.3.2. Design A, first prototype

For the reasons mentioned in section 3.3.1, the first prototype, design A, is made of three joints. As shown in Figure 3.12, the tendons are driven to strategic kinematical points

using pulleys. It is also noticed that pulleys connected to the PIP and DIP are connected together using a passive tendon. The pulley of the DIP joint is fixed to the distal phalange with a screw, so the phalange and the pulley rotate together. The metal pieces acting as phalanges are separated by washers to ease the rotation. The design of prototypes very close to design A are also discussed in the report of I. Berruezo Juandeaburre [234].

| (a) | (b) |
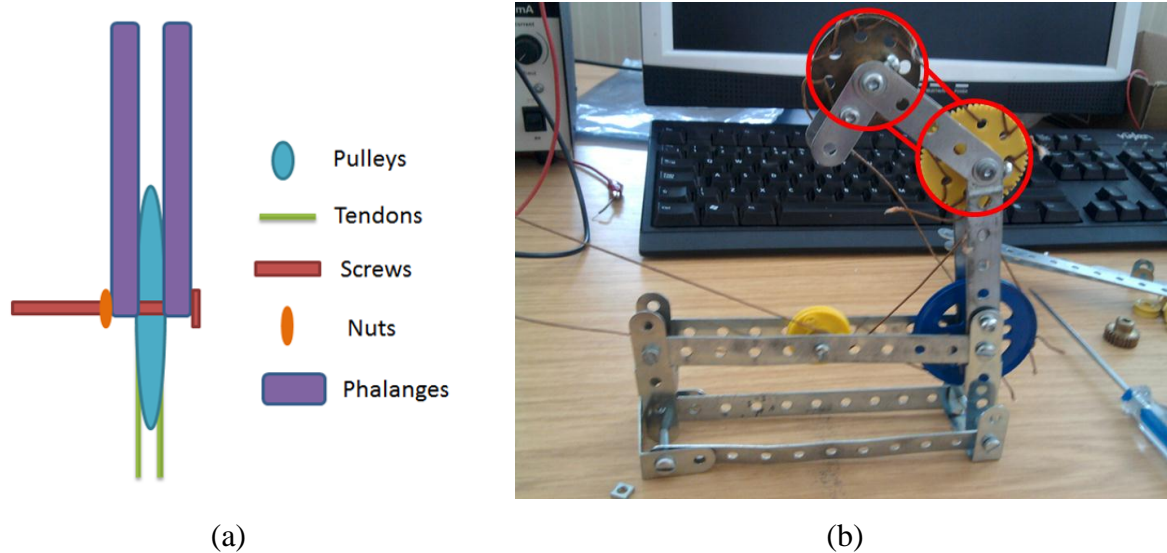
Figure 3.12: Design A, first prototype of robotic finger.
(a) shows how the pulleys are implemented and (b) is the actual implementation with Meccanos

For the first experiments, the proximal phalange is maintained motionless with a couple of screws holding it to the holding structure. Consequently, only two PAMs are used to actuate this prototype. The PAMs are put on a second holding structure shown in Figure 3.13.
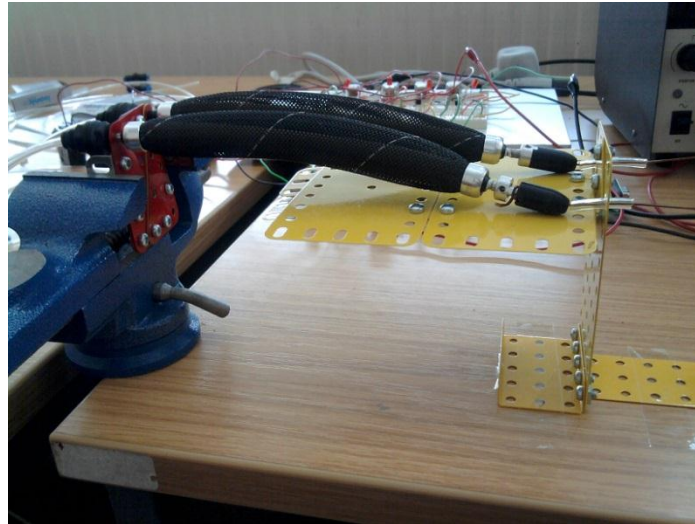
Figure 3.13: Holding structure designed for PAMs

Although the structure is properly actuated, the range of movements does not exceed 15° for the medial phalange and 25° for the distal phalange. The reason why the movements are so limited is because the pulleys' diameters, which are too big compared to the reduction ratio of PAMS' length. It is also noticed in Figure 3.12 (a) that the pulleys and the phalanges are tightened together, which provides a lot of friction. Therefore, Design B aims at increasing the pulling range of the PAMs and fixing the problem concerning friction.

As the first aim of the project is to amplify the range and as the maximum range is very limited, control functions are not implemented yet. The phalanges move by switching the valves ON/OFF, respecting the antagonistic behaviours of PAMs, until half of the PAMs contract to their maximum.

3.3.3. Design B, routing with different sizes of pulleys

As the PAMs' range is limited, the design B is built using different sizes of pulleys and a different tendon routing, shown in Figure 3.14. Indeed, the pulley fixed on the PIP joint has a diameter about twice smaller as the one fixed on the DIP joint. It is therefore expected to double the range provided by PAMs.
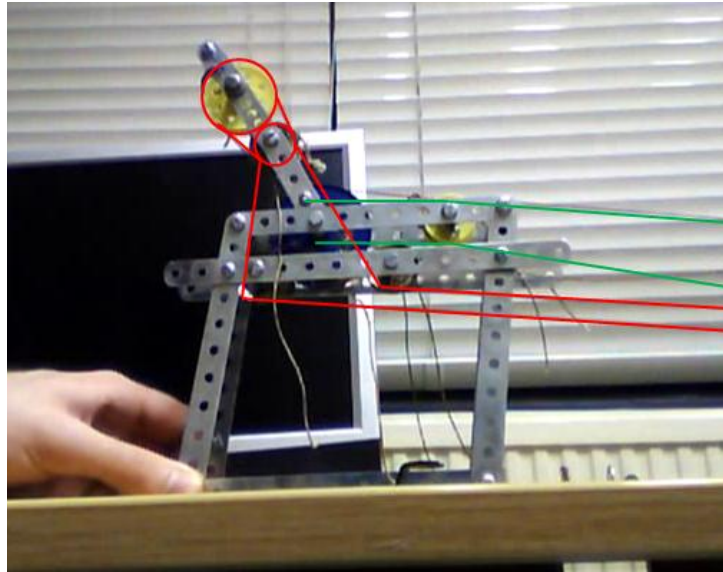
Figure 3.14: Design B, routing with different sizes of pulleys

The friction hindering the movements of Design A is also reduced by changing the architecture around the pulleys, as shown in Figure 3.15, which provides a smoother rotation of the system. This design is mainly used at the PIP joint, whereas pulleys are still screwed to the phalanges at MCP and DIP joints.
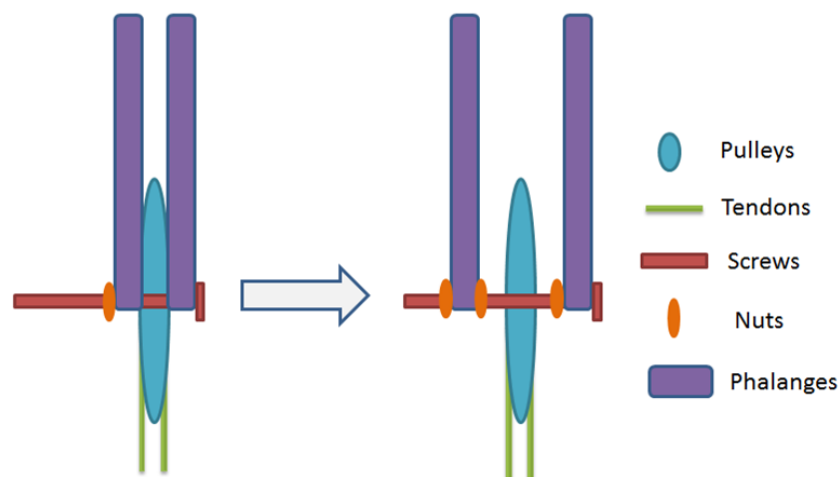
Figure 3.15: Modification of the implementation of pulleys from Design A to Design B

Contrary to Design A, Design B also aims at actuating the three phalanges, which means the four PAMs are connected to the SPCU. As medial and distal phalanges are coupled, the two longer PAMs are used to actuate these ones, whereas the proximal phalange that moves on its own is connected to the shortest PAMs.

However, the results obtained with Design B are barely better than the ones obtained with Design A. Indeed, the ranges of joints are respectively 40°, 0° and 10° for the proximal, medial and distal joints. The different sizes of pulley make the medial phalange motionless. Moreover the distal joint barely moves either, when it is actuated after the flexion of the proximal joint. This is explained because the tendons actuating the right side of the finger are routed to the right side, whereas the tendons actuating the left side are routed to the left side. Even though this routing choice seems logic, the tendons actuating the medial phalange become slack when the proximal phalange rotates first. Consequently, when the PAMs contract, most of their range is used to compensate the tendons' lose. The Design C aims at correcting these defects.

3.3.4. Design C, routing with coupled pulleys

The Design C uses the same concept tested in Design B about the coupling of pulleys, but this time the pulleys are directly connected together with screws, as shown in Figure 3.16. The aim is still to double the range of PAMs. For the pulleys fixed on the MCP joint, a bigger ratio is used to check if the efficiency of the method. Even though the size of the pulley cannot be used for the manufacturing of a more advanced design, it would be possible to use the same ratio. The current testing is indeed limited because the minimum diameter of the available pulleys, which is more than 120 mm. This dimension can be reduced by the manufacturing of smaller pieces.
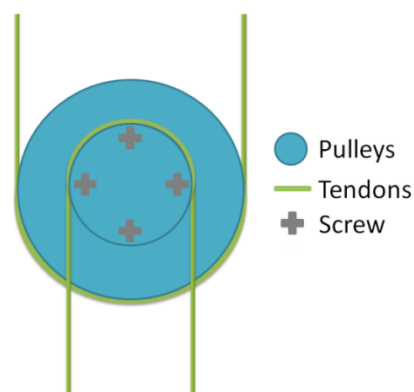
Figure 3.16: Two pulleys coupled together with screws

As shown in Figure 3.17, other differences with the Design B are the two pulleys fixed at the bottom of the structure that change the routing of tendons. This time, it is seen that the tendons actuating the medial and distal phalanges cross before reaching the MCP joint. In that way, tendons actuating the left side are routed from a starting point on the right side, and vice versa.
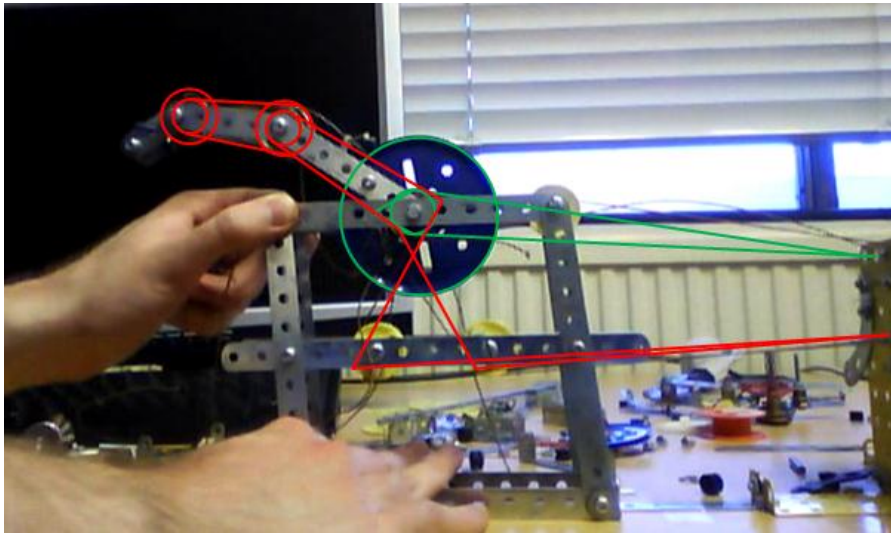
Figure 3.17: Design C, routing with coupled pulleys

The angular ranges obtained with Design C are respectively 80°, 100° and 150° for the proximal, medial and distal phalanges.

Contrary to expectations, the maximal range is far to be reached for the proximal phalange. This can be explained because of a lever effect. The proximal phalange is indeed screwed to a big pulley, which is itself connected to a first, smaller pulley. Consequently, for the rotation of the first pulley around a distance d_0 with a force F_0, the second pulley rotates around a distance d_1 applying a force F_1 on the following tendon, theoretically increasing the range by the ratio d_1/d_0. However, this system also causes a loss of force because of the increase of the range. The force F_1 provided to the MCP joint is indicated in equation (3.1).

$$F_1 = F_0 * d_0/d_1 \qquad\qquad (3.1)$$

Being multiplied by d_0/d_1, the force strongly decreases, which prevents the phalange to reach its maximal range. The sizes of pulleys will be explored deeper for Design D.

3.3.5. Design D, smaller sizes of pulleys

Design D aimed at improving the results reached with Design C by choosing more adapted sizes of pulleys, not belonging to Meccanos' kits. Despite the new diameters of pulleys that vary from 7.71 mm to 15.34 mm, the design and routing of Design D is technically the same as the one of Design C, except for the single pulley fixed at the DIP joint. The structure holding the PAMs is also modified. PAMs are implemented directly in the structure holding the finger to minimise any frictions.

Both the tendons routing and an image of Design D are shown in Figure 3.18.

(a)   (b)
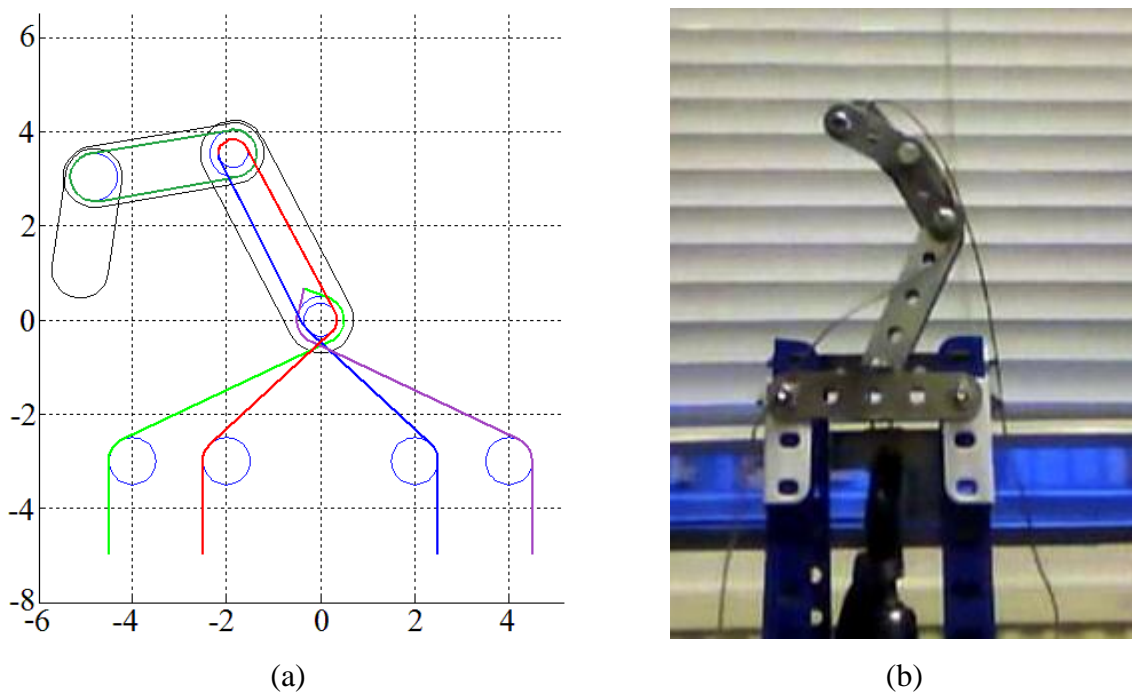
Figure 3.18: Design D, smaller sizes of pulleys
(a) the tendons routing and (b) the implementation of the prototype

The angular ranges obtained with Design D are respectively 165°, 165° and 83° for the proximal, medial and distal phalanges. For the first time, the ranges get close to the ones fixed by the initial requirements. Consequently, the next step consists in investigating a way to reduce the number of PAMs, which would limit the number of resources for the design of a whole Ambidextrous Robot Hand.

3.3.6. Design E, use of spring and racks

Design E investigates the possibility of replacing antagonistic PAMs by a spring. As the number of PAMs is reduced, Design E also aims to increase the range of PAMs to compensate the loss of the range of the antagonistic PAMs. The method used is different from Designs B and C, as Design E implements a spring, gears and racks. The implementation of springs to actuate hands driven by PAMs was proved to be efficient in the models introduced in [99], [106] and [98], as previously indicated in Section 2.1.3. However, as the use of a rack is very uncertain, only one PAM is connected to the system. The pulleys of the PIP and DIP joints are connected in the same way as Design D, whereas the MCP and PIP joints are connected together as shown in Figure 3.19. The aim is to actuate the three phalanges using a single PAM, and see if the spring can put back the phalanges in a position close their initial one. The structure holding the finger's prototype and the PAMs is modified again, to provide a smoother horizontal layout on which the rack can slide.
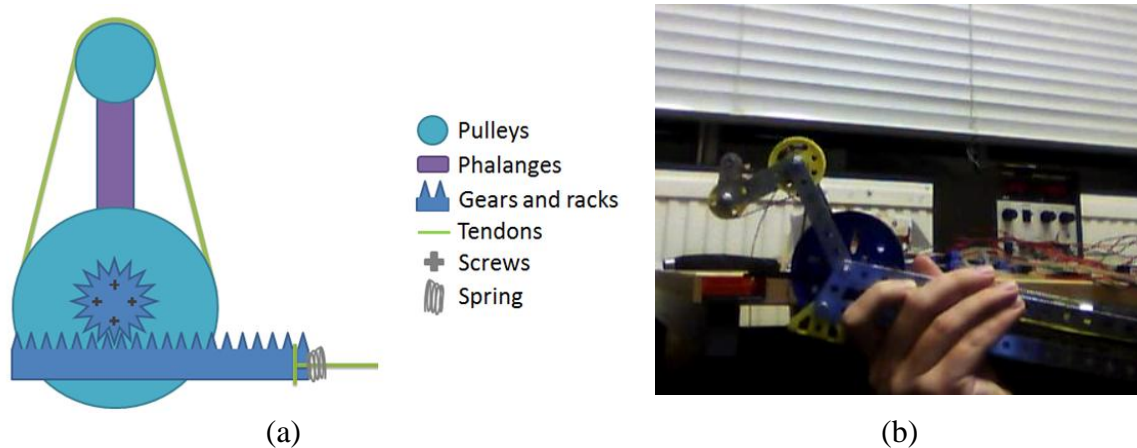
Figure 3.19: Design E, use of spring and racks
(a) a diagram showing how the gears and the racks are connected
and (b) the implementation of the prototype

The angular ranges obtained with Design E are respectively 0°, 0° and 235° for the proximal, medial and distal phalanges. The proximal and medial phalanges move on a range of about 20° but are unable to come back to their initial position. The reason why the actuation does not work properly is the same as the one mentioned for Design C in section 3.3.4. The lever effect does not allow a proper actuation of phalanges when a ratio between

two diameters is too big. Another attempt to reduce the number of PAMs is going to be investigated with Design F.

3.3.7. Design F, use of a rubber band

Design F investigates another possibility to replace antagonistic PAMs, using this time a rubber band. Despite its nonlinearity, rubber bands have already been used to actuate antagonistic movements of robot hands, as seen in [96]. Another example can be observed in [107], where the previous model of the hand of Swinburne University of Technology was actuated with rubber bands (although these ones were replaced by springs in a more recent design [99]).

Only one PAM is used to test Design F. Both the PAM and the spring are connected to the proximal phalange. The objective of the experiment is to see if the range reached by the Design C can be reached again using this new mechanism. The experiment is shown in Figure 3.20.

(a)   (b)

Figure 3.20: Design F, effect of the rubber band.
The PAM contracts in (a) and extends in (b)

The angular ranges obtained with Design F are respectively 80°, 0° and 0° for the proximal, medial and distal phalanges. Even though the range of the proximal phalange reached with Design F is close to the one reached with Design C, it is noticed the proximal phalange provides no force when it is to the side actuated by the rubber band. It makes the

interaction with objects impossible for one side of the Ambidextrous Hand, which is why the idea of Design F is not investigated further.

3.3.8. Design G, wrapping of tendons around pulleys

Design G investigates a new possibility to reach an ambidextrous behaviour with four PAMs. Contrary to Designs B to D, the tendons are this time wrapped around the pulley of the DIP joint. Even though the mechanism increases the friction of the system, it also prevents any loss of tendons when the finger is actuated. The type of pulleys used is the same as the one implemented in Design D. The structure holding the finger's prototype and the PAMs is also the same as the one holding Design D, as Design G does not include any more devices requiring a horizontal plane for early implementations.

The routing of Design G is shown in Figure 3.21.
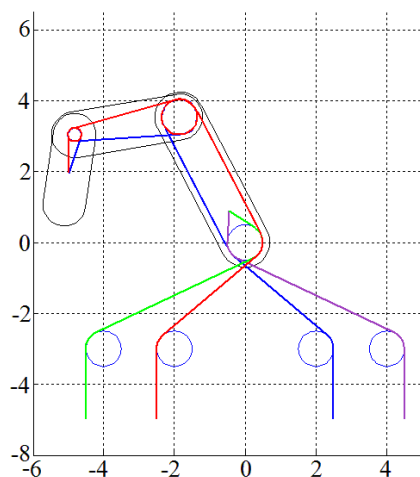
Figure 3.21: Routing of Design G

The angular ranges obtained with Design G are respectively 166°, 141° and 107° for the proximal, medial and distal phalanges. Video's snapshots of Design G under actuation are provided in Figure 3.22.

<div align="center">(a)   (b)   (c)</div>
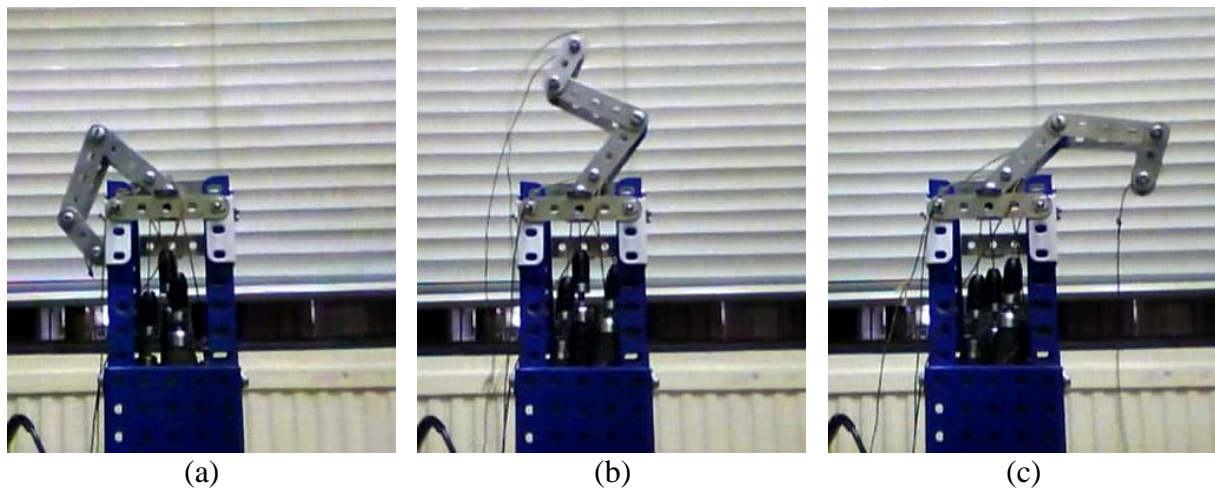
Figure 3.22: Video's snapshots of Design G.
The finger is on left/right side on (a), on an intermediate position on (b) and
on right/left side on (c)

For the second time, the ranges get close to the ones fixed by the initial requirements. The next step consists in analysing the models from Designs A to G, to see if one of them could be used to start a feasibility study about control theory.

3.3.9. Comparisons of mechanical features from Design A to Design G

The results obtained from Design A to Design G are investigated to see if one design is appropriate to start a feasibility study about control theory. The ranges obtained for each joint of each design are gathered in Table 3.2. In addition to their angle, their range is also compared to the initial requirements in percentages. The higher the percentage, the closer the prototype to the human anatomical behaviour, defined as the target. Prototypes reaching the highest percentages can consequently be used for further investigation.

Table 3.2: Comparison of the ranges of the different designs

Designs	# PAMs	Ranges obtained for each joint, in °			Ranges obtained for each joint, in % compared to initial requirements				Applicable for further investigation
		MCP	PIP	DIP	MCP	PIP	DIP	Average	
Target	N/A	180	200	160	100%	100%	100%	100%	
A	2	0	15	25	0%	7.5%	15.6%	7.7%	
B	4	40	0	10	22.2%	0%	6%	9.5%	
C	4	80	100	150	44.4%	50%	93.8%	62.7%	
D	4	165	165	83	91.7%	82.5%	51.9%	75.3%	✓
E	1	0	0	235	0%	0%	146.9%	49.0%	
F	1	80	0	0	44.4%	0%	0%	14.8%	
G	4	166	141	107	92.2%	70.5%	66.9%	76.5%	✓

Table 3.2 shows that the best behaviours are obtained for Designs D and G, which both reach more than 75% of the target. Their MCP joint, in particular, almost reaches the maximum angles of the initial requirements. Therefore, an additional investigation is done, concerning the maximum force applicable by each phalange of Design D and Design G.

These forces are collected using a Newton metre. The hook is linked to specific phalanges and a force is applied on the phalanges until their maximum angles decrease of about 10°. The performances of Design D and Design G are summarised in Table 3.3, which indicates the maximum angles reached by each joint, as well as the maximum forces applicable by their respective phalanges. The results are showed both for the left and right sides.

Table 3.3: Comparison of mechanical features between Design D and Design G

Designs	Joints	Maximum angles reached (°)		Maximum forces applied (N)	
		Left	Right	Left	Right
D	MCP	85	80	52	47
	PIP	80	85	9	10
	DIP	40	43	3	3
G	MCP	84	82	51	49
	PIP	70	71	12	13
	DIP	52	55	0	0

Table 3.3 shows that the maximum force applicable by the proximal phalange is much higher as the ones of the medial and distal phalange. This is normal, as PAMs are directly connected to the MCP joint, whereas the PIP and DIP joints are coupled. Moreover, the PAMs connected to the PIP joints are routed through a higher number of pulleys. Indeed,

they are routed around the MCP joint before being tied to the PIP joint, which adds friction to the system. However, the maximum forces applicable by medial and distal phalanges are very weak. It is noticed that distal phalanges cannot apply more than 3 N, which is not enough to interact with objects. Consequently, an additional design is going to be investigated. In addition to the angular range, the maximum force applicable by medial and distal phalanges is also going to be optimised.

3.3.10. Design H, use of torsion springs

Design H investigates the possibility to avoid unnecessary routings by replacing a number of pulleys by torsion springs. If tendons provide enough force to medial and distal phalanges, the finger would then be able to interact with objects. The design of such a model is discussed in the report of S. Chattoraj [235].

The tendon routing is shown in Figure 3.23. As for Design G, it is seen that the tendons actuating the medial and distal phalanges are not connected to the PIP joint but to the DIP joint. The tendons are also routed almost straight from the bottom of the structure to the DIP joint. The only curve is the one formed around the MCP joint.

The implementation of torsion springs under the PIP and DIP joints allows a synchronised bending of medial and distal phalanges. Design H also includes intermediate pulleys which avoid the tendons to get loose. Contrary to the method investigated for Design G, the tendon force is less reduced. Indeed, the only force that opposes the PAMs' contraction is the one provided by the spring, weaker than the one provided by the systems of pulleys of Design D and Design G.
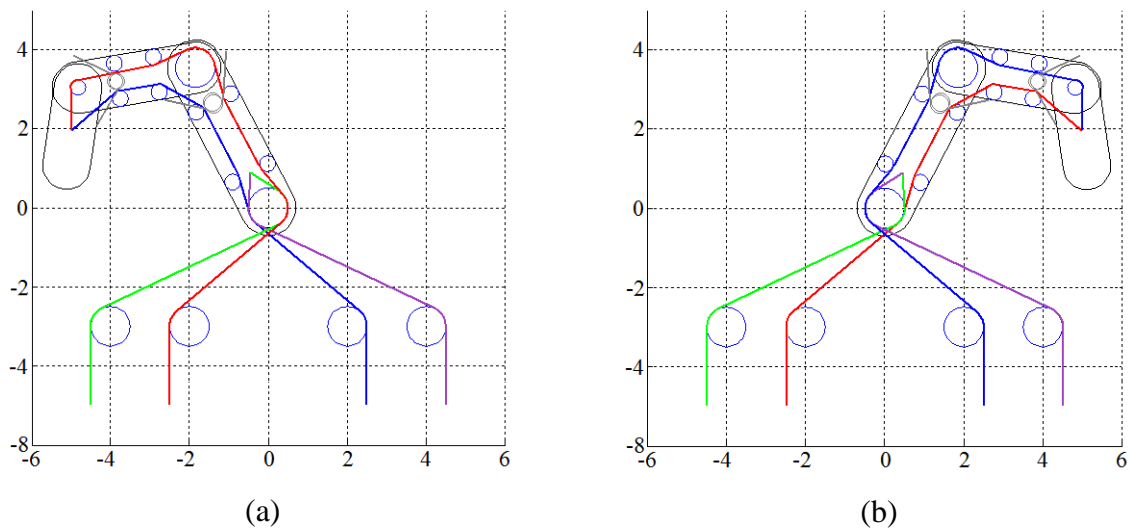
Figure 3.23: Tendon routing of Design H
(a) the left hand mode and (b) the right hand mode

However, the angular ranges reached by the original model introduced in [235] are limited compared to the ones obtained with Design D and Design G. The reasons of these restrictions are the same as the ones mentioned for Design C. Indeed, the sizes of the pulleys do not match with the ambidextrous behaviour and the PAMs at disposal. Consequently, optimal dimensions are investigated by repeating the same movements with different sizes of pulleys. The results of this experiment are summarised in Table 3.4.

Table 3.4: Maximum angles and forces obtained with different pulleys configurations of Design H

Joints	Pulleys' diameter (mm)	Max. angles reached (°)		Max. applied force (N)	
		Left	Right	Left	Right
MCP	23.81	58	54	91	86
MCP	15.34	85	80	53	49
MCP	7.71	90	90	38	31
PIP/DIP	23.81 / 15.34	54 / 10	60 / 19	59 / 4	62 / 11
PIP/DIP	15.34 / 15.34	73 / 29	77 / 36	30 / 18	35 / 22
PIP/DIP	7.71 / 2.95	75 / 51	80 / 55	21 / 10	23 / 13
PIP/DIP	2.95 / 2.95	88 / 68	90 / 72	12 / 3	15 / 4

Table 3.4 shows that the best pulley configuration to optimise the angle/force ratio is 15.34 mm for the MCP joint and 7.71 mm / 2.95 mm for the PIP/DIP joints. The maximum reachable angles can be increased using smaller pulleys, but it would then cause a significant loss of the applicable force. The maximum range of Design H is shown on video's snapshots gathered in Figure 3.24.

<div align="center">

(a)   (b)   (c)
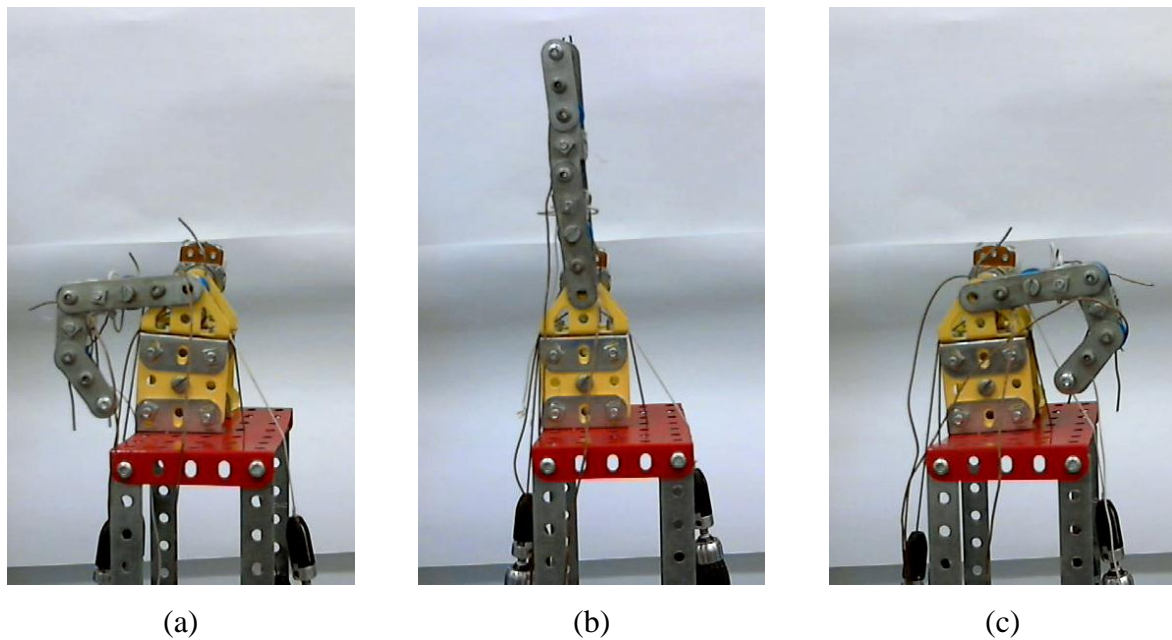
Figure 3.24: Maximum range of Design H
(a) the left/right position, (b) the vertical position and (c) the right/left position

</div>

The angular ranges reached by Design H are then compared with ranges of other robotic fingers, to check if its behaviour on a single side is close to other models.

3.3.11. Comparison of angular ranges between Design H and other robotic fingers

The ranges reached with Design H are compared with ranges of other robotic fingers to analyse its behaviours with others. The maximum angles reached with robot fingers are precisely mentioned in some articles. When the range of several fingers is mentioned, the forefinger is chosen as a reference for this comparison. Moreover, as the pictures of these devices show right hands, it is estimated that the provided range are the ones of right hands. The range of each joint of Design H is put in Table 3.5, both for left and right mode, with the range of some other robotic models. These other models are the robotic finger engineered by K.J. De Laurentis et al. [112], driven by SMAs, the wearable rehabilitation device developed by K. Xing et al. [172], actuated by PAMs, the Shadow Hand [74], which reaches the same angles when it is actuated by PAMs or by motors, the ACT hand [66], which is motorised, and the anthropomorphic robotic hand engineered by Z. Xu et al. [142], driven by air cylinders.

Table 3.5: Comparison of angular ranges between Design H and other robotic fingers

Hand or finger	MCP joint (°)	PIP joint (°)	DIP joint (°)
K.J. De Laurentis et al.[112], 2000	88	73	77
K. Xing et al.[172], 2009	88	90	63
Shadow Hand [74], 2013	90	90	90
ACT hand [66], 2013	90	110	90
Z. Xu et al. [142], 2013	110	90	90
Design H, left hand mode [39], 2013	85	75	51
Design H, right hand mode [39], 2013	80	80	55

Table 3.5 shows that even though the experiments are done with standard PAMs, the ambidextrous design has ranges relatively close to the ones of other models, both for left and right hand modes. Combined together, the two modes overreach the range of other models.

The range of Design H can be increased even further using more suitable PAMs. However, this range and the force it can apply are large enough to proceed with first tests of control theory.

3.4.   Feedback control applied to the ambidextrous fingers' prototypes

Another part of the feasibility study consists in controlling the prototype of the ambidextrous finger, to check if its actuation is possible.

As explained in section 2.4, a number of systems that implement PAMs are driven using PID controllers. It is for example the case of [236], for which a two-links PAM manipulator is driven with a PID loop supervised by a feedforward NN controller. It is also the case of a rehabilitation arm, which uses PID loops to control both the force and the position of the system [28]. The robot arm described in [104] and the robot hand discussed in [177] use a control based on a PID feedback as well. Finally, the Shadow Hand also uses PID controllers to operate either from sensor data or from values supplied by users [94]. Consequently, as PID controllers are widely used in the area of PAMs, conventional PID loops are used to control the early designs of the Ambidextrous Robot Hand.

The angular displacement will be investigated first. Then, the force applied by the fingertip and the interaction with objects will be discussed as well.

3.4.1. PID control theory

The pattern describing the basic functioning of a PID loop is provided in Figure 3.25.
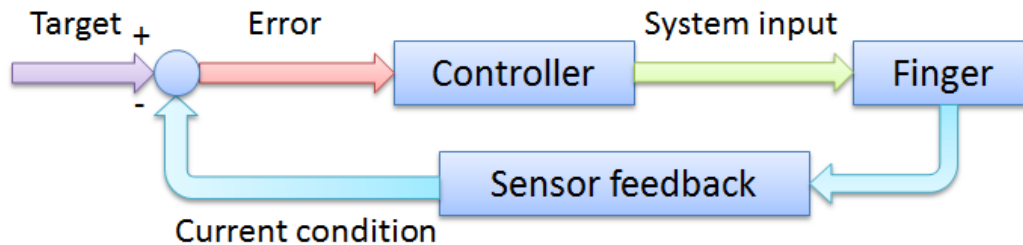
Figure 3.25: Control of a robotic finger using PID loops

Over a first phase, the target (or setpoint) is compared to the current condition of the system. The output $u(t)$ of a PID controller is defined as the sum of the proportional term, the integral term and the derivative term [237]. Equation (3.2) is an algebraic expression commonly used to calculate the output of a PID controller and is known as representing the parallel form of the transfer function [238].

$$u(t) =\ K_p e(t) + K_i \int_0^t e(\tau)d\tau +\ K_d \frac{d}{dt} e(t) \qquad (3.2)$$

It is observed in (3.2) that the three terms depend of the error signal $e(t)$, which is the difference between the target point and the process variable [239]. The different gain constants K_p, K_i and K_d respectively adjust the proportional, integrative and derivative terms set the ratio of the output response. Before understanding the interactions between the three terms and the signal output, it is necessary to get familiar with the control terminologies indicated in Figure 3.26.
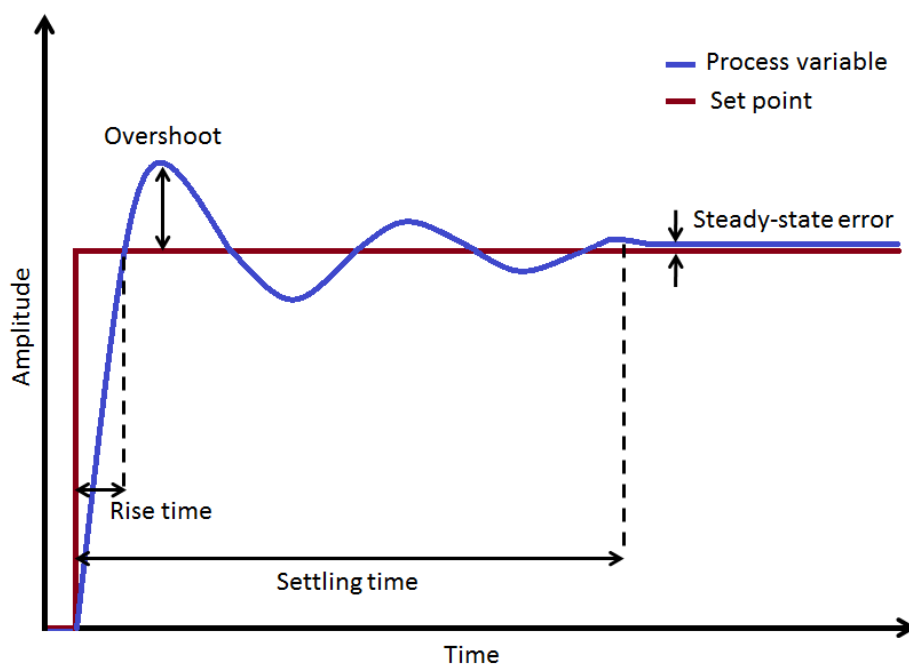
Figure 3.26: Representation of process variable and set point for a system controlled by PID loops, the terms being courtesy of PID terminology, such as in [240]

The overshoot is the maximum peak value reached by the error. The steady-state error is the final difference between the process variable and the set point. The rise time is the time taken by the signal to change from its initial value to the set point. The settling time is the time taken by the signal to change from its initial value. Oscillations are illustrated by the number of times the process variable crosses the set point. The steady-state error, or error band, is the margin of error of the process once it reaches a stable state.

The proportional term $K_p e(t)$ provides an overall control action depending only on the error signal. The higher is K_p, the fastest is the response, which increases both the speed and the sensitiveness of the system [238]. However, a too high gain constant may make the system unstable and oscillate out of control [238]. In the case of an angular target for the ambidextrous finger, it would make the phalange move very fast around the targeted set point.

The integrative component $K_i \int_0^t e(\tau) d\tau$ sums the error over time, which corresponds to the accumulate offset. It means that it is proportional to both the magnitude and the duration of the error [241]. Consequently, as long as the set point is not reached, the integrative term increases to reduce the steady-state error. Usually, increasing K_i makes the process variable reaches the set point faster, but also increases the overshoot. Combined

together, the proportional and integrative terms regulate the response time of the ambidextrous phalange to reach set points limiting the number of oscillations.

It is observed that a number of systems do not use derivative component, such as the ones described in [242], [243] or [244]. Nevertheless, the addition of this derivative component may allow adding more stability [245].

The derivative term $K_d \frac{d}{dt} e(t)$ depends on the slope of the error over time, which means it is proportional to the rate of change of the system's reaction. The more the process variable increases, the more the output decreases. Consequently, the derivative term theoretically permits to decrease the overshoot, to add more stability and to reduce the number of oscillations. These three outcomes are going to be verified on the ambidextrous finger. As for the other gain constants, a too high K_d may make the system unstable, because the higher K_d, the slower the system and the higher becomes $\int_0^t e(\tau)d\tau$ of the integrative term.

Now that the three terms of the PID control are explained, a more advanced scheme is provided in Figure 3.27. As it can be seen, the three terms are going to work in coordination. The final output is converted into PWMs by the SPCU. According to the widths of these PWMs, the PAMs contract and extend to make the finger reach its setpoint.
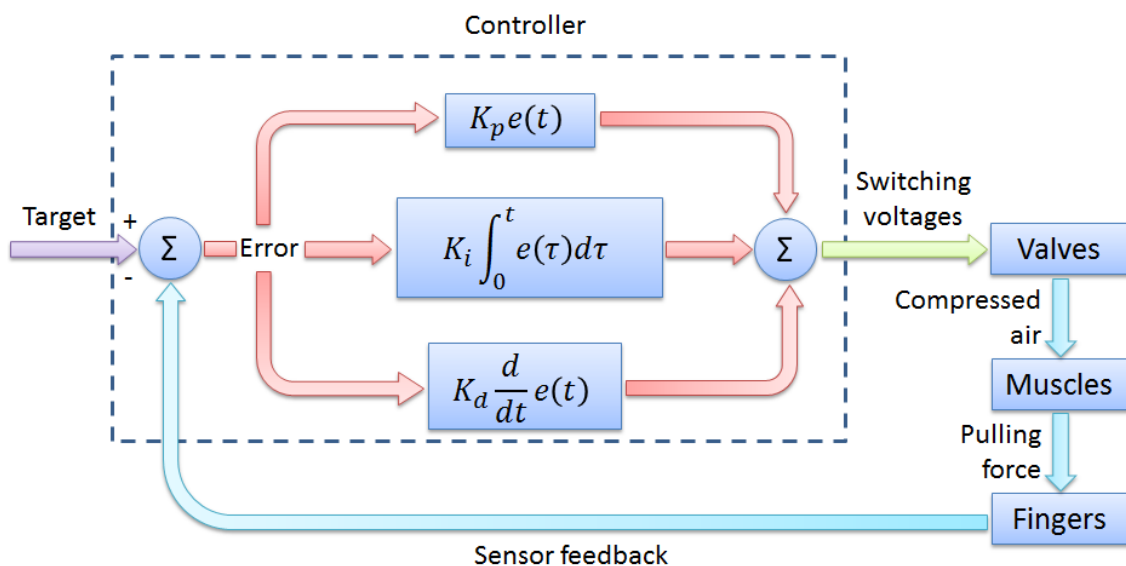
Figure 3.27: PID controller associated with the Ambidextrous Hand

First tests are going to be done for the angular position. Over a second phase, force control is going to be added to angular displacement.

3.4.2. Control of angular position

The control of the angular position is necessary for the actuation of an ambidextrous finger. It allows reaching specific angles and knowing if the finger is on its right side or on its left side.

A potentiometer RV120F-20-15F-B1K [246] is implemented to control the angular position of the ambidextrous fingers' prototypes. The mechanical implementation of the potentiometer inside the prototype's architecture is explained in [235]. A scheme of a potentiometer RV120F-20-15F-B1K is provided in Figure 3.28. When these potentiometers are connected to a 5 V DC power supply, the voltage feedback linearly varies according to the angle of the rotating contact by its two components. Therefore, potentiometers RV120F-20-15F-B1K can be used as angular sensors, which matches with the literature reviews done in sections 2.1.2 and 2.1.3.1, and 2.1.3.2. The difference between their maximum and minimum angles is about 270°, which is more than enough for ambidextrous fingers, for which the maximum range does not exceed 200°.
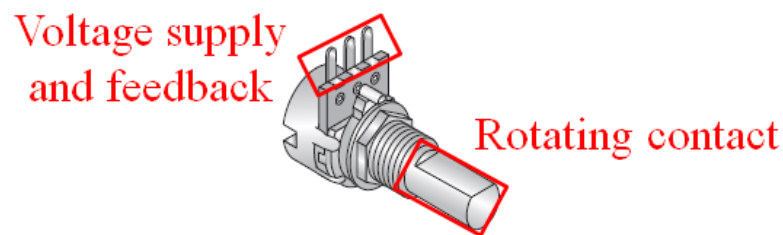
Figure 3.28: Scheme of potentiometer RV120F-20-15F-B1K [246]

When potentiometers RV120F-20-15F-B1K are connected to the SPCU, the ADC and the CPU indicates values varying from 00100_{16} to $15EFF_{16}$. Thus, if the sensor is positioned properly inside the finger, the vertical position corresponds with 08000_{16}. According to the desired position, the value read by the SPCU is set as a target.

As explained in chapter 3.2.2, the commands sent to a couple of I/O valves must be sent in an opposite way to the valves controlling the antagonistic PAMs. The

flexion/extension of the phalange depends on four inputs, which are the states (opening or closing) of the four valves actuating the two PAMs. Consequently, to reach a vertical position, the gain constants must switch whenever the phalange overreaches 08000_{16}. The valves working as inputs on the left side become outputs on the right side, and vice versa.

The calibration of the gain constants is done using manual PID tuning method. The manual tuning of a PID loop is one of the most famous ones and is described, for instance, in [237]. The method consists in calibrating the gain constants one after other. The experiment is done with the MCP joint of Design G. The aim is to reach a vertical position with the proximal phalange. The very first step of this experiment is illustrated in Figure 3.29. The proximal phalange oscillates six times and it takes itself about 1 sec to stabilise.

(a)   (b)   (c)   (d)
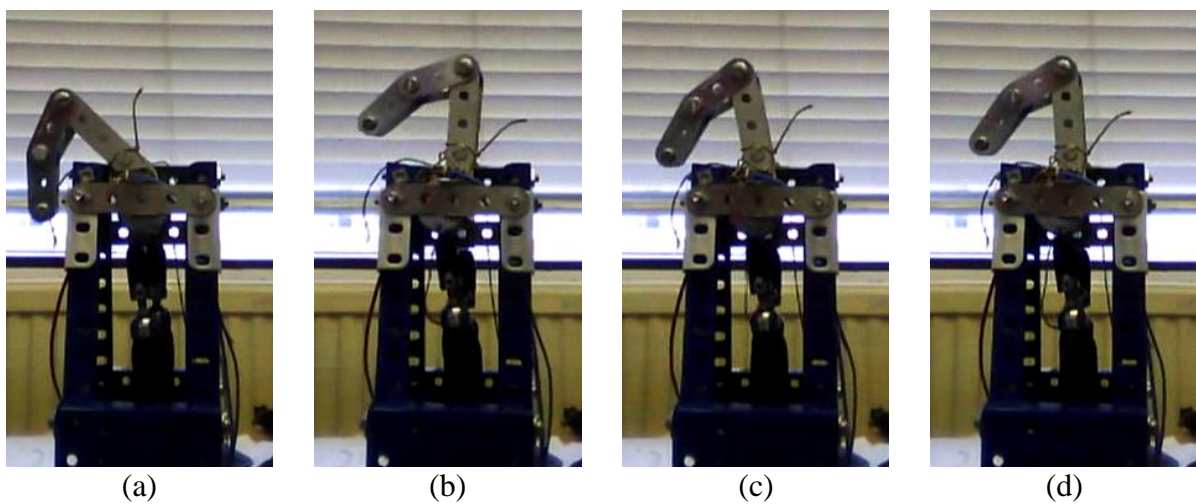
Figure 3.29: Video's snapshots of the first step of the tuning of a PID loop with Design G
In analogy with Figure 3.26, (a) the initial position, (b) the overshoot,
(c) an oscillation and (d) the steady-state error.

The next steps of the experiment are summarised and commented in Table 3.6. The gain constants are still tuned for a vertical position. The percentage of the overshoot is calculated according to the angle defined as the set point. Firstly, K_i and K_d are put to zero, whereas K_p is increased until rising time is fast enough. Secondly, K_p is reduced whereas K_i is increased until the overshoot almost disappears. The tuning was efficient for $K_p = 2$ and $K_i = 2$, yet, the system still oscillates around the setpoint. The system becomes less stable for $K_p = 2$ and $K_i = 3$, which is why K_d is tuned keeping $K_p = 2$ and $K_i = 2$. Whenever K_d is increased, it is noticed the oscillations stop from $K_d = 4$. The system keeps

being stable when K_d increases until $K_d = 10$, but the rising time becomes slower and slower. It is noticed the system oscillates again for $K_d > 10$.

Table 3.6: Tuning of the PID gain constants K_p, K_i and K_d for angular displacements to reach a vertical position

K_p	K_i	K_d	Rising time (sec)	% of overshoot	# oscillations	Settling time (sec)
1	0	0	0.70	15%	2	1.05
2	0	0	0.30	15%	4	0.65
3	0	0	0.15	30%	8	0.60
4	0	0	0.10	35%	∞	∞
3	1	0	0.10	20%	6	0.35
2	1	0	0.15	10%	5	0.25
2	2	0	0.10	5%	5	0.20
2	3	0	0.05	15%	6	0.25
2	2	1	0.10	10%	2	0.15
2	2	2	0.10	10%	2	0.15
2	2	4	0.10	5%	1	0.15
2	2	6	0.10	0%	0	0.10
2	2	8	0.15	0%	0	0.15
2	2	10	0.25	0%	0	0.25
2	2	12	0.30	10%	2	0.40
2	2	14	0.20	30%	3	0.40

The best gain constants K_p, K_i and K_d obtained in this experiment are respectively 2, 2 and 6. However, according to the desired rising time, K_d can be increased until 10 to make the movement slower.

A better tuning accuracy can be reached by dividing the SPCU's input by a large number. The maximum value $15EFF_{16}$ is almost equal to 90000_{10}. To keep an angular position close to 0.5°, a corresponding ratio must be found.

As the proximal phalange aims at rotating around 200° instead of the 270° provided by the RV120F-20-15F-B1K potentiometer, the value 90000 is first multiplied by $\frac{200}{270}$. Then, as an accuracy of 0.5° is aimed for the range of 200°, the first ratio is divided by $\frac{200}{0,5} = 400$. The full operation is shown in equation (3.3).

$$90000 * \frac{200}{270} * \frac{1}{400} \sim 167 \qquad (3.3)$$

A number close to 167 is found, which means that the SPCU's sensor's inputs can be divided by 150 and still have an accuracy higher than 0.5°.

As the angular position is controlled by two different PAMs, a safer option consists in fixing two different targets for the PAMs. For a desired angle of 90°, the first PAM may contract only for an angle inferior to 88°, whereas the second one would contract for an angle superior to 92°. This setting reduces the system accuracy but also limits the risk of oscillations.

Experiments show that vertical position is the most difficult one to reach. Indeed, contrary to other robotic fingers, the ambidextrous model does not have sockets to disable it to overreach that very position. Consequently, once the gain constants are settled for the vertical constants, these same coefficients can be used for any other positions. As shown in Figure 3.30 with Design H, the potentiometer can also be connected to a second one that transfers it a position in real-time. The same mechanism can be applicable later on, with two fingers and force sensors. In that way, the same force can be applied from both fingers, allowing the robot hand to grab objects. For rehabilitation process, the angles reached by users can also be forwarded to the robot hand, so the same positions can be transferred.

(a)   (b)
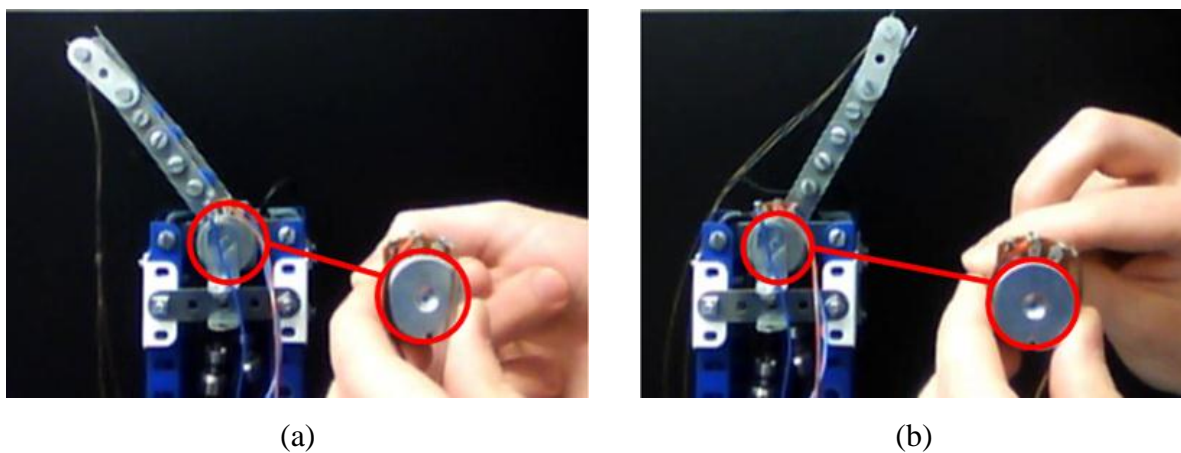
Figure 3.30: Transferring a position value from one angular sensor to another with Design H. (a) is the opposite behaviour of (b)

Next step consists in controlling the force applied by the fingertip.

3.4.3. Force control

The addition of force control on the ambidextrous finger's prototype allows detecting and interacting with objects. Thus, an adapted model of force sensor is chosen. The finger is then put in contact with an object. Finally, the kind of object is identified analysing both the angular and the force variations.

3.4.3.1.   *Choice of force sensors*

To control the force applied by fingertips, force sensors were looked for on the online-shop active-robots.com. A number of force sensors were found and classified. Their features are compared in Table 3.7. The force sensor must be able to detect at least 53 N, which is the maximum force provided by Design H, as shown in Table 3.4, whereas a minimum force of 1 N would allow to detect very light objects. It is also preferable to have a maximum error lower than 15% to permit accurate experiments. Finally, the contact area must not overreach a diameter of 8 mm, as it would not fit with the dimensions of the Design H.

Table 3.7: Features of force sensors

Sensors' names / codes	Min and max forces	Error max	Contact area
1131_0 Phidgets Thin Force sensor / 1131 [247]	N/A min, 20 N max	10%	12.7 mm diameter
Force Sensitive Resistor – Square / SEN-09376 [248]	1 N - 100 N	Between 5% and 25%	38.1 mm²
Force Sensing Resistor / FSR-01 [248]	1 N - 100 N	10%	5 mm diameter
Force Sensitive Resistor 0.5'' / SEN-09375 [248]	1 N - 100 N	10%	126.7 mm²
3103_0 Interlink Circular Force Sensing Resistor / 3103 [248]	1 N - 100 N	N/A	5 mm diameter

Both sensors SEN-09376 and SEN-09375 [248] are too big for the ambidextrous finger, whereas the sensor 1131_0 [247] cannot forces higher than 20 N. Sensors FSR-01 and 3103 are very similar [248], but the model FSR-01 is almost 25% cheaper, which is why it is chosen to experiment the force control.

3.4.3.2.   Interaction with objects

To apply a measurable force contact to objects, force sensing resistors FSR-01 are scotch taped to the fingertips and wired to the SPCU. Pressing a piece of metal against the force sensor, it is noticed that the feedback's value varies between 18000_{16} and $19A00_{16}$, according to the force applied by the human hand. Consequently, it is estimated that fixing targets between $19B00_{16}$ and $19C00_{16}$ would permit to provide enough force to hold this same piece of metal, in interaction with a human finger. The gain constants of the PID controller are tuned the same way as the one described in chapter 3.4.2. However, contrary to the vertical position, there are no losses of balance caused by accurate antagonistic ratios, which makes the tuning of gain constants much faster. With Design H, the finger's prototype can grab the piece of metal at the first attempt. The grasping stability is increased at the second attempt and becomes very stable at the third attempt. The best experimental results are obtained with $K_p = 50$, $K_i = 20$ and $K_d = 10$. Video's snapshots are provided in Figure 3.31.
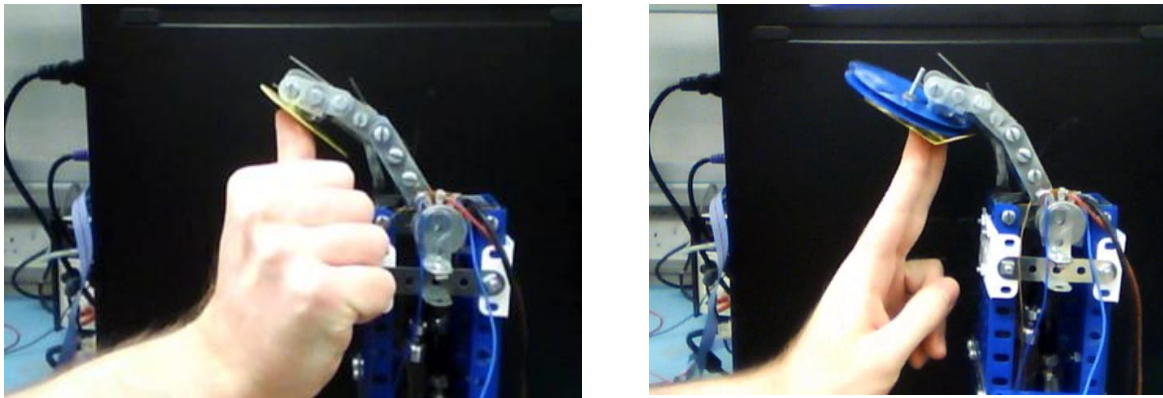
Figure 3.31: Video's snapshots of Design H maintaining pressure on two different metallic pieces, with the same setpoint and the same gain constants

The experiment shown in Figure 3.31 combines both the angular control of the proximal phalange and the force pressure applied by the distal phalange. It means that two PID controllers are running in parallel. The flowchart of the process is provided in Figure 3.32. As it can be seen, the first PID controller deals with the angular displacement of the proximal phalange even when the distal phalanges are moving. This process allows parallel motions and control of the three phalanges of the finger.
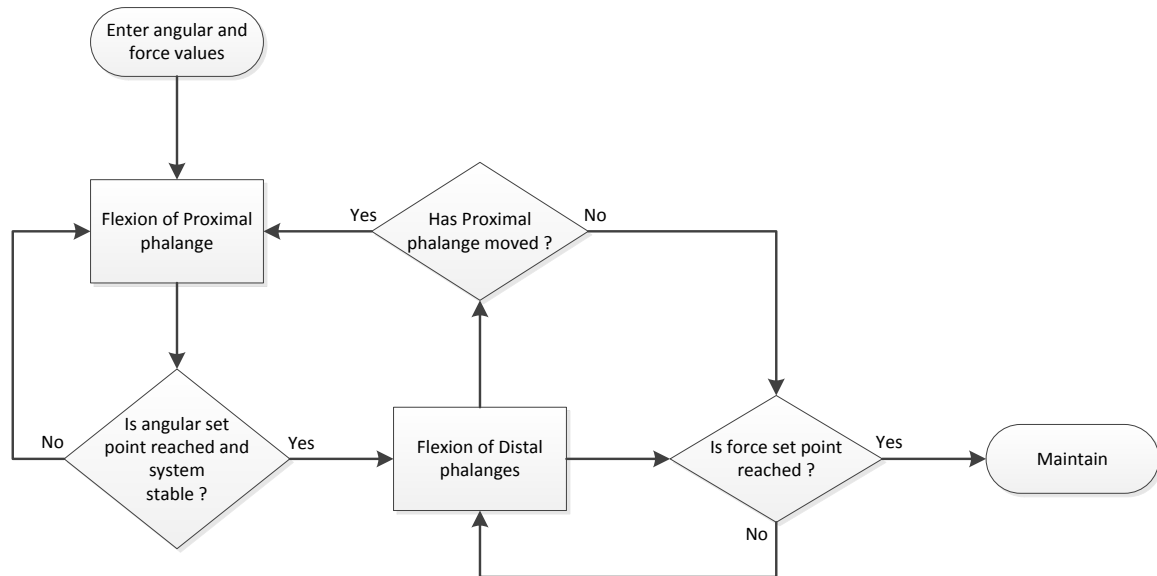
Figure 3.32: Flowchart of force applied on a piece of metal

Force control is investigated further with objects' detection.

3.4.3.3.   *Detection of objects*

The recognition of objects allows robotic structures to become more autonomous, as they do not require any other commands sent by a human to trigger an appropriate process. The holding of objects, which includes its detection, is already introduced in Section 3.4.3.2. However, if the control function aims at touching an object without pressing it, then the setpoint of the PID must be reduced. Therefore, to touch light material such as paper, the target of the sensor's feedback is fixed to a value close to its minimum, such as 8_{16} or A_{16}. Video's snapshots of this experiment are provided in Figure 3.33. It is observed that the robotic finger goes backward when the piece of paper is in contact with the fingertip, whereas the finger bends when the paper does not touch the fingertip. The gain constants used are the same as the ones of the experiments shown in Figure 3.31.
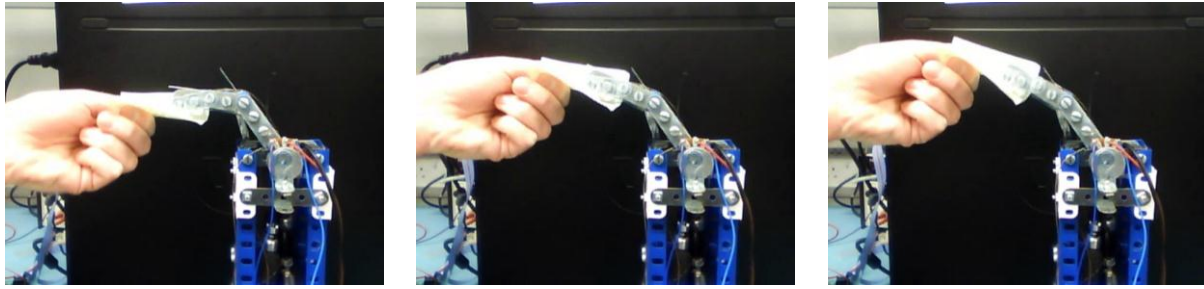
Figure 3.33: Video's snapshots of Design H detecting a piece of paper.
Paper is touched in (a). Finger goes backward in (b) and (c) when the paper is maintained on the fingertip.

To recognise if the object in contact is solid or light, additional steps are added to the control loops. The full flowchart of object interaction is provided in Figure 3.34. First, the flexion of the proximal phalange stops when an object is touched. Its current position is then slightly reduced (by 3°) because of the small delay between the contact of the object and the creation of an angular setpoint. Next, if the medial and distal phalanges are not in contact with the object, they bend until they touch it. As soon as the force feedback overreaches 20_{16}, it is estimated the object is not a piece of paper. Therefore, depending on this inequality, the force target is selected either to grab a solid object or to make the finger goes backward if the object is identified as being very light.
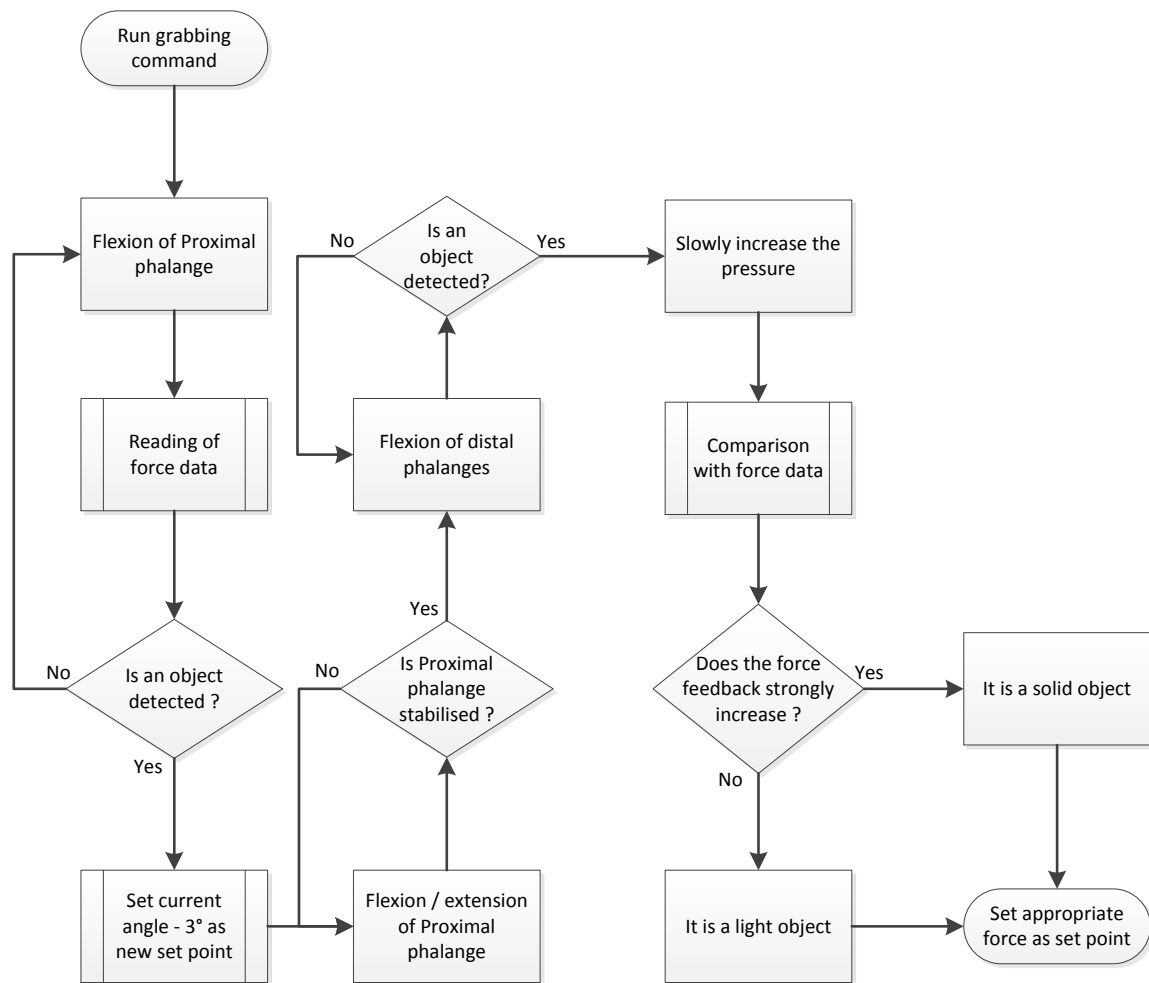
Figure 3.34: Flowchart of object interaction

The overall architecture of the project can be summarised as in Figure 3.35. The mechanical structure is connected to PAMs that are actuated by compressed air. According to the sensors' data feedback received by the electronic board, the electronic board sends signals to the valves to activate the PAMs until the target is reached by the mechanical structure.
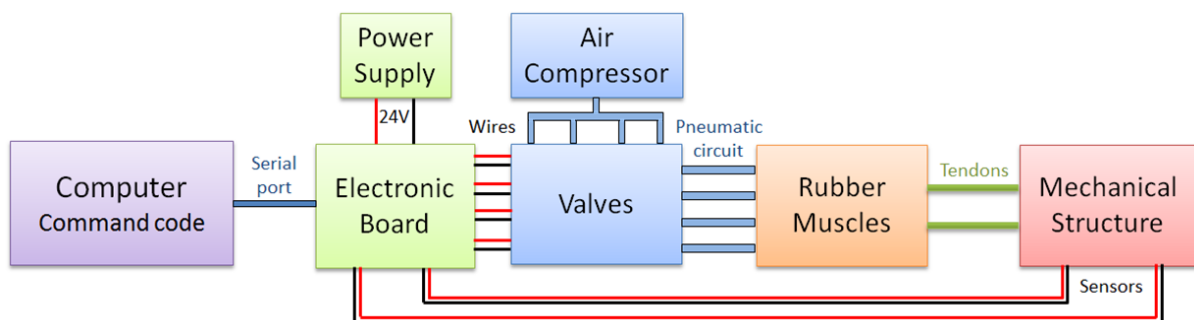
Figure 3.35: Feasibility study's architecture of the project

The control functions are then gathered in a GUI to ease the interactions between the finger and the user.

3.5. Implementation of control functions into a graphical user interface

Interactions between the robotic prototype and the user are increased by the design of a GUI. Therefore, the different control functions can directly be selected by clicking on the corresponding buttons. For this, the implementation of a free software and cross-platform library is investigated. As the Ambidextrous hand aims at being accessible on-line for a maximum of persons, the software must be compatible for Windows, Mac and Linux. The software Qt4 developed by Nokia [249] matches with all these standards, which is the reason why Qt4 is chosen to design a GUI integrating the commands of the Ambidextrous Hand.

The buttons are connected to widgets which direct the different functions to the files containing the actual finger's commands, written in C. A screenshot of the GUI is shown in Figure 3.36.
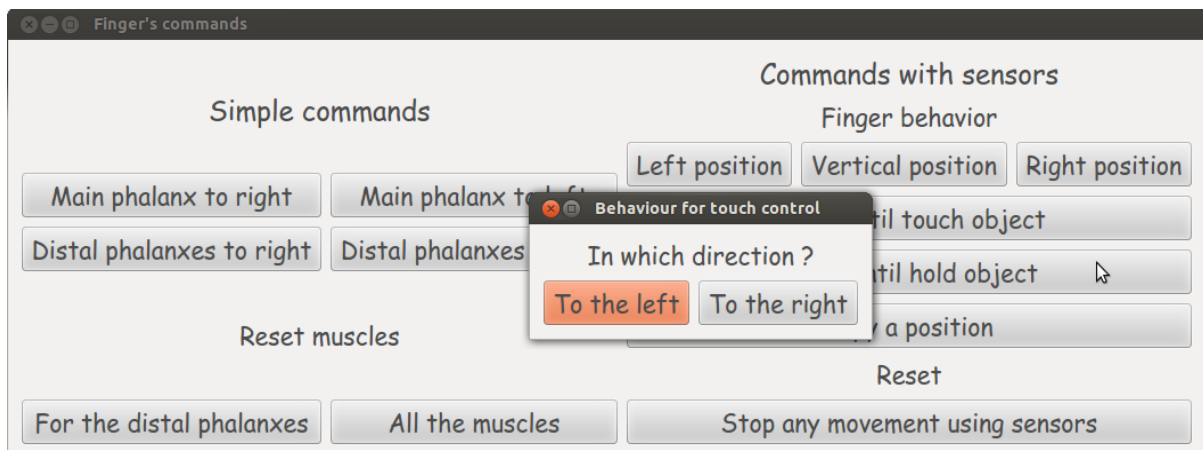
Figure 3.36: Screenshot of the GUI designed from Qt4

Additional functions are also connected to a number of buttons. Whenever buttons are clicked, processes are triggered to make secondary windows appear. Thus, the command can be executed either on the left or on the right side of the prototype.

The control functions called from the GUI are identical to the ones called from the RCI.

3.6.   Remote control interface

The RCI aims at providing a free and easy access to users from internet. Thus, the control functions discussed in Section 3.5 are integrated in a server connected to the robotic structure. It allows the robotic structure to execute commands received from its client through internet. This structure is close to the one described in [160] and mentioned in Section 2.3. Secondly, the internet network is connected to the Ambidextrous Robot Hand website, which acts as a second client, allowing user to send commands without downloading any client applications.

3.6.1. Connection with the server

The server does the connection between the control functions and the commands received from internet. The server architecture is shown in Figure 3.37. Even though the server is embedded on a Linux system, the use of Qt permits the users to access the Ambidextrous Hand from other OS. The development of the server is discussed in the report of A. Dilly [31], whereas the integration of the control functions in the server are discussed in the report of Z. Liu [250].
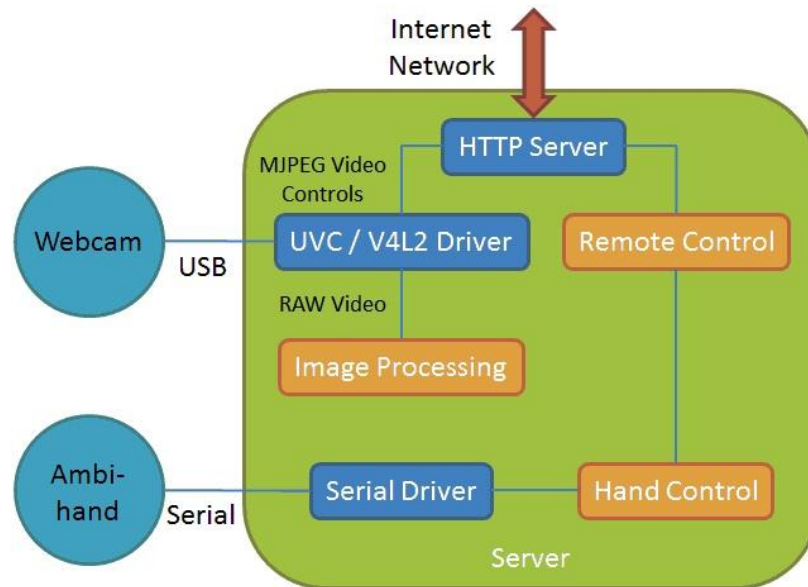
Figure 3.37: Server's architecture [31]

In addition to the remote actuation of the Ambidextrous Hand, the server allows to stream a video in real-time as feedback. The stream and the control functions are sent from the HTTP server, based on TCP/IP protocol. The server deals with HTTP requests, sending back the appropriate HTTP headers and XML messages to the two different clients developed for this application. The first one is a client developed on Qt4, described in [31] and [250]. It would allow the communication with the Ambidextrous Hand using advanced hardware devices, such as EMG signals.

The second client is a Web application, easily accessible from the Ambidextrous Robot Hand's website or from its Facebook application. It allows communicating with the robotic structure without downloading any clients. The design of this Web application is discussed in the report of F. Jourdan [251].

3.6.2. Interactions with the robot hand from the website

Although the Ambidextrous Robot Hand's website provides some visual information about the project's development, its main aim is to interact with the robotic structure online. The design of the website is described in the report of M. Heinrich [252]. Among the four different ways to interact with robotic movements, two are introduced in this section. The first one is possible by connecting to the Ambidextrous Hand's server. The second one is

about pre-recorded videos that are always accessible, even when the server is not running. The third and fourth ones are about HGR and EMG and are respectively introduced in [31] and [32].

3.6.2.1.   *Use of the server*

The Ambidextrous Hand's website includes a GUI permitting the communication between the user and the robotic structure. Thus, the work introduced in [251] is embedded in the design of the website [252]. When the user is connected to the server, a vision feedback is transferred from the embedded webcam. The implementation of the embedded webcam is discussed in [31].

Another GUI is designed for the website and Design H is replaced by a Science Museum Robotic Hand [35] to test the RCI. The Science Museum Robotic Hand is a device representing a right human hand actuated when a user pulls one of its tendons. Its elastic structure permits each of its fingers to come back to its vertical position when the user releases the tendon. Consequently, the hand can be actuated with five PAMs. As only four PAMs are at disposal, the ring and little fingers are tied together and cannot move independently. An example of the Science Museum hand control through the website is provided in Figure 3.38. Once the middle finger has been bent, the thumb bends as well in (a) and the hand is fully opened in (b).
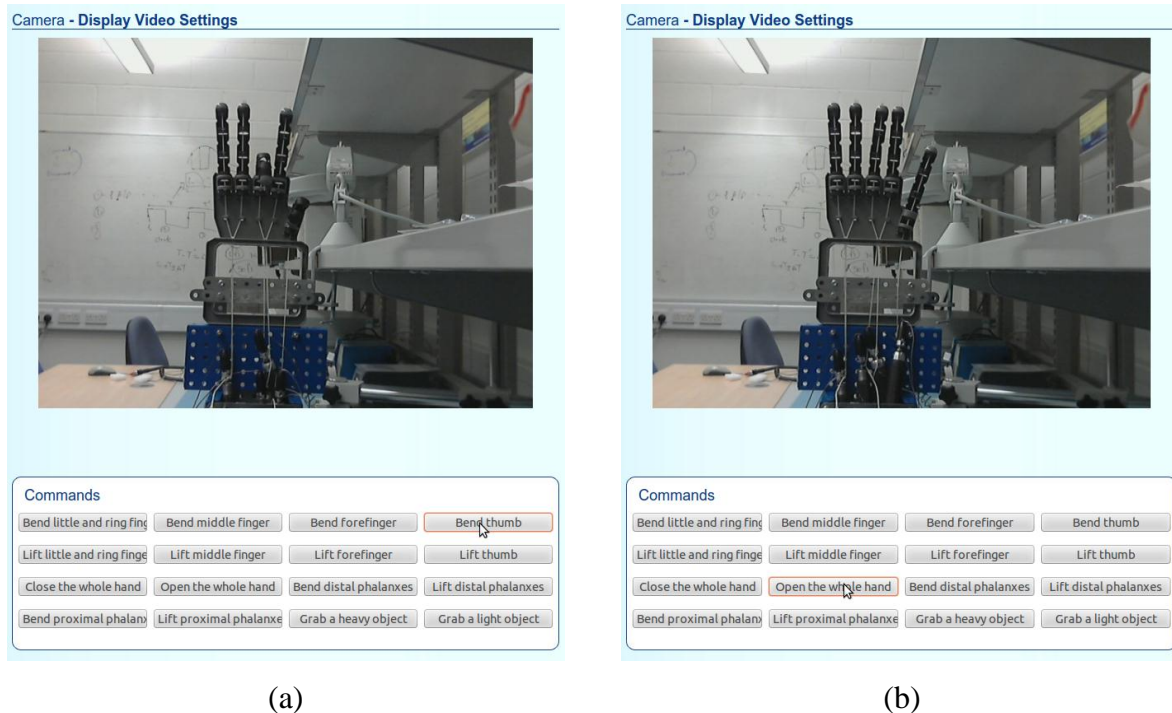
<div align="center">(a)   (b)</div>

Figure 3.38: Further examples of website's RCI.
(a) execution of "Bend thumb" button and (b) execution of "Open the whole hand button"

As VR contributes to ease the PLP, such as in [11] or [24], the RCI aims at being instantly accessible on internet and allowing an online HCI. Thus, the HCI permits the user to control a robot hand from distance. As for the mirror boxes, observing mirrored movements of an artificial limb can cause additional neural activity in motor areas located in the affected brain's hemisphere and thus lead to cortical reorganisation [21]. Watching the robot hand replicate the gestures imagined by the user can therefore allow the recovery of cortical maps [17]. As the PLP experienced after amputation is reduced according to the amount of cortical reorganisation [15], the pain of the user can therefore be reduced, using the same principle as the one of the mirror boxes [18], except that the Ambidextrous Hand's website is accessible from any places with an internet access. Nevertheless, other control methods based on HGR and EMG are explored in [31] and [32], as it would make the control of the hand more intuitive.

3.6.2.2.   *Comparison with other RCIs*

The RCI designed for the Ambidextrous Hand project is compared with the RCIs of other robotic limbs projects in Table 3.8. RCIs are not automatically implemented on robotic limbs projects, as for the bionic structures [26], [45] and [46] that aim at being directly

connected to the user's body and controlled by EMG signals. Another example of robotic device without RCI is the rehabilitation robot [28] which consists in a wearable exoskeleton used for rehabilitation exercises as a treatment available in a laboratory environment. Some articles specify that RCI or EMG interfaces should be integrated to specific projects. For example, the implementation of neural commands is discussed for the ACT Hand [27]. Another example is considered in [123], which indicates that the hand engineered by T. Maeno and T. Hino is designed for remote applications, even though nothing specifies that these RCIs have been developed. The DEXMART Hand is controlled by actuators remotely located in the forearm, but no other information is provided about the RCI [282]. It is also observed that data gloves are often used to control robotic structures, as for the hands [253], [72], [99], [143] and [62]. Robot hands can be controlled from distant locations with stereo display, such as [253] or [148]. However, none of these models propose a robot structure accessible from the website of their respective projects or an access from a social media interface. These features are consequently specific to the Ambidextrous Hand project.

Table 3.8: Comparison of the RCI of the Ambidextrous Hand project with RCIs of other robotic limbs projects

Robotic hands or arms	RCI	Video feed-back	Data gloves / wearable exoskeleton	EMG	Website application	Accesible from social media interface
DLR Hand [253], 2003	✓	✓	✓			
T. Maeno and T. Hino [123], 2006	N/A					
T. Kato et al. [148], 2010	✓	✓				
X. Jiang et al. [28], 2010			✓			
AMO arm [26], 2011	N/A			✓		
OCU Hand II [72], 2011	✓		✓			
C.Y. Lau and A. Chai [99], 2012			✓			
Bebionic3 [45], 2012				✓		
ExoHand [143], 2012	✓	✓	✓			
Shadow Hand [62], 2013	✓	N/A	✓			
ACT Hand [66], 2013	N/A					
Ambidextrous Hand project [39], 2013	✓	✓			✓	✓
I-limb ultra revolution [46], 2014				✓		
DEXMART Hand [282], 2014	✓					

3.6.2.3.   Use of pre-recorded videos

The remote control of the Ambidextrous Hand project is only possible when the server is running. However, the server is not constantly running as the robotic structure is often inaccessible because of software or hardware upgrades. An alternative solution is consequently investigated.

Recorded videos of the robot hand movements are included on the project's website. They allow simulating interactions with the robotic structure even when the computer system is not running or when the mechanical architecture is under maintenance.

Thus, the behaviour of the hand is reduced to 32 videos, which represent the basic fingers' movements feasible from an initial position. This starting position is chosen as the one with the five fingers extending. Two main behaviours are then possible for each finger: to bend or to stay motionless. It makes a total of 2^5, i.e. 32 possibilities. Both bending and extending are recorded on the videos to reach a total of 64 different gestures.

As no complex movements are recorded, it is this time possible to design a GUI without any text, more intuitive and easier to familiarise with. Thus, five coloured buttons are put underneath the fingers they represent. Clicking the buttons makes their colour switch from blue to red or from red to blue and indicates which fingers bend if the corresponding video is played. An example of the application is showed in Figure 3.39, with the bending of index and middle finger.

(a)   (b)
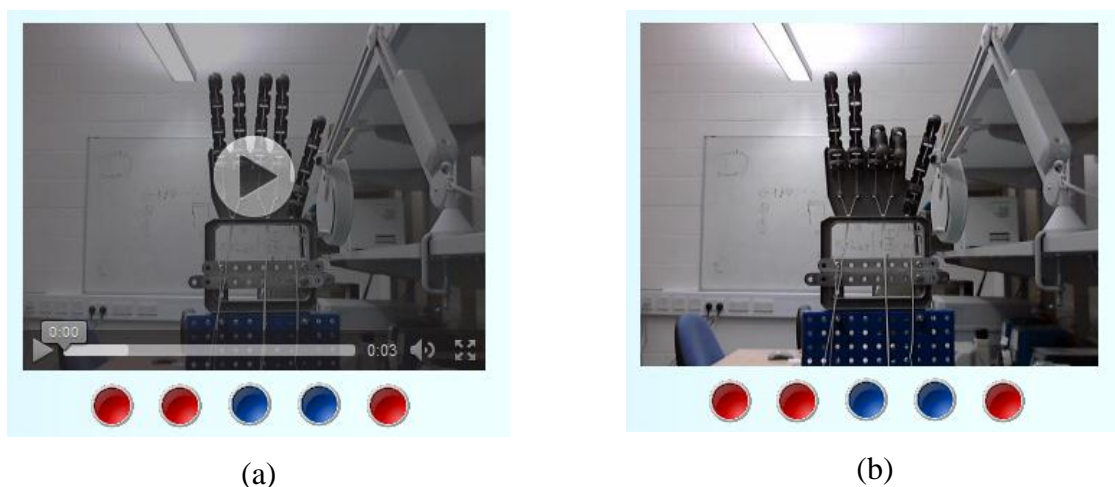
**Figure 3.39: Example of the videos' application on the Ambidextrous Robot Hand's website
(a) shows the selection of fingers whereas (b) shows the actuation of the selected fingers**

3.7. Chapter summary

This chapter has summarised the feasibility study for the Ambidextrous Robot Hand project.

It first started with the introduction of the material that is used for the experiments. This includes the pneumatic and the electronic interfaces, as well as the ways they are connected and depend of each other.

Secondly, the chapter discussed with a number of ambidextrous fingers prototypes designed with Meccanos. The section contained an analysis of their different mechanical features as well as descriptions of mechanisms used to actuate the different prototypes.

A feasibility study about control theory was also presented. As the mechanical design has not reached its final form yet, only PID controllers were used to control the finger's prototype. PID loops were chosen as they are very widespread in the area of embedded systems, even for PAM technology. The PID loops were combined with angular and force sensors. Their implementation was successful in both cases.

Finally, the control functions were connected to an RCI. The RCI is proper to the project as it makes the robotic structure instantly accessible and controllable through internet, from the website of the project.

The preliminary experimental results of the feasibility study demonstrate that it is possible to design and provide stable control with ambidextrous features. Thus, further enhanced designs of ambidextrous fingers and, consequently, of a robot hand are considered in the following Chapter.

Chapter 4: From a single finger to a whole ambidextrous robot hand

This chapter focuses on further architectural development. The mechanical, electronic and pneumatic interfaces are further enhanced and applied to control an ambidextrous robot hand.

First, the implementation of an interface to test advanced prototypes of ambidextrous fingers is discussed. Specifically, the focus is on the choice of sensors, the way they are implemented, the design of a testbench, the mechanical features of the final prototypes and the analysis of data collected from the experiments.

Secondly, the different electronic and pneumatic requirements from a single robotic finger to a whole ambidextrous robot hand are explored. Therefore, the electronic and pneumatic interfaces are adapted to the scope of a robot hand.

Finally, this chapter describes the mechanical specifications of the Ambidextrous Robot Hand. These characteristics have to be taken into account before discussing the control algorithms introduced in Chapter 5.

4.1. Testing of advanced prototypes

This Section discusses the implementation of interfaces used to test advanced prototypes of ambidextrous fingers, most of them being designed using 3D printing. Indeed, the design of ambidextrous fingers aims at being optimised before being integrated in a whole robot hand. The methodology and the process of these designs are discussed in the report of A. Nimmo, L. Kavanagh, L. Steele and M. Simko [254].

Prior to testing such prototypes, a test rig needs to be implemented. The test rig must include a surface suitable for the experiments. Therefore, it must include devices to hold PAMs, pulleys and the fingers' prototypes. It must also incorporate sensors to collect and compare data from the different prototypes.

First, this Section consequently discusses the choice of the material, to investigate which are the most suitable choices for the testing of prototypes. Secondly, it describes the design of the testbench itself. Next, it introduces the way the sensors are implemented in the system. The behaviour of PAMs is then analysed in detail so that their mechanical characteristics can be taken into account for the designs of prototypes. Finally, the features of ambidextrous fingers are collected and analysed prior to designing a whole ambidextrous hand.

4.1.1. Choice of the material

Specific devices are chosen to collect data when the advanced prototypes are running.

The first devices discussed in this Section are load cells, which allow measuring the force provided by PAMs. Their accuracy and their maximum capacity must be compatible with the PAMs' mechanical features.

The second devices are pressure transducers, which measure the pressurised air introduced in PAMs. As for load cells, both their accuracy and their maximum capacity must be compatible with the PAMs' characteristics.

The third devices are turnbuckles, which permit adjusting the tendons' length before the experiments. Their length if the main feature that is investigated, as an optimal length would reduce the area of the testbench.

The assembling structure of these three devices with PAMs is illustrated in Figure 4.1. The PAM is connected both to a pressure transducer and a load cell that respectively measure the pressure and the force of the device. A turnbuckle adjusts the length of the set up, as the PAM must be connected to a mechanical architecture and the load cell must be fixed on a test rig.
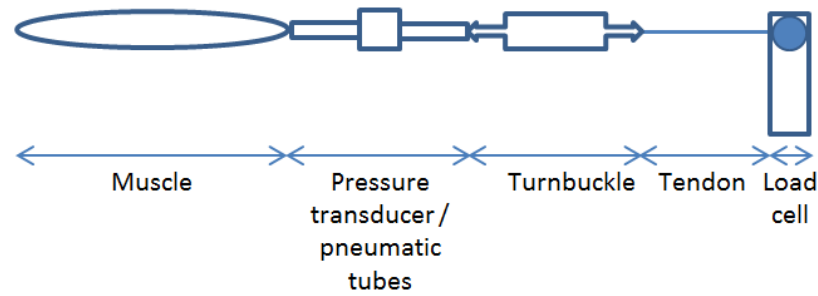
Figure 4.1: Set up of a PAM, a pressure transducer, a turnbuckle and a load cell

Other devices are implemented to collect data from the experiment, but they are not discussed in this thesis. Indeed, position sensors are also developed to be combined with load cells and pressure transducers. Their development is introduced in [254] and in the report of A. Huynh [255].

4.1.1.1.   *Load cells*

Load cells are investigated to be fixed at the base of PAMs. Thus, the force that PAMs apply to fingers can be obtained to provide mechanical feedback.

Prior to being implemented, load cells must be chosen according to their technical features, which must be compatible with the PAMs and the test rig. According to [80], SPAMs can hold up to 12 kg, which is why load cells must have a maximum capacity at least equal to this mass. The shape of the load cells is another parameter to be taken into account. The S-shaped load cells can indeed be fixed directly on the holding pieces of the testbench, whereas rectilinear load cells require more room and a specific shaping of pieces before being fixed. Thirdly, a low rate of error allows collecting more accurate data. Consequently, the main features investigated for the type of load cells are their maximum capacity, their shape and their accuracy. A list of different types of load cells currently available on the market is provided in Table 4.1, with a comparison of their main features.

Table 4.1: Comparison of technical features between different load cells

Sensors' names / codes	Maximum capacity (kg)	Shape	Implementation	Error max. (%)
TSA Alloy Steel S Type Load Cell / 1131 [256]	100	S	Compact	0.015
S Type Load Cell - Model 615 [257]	200	S	Compact	0.05
3134_0 Micro Load Cell CZL635 [258]	20	Rectilinear	Bulky	0.05
3135_0 Micro Load Cell CZL635 [259]	50	Rectilinear	Bulky	0.05
3132_0 Micro Load Cell CZL616C [260]	0.78	Rectilinear	Bulky	0.05

Because of the "S" shapes of the load cells 1131 [256] and 615 [257], these models are the easiest to implement. However, they are about fifteen times more expensive than the two models CZL635, [258] and [259], or than the model CZL616C [260]. This is the reason why the "S" shapes are not considered any more. As PAMs can hold up to 12 kg and that the 3134_0 micro load cell CZL635 has a maximum capacity of 20 kg, it is the chosen load cell to proceed with the tests. The 3135_0 Micro Load Cell CZL635 has the same price, but its higher range would imply longer electronic calibrations to reach accuracy as high as the one obtainable with the 3134_0 micro load cell CZL635.

4.1.1.2. *Pressure transducers*

Pressure transducers are investigated to measure the air pressure of PAMs and to collect data during the testing of models. The range of their pressure readings is the main technical feature that is considered. The transducers must have a minimum pressure reading of 0 bars and a maximum one at least 3.5 bars, as it is the maximum pressure used to actuate the SPAMs [80]. However, it is preferable to aim for a higher pressure reading in case SPAMs would be replaced by FPAMs for a next stage of the project. Indeed, FPAMs have a higher maximum input pressure that can vary between 6 and 8 bars according to the models [81]. [80] and [81] also indicate that the PAMs' hysteresis may change their extending from 3% to 7%. Consequently, the transducers' maximum error must be lower than 1% to collect applicable data.

The two other parameters relative to pressure transducers do not depend on PAMs characteristics. The first of them is their pressure measurement type, which can be absolute,

gauge or differential. Absolute measuring transducers compare the air pressure of PAMs with perfect vacuum, whereas gauge ones compare it with atmospheric pressure and differential ones compare it with the pressure another joint, which can be connected to atmospheric pressure as well. The type of measure must be taken into account in a second stage, for the implementation of the transducers, but does not interfere with the accuracy of data collection. The second parameter that must be taken into account is the port style, which can be dual or single axial as well as barbed or barbless. As PAMs work in an independent way, only single axial transducers must be investigated. Barbless ports prevent connecting directly the transducers to the pneumatic tubing, which is why barbed ports are more adapted to the pneumatic system.

A number of pressure transducers currently available on the market and reading a maximum of more than 3.5 bars are gathered in Table 4.2. The minimum pressure reading for each of these sensors being of 0 bars, this feature is not indicated.

Table 4.2: Comparison of technical features between a number of pressure transducers

Pressure transducers' name / code	Maximum pressure reading (bars)	Pressure measurement type	Port style	Error max. (%)
Absolute pressure sensor for air, MPX5700AS [261]	7.00	Absolute	Single Axial Barbed	2.5
Absolute pressure sensor for air, MPX5700AP [261]	7.00	Absolute	Single Axial Barbed	2.5
Honeywell S&C - HSCMANN100PGAA3 [262]	6.89	Gauge	Single Axial Barbed	0.35
Honeywell S&C - TBPLLNN060PGUCV [263]	4.14	Gauge	Single Axial Barbless	0.15
Honeywell S&C - NSCDANN150PGUNV [264]	10.34	Gauge	Single Axial Barbed	0.25
Honeywell S&C – 40PC150G2A [265]	10.34	Gauge	Single Axial Barbless	0.25

First, Table 4.2 indicates that the two models MPX5700 [261] have a maximum error of 2.5%, which make them not accurate enough to collect applicable data. However the sensors designed by Honeywell [262], [263], [264] and [265] match with the required accuracy. Contrary to the MPX5700 models, it is noticed their pressure measurement type is gauge instead of absolute. The model TBPLLNN060PGUCV has a barbless port, which prevents the direct connection of pneumatic tubing. Barbed ports are indeed more adapted to the pneumatic tubing as the tubes can fit directly to the transducers. Moreover, the maximum pressure reading of the model TBPLLNN060PGUCV is 4.14 bars. Although it is enough for

the SPAMs, it is preferable to aim for a higher pressure reading, in case the PAMs of the project are changed for a next stage. As FPAMs have a maximum input pressure varying between 6 and 8 bars [81], it is more suitable to choose sensors able to read up to 8 bars. As the model TBPLLNN060PGUCV, the model NSCDANN150PGUNV requires the design of an analogic amplifier to read its output signal properly. Given that the model 40PC150G2A is barbless and about 50% more expensive than the model HSCMANN100PGAA3, the model HSCMANN100PGAA3 is chosen. Even though it can only read up to 7 bars instead of 10.34, it is specified in [262] that it can endure a pressure up to 17.24 bars.

4.1.1.3.   Turnbuckles

Turnbuckles are investigated to be fixed between the PAMs and the load cells. Their aim is to adjust the tendons' length during mechanical calibrations, prior to testing the range of the prototypes. The length of the turnbuckles is the first mechanical feature to be considered, as it is preferable they take a minimum of place on the testbench. The second main feature is the diameter of the screws. The larger the screws, the higher the work load limit. The work load limit must be high enough to endure the maximum of 12 kg provided by the SPAMs. According to [266], an M3 screw allows a maximum load of 200 kg whereas an M4 screw permits a maximum load of 325 kg, which make them compatible both with SPAMs and FPAMs. These two characteristics are compared in Table 4.3.

Table 4.3: Comparison of mechanical features between a number of turnbuckles

Turnbuckles' name / code	Length (mm)	Diameter of the screw
M8 xy2cz404 [267]	70	M8
M6 xy2cz402 [268]	60	M6
Hook-eye bzp zinc plated 6mm [269]	155	M6
8mm hook-eye OBTHE-08 [266]	200	M8
4mm Eye-Eye LBEE-04 [270]	143	M4

Each turnbuckle summarised in Table 4.3 has a screw with a diameter equal or higher to M4. Each turnbuckle consequently has a maximum load equal or higher than 325 kg [270], which make them compatible with PAMs (SPAMs endure a maximum load of 12 kg [80]). The model M6xy2cz402 [268] is the shortest ones, and its price barely exceeds the ones of the models hook-eye bzp zinc plated 6mm [269] or the model 8mm hook-eye OBTHE-08 [266]. The model M6xy2cz402 is consequently chosen.

4.1.2. Design of the testbench

The design of the testbench consists in having a working environment suitable for testing and data collecting. The mechanical disposal is consequently divided into two parts, which are the testbench itself and the holding pieces, designed to hold the electronic devices and the prototypes of ambidextrous fingers.

4.1.2.1. *Global pattern of the testbench*

The testbench is divided into five main parts. The first part is made of the structures holding the load cells, which provide feedback about the force applied by PAMs. The second part is the routing between the PAMs and the load cells. This second part includes the turnbuckles that settle the length of tendons as well as the pneumatic connections. These pneumatic connections include the PAMs' inputs and an output that is directed to the pressure transducers. The third part of the testbench is used for letting enough room to the PAMs themselves. The fourth part consists in the routing between the PAMs and the prototypes. This fourth part is made of pulleys and distance sensors, the development of which being discussed in [254]. The fifth part is made of the structure holding the prototypes. A global pattern of the Ambidextrous Robot Hand's testbench is shown in Figure 4.2. A similar testbench structure can be seen in [271], which introduces a solution to measure tendon tension and joint torque of tendon-driven robots.
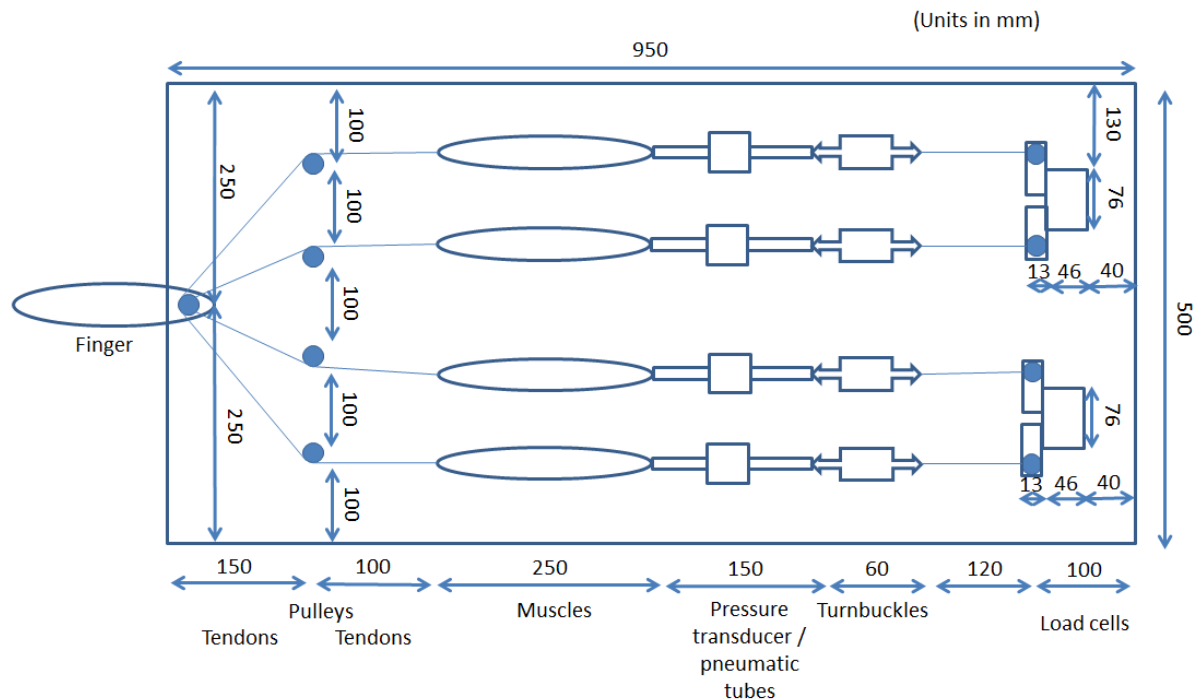
Figure 4.2: Global pattern of the testbench

As specific lengths are required between the devices, the most suitable way to have such a testbench is to design it. Hard wood is strong enough to endure PAMs' contraction without any deformations, can be drilled easily and is cheap, which is why it is the chosen material to design the testbench. The board has dimensions of 950 mm × 500 mm × 3.3 mm. It is both long and large enough to dispose the robotic architecture and thick enough not to be deformed by the finger's actuation. A row of four holes is drilled in the testbench, at 63 mm of the side of the load cells. Structures holding the load cells will be screwed at these points. After having the experimental surface set up, the design of additional structures is explored.

4.1.2.2.   *Design of wooden cuboids*

Holding structures are designed to be fixed on the testbench. These structures are chosen to be wooden cuboids, are this shape fits with the platform's requirements. Their width must be thick enough not to deform themselves when the PAMs contract. Their length must be long enough to hold a couple of load cells CZL635 [258], for which the dimensions are 55.25 mm × 12.7 mm × 12.7 mm. However, only one of the load cells' extremities is fixed to the cuboid. The second one is linked to the PAMs. Therefore, less than half of their length is hold by the cuboids. The cuboids must also hold the load cells high enough to

connect them to the PAMs, themselves connected to the prototypes. It is so decided to shape cuboids of dimensions 76 mm × 46 mm × 55 mm, as it fits with the requirements.

A part of the load cells 3134_0 CZL635 is made of resin to cover the stress gauge [258]. Thus, metal pieces are shaped to be fixed on the metal parts of load cells and isolate the resin. Holes of 4 mm and 6 mm are then drilled to put M4 or M6 screws inside the cuboids. Two load cells screwed to a cuboid are shown in Figure 4.3. The screw fixing the cuboid is cut in a thread. Its first extremity is fixed with a locknut, whereas its second extremity is tight with two nuts, to prevent any displacements during the measures.

(a)

(b)
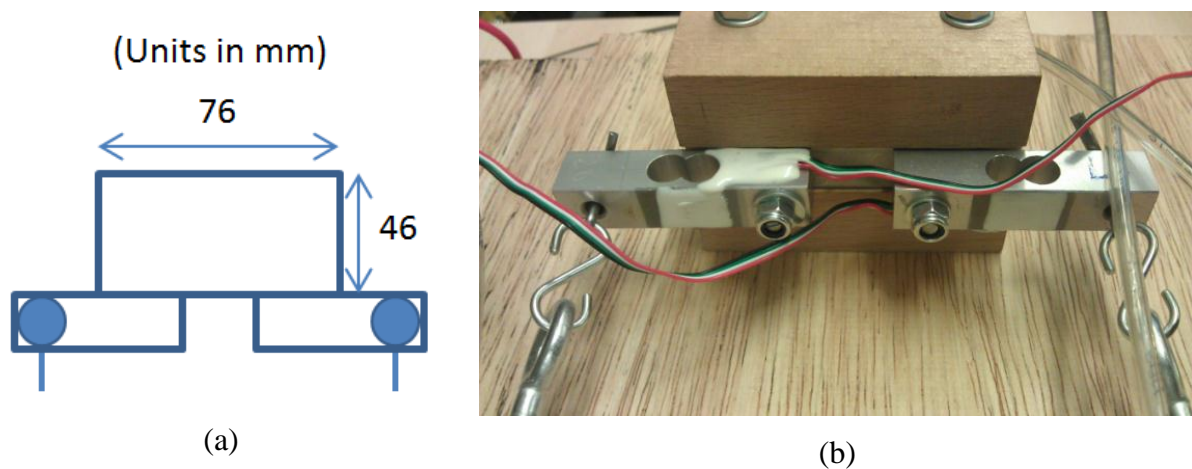
Figure 4.3: Wooden cuboid holding two load cells
(a) a scheme from Figure 4.2 and (b) the actual implementation

A picture of the overall implemented testbench is showed in Figure 4.4. The load cells are connected to the turnbuckles, themselves connected to the PAMs. The implementation of pulleys is discussed in [254].

Figure 4.4: Picture of the testbench with the PAMs connected to a finger prototype

4.1.3. Implementation of sensors

The third stage of the testing of advanced prototypes consists in implementing the sensors in the system and making their feedback compatible with the MCU. The MCU used at this stage of the project is an Arduino Mega 2560, for which the choice and the development of the hardware are introduced in [255].

In this Section, the implementation of load cells mainly consists in designing amplifiers and calibrating the output signal.

On another hand, the implementation of pressure transducers consists in calibrating their output signals with a Dead Weight Pressure Gauge and to convert the obtained values into bars.

4.1.3.1.   Implementation of load cells

Experimental work shows that the output voltage provided by the load cells 3134_0 CZL635 [258] only varies from 0 mV to 5 mV when the weight to which it is connected varies from 0 kg to 12 kg. Such a voltage difference would not allow detecting variations caused by a force's difference of 1 kg. Indeed, the voltage difference should be large enough to detect a variation caused by a weight of 100 g. Thus, the data collection would be sufficiently accurate to properly analyse the PAMs' behaviour. Amplifiers are therefore

designed for this purpose. Next, an experiment is run to check if the data collected from the load cells matches with expected values determined by calculations.

4.1.3.1.1.   Design of electronic amplifiers for load cells

Based on experimental observation, it is noticed that the output of load cells must be connected to amplifiers. Indeed, applying a load of 10 kg on the 3134_0 CZL635 load cell, the output voltage only varies from 0.00 V to 0.04 V. As this voltage is not high enough for accurate measures, amplifiers must be designed prior to using load cells for the experiments.

As the Arduino MCU receives inputs of a maximum of 5 V [150], the design of an amplifier multiplying the input by 100 is a suitable option. As the SPAMs are not designed to exceed a pulling force of 12 kg [80], the output voltage obtained for such a force would be 4.8 V. Such a voltage suits with the MCU's specifications.

Consequently, a two steps amplifier is designed using chips LF356 [272]. A scheme of the amplifier is shown in Figure 4.5.
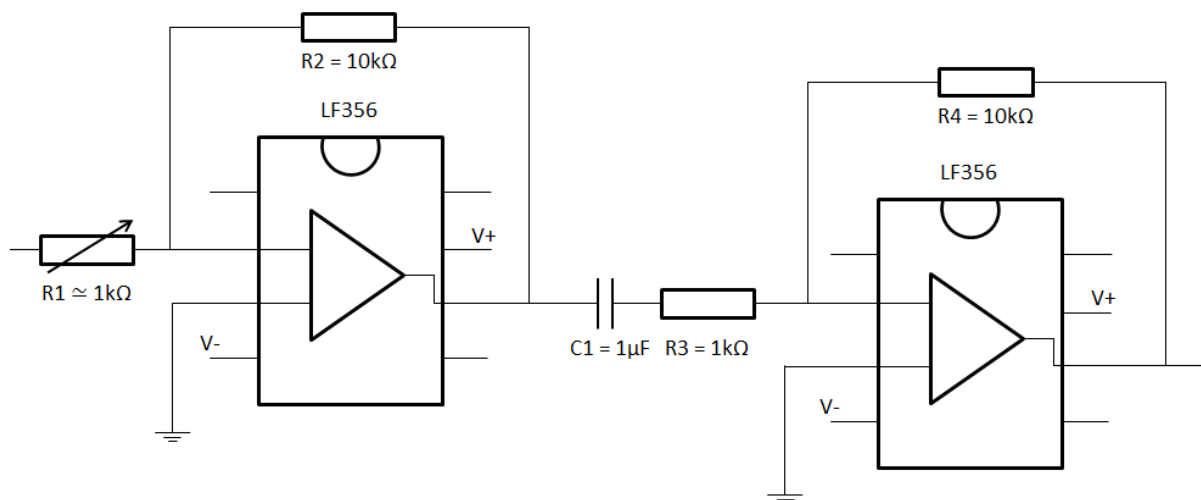
Figure 4.5: Amplifier × 100 using LF356 [272]

The theoretical value of the amplification *A* is obtained in equation (4.1).

$$A = \frac{R2}{R1} * \frac{R4}{R3}$$

(4.1)

$$A = \frac{10k}{1k} * \frac{10k}{1k} = 100$$

Even though the output voltage is amplified 100 times, the output of the amplifier depends of the accuracy of the components. The next step is to test the accuracy of the amplifier by hanging weights to the load cells.

4.1.3.1.2.   Calibration of load cells

The calibration of load cells is made using testing. Thus, experiments are done hanging weights to load cells and reading the output voltage on a voltmeter. The structure of the experiment is shown in Figure 4.6.

(a)   (b)
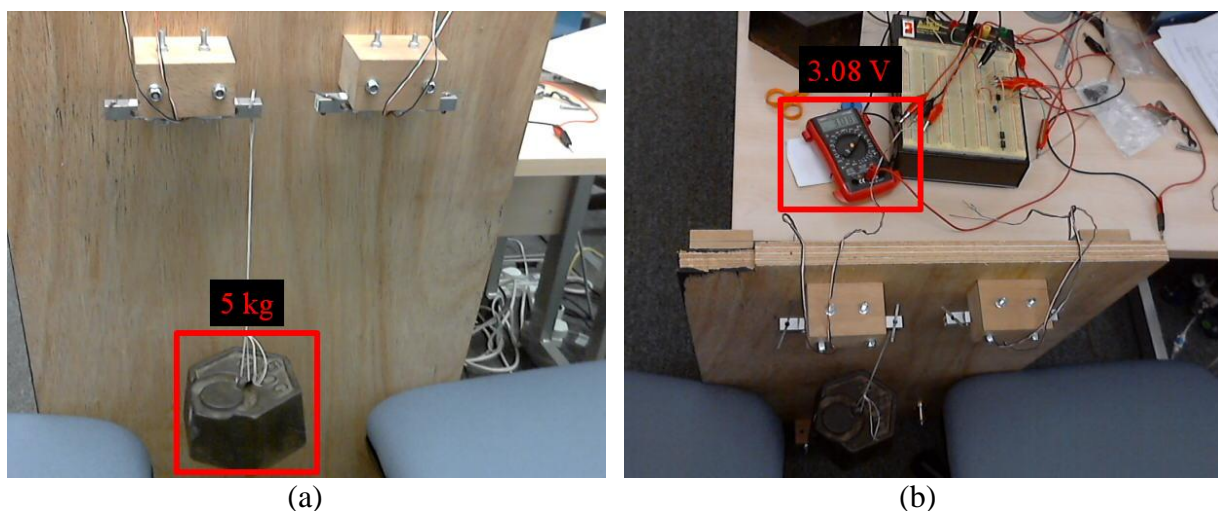
Figure 4.6: Load cell connected to a weight of 5 kg
(a) shows the weight and (b) the voltage received at the output of the amplifier

For a weight of 5 kg, the expected value readable on the voltmeter is 2.00 V. However, the experiment first shows a value of 3.08 V. Thus, the variable resistance is adjusted to reach exactly 2.00 V with 5 kg. A picture of the amplifier, which includes the variable resistance, is provided in Figure 4.7.
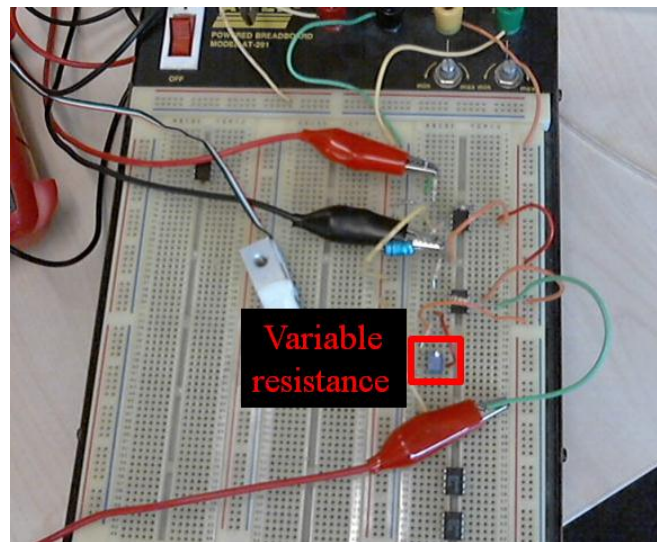
Figure 4.7: Operational amplifier connected to the load cell's output

From this calibration are tested other weights, from 1 kg to 12 kg. The expected values and the obtained values are gathered in Table 4.4.

Table 4.4: Load cell's calibration

Weights (kg)	Expected voltage (V)	Measured voltage (V)	Calculated error (%)
0	0.00	0.00	0.00
1	0.40	0.40	0.00
2	0.80	0.80	0.00
3	1.20	1.19	0.83
4	1.60	1.60	0.00
5	2.00	1.98	1.00
6	2.40	2.40	0.00
7	2.80	2.78	0.71
8	3.20	3.19	0.31
9	3.60	3.60	0.00
10	4.00	3.99	0.25
11	4.40	4.39	0.23
12	4.80	4.78	0.42

Analysis of Table 4.4 shows that the system is not totally stable, as the previous output obtained with 10 kg was 4.00 V, whereas 3.99 V are obtained during the experiment. It is however noticed that the maximum error never exceeds 1%, which is suitable to collect data from the experimental setup. The conversion of the output voltage to newtons by the MCU is explained in [255].

The same scheme is then repeated with the three other load cells, so parallel data can be collected from a maximum of four PAMs.

4.1.3.2.   *Implementation of pressure transducers*

Contrary to load cells, the output voltage received from pressure transducers perceptibly varies when they are connected to the pneumatic circuit. The values collected from the Arduino Mega 2560 MCU [150] must however been converted into an applicable unit to be efficiently applicable. Pressure transducers are consequently calibrated using a Dead Weight Pressure Gauge Tester prior to converting their feedback values into bars. The following experiments have been completed in collaboration with [255].

4.1.3.2.1.   *Calibration of pressure transducers*

Pressure transducers must be calibrated before obtaining interpretable data as feedback. After the calibration, it will be possible to identify what is the ratio between the feedback of the MCU and the actual pressure which is measured. As the Arduino Mega 2560 MCU [150] converts the analogic feedback from 0 V to 5 V to an integer from 0 to 1023, the values must be converted into interpretable units, such as Pa or bars. Thus, pressure is measured using a Dead Weight Pressure Gauge tester while data is collected from the MCU. Picture of the Dead Weight Pressure Gauge are shown in Figure 4.8.

(a)

(b)

Figure 4.8: Dead Weight Pressure Gauge Tester, (b) is a zoom on (a)

The Dead Weight Pressure Gauge includes a chamber filled with oil, for which the pressure can be regulated turning a wheel. The experiment consists in connecting the pressure transducer to the output varying the oil level. Meanwhile, different weights are placed around a piston. When they lift, it means the pressure to which they match, indicated in PSI, is reached. The experiment has been repeated until reaching 6.5 absolute bars, which is close to the maximum readable value indicated by the datasheet of the transducer HSCMANN100PGAA3 [262]. Even though SPAMs do not exceed 3.5 bars for a safe actuation [80], calibrating the transducers up to 6.5 bars can be useful if SPAMs are substituted by FPAMs [81].

The average results of the experiments are shown in Table 4.5. The conversion from PSIs to bars is done using the equality 1 PSI = 0.0689475729 bars. As the transducer HSCMANN100PGAA3 is made of a vacuum gauge [262], atmospheric pressure is taken into account, which is why bars are read from a value of 0 instead of 1. It is also the reason why the averaged Arduino Mega 2560 MCU [150] values start from 100 instead of 0.

Table 4.5: Calibration of pressure transducers

Averaged Arduino Value	PSI	Bars
100	0	0.00
184	10	0.69
225	15	1.03
266	20	1.38
307	25	1.72
347	30	2.07
389	35	2.41
430	40	2.76
471	45	3.10
513	50	3.45
554	55	3.79
596	60	4.14
638	65	4.49
680	70	4.83
722	75	5.17
764	80	5.52
806	85	5.86
848	90	6.20
890	95	6.55

The graph corresponding to the values of Table 4.5 is shown in Figure 4.9.
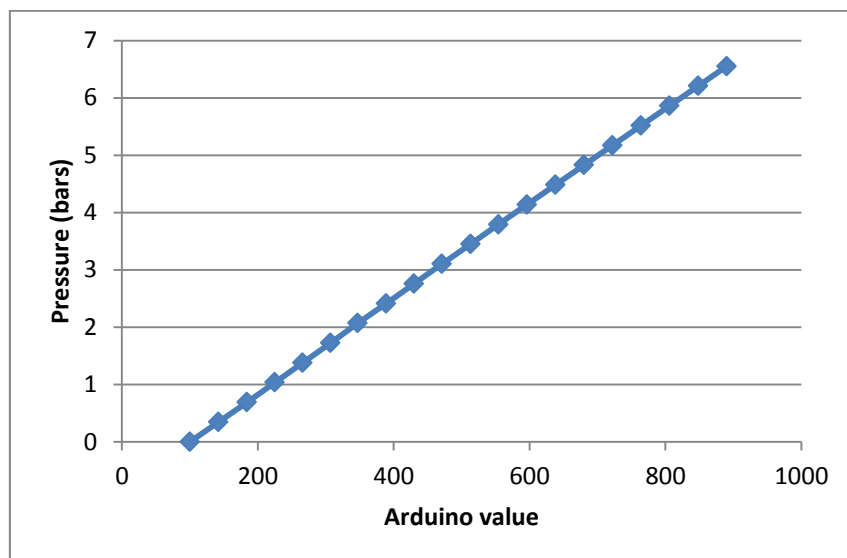
Figure 4.9: Graph of Arduino's numerical values against pressure (bars)

As the voltage input is proportional to the pressure, it is possible to check that the sensor HSCMANN100PGAA3 [262] is linear, the Arduino value increasing averagely of 41

106

units per 5 PSI. The next step consequently consists in finding coefficients to convert the values of the Arduino MCU into a unit applicable to pressure, such as PSI, kPa or bars.

4.1.3.2.2.   Conversion of the output of the pressure transducers

The numeric voltage indicated by the Arduino MCU needs to be converted into another unit applicable to pressure, such as bars. Thus, the relationship between the voltage V and the pressure p can be found identifying the coefficients of the line using equation (4.2).

$$p = aV + b \qquad (4.2)$$

where a is the slope of the line and b is the intercept.

The coefficient a can be obtained calculating the difference between the points coordinates of pressure and voltage of Figure 4.9, as done in (4.3).

$$a = \frac{p_2 - p_1}{V_2 - V_1}$$

$$a = \frac{6.55 - 0}{890 - 100} \qquad (4.3)$$

$$a = \frac{6.55}{790} \simeq 0.00829$$

Using the value of a, the coefficient b is calculated in (4.3), from the point $p = 6.55002$.

$$b = p - aV$$

$$\qquad (4.4)$$

$$b = 6.55002 - 0.00829 * 890 \simeq -0.82808$$

The relation between bars, noted p, and the MCU's feedback, noted V, is therefore defined in (4.5).

$$y = 0.00829x - 0.82808 \qquad (4.5)$$

Implementing the equation (4.5) in the Arduino MCU, the feedback signals received from pressure transducers can be converted into bars.

4.1.4. Measures of the variation of the muscles' lengths

The design of advanced prototypes requires measuring the PAM's behaviour with much accuracy as the simple measures made in Section 3.1.2.

The PAMs' behaviour is not only about the difference between their minimum and maximum lengths. As PAMs have an elastic behaviour, their length can vary for a same pressure, is the PAM is on a contracting mode or on an extending mode.

Thus, experiments are done linking weights to PAMs. The pressure is measured using a pressure transducer whereas the tendon displacement is indicated by a position sensor. The position sensor is in fact a Hall effect sensor, for which the design and the implementation are discussed in [254] and [255]. As shown in Figure 4.10, the rotating contact is connected to a magnet, itself connected to a rotary encoder that provides different voltage feedbacks according to the contact's angle.
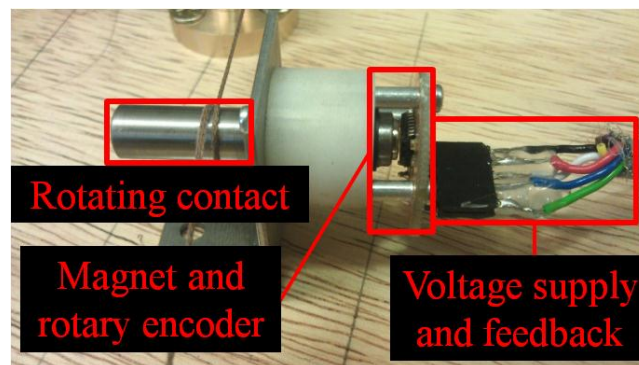
Figure 4.10: Hall effect sensor, [254] and [255]

A block diagram of the experiment is shown in Figure 4.11 (a). The weight varies from 0.5 kg to 10 kg. The experiments are run onward and backward five times, so the obtained results can be averaged. A picture of an early set up is provided in Figure 4.11 (b). Experiments were first done using a ruler to measure the length's displacement. These experiments have been completed in collaboration with [255].
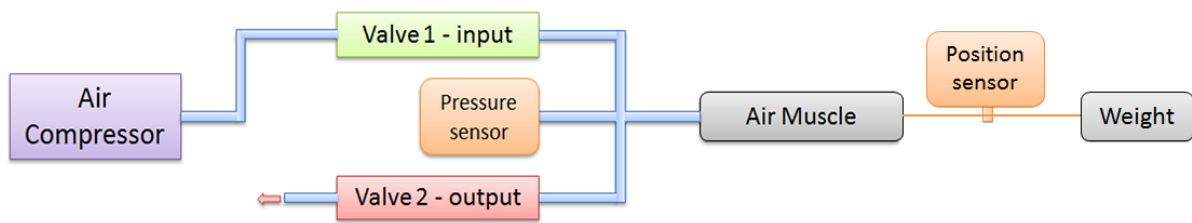
(a)
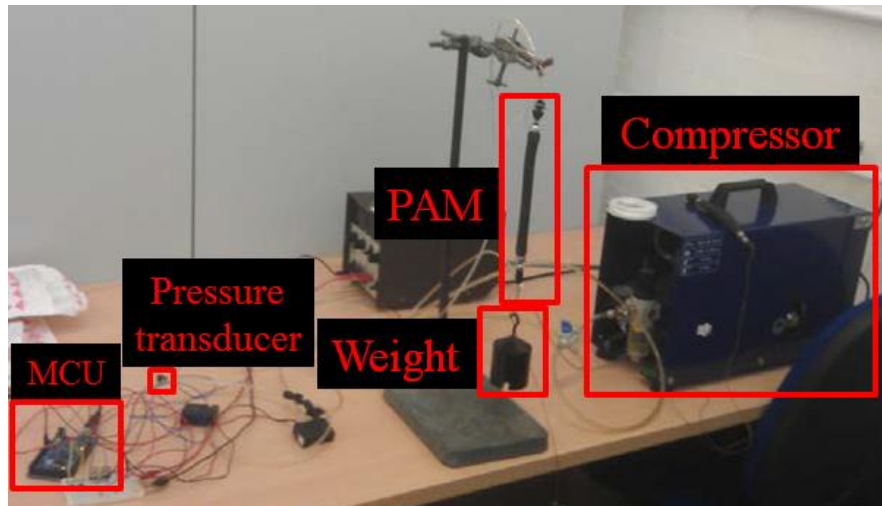
(b)

Figure 4.11: Set up of the SPAM's length's measure experiment.
(a) a block diagram and (b) the implementation with actual devices

In a second stage, the PAM is fixed to the testbench and connected to position sensors for a more accurate calibration. The 30 first values obtained with a weight of 500 g are gathered in Table 4.6, when the PAM is contracting. The same process is repeated when the PAM is extending.

Table 4.6: Measure of pressure and length when a SPAM is contracting

1st run		2nd run		3rd run		4th run		5th run	
Pressure (bars)	Length (mm)	Pressure (bars)	Length (mm)	Pressure (bars)	Length (mm)	Pressure (bars)	Length (mm)	Pressure (bars)	Length (mm)
0.00	252.1	0.00	252.1	0.01	252.1	0.01	252.1	0.00	252.1
0.14	252.1	0.17	252.1	0.15	252.1	0.15	252.1	0.15	252.1
0.29	252.1	0.32	252.1	0.29	252.1	0.30	252.1	0.29	252.1
0.42	252.1	0.44	252.1	0.42	252.1	0.42	252.1	0.42	252.1
0.54	252.1	0.56	252.1	0.54	252.1	0.55	252.1	0.53	252.1
0.64	252.4	0.66	252.7	0.64	252.5	0.64	252.1	0.62	252.3
0.72	253.2	0.73	253.1	0.72	253.1	0.72	253.1	0.71	253.0
0.79	254.2	0.80	253.8	0.80	253.8	0.80	253.8	0.78	253.5
0.85	255.0	0.86	254.4	0.85	254.4	0.85	254.4	0.84	254.2
0.91	255.2	0.92	254.4	0.91	254.4	0.91	254.4	0.90	254.4
0.97	255.2	1.00	253.1	0.98	253.3	0.97	253.5	0.97	253.8
1.05	253.8	1.13	249.4	1.12	249.6	1.12	249.8	1.11	250.2
1.22	250.0	1.27	246.4	1.26	246.4	1.26	246.6	1.25	246.8
1.30	248.0	1.43	243.3	1.41	243.4	1.41	243.6	1.41	243.8
1.45	245.1	1.57	241.1	1.57	240.9	1.56	241.1	1.54	241.3
1.61	242.8	1.72	238.8	1.72	238.8	1.71	239.0	1.70	239.2
1.76	240.8	1.87	237.1	1.87	237.2	1.86	237.3	1.85	237.3
1.91	239.0	2.03	235.6	2.01	235.7	2.01	235.8	2.00	235.8
2.03	238.0	2.17	234.4	2.16	234.5	2.15	234.5	2.14	234.5
2.20	236.2	2.31	233.3	2.30	233.3	2.29	233.5	2.28	233.5
2.33	235.2	2.45	232.4	2.43	232.2	2.43	232.4	2.42	232.4
2.46	234.3	2.58	231.5	2.56	231.4	2.55	231.6	2.55	231.6
2.71	233.1	2.70	230.7	2.70	230.7	2.68	231.0	2.66	230.9
2.82	232.4	2.86	229.8	2.81	230.1	2.79	230.3	2.84	229.8
2.93	231.9	3.02	229.2	2.92	229.7	2.95	229.5	3.00	229.2
3.08	231.2	3.15	228.6	3.07	229.0	3.10	229.0	3.14	228.6
3.21	230.7	3.28	228.2	3.20	228.4	3.23	228.4	3.25	228.2
3.33	230.3	3.39	227.8	3.32	228.0	3.34	228.0	3.36	227.8
3.43	230.1	3.49	227.6	3.42	227.8	3.45	227.8	3.45	227.6
3.51	229.7	3.56	227.4	3.51	227.6	3.53	227.6	3.53	227.4

Data from Table 4.6 reveals that the lengths obtained on the first run are a bit longer than the others. The same phenomenon happens with weights heavier than 0.5 kg. As the PAM is not stretched yet, its elasticity interferes in a different way for the first experiment. Consequently, first runs of the experiments are not taken into account to draw curves and analyse the behaviour of PAMs.

The same experiment is repeated and the average results obtained for weights from 0.5 kg to 10 kg are turned into curves, as showed in Figure 4.12. The shorter lengths are obtained during the PAM's contraction whereas the longer ones are obtained during the PAM's relaxation.
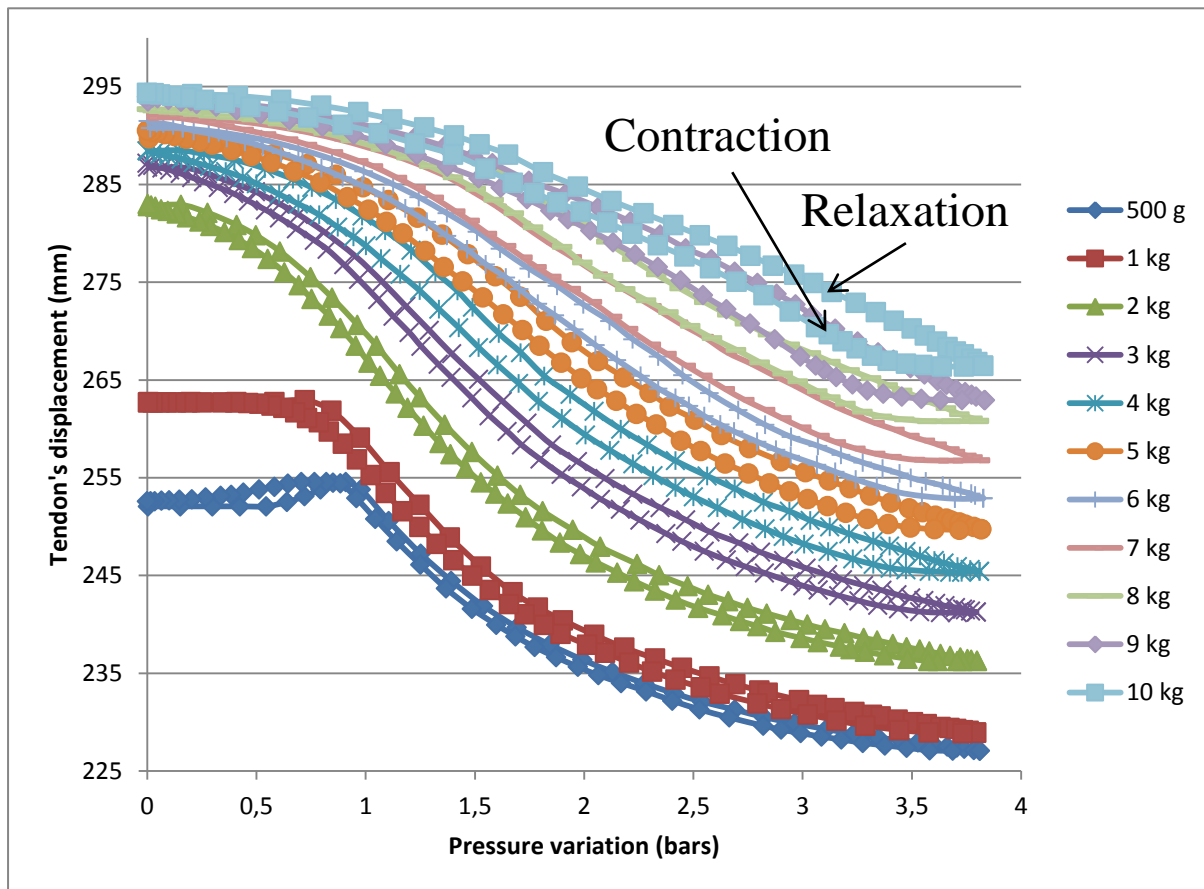
Figure 4.12: Pressure against tendon's displacement for different weights
Longer lengths are obtained during the PAM's relaxation

The PAMs' hysteresis is clearly visible from Figure 4.12. The nonlinearity increases both with pressure and weights. It is also noticed that PAMs extend before contracting when they pull a weight of 1 kg or less. This is explained by the fact PAMs are not fully stretched when they are linked to a weight not heavy enough. Therefore, the compressed air fills their length before expanding widthways and starting the contracting motion.

The obtained data is taken into account to design prototypes of ambidextrous fingers.

4.1.5. Mechanical features of the final version of ambidextrous fingers

The mechanical features of the final version of the ambidextrous finger are investigated prior to developing control algorithms in Chapter 5.

Thus, the specifications of the mechanical routing are explained first.

Next, data is collected when the ambidextrous finger moves from some positions to other ones. Experimental data is then analysed to see which sensors would be the most suitable for a full ambidextrous robot hand.

4.1.5.1.   *Tendon routings of the final version of ambidextrous fingers*

A number of more advanced prototypes have been tested before reaching an ambidextrous behaviour. The experimental methodology is the same as the one described in Section 3.3; the weak point of each prototype is analysed to reach better performances with next designs. The evolution of advanced prototypes of ambidextrous fingers is discussed in [254]. Prior to understanding the way data is collected in section 4.1.5.2 or to develop control algorithms, it is necessary to understand the tendon routing of the last prototypes.

As for most of the prototypes designed in Section 3.3, the first prototypes discussed in [254] use a symmetrical routing. Thus, the proximal phalange is driven by two tendons whereas the medial and distal phalanges are coupled and driven by two other tendons. Therefore, the actuation of the fingers is antagonistic. However, more advanced prototypes use a three tendons routing to minimise the number of PAMs. The two different kinds of routings are shown in Figure 4.13. These schemes were done using the Matlab software introduced in [38].
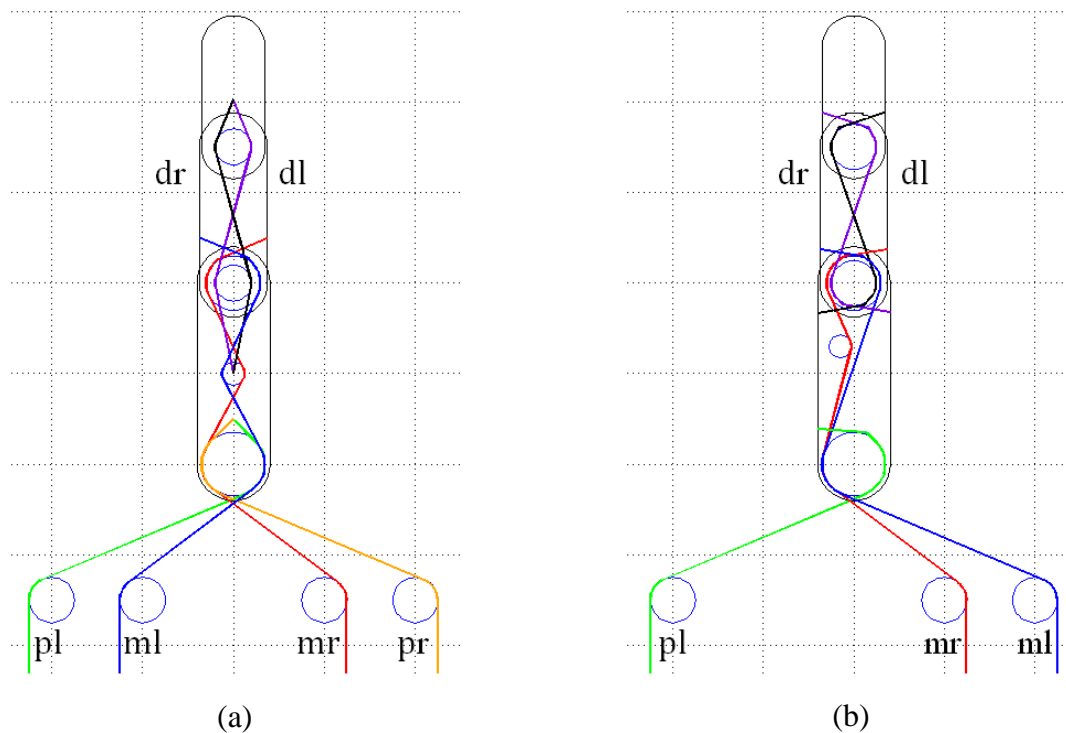
Figure 4.13: Evolution of tendons routings
(a) is a four tendons routings and (b) a three tendons routings

Figure 4.13 shows that black "dr" and violet "dl" tendons are passive tendons assuring a coupled motion between distal and medial phalanges. On another hand, green "pl", blue "ml", red "mr" and orange "pr" are active tendons, respectively actuating proximal left, medial left, medial right and proximal right phalanges. Furthermore, the proximal phalange observed in Figure 4.13 (b) is only driven by the green tendon "pl", instead of the two antagonist tendons "pl" and "pr" seen in Figure 4.13 (a). Therefore, it means the PAM actuating the proximal phalange on its right side is missing. The removed tendon action is compensated by pulling the two tendons "ml" and "mr" in synchronisation. Even though they actuate the medial and distal phalanges, the engineered routing allows the tendon to bend the finger to the right when they are pulled together.

The specificity of such a design is investigated through a collection of data.

4.1.5.2.   *Analyse of data collection*

Data is collected from the last ambidextrous finger prototype when it is driven to specific positions. Each of its phalange has three extreme positions: right, left and straight. As the finger's prototype is made of one proximal phalange and two other phalanges for which

the movement is coupled, it means the finger has nine extreme positions. These positions are numbered from 1 to 9. Position 1 refers to the proximal and medial/distal phalanges reaching both the maximum range on their left side. Position 2 refers to the proximal phalange reaching its maximum range on its left side, whereas the medial/distal phalanges are straight. Position 3 refers to the proximal phalange being on its maximum range on its left side, whereas the medial/distal phalanges are on their maximum range on the right side. Using the same code, positions 4 to 6 refers to the finger when the proximal phalange is straight. Last position, position 9, is when the proximal and medial/distal phalanges reach both the maximum range on their right side.

The fingers' prototype is driven to these positions using electronic pulses. An image and a block diagram of the experiment are shown in Figure 4.14. Most of the mechanical interface can be seen in Figure 4.14 (a) whereas the pneumatic and electronic connections are mostly illustrated in Figure 4.14 (b). Data is collected from pressure, force and position sensors. The feedback signals of these sensors are directed to the control module. The aim of this experiment is to analyse the ratio between pressure and force, respectively provided by pressure transducers and load cells.

(a)

(b)
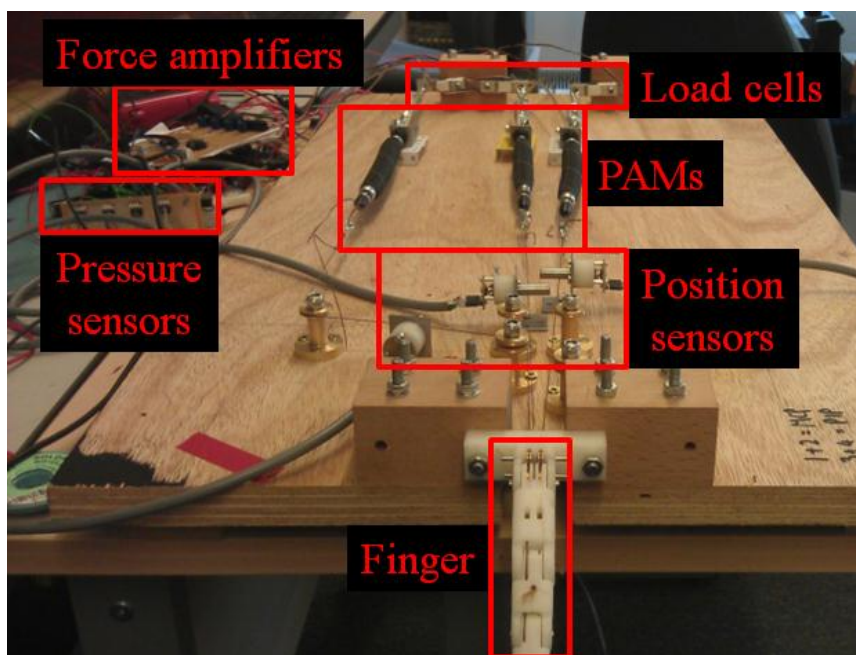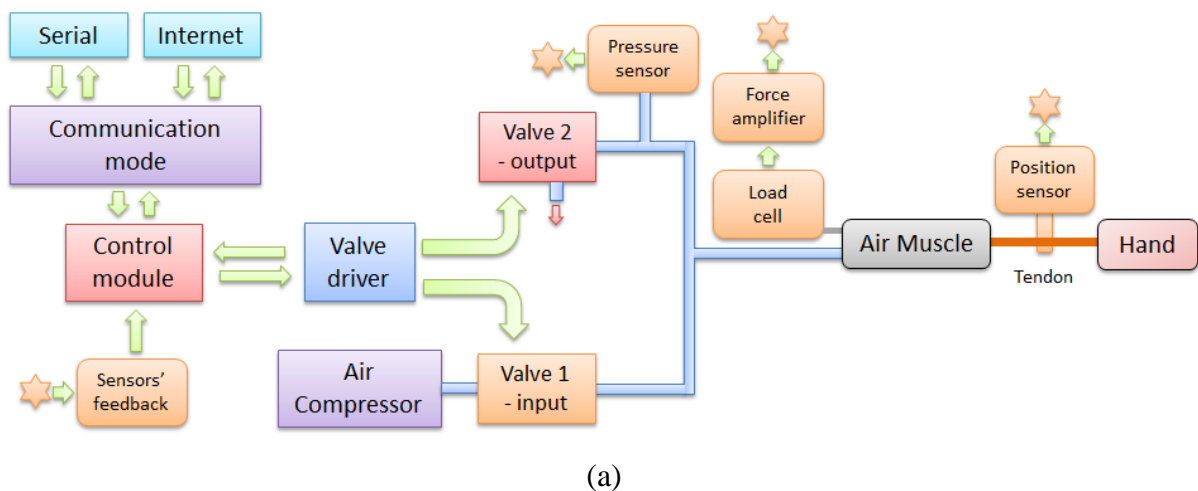
Figure 4.14: Implementation of a prototype driven by three PAMs
(a) a block diagram and (b) the actual implementation

Each time the prototype reaches one of its extreme positions, data is collected from pressure transducers, position sensors and load cells. The experiment is run thrice. The averaged experimental results of the runs are summarised in Table 4.7. The abbreviations PT, HS and LC respectively refer to pressure transducer, Hall sensor and load cell.

Table 4.7: Averaged data collection of the three runs, from extreme positions of a prototype

No. of position	PT[a]0 (bars)	PT[a]1 (bars)	PT[a]2 (bars)	HS[b]0 (mm)	HS[b]1 (mm)	HS[b]2 (mm)	LC[c]0 (N)	LC[c]1 (N)	LC[c]2 (N)
1	2.497	1.173	0.017	15.1	-0.2	-21.7	24	8	19
2	4.028	0.250	0.782	14.9	15.5	15.4	47	21	20
3	3.129	0.175	1.481	14.6	6.6	27.1	35	21	22
4	1.972	1.406	0.017	1.6	13.3	-8.2	26	20	20
5	2.954	1.115	2.363	1.8	1.9	3.3	55	17	42
6	1.643	0.357	2.617	2.0	-8.4	13.1	38	11	28
7	0.038	2.725	1.227	-13	26.4	5.2	17	13	17
8	0.022	1.411	2.039	-13	14.0	13.9	17	15	18
9	0.008	0.491	2.990	-13	4.5	25.1	17	7	16

[a] Pressure transducer
[b] Hall sensor
[c] Load cell

The values obtained from pressure sensors and load cells are averaged. Curves are then designed from these values, taking the position of the finger into account. The curves obtained for the sensors PS0 and LC0, which actuate the proximal left tendon of the finger, are showed in Figure 4.15. A multiplicative factor of seventeen is experimentally defined and applied on the value of pressure, to normalise it with the one of the force.
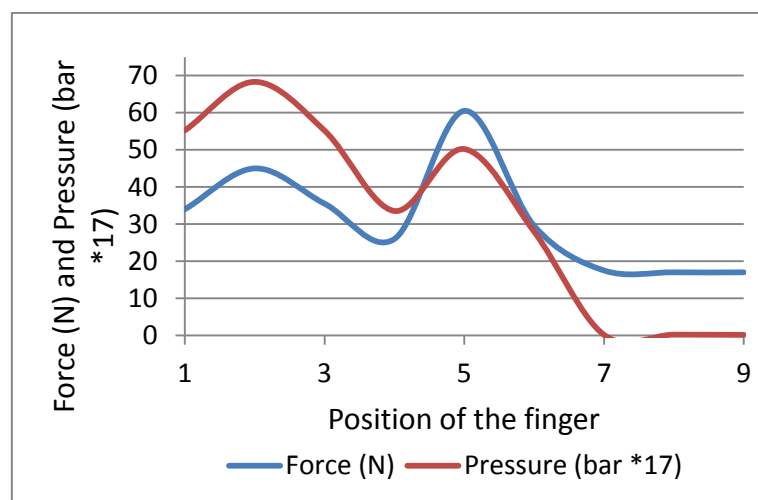
Figure 4.15: Force and pressure collected for the proximal left PAM against the position of the finger

Figure 4.15 shows that force and pressure have close behaviours for the proximal left PAM. The main difference can be seen from positions 7 to 9, when the proximal phalange is to its right side. Even though the proximal left PAM contains no compressed air, its tendon is stretched because of the force provided by the antagonistic PAM.

Feedback obtained with sensors PS1, LC1, PS2 and LC2 are drawn as well. The curves can be seen in Figure 4.16.

(a) Distal left PAM   (b) Distal right PAM
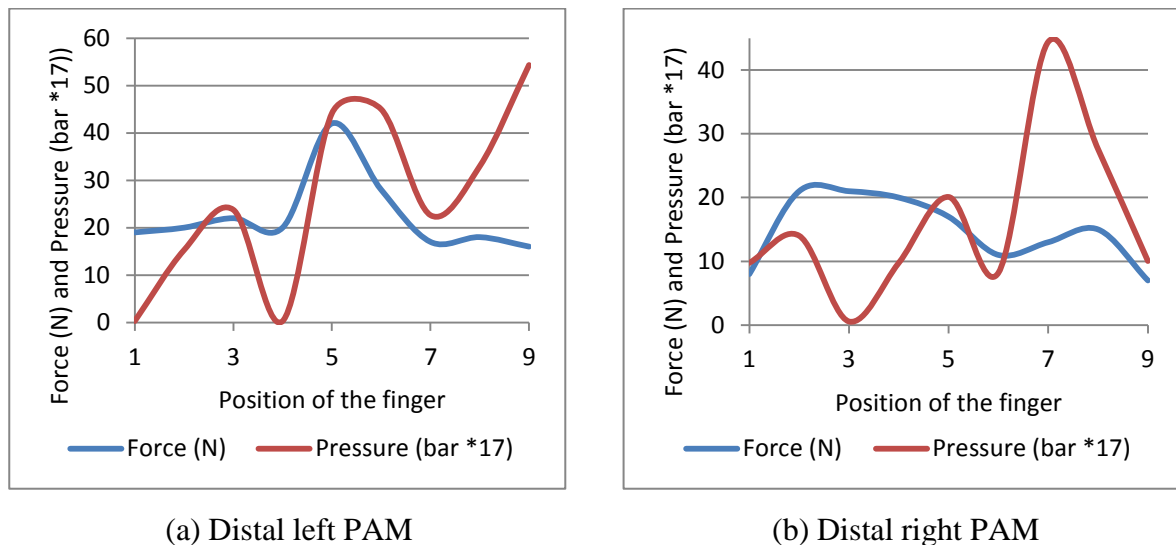
Figure 4.16: Force and Pressure collected for left distal muscle and right distal muscle against the position of the finger.
(a) is for the distal left muscle and (b) is for the distal right muscle.

Contrary to the curves obtained with the proximal left PAM illustrated in Figure 4.15, Figure 4.16 shows that pressure and force evolve in different way for the distal PAMs. Their behaviour can even be opposite, such as for the position 9 with the distal left PAM or position 3 with the distal right PAM. Once again, this is due because PAMs stretch when the antagonistic PAMs contract. Therefore, the values collected from the load cells is not related to the force provided by the finger. Contrary to the force sensors used in Section 3.4.3, it implies the load cells' feedback cannot efficiently be used to interact with objects. Moreover, as the implementation of load cells would complicate the manufacturing of the Ambidextrous Hand's forearm, it is decided to remove them from the system. The mechanical issues concerning the implementation of the load cells inside the forearm structure are explained in [254].

4.2.   Upgrade of electronic and pneumatic interfaces

Compared to a single finger, the actuation of a whole robotic hand implies more resources. From the pneumatic and electronic sides, this increase of resources mainly

concerns the numbers of PAMs, valves, and MCUs. This section first describes the upgrade of the equipment.

Next, the section mentions the mechanical features of the Ambidextrous Robot Hand, necessary to develop the control algorithms discussed in Chapter 5.

4.2.1. Upgrade of the electronic interface

The control of a full robot hand requires a MCU with more I/O as the SPCU, discussed in Section 3.2.2. Therefore, hardware based on Arduino Mega 2560 MCU [150] is developed. The implementation of this remote-controlled hardware is described in [255]. The early block diagram illustrated in Figure 3.35 is consequently modified. The control interface is indeed divided into three different Arduino Mega 2560 MCU [150]. As shown in Figure 4.17, the first board controls the PAMs actuating the thumb, the forefinger and the middle finger. The second board controls the PAMs actuating the ring finger, the little finger and the palm. The third board deals with the communication between the two first MCUs and the RCI.
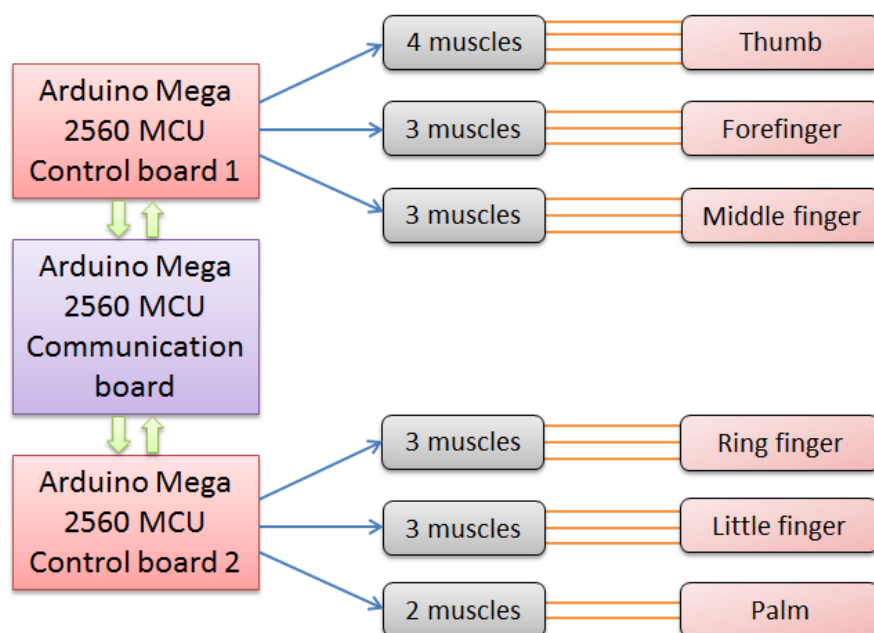
Figure 4.17: Connection between control boards, muscles and fingers

Arduino Mega 2560 MCU [150] deliver outputs of 5 V DC, contrary to the SPCU which provides output voltages of 24 V DC [226]. As mentioned in section 3.2.1, the solenoid valves manufactured by Mead Fluid Dynamics are actuated by 24 V. Thus, a relay interface is required between the valves and the MCUs. The aim is to switch from 0 V to 24 V when an input of 5 V is received. Transistors match with this function. As explained in [255], MOSFETs (metal-oxide-semiconductor field-effect transistors) were firstly used to assure the junction between an Arduino MCU and the valves of a single finger. Nevertheless, implementing enough MOSFETs to control a full robot hand would make the relay interface bulky. Therefore, chips containing as many transistors as possible are investigated. ULN2803A Darlington Arrays [273] are the best choice for this purpose, as they contain eight relays for eighteen pins. They can receive up to 30 V and emit up to 50 V, which matches with the electronic requirements. The diagrams of these Darlington Arrays are provided in Figure 4.18.
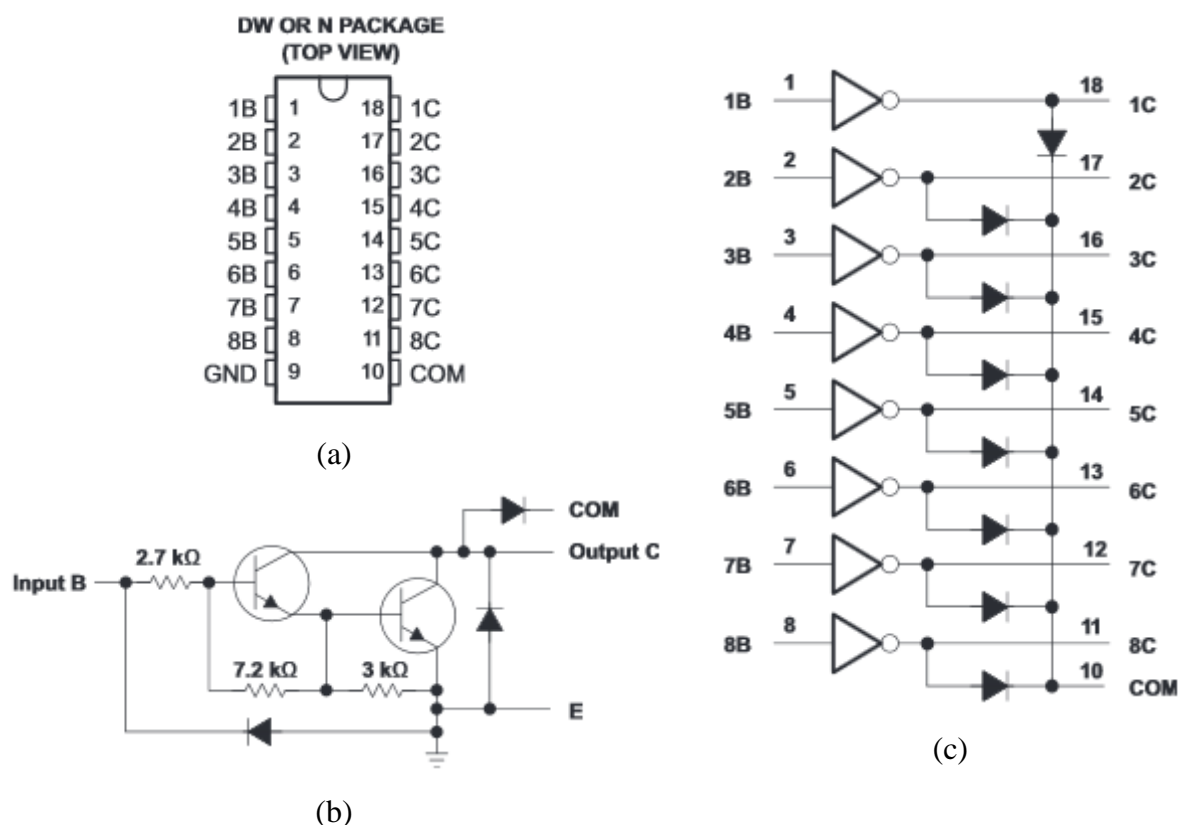
Figure 4.18: ULN2803A Darlington Transistor Arrays [273]
(a) is the top view of the chip and (b) is the schematic for each Darlington pair and
(c) is the logic diagram

The 24 V supply is linked to the tenth pin. Thus, the 24 V voltage can be provided to the Darlington Transistor Arrays' outputs. As seen in Figure 4.18 (b), the disposal of the transistors prevents the voltage to reach the outputs, except if the corresponding input receives a DC signal. When a Darlington pair is supplied with 5 V, it acts like a switch and provides a 24 V output. Additionally, 100 nF capacitors are put between pins 9 and 10 to stabilise the voltage supply.

As the Ambidextrous Robot Hand is actuated by eighteen PAMs, it means the system is controlled by 36 solenoid valves. As eight valves can be connected to a single Darlington Transistor Array, it implies the Ambidextrous Robot Hand requires a total of five Darlington Transistor Arrays to switch from 5 V to 24 V.

The electronic interface, as well as the transition from MOSFETs to ULN2803A Darlington Arrays is shown in Figure 4.19, where it is seen that the size of the chips ULN2803A significantly reduces the size of the relay interface.
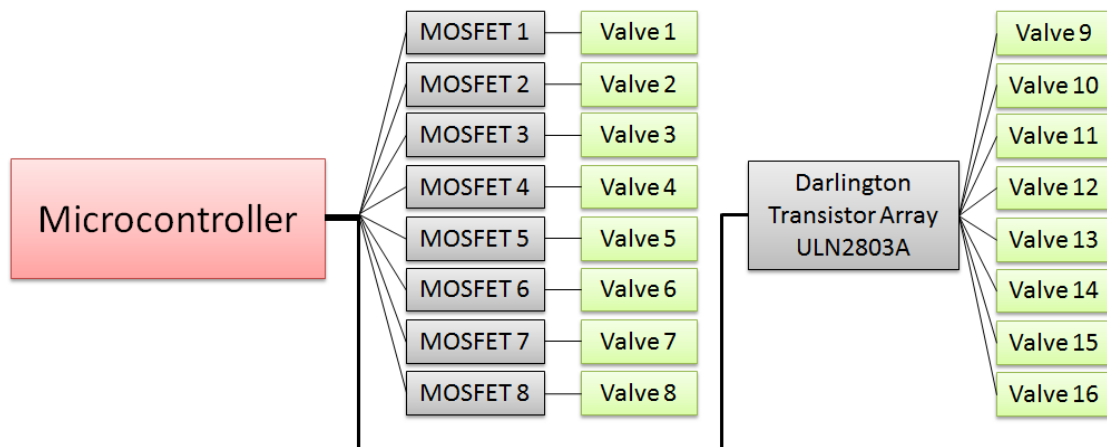
(a)
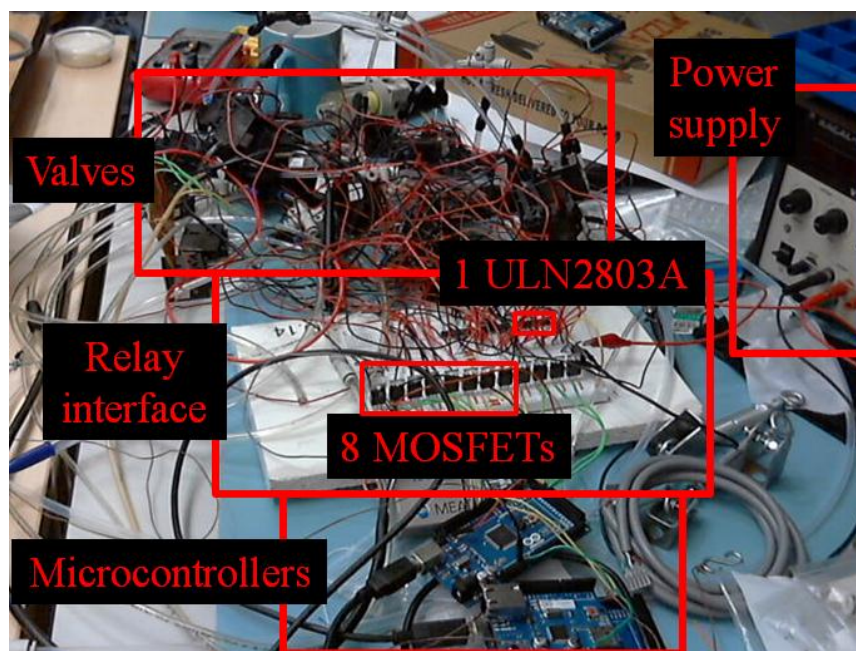
(b)

Figure 4.19: Comparison of sizes between 8 MOSFFETs and 1 ULN2803A in the electronic interface (a) a scheme and (b) the actual devices

4.2.2. Upgrade of the pneumatic interface

The upgrade of the pneumatic interface is divided into two main points. First, the air flow must be fast enough to make five fingers move in parallel. Thus, manifolds are implemented in the system. Secondly, the air compressor must have a tank big enough to supply a full robot hand or, for future stage of the project, an ambidextrous robot arm. These two points are investigated in this section.

121

4.2.2.1.   *Implementation of manifolds*

Switching from a single finger to a full hand also implies that a higher number of PAMs would be contracting or extending at same time. PAMs have an input of 2.5 mm ID. They are connected to a pneumatic input, of 2.5 mm ID as well. As it could be seen in Figure 3.9, the airflow divides itself when several input valves are opened in the same time. Thus, the airflow decreases according to the number of valves that are opened. The movement speed of the hand would consequently decrease when the five fingers move in parallel. Therefore, manifolds with a maximum OD input are ordered.

To avoid any compatibility issues, manifolds are ordered from Mead Fluid Dynamics, which are the same manufacturers as for the solenoid valves. The manifolds can be manufactured with a maximum OD input of 6 mm [225]. Two different diameters of pneumatic tubing are therefore ordered. The chosen tubing are made of fluoropolymer, a material that withstands a maximum pressure of 20 or 22 bars when the tube's OD does not exceed 6 mm [274]. As SPAMs and FPAMs respectively contract at maximum pressures of 3.5 and 8 bars, fluoropolymer tubes fit with the pneumatic interface of the Ambidextrous Hand. Some tubing is ordered with an OD of 6 mm and ID of 4 mm to connect the manifolds to the air compressor, whereas other tubing is ordered with an OD of 4 mm and ID of 2.5 mm to connect the valves to the PAMs. Additional push-in fitting connectors, as the ones shown in Figure 3.5, are also ordered with appropriate diameters to link the devices together.

This upgraded pneumatic interface is connected to the electronic interface and is shown in Figure 4.20.
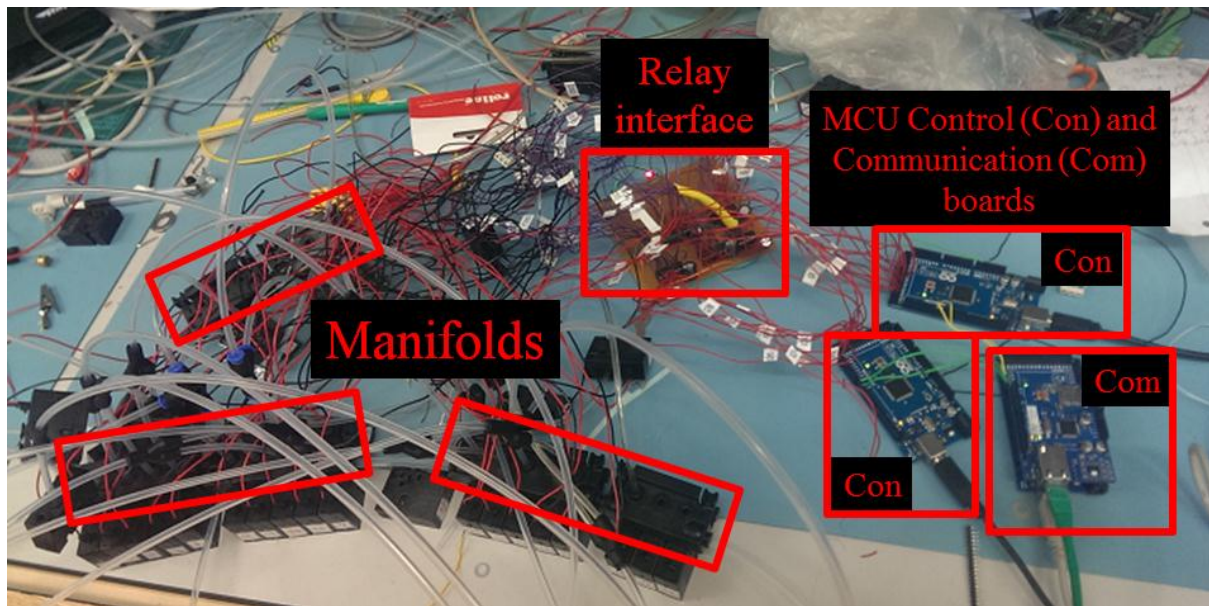
Figure 4.20: Electronic and pneumatic interfaces to actuate a whole ambidextrous robot hand

Figure 4.20 shows that the valves are fixed on manifolds, whereas two of the MCUs are connected to the relay interface. An Ethernet cable is linked to the third MCU, so it can transfer the remote commands to the two first MCUs.

4.2.2.2.   *Choice of an air compressor*

The parallel contraction of a higher number of PAMs requires an air compressor with adequate pressure supply, air flow and tank capacity. Indeed, the compressor must provide enough pressure to make the PAMs contract to their maximum rate. SPAMs contract to a maximum pressure of 3.5 bars; therefore all the compressors that are investigated must fit with this feature. However, as seen in Section 3.3, the range of ambidextrous fingers was often limited because of the limitation of the PAMs' contraction rate. Therefore, future stages of the project may imply to use FPAMs instead of SPAMs. According to the models, FPAMs have a maximum contraction rate varying from 6 to 8 bars, which is why it is preferable to investigate for compressors able to supply a pressure up to 8 bars. Besides, an ambidextrous arm would require longer and bigger PAMs, which is why it is estimated that the air compressor should have a minimum tank capacity of 3 L and a minimum air flow of 25 L/min. In addition to pneumatic features, it is also preferable to look for a low noise compressor suitable with a lab environment. Thus, only compressors that do not exceed a noise of 40 db are investigated in Table 4.8.

Table 4.8: Technical features of air compressors

Air compressor's names	Maximum pressure (bar)	Maximum air flow (L/min)	Tank capacity (L)	Noise (db)
G 1/4 Norgren Air Reservoir [275]	10	N/A	2	N/A
Werther Sil Air 15A Compressor [276]	6	17	1.5	30
Werther Sil Air 15D Compressor [276]	6	17	4	30
Werther Sil Air 30-12 Silent Airbrush Compressor [277]	8	25	6	40
Werther Sil Air 30D Silent Airbrush Compressor [278]	8	25	4	40
Werther Sil Air 50D Compressor [279]	8	50	6	40

First, Table 4.8 shows that the Werther Sil Air 15A and 15D compressors [276] do not fit with the potential implementation of FPAMs, as they can only supply a maximum pressure of 6 bars. The tank capacity of the G 1/4 Norgren Air Reservoir [275] is suitable to actuate a full robot hand but does not fit with the requirements of a robot arm. The technical features of the Werther Sil Air 30-12 [277] match with the needs, but its shape makes it very difficult to move, contrary to the two other models designed in a portable device provided with a handle. The model Werther Sil Air 50D [279] has the highest features, but the model Werther Sil Air 30D [278] is about 20% cheaper. Besides, the model Werther Sil Air 30D has an air flow high enough to actuate an ambidextrous robot arm, which is why it is chosen for the project.

A hose tail barb with an ID of 4 mm is screwed directly into the compressor. This connector allows transferring the air from the compressor to the manifolds. As there are two inputs with IDs of 4 mm for the manifolds, it is noticed the fingers' movements can be increased even further with a hose tail barb of an ID of 6 mm. Additional pneumatic tubing and connectors would then be necessary to convert the input's ID and split it before connecting it to the manifolds.

4.3. Mechanical features of the Ambidextrous Robot Hand

The whole features of the mechanical evolution of advanced prototypes of ambidextrous fingers are discussed in [254]. The possibilities and limitations of the design must be considered prior to investigating the movements' abilities discussed in Chapter 5.

This Section summarises the mechanical characteristics of the Ambidextrous Hand prior to comparing them with the ones of other robotic models.

4.3.1. Summarise of mechanical features of the Ambidextrous Hand

The full Ambidextrous Robot Hand is actuated by eighteen PAMs. As explained in Section 4.1.5.1, each of the four ambidextrous fingers has their flexion and extension actuated by three PAMs. As medial and distal movements are coupled, it is then said each finger have two DOFs actuated by three PAMs. In addition to flexion and extension, abduction and adduction are added to the forefinger to provide more possibility of movements. The abduction is controlled by a single PAM, whereas the adduction is automatically triggered by a spring when the PAM extends. The same system is used for the ring and little fingers, except that their abduction and adduction are coupled. The addition of abduction and adduction to the four ambidextrous fingers consequently adds two PAMs and two DOFs to the robot hand.

The structure of the thumb is different. Contrary to the four other fingers, its phalanges cannot bend in one way or another. Its rotational axe is the only one to be increased, to fit with the ambidextrous design of the hand. Its rotational axe, which corresponds to abduction and adduction, is actuated by two antagonistic PAMs. This antagonistic tendon routing is much more classical than the asymmetrical routing used for the four ambidextrous fingers. Indeed, similar routing can be seen for the work of S. Boudoua et al. [102], previously illustrated in Figure 2.1. The same system was used for the prototypes of section 3.3, such as the routing of Design D shown in Figure 3.18. The symmetrical routing was also used for the first designs of ambidextrous fingers, as seen in Figure 4.13 (a). The flexion of the proximal phalange of the thumb is actuated by a third PAM. The extension is automatically actuated by a spring when the PAM deflates. The flexion of the distal phalange

of the thumb is actuated in the same way, with a fourth PAM. The thumb consequently has three DOFs actuated by four PAMs. As explained in [254], a future version of the Ambidextrous Robot Hand should include two additional DOFs for the thumb, to allow it to be opposable to the other fingers and to permit more anthropomorphic movements.

(a)   (b)
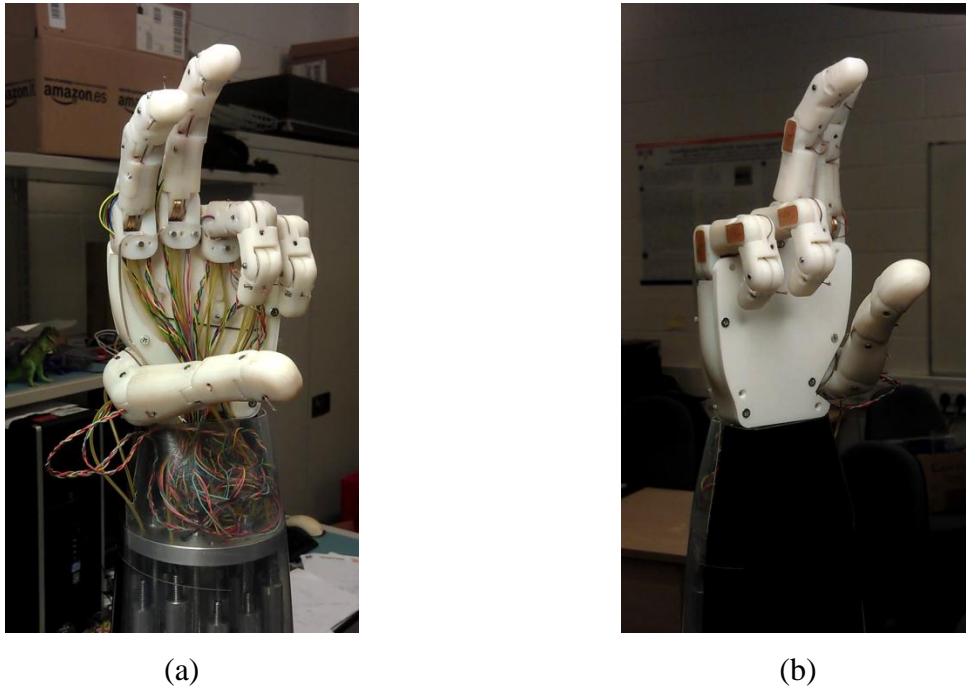
Figure 4.21: Ambidextrous Robot Hand
(a) the left mode and (b) the right mode

In addition to the mechanical architecture, the Ambidextrous Robot Hand includes a total of eleven Hall effect sensors. They are the same as the ones previously used as position sensors, except that they are directly embedded inside the mechanical architecture. The design and the implementation of these sensors are discussed in [254]. Ten of them are connected to the independent flexions/extensions of each phalange. The eleventh one is connected to the adduction/abduction of the thumb. Consequently, the Ambidextrous Robot Hand has eleven sensors for thirteen DOFs. The two DOFs without any sensors are the adduction/abduction of the forefinger and the adduction/abduction of the ring and little fingers.

The pressure transducers can be implemented on electronic boards. Only five pressure transducers were at disposal during the testing of advanced fingers prototypes. PAMs' pressure is directly related to their contraction rate, and consequently to the force applied by each phalange. In case the Ambidextrous Robot Hand would include as many pressure

transducers as PAMs, it would reach a total of eighteen pressure sensors, allowing controlling both the angles and the pressures from the hardware system.

As only four SPAMs were at disposal to experiment the fingers' behaviours, the SPAMs are replaced by eighteen FPAMs to allow the full actuation of the whole Ambidextrous Robot Hand. Longer lengths of PAMs were chosen to fit with the ambidextrous range of the robotic hand. Therefore, the PAMs have a length of 300 mm each when they are deflated and can contract up to a maximum pressure of 8 bars. Their contraction rate of 25% [81] makes their initial length reduce of 75.0 mm, which is much more than the one of SPAMs previously investigated in Section 4.1.4. Contrary to SPAMs, FPAMs only have a passive range of 5% and are consequently almost unable to extend. An error margin must therefore be considered with the tendons' implementation, to allow antagonistic movements of the Ambidextrous Hand.

4.3.2. Comparison of mechanical characteristics with other robotic hands

The mechanical characteristics of the Ambidextrous Robot Hand are summarised in Table 4.9, where the same features are also indicated for other five-fingered robot hands actuated by PAMs. In addition to be the only one with an ambidextrous behaviour, it is also noticed that the Ambidextrous Hand has a ratio of 0.72 between its number of DOFs and its number of PAMs. It is higher than most of the ratios of Table 4.9, which is explained because of the three tendons routing of the Ambidextrous Hand. Robot Hands with higher ratios, i.e. [96], [106], [99] and [98], have anthropomorphic ranges that allow the implementation of additional springs or rubber bands as return mechanisms. The ratio of 0.68 obtained by the hand [90] is also close to the one of the Ambidextrous Hand, the PAMs are directly implemented inside the architecture of its fingers. Nevertheless, Table 2.1 revealed that the ratio between the number of DOFs and actuators is almost always higher for motorised hands. The only exceptions are the DLR hand [67] and the ACT hand [66], which respectively aim at being the most robust and the most flexible as possible. Otherwise, it can be noticed that the motorised hands [64], [71], [68], [69], [72] and [62] all have a ratio equal or higher than 1.

Table 4.9: Comparison of mechanical characteristics between the Ambidextrous Hand and other robotic hands controlled by PAMs

Robot hands	# DOFs	# PAMs	Ratio #DOFs/#PAMs	# and type of sensors	Ambi-dexterity
P. Scarfe and E. Lindsay [95], 2006	10	20	0.50	N/A	
S. Nishino et al. [96], 2007	~13[a]	~16[ab]	~0.81[ab]	~10[a] position, 1[a] force and 16[a] pressure sensors	
P.Y. Chua et al. [106], 2006	21	~20[a]	~1.05[a]	N/A tactile and pressure sensors	
Y. Honda et al. [90], 2010	17	25	0.68	N/A angle sensors	
The Festo Hand [97], 2010	~15[a]	~25[a]	~0.60[a]	N/A	
J.Y. Nagase et al. [98], 2011	4	4[b]	1.00[b]	4 force sensors	
C.Y. Lau and A. Chai [99], 2012	16	14	1.14	14 linear potentiometers	
A. Uribe et al. [100], 2012	14	28	0.50	N/A	
The Shadow Dexterous Hand E1P1R, E1P1L [94], 2013	20	40	0.50	N/A Position, tactile and pressure sensors, total $\geq$ 56	
Ambidextrous Robot Hand [38], 2013	13	18	0.72	11 angle and 18 pneumatic sensors	✓

[a] Estimations are done from pictures, videos or descriptions of the robot hands
[b] Actuators are referred as pneumatic ballons instead of PAMs; both function in identical ways

4.4.   Chapter summary

This chapter has presented the progress of the Ambidextrous Robot Hand's project, from a single finger made of Meccanos to a full hand designed with 3D printing, mainly focusing on the testing platform, electronic and pneumatic interfaces.

The testing of the advanced prototypes required to prepare a testbench specific to the project. First, a number of sensors were chosen among others to be implemented on the testbench. They were calibrated, implemented to their respective interfaces and additional electronic circuits were designed to collect accurate feedback. Secondly, the testbench was designed to be suitable with both the electronic and mechanical requirements.

The electronic and pneumatic interfaces were upgraded to fit with the needs of a full Ambidextrous Robot Hand.

Finally, the mechanical characteristics of the Ambidextrous Hand were compared to the ones of other robotic models driven by PAMs, revealing that, in addition to its ambidextrous feature, the Ambidextrous Hand has a ratio between its number of DOFs and its number of actuators higher than the one of a number of robot hands driven by PAMs. The mechanical features were also considered to engineer suitable control algorithms in the next Chapter.

Chapter 5: Control algorithms

This chapter focuses on control algorithms implemented for the Ambidextrous Robot Hand.

First, the control of angular displacements is investigated based on the literature review summarised in Section 2.5.

Next, algorithms are engineered to control the grasping force of the robot hand. The grasping force is investigated based on two different kinds of feedbacks, namely pressure received from PAMs and force received from fingertips.

For each of these three cases, algorithms are selected according to the similarities existing between the Ambidextrous Hand and other pneumatic robotic systems. These similarities have the nature of either of the mechanical structure or the type of sensors' feedbacks. Control loops are then engineered to be suitable with the asymmetrical routing of the Ambidextrous Hand. The ambidextrous range is also taken into account for the angular displacements as well as the PAMs' nonlinearity when the grasping mode is controlled from pressure feedback.

5.1. Angular displacement

This Section discusses the control of the fingers' angular displacement. Such a control is firstly investigated using PID loops. Then, oscillations zones are defined and a phasing plane switch control makes the gain constants of the PID loops switch to dynamic coefficients.

The work introduced in this Section is based on the hardware developed in [255]. The algorithms described in Section 5.1.1 and Section 5.1.2 have also been completed in collaboration with [255].

5.1.1. Angular displacement driven by PID control

It was previously noted in Section 2.5 that PID controllers are widely used to control the angular displacement of robotic structure. Moreover, a number of papers discussed in Section 2.5 deal with robot hands instead of robot arms or robot manipulators, which proves the robustness of PID control in this area.

This is explained because, as observed in Section 2.1.3, a number of robot hands include angular or position sensors. Angular feedback is therefore measured straight from joints, preventing the PAMs' nonlinearity to directly interfere with the control of phalanges displacements. Consequently, the chosen solution consisted in adapting the previous control algorithms used in Section 3.4.2 to the new asymmetrical design of the system detailed in Section 4.3. Thus, the data collection introduced in Table 4.7 is used again to analyse the behaviour of ambidextrous fingers. Contrary to Figure 4.15 and Figure 4.16 that compared pressure feedback with load cells' feedback, Figure 5.1 represents the PAMs' pressure variation according to the fingers' extreme positions. As previously explained in section 4.1.5.2, position 1 refers to the proximal and medial/distal phalanges reaching both the maximum range on their left side. Position 2 refers to the proximal phalange reaching its maximum range on its left side, whereas the medial/distal phalanges are straight. Position 3 refers to the proximal phalange being on its maximum range on its left side, whereas the medial/distal phalanges are on their maximum range on the right side. Positions 4 to 6 refers to the finger when the proximal phalange is straight while the medial/distal phalanges go from left side to their right side. Last position, position 9, is when the proximal and medial/distal phalanges reach both the maximum range on their right side.
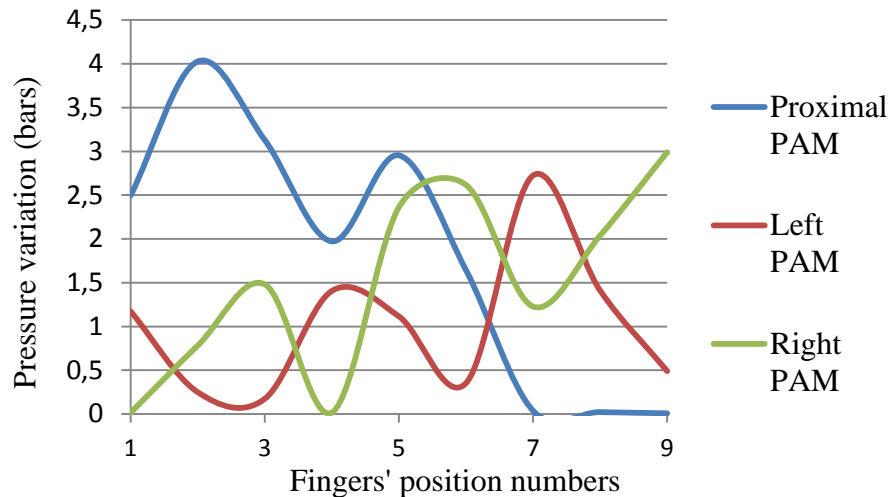
Figure 5.1: PAMs' pressure variation according to fingers' extreme positions

First, Figure 5.1 shows that the right and left PAMs function in antagonist way, which means they vary according to the same amount of pressure (and consequently at the same speed) to make the medial and distal phalanges reach an angular target θ_t. The parallel form of a PID controller used in section 3.4 can consequently be used again to control the angular displacement. Therefore, the same gain constants are attributed to both of these PAMs, but reacting in opposite ways, which means the first one contracts whenever the second one relaxes. However, it is also observed that the proximal PAM's pressure is often about twice as large as the sum of the two others when the proximal PAM is involved, and so can be its pressure variation from one position to another. This is the reason why an approach similar to the one of the antagonistic ratios engineered by Y. Honda et al. in [90], [177] or [178] is implemented. Pressure variations are estimated from the data collection, so the ratio is applied to the constant gains of the proximal PAM. Its proportional and integrative terms are consequently twice lower than the ones of left and right PAM, which equilibrates the speed of the system. As the sum of pressures for the left and proximal PAMs on the finger's left side corresponds to the sum of pressures for the left and right PAMs on the finger's right side, this provides a kind of symmetry that makes the system possible in most of cases. However, this symmetry deforms itself when the proximal phalange is close to a vertical position, which makes the system oscillates in most cases. This is why the vertical position must be predicted to replace the gain constants by dynamic values.

5.1.2. Implementation of a phasing plane switch control

It was observed in Section 2.5.1.1 that PID control was often combined with AI-based algorithm to compensate the PAMs' nonlinearity. In section 2.5.3.1, it was observed that K.K. Ahn et al. connect a NN to PID loops in [211], creating an intelligent PPSC to overcome the nonlinearities of PAMs' pressure feedback. Some parameters of the PID controller are self-tuned because of a learning algorithm of NN, which triggers the PPSC [212]. In the case of the angular displacement of ambidextrous fingers, neither learning algorithms nor NNs are necessary, as the unstable behaviour systematically occurs around the same area. A PPSC is consequently implemented around the vertical position of ambidextrous fingers.

5.1.2.1. *Identification of the unstable area*

A range of critical angles is therefore defined as $\{\theta_c\}$ around the proximal phalange's vertical position. $\{\theta_c\}$ is delimited by θ_{cl} on the left side and by θ_{cr} on the right side. The aim of the PPSC is to anticipate $\{\theta_c\}$ and to switch the classic PID loops' gain constants into dynamic coefficients. To allow these dynamic coefficients to relay the classic ones before the proximal phalange enters in $\{\theta_c\}$, a danger zone noted $\{\theta_d\}$ is defined as:

$$2\theta_{cl} - \frac{\pi}{2} \leq \{\theta_d\} \leq 2\theta_{cr} - \frac{\pi}{2} \tag{5.1}$$

The limits of $\{\theta_d\}$ introduced in (5.1) are noted θ_{dl} on the left side and θ_{dr} on the right side. As shown in Figure 5.2, $\{\theta_d\}$ permits doubling the area of $\{\theta_c\}$ keeping the proportions around the vertical position.

$$2\theta_{cl} - \pi/2 \leq \{\theta_d\} \leq 2\theta_{cr} - \pi/2$$
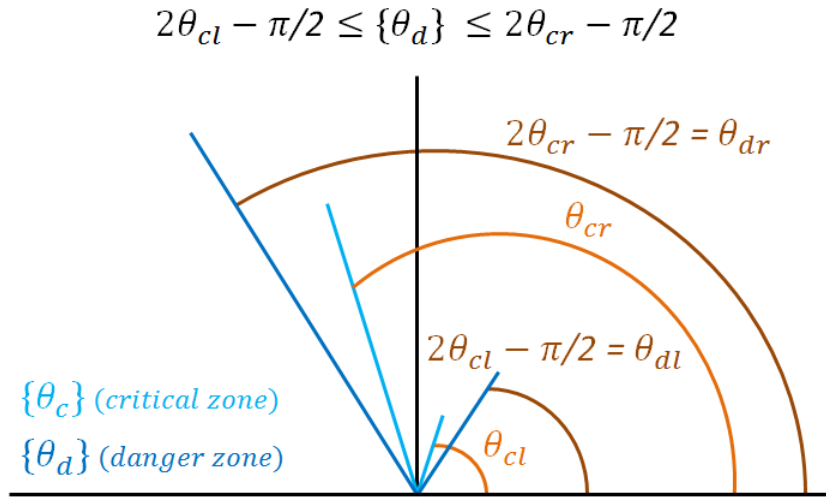
Figure 5.2: Representations of the critical zone and of the danger zone

Experiments show that the finger can oscillate when it stands between $\theta_{cl} = 78°$ and $\theta_{cr} = 99°$, meaning that:

$$\{\theta_c\} = \{78°, 79°, 80°, \dots 99°\} \tag{5.2}$$

$$\{\theta_d\} = 2 * \{\theta_c\} - 90° = \{66°, 67°, 68°, \dots 108°\} \tag{5.3}$$

The next step consists in calculating appropriate dynamic coefficients to efficiently control the finger around $\{\theta_c\}$. It is known that an object in motion depends on three parameters, which are position, velocity and acceleration. For an angle θ, the finger's position is calculated from the equation (5.4):

$$\theta(t) = \theta_0 + \omega t - \alpha t^2/2 \tag{5.4}$$

with ω its velocity and α its acceleration. As ambidextrous fingers belong to nonlinear systems, their values are estimated from their instantaneous equations, defined as:

$$\omega = \Delta\theta/\Delta t \tag{5.5}$$

$$\alpha = \Delta\omega/\Delta t \tag{5.6}$$

Acceleration is obtained from the derivative of speed, itself obtained from the derivative of the position. Consequently, these three values are assimilated to the three terms of the PID controller, based on the error $e(t)$, its integral $\int_0^t e(\tau)d\tau$ and its derivative $\dot{e}(t)$. Based on the equations (3.2), (5.1), (5.4) and (5.5), the dynamic parameters of the proximal

phalange are compared to the following values whenever the finger goes from its left side to a vertical position or to its right side:

$$K_p * e(t) < [\pi/2 - \theta_{dl} - \theta(t)]/\Delta t \qquad (5.7)$$

$$K_i * \int_0^t e(\tau)d\tau < \pi/2 - \theta(t) \qquad (5.8)$$

$$K_d * \dot{e}(t) < [2K_p e(t)\Delta t - \theta(t)]/\Delta^2 t \qquad (5.9)$$

When the finger is on its right side, $\theta(t)$ takes its values from $180°$ instead of $0°$. The signs of $\theta(t)$ and $\pi/2$ of equation (5.7) must then be changed. On the right side, equation (5.7) therefore becomes:

$$K_p * e(t) < [\theta(t) - \pi/2 - \theta_{dr}]/\Delta t \qquad (5.10)$$

with θ_{dr} taken into account instead of θ_{dl}.

As soon as the inequality goes wrong either for the position term, or both the velocity and acceleration terms, it implies that the proximal phalange is going to reach $\{\theta_c\}$, which triggers the PPSC. The constant gains of the PID are consequently switched to dynamic values noted K_{dp}, K_{di} and K_{dd}.

5.1.2.2. *Tuning of dynamic coefficients*

The process of identification of dynamic values is then considered in details. The dynamic values are defined experimentally.

It is noted that the system becomes unstable when $\theta(t)$ gets close to $\pi/2$. The calibration therefore starts from $K_{dp} = \pi/2 - \theta(t)$, $K_{di} = 0$ and $K_{dd} = 0$, for the left side of the hand, using the same tuning method as the one described in section 3.4.2. For a setpoint defined as vertical position, as the sign of the error becomes negative for $\theta(t) > \pi/2$, the symmetrical calibration from the right side starts from $K_{dp} = \theta(t) - \pi/2$, $K_{di} = 0$ and $K_{dd} = 0$, so that the sign of $K_{dp} * e(t)$ only depends on the sign of $e(t)$. Absolute value is added to prevent $e(t)$ to increase for $\theta(t) > \pi/2$. The different steps of the tuning process are summarised in Table 5.1. The setpoint is defined with an error margin of $1.25°$, to avoid a too high number of oscillations.

Table 5.1: Tuning of dynamic coefficients of angular displacement driven by PID control

K_{dp}	K_{di}	K_{dd}	Rising time (sec)	% of over-shoot	# of oscil-lations	Settling time (sec)
$\|\pi/2 - \theta(t)\|$	0	0	0.45	10%	7	1.00
$\|\pi/2 - \theta(t)\| + 3$	0	0	0.30	25%	9	0.75
$\|\pi/2 - \theta(t)\| + 1$	$\|\pi/2 - \theta(t)\|$	0	0.25	20%	8	0.60
$\|\pi/2 - \theta(t)\| + 1$	$\dfrac{\left\|\left(\frac{\pi}{2} - \theta(t)\right)\right\|}{\|e(t)\| + 1}$	0	0.35	15%	6	0.65
$\|\pi/2 - \theta(t)\| + 1$	$\dfrac{\left\|\left(\frac{\pi}{2} - \theta(t)\right) * e(t)\right\|}{\|e(t)\| + 1}$	0	0.25	20%	∞	∞
$\|\pi/2 - \theta(t)\| + 1$	$\dfrac{\left\|\left(\frac{\pi}{2} - \theta(t)\right) * \dot{e}(t)\right\|}{\|e(t)\| + 1}$	0	0.30	10%	3	0.40
$\|\pi/2 - \theta(t)\| + 1$	$\dfrac{\left\|\left(\frac{\pi}{2} - \theta(t)\right) * \dot{e}(t)\right\|}{\|e(t)\| + 1}$	$\|\pi/2 - \theta(t)\|$	0.35	20%	∞	∞
$\|\pi/2 - \theta(t)\| + 0.5$	$\dfrac{\left\|\left(\frac{\pi}{2} - \theta(t)\right) * \dot{e}(t)\right\|}{\|e(t)\| + 1}$	$\dfrac{\theta(t) * K_{di}}{\pi/2}$	0.40	5%	2	0.45
$\|\pi/2 - \theta(t)\| + 0.5$	$\dfrac{\left\|\left(\frac{\pi}{2} - \theta(t)\right) * \dot{e}(t)\right\|}{\|e(t)\| + 1.1}$	$\dfrac{\theta(t) * K_{di}}{\pi/8}$	0.55	10%	5	0.65
$\|\pi/2 - \theta(t)\| + 0.6$	$\dfrac{\left\|\left(\frac{\pi}{2} - \theta(t)\right) * \dot{e}(t)\right\|}{\|e(t)\| + 1.1}$	$\dfrac{\theta(t) * K_{di}}{\pi/4}$	0.45	5%	4	0.55
$\|\pi/2 - \theta(t)\| + 0.6$	$\dfrac{\left\|\left(\frac{\pi}{2} - \theta(t)\right) * \dot{e}(t)\right\|}{\|e(t)\| + 1.1}$	$\dfrac{\theta(t) * K_{di}}{\|e(t)\| + 1}$	0.30	0%	0	0.30

It is noticed that the speed of the system varies too much for $K_{dp} = |\pi/2 - \theta(t)|$. Indeed, when $\pi/2 - \theta(t) \to 0$, the loop's speed decreases before increasing again. This is corrected by the addition of a constant C_{dp}. As it was noticed in Section 3.4.2 that the PID loop was already fast enough for $K_p = 3$, it is decided to have $C_{dp} = 3$ as well, which would correspond to the slower speed of the loop. However, for the next steps of the process, C_{dp} is reduced to 1, as K_p is also meant to be reduced.

Secondly, to reduce the overshoot and the oscillations, the tuning of the dynamic integrative gain is started from $K_{di} = |\pi/2 - \theta(t)|$ as well. Yet, the system still has an overshoot and oscillates because the chosen value of K_{di} is too high. It is then decided to divide K_{di} by $e(t)$. Thus, the farer it is from $\pi/2$, the slower is the movement. An absolute

value is put to the divisor, to which is added a constant $C_{di} = 1$, to avoid any division close to 0 that would considerably increase K_{di}. It is observed that very irregular movements can be created at the limits of $\{\theta_d\}$. K_{di} is therefore multiplied by $e(t)$ to compensate the effect of the division and see if the influence of C_{di} is enough to stabilise the system. However, the movements become too fast and run out of control. Thus, $e(t)$ is replaced by $\dot{e}(t)$, which also depends on the distance between the setpoint and $\pi/2$ but which is smaller than $e(t)$. Using these coefficients, the setpoint is reached with a rising time's speed barely varying and a small overshoot. The only problems remaining are some oscillations, which must be fixed by the tuning of K_{dd}.

As for K_{dp} and K_{di}, K_{dd} is initialised at $\pi/2 - \theta(t)$, which causes again a huge overshoot and many oscillations. As the coefficient found for K_{di} was stable, it is decided to put $K_{dd} = \theta(t) * K_{di}$, but divided by $C_{dd} = \pi/2$ to reduce the impact of the multiplication by $\theta(t)$. As the system does not stabilise properly, it is then tried with $C_{dd} = \pi/8$, which makes the system much slower and oscillating again. With $C_{dd} = \pi/4$, the system oscillates as well. Therefore it is decided to use the error as a divisor, so the divisor varies according to $\theta(t)$. The constant C_{dd} is fixed as $C_{dd} = 1$ to prevent any division by 0.

The final coefficients found for the dynamic PID control are:

$$K_{dp} = |\pi/2 - \theta(t)| + C_{dp} \tag{5.11}$$

$$K_{di} = \frac{\left|\left(\frac{\pi}{2} - \theta(t)\right) * \dot{e}(t)\right|}{|e(t)| + C_{di}} \tag{5.12}$$

$$K_{dd} = \frac{\theta(t) * K_{di}}{|e(t)| + C_{dd}} \tag{5.13}$$

with:

$$C_{dp} = 0,6 \tag{5.14}$$

$$C_{di} = 1,1 \tag{5.15}$$

$$C_{dd} = 1 \tag{5.16}$$

where C_{dp} is a small positive constant preventing the system to become motionless, whereas C_{di} and C_{dd}, also positive, stabilise the speed and the acceleration for an angle close to $\pi/2$. Contrary to the constant coefficients, the dynamic ones take the angular distance into account as well as the error; they react in different ways depending on if θ_t belongs to $\{\theta_d\}$ or to the finger's right side. In the first case, the motion prepares to slow down as the setpoint is very close, whereas in the second case the speed aims to be constant. An identical method is symmetrically applied when the finger starts from its right position. In both cases, it is noted that the dynamic coefficients are specific to positions close to vertical and so cannot be used permanently (as the finger motion would be very slow or otherwise irregular) which is why the PPSC is required.

5.1.2.3.   *Experimental results obtained using the PID controllers with the PPSC*

The positions reached using the PID loops coupled with the PPSC are shown in Figure 5.3, where snapshots (a) to (i) correspond to the positions 1 to 9 as defined in section 4.1.5.2. Snapshots (d) to (f) are obtained with the dynamic coefficients whereas snapshots (a) to (c) and (g) to (i) are obtained with classic PID control.

(a)   (b)   (c)

(d)   (e)   (f)

(g)   (h)   (i)
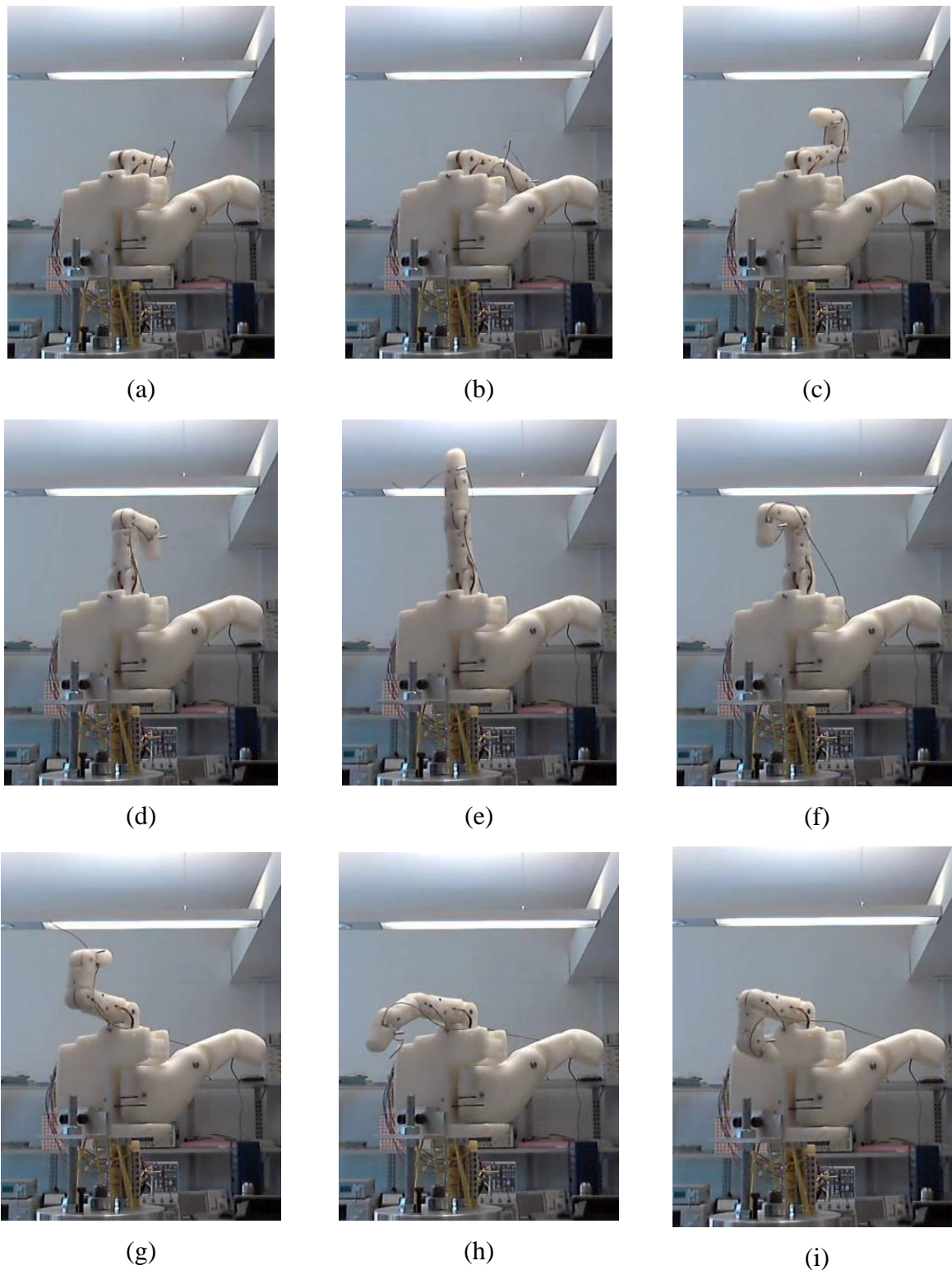
Figure 5.3: Video snapshots of finger positions obtained with PID loops coupled with PPSC Positions (a) to (i) respectively represent the positions 1 to 9 as defined in section 4.1.5.2

Even though the system stays stable when the finger goes from one position to another, it is noted that the PPSC can make the finger speed vary when θ_t belongs to $\{\theta_d\}$.

139

However, the same process can be applied to the five fingers of the Ambidextrous Robot Hand, to allow parallel movements of the structure. Screenshots are provided in Figure 5.4.
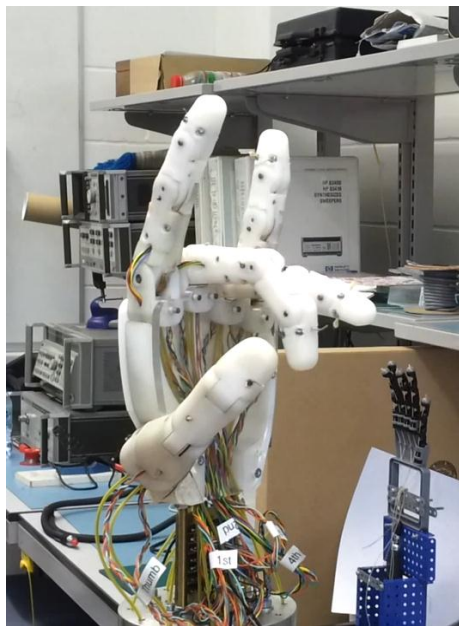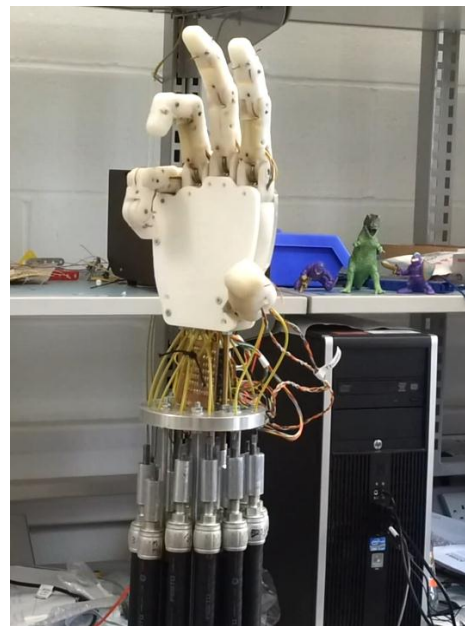
(a)   (b)
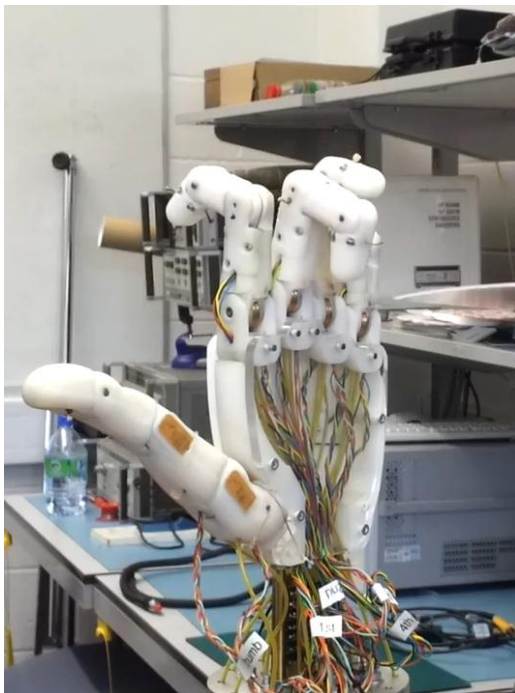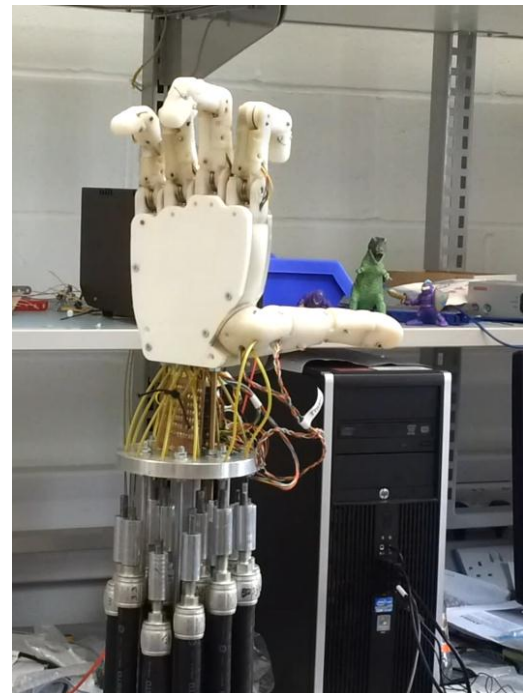
(c)   (d)

Figure 5.4: Video snapshots of the Ambidextrous Robot Hand in movement [283]
(a) Shows a right hand behaviour and (b) a left hand behaviour whereas
(c) and (d) show ambidextrous behaviours

Because of the asymmetrical tendons routing, the speed varies when the fingers move from right to left or from left to right. The ambidextrous fingers are indeed faster when moving from right to left, as the angular speed reaches about 140 deg/sec, against about 110 deg/sec from left to right (these values do not match with the rising and settling times indicated in Table 5.1 as the compressed air circulates slower when a higher number of PAMs is inflating). The angular speed of a single ambidextrous finger can also approximate 300 deg/sec when the other fingers are not actuated, as a lower number of PAMs, and consequently a lower air flow, is involved. Its maximum speed is however about four times slower than the maximum speed of a human hand. It is indeed indicated in [63] or in [178] that human fingers move up to a frequency of 5.5 Hz. As human fingers achieve a motion of about 90°, then their angular speed can be approximated to about 500 deg/sec:

$$\omega = \Delta\theta/\Delta t$$

$$\omega \simeq 90 * 1/5.5 \qquad\qquad (5.17)$$

$$\omega \simeq 495 \; deg/sec$$

The speed of the Ambidextrous Hand could be increased if the PAMs were shorter. Indeed, the PAMs that actuate the structure have a length of 300 mm and can contract up to 8 bars. However, the pressure never overreaches 4 bars when the fingers are in motion. Shorter PAMs can consequently actuate the robotic structure. PAMs would contract faster, and therefore increase the movement's speed of the fingers. The experiment summarised in Table 3.6 indeed showed that an early prototype could move about thrice faster than 3D printed fingers, as it was actuated by shorter PAMs.

5.1.3. Comparison with angular controls of other robotic models

The angular accuracy and the overall behaviour of the Ambidextrous Hand obtained with the PID control coupled with the PPSC are summarised in Table 5.2, where they are compared with the ones of other robotic models. Most of these robotic models are robot hands, but some robot arms and manipulators are also included, as the only PPSC revealed by the literature review, in [211] and [212], is not implemented on a robot hand. Moreover, the algorithms implemented on robot arms and manipulators are more varied, which allows additional comparisons with the Ambidextrous Hand.

141

PID and PD controllers are indeed almost systematically implemented to control the angular displacements of the robot hands summarised in in Table 5.2. The DLR hand [281] and the hand engineered by Z. Xu et al. [142] are exceptions; the first is driven by cascade control and the second uses bang-bang to test the speed capabilities of the robotic model. Robotic structures using AI-based algorithms (fuzzy logic, GAs, PSOs or NNs) are generally much more accurate than the ones using PID control. Nevertheless, their reaction speed is also about ten times slower and the number of their DOFs never exceeds three. An exception concerning the accuracy of robot hands is the High-speed model [280], which is both the second most accurate robotic structure of Table 5.2 and the fastest one, as it is more than ten times faster than most of the other robotic models. This high speed is the reason why the control loops do not include integrative control. As observed in the transfer function of PID controllers (3.2), the integrative term is not significant when the setpoint is quickly reached, which is why the High-speed hand [280] is driven by PD control.

Other models using actuators different from PAMs are summarised in Table 5.2. The SMA Hand [115] and the miniature five-fingered robot hand [123] are both actuated by SMAs. Because of the slow speed of its actuators, the SMA Hand [115] is the third slower hand of Table 5.2, whereas the miniature five-fingered robot hand [123] has an average speed, although it is also the only hand of Table 5.2 being a miniature version of a human hand. The hand engineered by Z. Xu et al. [142] is driven by air cylinders, and the maximum speed obtained with a single finger is close to the speed of motorised fingers. However, the speed of several fingers moving in parallel would certainly be slower than the one indicated in [142], as the pressurised air would not flow as fast in a higher number of cylinders. The hand designed by I. Yamano and T. Maeno [63], the hand engineered by S. Takamuku et al. [71], the ACT hand [175], the DLR Hand [281], the DEXMART Hand [282] and the Shadow Hand [62] are other hands driven by motors. Their technical features show that motorised robot hands are generally more accurate and, most often, at least twice faster than the pneumatic models. However, the angular displacement of the ACT hand [175] is among the less accurate ones engineered since 2008 in Table 5.2. The other ones are the control algorithms implemented on the hand designed by Y. Honda et al., in [177] and [178]. It is noticed that both of these hands have an asymmetrical tendons routing, which makes the angular accuracy more challenging. The Ambidextrous Hand also has an asymmetrical tendons routing, however it is noticed that its angular accuracy is higher than for the hands [175] and [178]. Without taking the robotic structures with less than five DOFs into account,

the Ambidextrous Hand is also one of the most accurate hands summarised in Table 5.2, with a maximum angular error of 1.25°, the exceptions being [280], [96], [183], [94] and [62], with respective errors of 0.012°, 1.2°, 1.2°, 1° and 1°. However, many robot hands have an angular speed faster than the one of the ambidextrous fingers. Indeed, robot hands can reach about 200 deg/sec, such as [123], [71] and [282], reach between 300 deg/sec and 500 deg/sec for [62], [94] and [142] or even reach between 800 deg/ sec and 2000 deg/sec for [280], [63] and [281]. Among these models, the Shadow Hand [94] is the only one of these hands that is driven by PAMs. It can therefore be deduced that the Ambidextrous Hand is among the fastest robot hands actuated by PAMs. According to equation (5.17), the Shadow Hands [94] and [62] are the models of Table 5.1 for which the angular speed is the closest to the one of human fingers, as they move to a speed close to 500 deg/sec.

Table 5.2: Comparison of angular control between the Ambidextrous Hand and other robotic models

Robotic models	Robot hand	Five fingers	Driven by PAMs	Asymmetrical tendons routing	# DOFs	Control algorithms	Max angular error	Speed (deg/sec)	Ambidexterity
SMA Hand [115], 2002	✓				1[a]	N/A	N/A	30	
Gifu Hand II [291], 2002	✓	✓				PD	1.1°[a]	140[a]	
P. Pomiers [104], 2003		N/A	✓		3	PID, cascade	1°	50	N/A
High-speed hand [280], 2003	✓			N/A	8	PD	0.012°	1800	N/A
I. Yamano and T. Maeno [63], 2005	✓	✓			20	N/A	N/A	900	
T.D.C. Thanh and K.K. Ahn [212], 2006		N/A	✓		1	PID, NN, PPSC	0.025°	67[a]	N/A
Miniature five-fingered robot hand [123], 2006	✓	✓			20	N/A	N/A	200[a]	
K.K. Ahn and H.P.H. Anh [179], 2006		N/A	✓		2	Fuzzy logic, NN	3.01°	22[a]	N/A
S. Takamuku et al. [71], 2007	✓	✓			18	N/A	2°[a]	200[a]	
K.K. Ahn and N.H.T. Chau [211], 2007		N/A	✓		2	PID, NN, PPSC	1°	36[a]	N/A
K.K. Ahn and H.P.H. Anh [218], 2007		N/A	✓		2	GAs	0.2°[a]	32[a]	N/A
S. Nishino et al. [96], 2007	✓	✓	✓		13	PID	1.2°[a]	75[a]	
ACT Hand [175], 2009	✓	✓		✓	23	PID	1.7°[a]	49[a]	
J. Wu et al. [183], 2009	✓		✓		N/A	PID, fuzzy logic	1.2°[a]	7.8[a]	

Robotic models	Robot hand	Five fingers	Driven by PAMs	Asymmetrical tendons routing	# DOFs	Control algorithms	Max angular error	Speed (deg/sec)	Ambidexterity
Y.P.H. Anh and N.H. Phuc [213], 2010		N/A	✓		2	NN, PSO	<0.004°	35[a]	N/A
X. Jiang et al. [28], 2010		N/A	✓		9	PID	1°[a]	N/A	N/A
S. Boudoua et al. [102], 2010		N/A	✓		3	PID, SMC, NN	0.1°[a]	5.7[a]	N/A
Y. Honda et al. [177], 2010	✓	✓	✓	✓	17	PID	10°[a]	75[a]	
Y. Honda et al. [178], 2012	✓	✓	✓	✓	17	PID	4°[a]	40[a]	
DLR Hand [281], 2012	✓	✓		N/A	19	Cascade	N/A	1680	
Shadow Hand [94], 2013	✓	✓	✓		20	PID	1°	450[a]	
Shadow Hand [62], 2013	✓	✓			20	PID	1°	500[a]	
Z. Xu et al. [142], 2013	✓	✓			20	Bang-bang	N/A	330[b]	
DEXMART Hand [282], 2014	✓	✓			20	N/A	N/A	250[a]	
Ambidextrous Hand from right to left [40], 2014	✓	✓	✓	✓	13	PID, PPSC	1.25°	110[c]	✓
Ambidextrous Hand from left to right [40], 2014	✓	✓	✓	✓	13	PID, PPSC	1.25°	140[c]	✓

[a] Estimations are made from curves, pictures or videos of the robot hands
[b] Tests being done on a single finger, the air flow would be slower in case of a parallel motion
[c] Averaged speed obtained with manifolds, with a parallel motion of the five fingers

In conclusion, the Ambidextrous Hand is the only robot hand with an ambidextrous range, making the range about twice larger than other robot hands. Despite the wider angular positions that the ambidextrous fingers must reach, their angular speed is higher than some of the robot hands summarised in Table 5.2, and among the fastest fingers driven by PAMs. As indicated by Y. Honda et al. in [177] and [178], a higher speed can be obtained with higher inner diameters of the pneumatic tubings or shorter lengths for the tubes standing between the solenoid valves and the PAMs. The Ambidextrous Hand is also a robotic model with a low angular error, and with the highest accuracy among the hands driven by asymmetrical tendons routings. It is also the only robot hand for which the angular displacement is controlled by a combination of PID controllers and PPSC.

5.2.   Force control from pressure and angular feedbacks

This Section discusses the control of force provided by the fingers using pressure feedback. This force control is firstly investigated using PID loops prior to be driven by SMC, for which angular control is combined with pressure feedback.

5.2.1. Pressure feedback driven by PID control

PID loops are implemented receiving feedback from pressure transducers to control the force applied by fingers. Pressure to reach grasping positions can be investigated analysing the data collection of Figure 5.1. On the left side, fingers have a grasping position when the left PAM contracts at 1.2 bars and the proximal PAM contracts at 2.5 bars. On the right side, the left PAM contracts at 0.5 bars whereas the right PAM contracts at 3 bars. These values were obtained without holding any objects. Using a method similar to the one investigated in section 3.4.3.2 to maintain pressure on metal pieces, the pressure values obtained without objects are increased from 10% to 30% to provide more force to the fingers, before being put as targets to PID control. This method allows grasping relatively heavy objects, with a weight such as 0.5 kg, as shown in Figure 5.5.

| (a) | (b) |
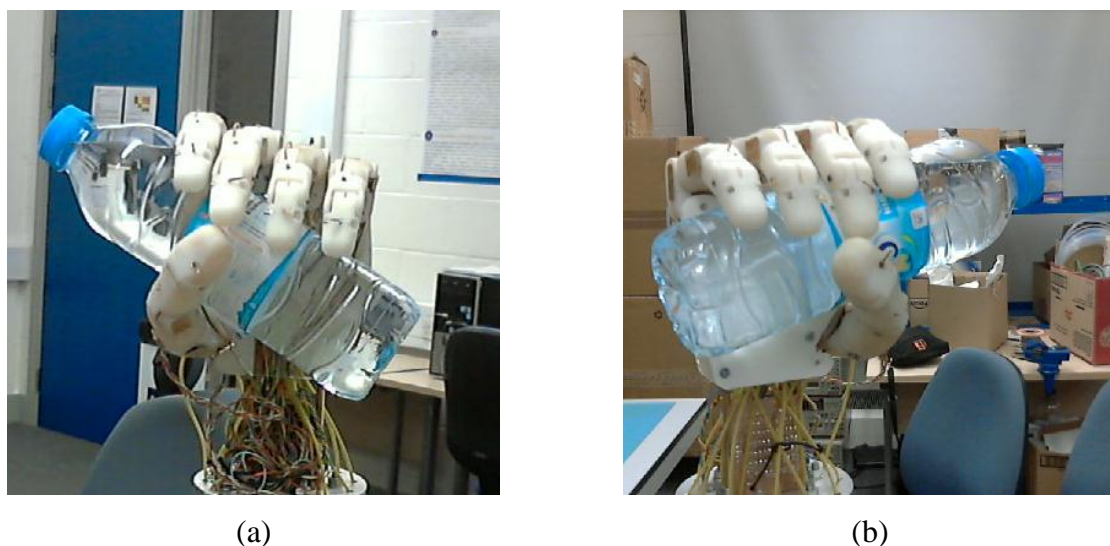
Figure 5.5: Ambidextrous Robot Hand grasping a 500 mL bottle of water
(a) the left hand mode and (b) the right hand mode

However, because of the PAMs hysteresis shown in Figure 4.12, this method would not be accurate enough to grab light objects. This is the reason why PID controllers were most often combined with AI-based algorithms or implemented in cascade control in the literature review done in section 2.5.1.1.

Another control algorithm is consequently investigated to interact with light objects.

5.2.2. Pressure and angular feedbacks driven by SMC

Section 2.5.1.1 revealed that PID controllers were often combined with other types of algorithms to compensate the hysteresis effect of PAMs. The analysis of the literature review in Section 2.5.4 shows that feedback, feedforward and IA-based algorithms have already been implemented on robot hands driven by PAMs, notably using PID controllers, cascade control and fuzzy logic. However, no robot hands driven by PAMs have been revealed to be controlled by nonlinear control algorithms, such as SMC or BSC. It was shown that SMC and BSC were always implemented to drive the angular position of robotic arms or robotic joints, but none of them have been implemented on pneumatic structures to grab objects. These two algorithms are therefore compared to know which one would be the most suitable to grab objects with the Ambidextrous Robot Hand.

As discussed in Sections 2.5.1.3 and 2.5.2, H. Aschemann and D. Shindele have published many papers in the area of nonlinear control, such as [195], [196], [197] or [201]. As their work discussed in [202] compares the results achieved with BSC and SMC and presents more accurate results for SMC, SMC looks to be a more suitable option than BSC. Moreover, [285] reveals that SMC is compatible with variable and discontinuous structure systems. It is also specified that the SMC switched between two distinctively different system structures, which is the target aimed to be reached to grab light objects, as the fingers must stop tightening when enough pressure is provided as feedback. Finally, as SMC is defined as being robust and finite-time convergence as well as reducing-order compensated dynamics in [284], the possibility to grab objects using SMC is explored.

Some exceptions of robotic models grabbing objects using SMC can almost be found. The robot hand introduced in [286] grabs objects because of an SMC, but the hand is driven by motors and the SMC is engineered receiving feedback from tactical sensors. This SMC

aims at calculating the coordinates of the hands, instead of the force applied by the fingers. The SMC implemented on the motorised prosthesis hand [287] controls the force applied by the robotic fingers from force feedback, but the robotic design only includes two fingers that move according to a single DOF. As the Ambidextrous Hand is pneumatically actuated and as the data feedback is received from pressure sensors, the implementation of a SMC to grab objects would therefore be different from the ones of [286] or [287]. Grabbing objects using an SMC would consequently bring more originality to the project.

5.2.2.1.   *Definition of the state trajectory*

As explained in [285], SMC allows driving a state trajectory defined as an error toward a predefined phase plane and to slide along its surface.

First, the object must be detected to trigger the SMC. Thus, experiments similar to the one illustrated in Figure 4.12 are realised. PAMs driving the angular displacement of the fingers' proximal phalanges are inflated and deflated, both pressure and angles being collected for each step. When the finger goes from right side to left side, the proximal PAM is the only one to contract. However, when the finger goes from left side to right side, left and right PAM must inflate in parallel. Numerical data of the experiment showed in Table 4.7 is consequently analysed to find appropriate ratios allowing such a movement. Pressures are consequently compared between position 2, referring to left straight position, and position 5, referring to right straight position. The averaged pressures obtained for each of them are respectively 0.250 bars and 1.115 bars for the left PAM, against 0.782 bars and 2.363 bars for the right PAM. The ratio between both PAMs is calculated in equation (5.18):

$$r = \frac{1.115 - 0.250}{2.363 - 0.782}$$

$$r = \frac{0.865}{1.581} \tag{5.18}$$

$$r \simeq 0.547$$

A ratio of 0.547 must therefore be applied between pulses sent to right and left PAMs from left to straight position. The same method is used between right straight and vertical positions, comparing the pressures obtained from position 8 to position 5 from the experiment

illustrated in Table 4.7. The averaged pressures obtained for each of them are respectively 1.115 bars and 1.411 bars for the left PAM, against 2.039 bars and 2.363 bars for the right PAM. The ratio between both PAMs is calculated in equation (5.19):

$$r = \frac{1.411 - 1.115}{2.039 - 2.363}$$

$$r = -\frac{0.296}{0.324} \tag{5.19}$$

$$r \simeq -0.914$$

The left PAM consequently deflates whereas the right PAM inflates going from position 5 to position 8, using a ratio of 0.914.

The curve obtained when the finger goes from right to left is shown in Figure 5.6. Using the ratios calculated in equations (5.18) and (5.19), the curve obtained when the finger goes from left to right is shown in Figure 5.7. The pressure indicated in Figure 5.7 is a sum of right and left PAM's pressure.
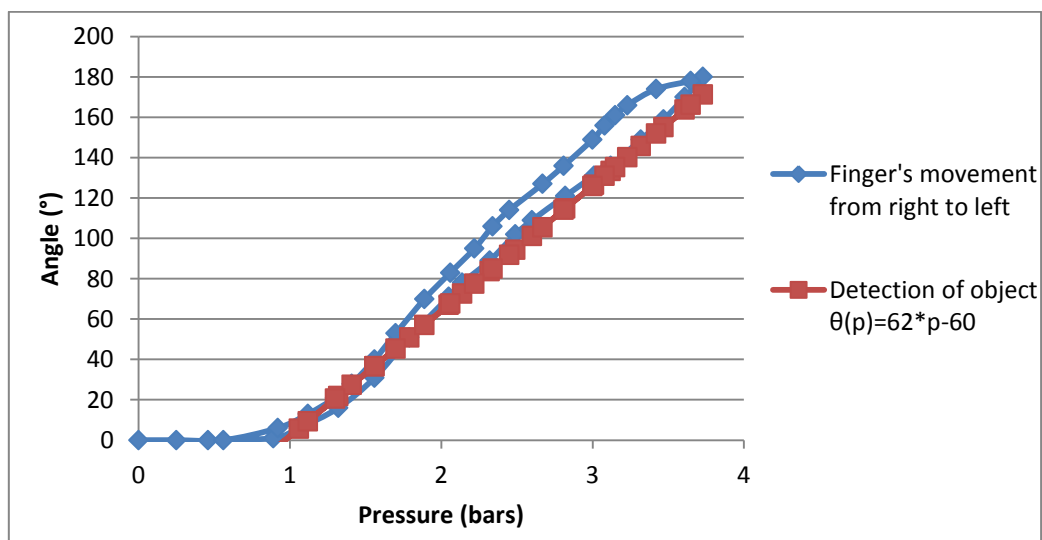
Figure 5.6: Angle of proximal phalange against pressure of proximal PAM when finger goes from right to left
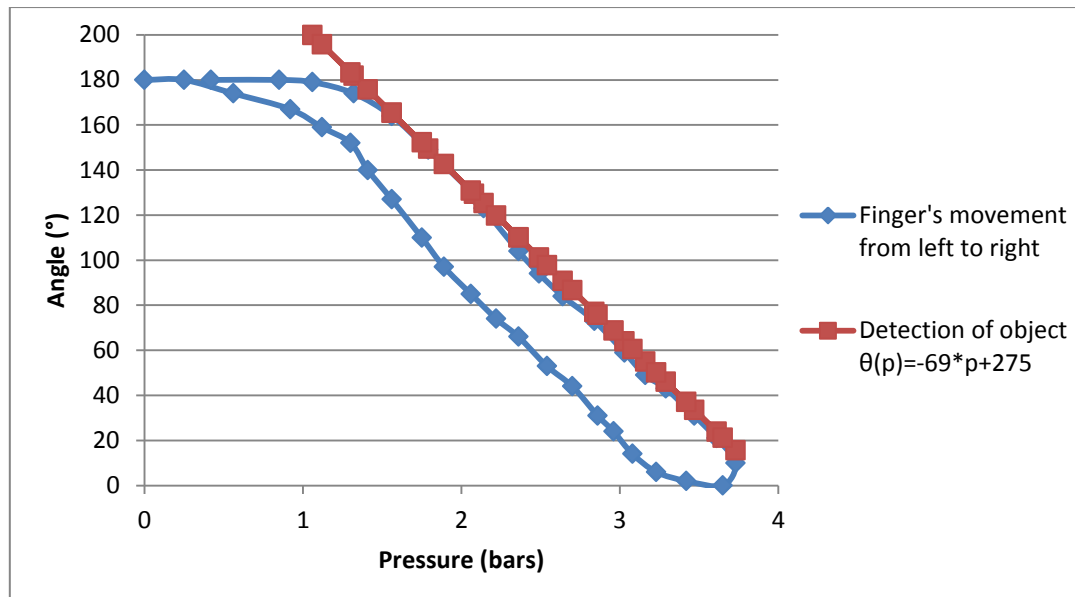
Figure 5.7: Angle of proximal phalange against pressure of right and left PAMs when finger goes from left to right

Contrary to SPAMs for which curves are shown in Figure 4.12, FPAMs' behaviour is much more linear between 2 bars and 4 bars. This is explained because their maximum contraction rate is reached for 8 bars instead of 4 bars [81]. Consequently, FPAMs are still far from their maximum contraction when they inflate at 4 bars. Secondly, it can be observed that the hysteresis effect is about twice more important in Figure 5.7 than in Figure 5.6. This is due because of the coordination of two PAMs when the finger goes from left side to right side. It is also noticed that the proximal phalange barely moves when pressures vary from 0 to 1 bar, contrary to the values collected in Table 4.7. This difference is explained because of a mechanical margin error provided as a safety mechanism. The technology of turnbuckles has indeed been imitated to calibrate the strings' length at the top of PAMs, using small devices based on screws, the development of which being explained in [254].

Because of the behaviour close to linearity obtained between 2 and 4 bars, linear functions can be drawn as comparison. It is observed that the curve obtained in Figure 5.6 is close to:

$$\theta(p) = 62 * p - 60 \tag{5.20}$$

whereas the curve obtained in Figure 5.7 is close to:

$$\theta(p) = -69 * p + 275 \tag{5.21}$$

For Figure 5.6 it is noticed that the line defined in (5.20) does not match the requirements when pressure is below 2.1 bars, which does not interfere with the grasping movement, as the angle does not reach 90° yet.

Using equations (5.20) and (5.21), it is deduced that the fingers touch an object if their trajectories overreach the fixed boundaries. Thus, the SMC is triggered.

5.2.2.2.   *Implementation of the SMC*

Once the fingers are in contact with objects, both pressure and angles must adjust in coordination. Therefore, instead of observing the angle according to the evolution of the pressure as in (5.20) and (5.21), the evolution of both values is taken into account according to the time. Therefore, $\Delta\theta(t)$ and $\Delta p(t)$ must be at the same side of the equation. Prior being integrated in the SMC, the evolutions of the angle and of the pressure are analysed according to:

$$\begin{bmatrix} \Delta\theta(t) * K_\pi \Delta p(t) \\ \Delta\dot{\theta}(t) * K_\pi \Delta\dot{p}(t) \end{bmatrix} < \begin{bmatrix} K_{\Delta\theta(t)\Delta p(t)} \\ K_{\Delta\dot{\theta}(t)\Delta\dot{p}(t)} \end{bmatrix} \tag{5.22}$$

when the fingers move from right to left, whereas the relational sign "$<$" is changed to "$>$" when the fingers move from left to right. In both cases, K_π is defined as:

$$K_\pi = \theta_{Max}/p_{Max} \tag{5.23}$$

so angles and pressure have an equivalent impact in the inequality. It is also noticed that data feedback is derived to design the sliding surface of the SMC. $K_{\Delta\theta(t)\Delta p(t)}$ and $K_{\Delta\dot{\theta}(t)\Delta\dot{p}(t)}$ are values defined and obtained from the equations (5.20) and (5.21). When the boundary fixed by the equations (5.20) is not overreached at a time t_s but is overreached at a time t_{s+1}, then:

$$K_{\Delta\theta(t)\Delta p(t)} = 62 * \Delta\theta(t) * \Delta p(t) - 60$$

$$\tag{5.24}$$

$$K_{\Delta\theta(t)\Delta p(t)} = 62 * [\theta(t_{s+1}) - \theta(t_s)] * [p(t_{s+1}) - p(t_s)] - 60$$

$$K_{\Delta\dot{\theta}(t)\Delta\dot{p}(t)} = 62 * \Delta\dot{\theta}(t) * \Delta\dot{p}(t)$$

(5.25)

$$K_{\Delta\dot{\theta}(t)\Delta\dot{p}(t)} = 62 * [\dot{\theta}(t_{s+1}) - \dot{\theta}(t_s)] * [\dot{p}(t_{s+1}) - \dot{p}(t_s)]$$

whereas, when the boundaries fixed by the equation (5.21) is overreached at a pressure p_0, then:

$$K_{\Delta\theta(t)\Delta p(t)} = -69 * \Delta\theta(t) * \Delta p(t) + 275$$

(5.26)

$$K_{\Delta\theta(t)\Delta p(t)} = -69 * [\theta(t_{s+1}) - \theta(t_s)] * [p(t_{s+1}) - p(t_s)] + 275$$

$$K_{\Delta\dot{\theta}(t)\Delta\dot{p}(t)} = -69 * \Delta\dot{\theta}(t) * \Delta\dot{p}(t)$$

(5.27)

$$K_{\Delta\dot{\theta}(t)\Delta\dot{p}(t)} = -69 * [\dot{\theta}(t_{s+1}) - \dot{\theta}(t_s)] * [\dot{p}(t_{s+1}) - \dot{p}(t_s)]$$

When at least one inequality of (5.22) goes wrong, it means a phalange is in contact with an object. Even though the same reaction can be deduced from (5.20) and (5.21), the way angles and pressure interact with each other in the system of inequations (5.22) permits them to be implemented in the SMC.

Using the equation of SMC applied to PAM technology, such as the one described in [202], the sliding surface is defined as:

$$S(t) = K_{\theta p}[\Delta\theta(t) * K_\pi \Delta p(t)] + \Delta\dot{\theta}(t) * K_\pi \Delta\dot{p}(t)$$

(5.28)

$$\dot{S}(t) = K_{\theta p}[\Delta\dot{\theta}(t) * K_\pi \Delta\dot{p}(t)] + \Delta\ddot{\theta}(t) * K_\pi \Delta\ddot{p}(t)\Delta\ddot{\theta}(t)$$

(5.29)

However, contrary to the equation shown in [202], the coordinates of the system are replaced by a ratio between angles and pressures to allow the hand to grab objects. As K_π for equation (5.23), $K_{\theta p}$ is defined as:

$$K_{\theta p} = [\Delta\dot{\theta}(t) * K_\pi \Delta\dot{p}(t)_{Max}]/[\Delta\theta(t) * K_\pi \Delta p(t)]_{Max}$$

(5.30)

Then the convergence to $\{S(t), \dot{S}(t)\}$ is achieved using a Lyapunov function to bring the system to an equilibrium point:

$$L = K_{PAM} * S(t) * \dot{S}(t)$$

(5.31)

In the case of PAM technology, K_{PAM} is usually chosen as ½, such as in [102] or in [199] but, because of the fingers' asymmetrical tendon routing, the coefficient attributed to each PAM varies from one to another, as seen for the ratios calculated in Section 5.2.2.1. Thus, the maximum value of K_{PAM} is defined as ½, but is often reduced according to the phalange position provided by $\theta(t)$. Using the same algebraic transformation as the one shown in [202], the boundary surface is then described as:

$$l = K_{PAM}\dot{S}(t) + tanh(K_{PAM} * S(t)/\varepsilon_b) \qquad (5.32)$$

with $\varepsilon_b > 1$. As arctangents increase very slowly for values higher than 3, ε_b increases the parameters from which is calculated the $tanh$, to amplify the difference obtained between two values. It is indeed noticed that:

$$\forall k \in [10; 20]$$

$$9.9 * 10^{-3} < tanh(k + 5) - tanh(k) < 3.3 * 10^{-2} \qquad (5.33)$$

whereas:

$$\forall k \in [1; 2]$$

$$8.3 * 10^{-2} < tanh(k + 0.5) - tanh(k) < 2 * 10^{-1} \qquad (5.34)$$

The constant is therefore fixed to $\varepsilon_b = 10$ for the experiments, which adds sensitivity to the system.

Next, the phalanges tighten around the object according to the limit defined by (5.32) until:

$$\Delta\theta(t) < \varepsilon_o \qquad (5.35)$$

where ε_o is a small constant, aiming at stopping the SMC when the angle barely varies between two successive feedbacks. The bigger ε_o, the more delicate the object is that the Ambidextrous Hand can grab; the smaller the grabbing force.

The whole process is illustrated in Figure 5.8.
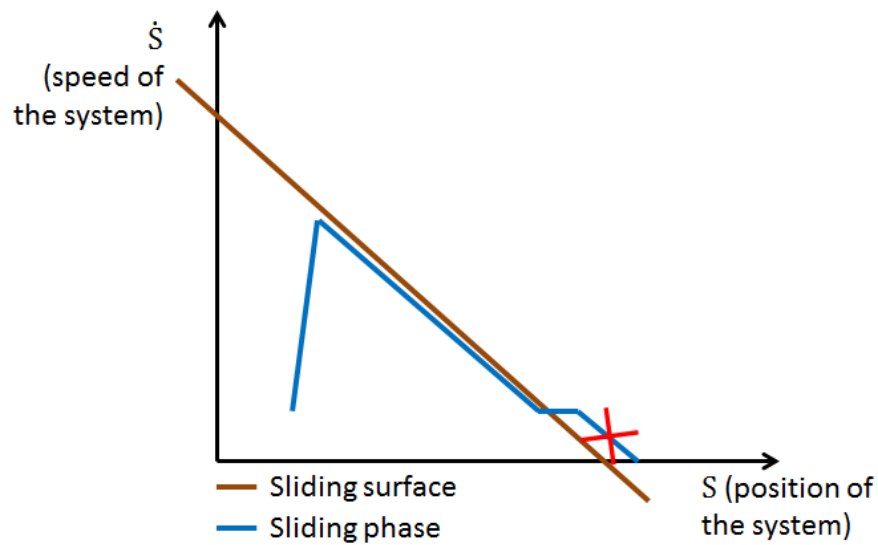
Figure 5.8: Implementation of a SMC to grab an object

As long as the inequality (5.35) is not verified, the sliding phase slides against the sliding surface defined by the equations (5.28) and (5.29). The sliding phase has to cross the sliding surface without overreaching it too much, as it would increase the force applied on objects. The overreaching of the sliding surface depends on the constant ε_o, defined in the inequality (5.35)

5.2.2.3.   *Experimental results obtained with the SMC*

The grasping abilities of the Ambidextrous Hand using the SMC are shown in Figure 5.9.
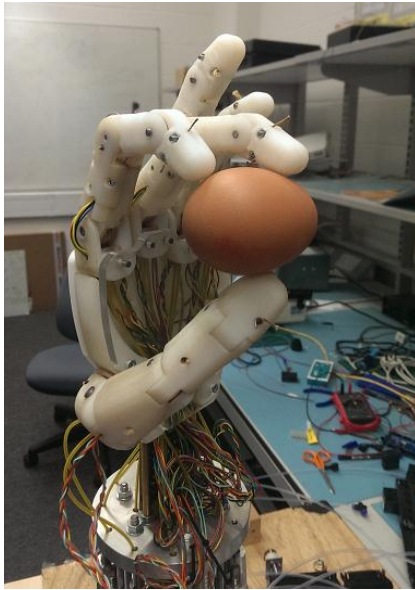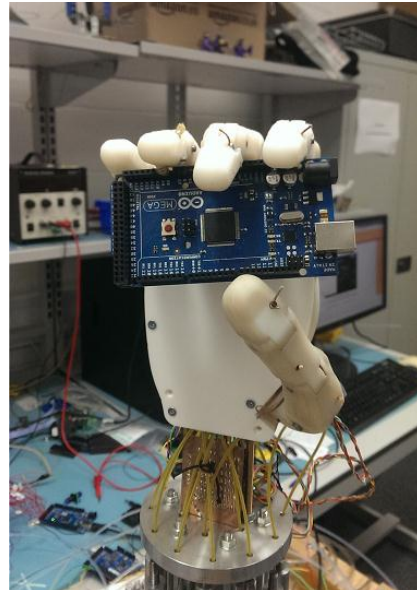
<div align="center">(a)   (b)</div>

Figure 5.9: Grasping mode using sliding-mode control
(a) a left hand mode grasping an egg and
(b) a right hand mode grasping an Arduino microcontroller

Figure 5.9 (a) shows that the ring and little fingers are close to vertical position, contrary to their position in Figure 5.9 (b). When the SMC ends, values are read from angular sensors. If fingers have an angle close to their extreme positions, it is estimated they do not touch the object and are consequently put back to a position close to vertical. The different steps of the grasping shown in Figure 5.9 (a) are illustrated in Figure 5.10.
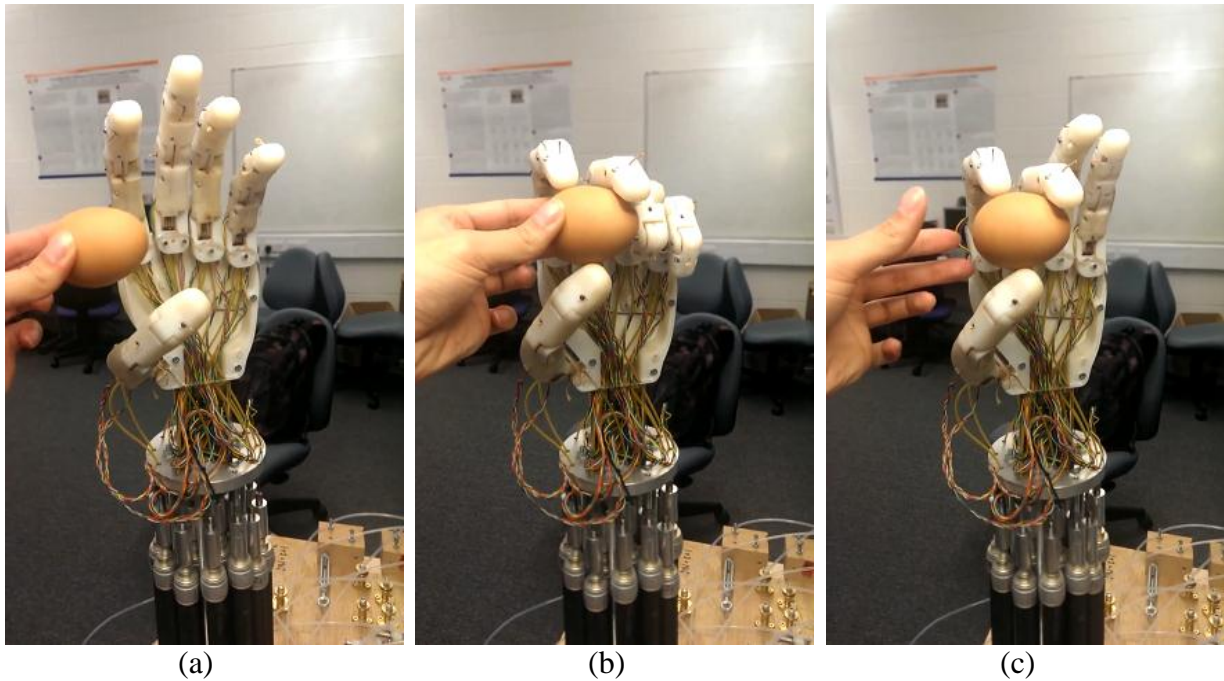
Figure 5.10: Video snapshots of the Ambidextrous Hand grasping an egg [288]
The hand opens itself in (a), closes in (b) and
ring and little fingers come back to vertical position in (c)

The SMC runs for a very short time as, in average, from the position illustrated in Figure 5.10 (a), the SMC is triggered after 0.20 sec and stops after 0.23 sec. Contrary to the angular displacements observed in Section 5.1.3, the lack of speed barely interferes when the Ambidextrous Hand grabs objects. This is explained because every PAMs and tubings already contain pressurised air when the hand opens, whereas a number of them can be totally empty at some angular positions. A shorter air flow is consequently necessary for grasping movements.

The experiment illustrated in Figure 5.10 is repeated a number of times to collect data. Putting the egg at close initial positions for each run, the final angles reached by the concerned MCP and PIP joints are summarised in Table 5.3 and Figure 5.11.

Table 5.3: Joints angles when the Ambidextrous Hand holds an egg (deg)

Run of the experiment	1	2	3	4	5	6
Forefinger's MCP	66.5	61.5	61.5	63.4	62.8	66.3
Forefinger's PIP	37.1	40.6	41.8	39.1	40.6	37.9
Middle finger's MCP	49.0	48.1	49.6	51.8	47.8	50.2
Middle finger's PIP	63.3	63.8	61.6	60.3	64.2	62.3
Thumb's adduction	42.0	41.7	42.6	43.1	42.8	44.5
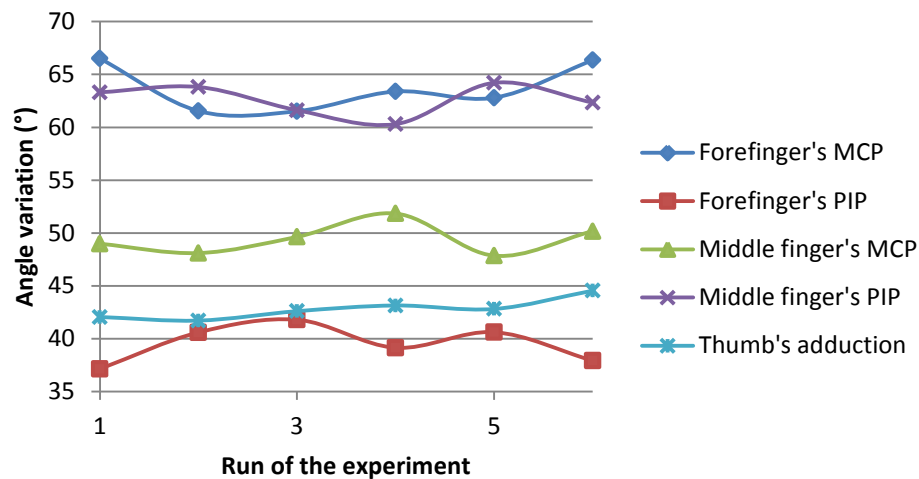
Figure 5.11: Joints angles when the Ambidextrous Hand holds an egg

Table 5.3 and Figure 5.11 show that MCP and PIP joints depend on each other: when one decreases, the other one increases to secure the grasping. As the design of the Ambidextrous Hand stepped aside the thumb opposition in favour of its abduction / adduction, it is also noted that only the force of the thumb's adduction is applied to the object.

During these same experiments, in addition to joint angles, the pressure of PAMs is also collected. Their grasping values are summarised in Table 5.4 and Figure 5.12.

Table 5.4: PAMs' pressure when the Ambidextrous Hand is holding an egg (bars)

Run of the experiment	1	2	3	4	5	6
Forefinger's MCP	2.42	2.59	2.60	2.51	2.56	2.43
Forefinger's PIP	2.19	2.06	2.01	2.15	2.03	2.17
Middle finger's MCP	2.85	2.89	2.79	2.72	2.95	2.79
Middle finger's PIP	1.75	1.74	1.82	1.86	1.71	1.77
Thumb's adduction	0.85	0.84	0.88	0.90	0.88	0.92
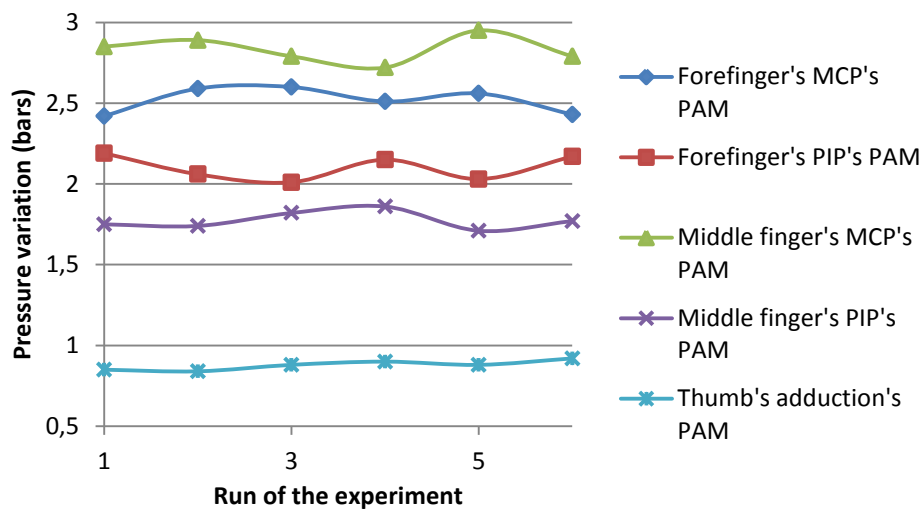
Figure 5.12: PAMs' pressure when the Ambidextrous Hand is holding an egg

Except the thumb's adduction that is controlled by its right PAM, the other joints show that the higher the pressure, the smaller the angle and that the PAMs connected to the MCP joints require more pressure than PIP's ones.

The global diagram of this whole control approach, combining PID controls, PPSC and SMC is shown in Figure 5.13. The PPSC switches between the PID loops tuned with classic gain constants or dynamic coefficients according to $\theta(t)$. The PID loops stop when $\theta(t)$ and $p(t)$ trigger the SMC. Another PPSC makes the SMC loops carry on until $\Delta\theta(t) < \varepsilon_o$. When the SMC stops, the grasping angle is put as the new setpoint of the system.
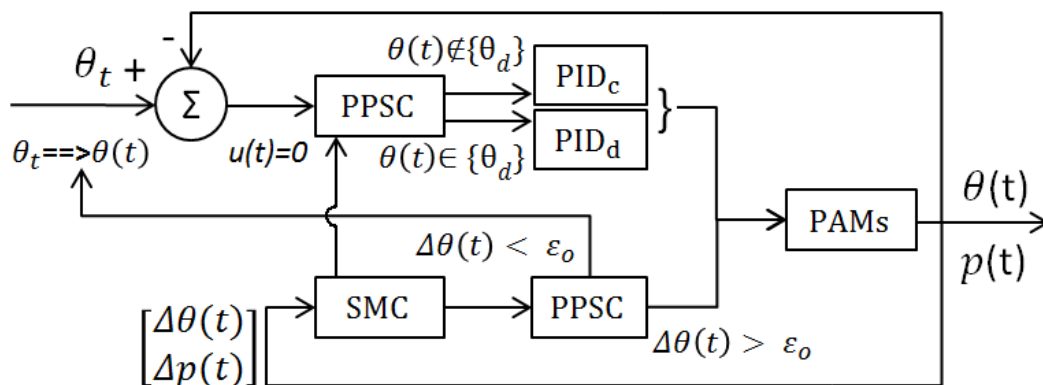
Figure 5.13: Global diagram of the whole system approach

5.2.3. Comparison with other SMCs

Because of the Ambidextrous Robot Hand architecture, the objects are not in contact with the inside of the thumb but with its side (as seen in Figure 5.9), which makes the grasping not as human-like as the ones that would be possible, for instance, with the ACT Hand and the joint torque control introduced in [175]. This is due because of the limited number of DOFs of the Ambidextrous Hand's thumb, which only has three, whereas robot thumbs usually include at least four DOFs to allow motion relative to the palm, as explained in [291], [52] or [54]. However, the holding features of the Ambidextrous Hand are still more anthropomorphic than the ones of the two-fingered and three-fingered motorized robot hands respectively concerned in [61] and [51], even though these two models have other advantages. Indeed, as explained in section 2.1, changing the shape of the hand, as well as the position and the number of fingers, can ease the implementation of control algorithms, allowing a stronger grasp and so an accurate manipulation of objects, as shown by the stability of the system described in [292]. Nevertheless, despite its thumb limitation, the experiments proved that the Ambidextrous Hand can grab objects in a similar way to that of other robot hands, such as the ones illustrated in [293].

The technical characteristics of the SMC are summarised in Table 5.5, with the technical characteristics of SMCs implemented on other robotic devices. These other robotic devices are mainly actuated by PAMs. It is observed that none of these pneumatic devices are robot hands or robot fingers, but rather bigger structures, such as robot arms, as in [205] or [203], robot axes [201] or manipulators [200]. None of these devices exceed five links, and

the robot arm engineered by K. Braika et al. [203] is the only structure summarised in Table 5.5 that exceeds four DOFs and that is pneumatically actuated. This proves the originality of the SMC introduced in Section 5.2.2, as it is the unique SMC engineered on a robotic device actuated by PAMs as sophisticated as the Ambidextrous Hand. Indeed, the Ambidextrous Hand is made of fourteen links (which, in this case, are phalanges) and its SMC is implemented on nine of its thirteen DOFs (the abduction/adduction of the forefinger, ring finger and little finger as well as the flexion/extension of the thumb being not integrated in the algorithm).

In addition to structures driven by PAMs, the motorised robot hands [287] and [286] are also summarised in Table 5.5, as they are the projects for which the use of the SMC is the closest to the one of the Ambidextrous Hand. Indeed, the hand [286] is the only robotic structure of Table 5.5 that has as many phalanges as the Ambidextrous Hand, whereas the hand [287] is the only one that uses SMC as force control. However, the SMC of the Ambidextrous Hand is the only one that controls the force of its structure from pressure and angular feedbacks. This feature is one of the most original points of the Ambidextrous Hand's SMC and allows the robotic structure to grab objects without integrating force sensors and wires in the fingers' mechanical architecture, which eases the design of the 3D printed pieces. The other original features of this SMC are summarised in Table 5.6, in comparison with the same robotic models that are summarised in Table 5.5.

Table 5.5: Comparison of SMC's characteristics between the ones of the Ambidextrous Hand and the ones of other robotic models

SMC	Robotic device	Type of actuators	Aim of the SMC	SMC's input(s)	# links or phalanges	# DOFs	# actuators
P. Carbonell et al. [199], 2001	N/A, single PAM	PAM	PAM's length control	Pressure feedback	N/A	N/A	1
M. Van Damme et al. [200], 2007	Mani-pulator	PAMs	Angular control	Force feedback	2	2	14
M. Chettouh et al. [205], 2008	Arm	PAMs	Position control	Position feedback	3	3	6
H. Aschemann and D. Schindele [201], 2008	Axis	PAMs	Position control	Angular feedback	1	1	2
E.D. Engeberg and S.G. Meek [287], 2009	Two fingers	Motor	Force control	Force feedback	4	1	1
S. Boudoua et al. [102], 2010	Arm	PAMs	Trajectory control	Pressure feedback	3	3	6
D. Schindele and H. Aschemann [196], 2010	Parallel robot	PAMs	Position control	Position and angular feedbacks	2	2	4
K. Braika et al. [203], 2010	Arm	PAMs	Angular control	Pressure and angular feedbacks	3	7	N/A, ≤ 7[a]
Z. Tong et al. [206], 2011	Joint model	PAMs	Trajectory control	Angular feedback	1	1	2
A. Rezoug et al. [204], 2012	Arm	PAMs	Angular control	Position feedback	2	2	N/A, ≤ 4[a]
J. Jalani et al. [286], 2013	Hand	Motors	Compliance and posture control	Force feedback	14	N/A, ≤ 10[a]	N/A, ≤ 10[a]
E. Akyürek et al. [40], 2014	Hand	PAMs	Force control	Pressure and angular feedbacks	14	9[b]	14[b]

[a] Estimations are made from pictures or details in the article
[b] Four DOFs and four actuators are not used for the SMC

Table 5.6: Originality of the SMC implemented on the Ambidextrous Hand

SMC	Structure actuated by PAMs	Structure actuated by motors	# actuators > 10	Implemented on a robot hand	Implemented to grab objects	Sliding surface purposely crossed	Ambidextrous behaviour
P. Carbonell et al. [199], 2001	✓						N/A
M. Van Damme et al. [200], 2007	✓						N/A
M. Chettouh et al. [205], 2008	✓						N/A
H. Aschemann and D. Schindele [201], 2008	✓						N/A
E.D. Engeberg and S.G. Meek [287], 2009		✓		✓	✓		
S. Boudoua et al. [102], 2010	✓						N/A
D. Schindele and H. Aschemann [196], 2010	✓						N/A
K. Braika et al. [203], 2010	✓						N/A
Z. Tong et al. [206], 2011	✓						N/A
A. Rezoug et al. [204], 2012	✓						N/A
J. Jalani et al. [286], 2013		✓		✓	✓		
E. Akyürek et al. [40], 2014	✓		✓	✓	✓	✓	✓

Table 5.6 shows that, in addition to be the only SMC implemented on a robot hand driven by PAMs and that controls force from pressure and angular feedbacks, the Ambidextrous Hand's SMC is the only one that is implemented on a structure having more than ten actuators, for which the crossing of sliding surface is a part of the process, and that is implemented on a hand with an ambidextrous behaviour.

The grasping abilities of the Ambidextrous Hand will be compared with other models more in detail in Section 5.3, where a more common control algorithm will be implemented.

5.3.   Force control from tactile feedback

In addition to be controlled by pressure and angular feedbacks, the force applied by the ambidextrous fingers can also be controlled by tactile feedback. As pressure sensors are quite expensive, this cheaper solution is investigated. Indeed, the pressure transducers selected in Section 4.1.1.2 are about six times more expensive than the force sensors selected in Section 3.4.3.1. Therefore, the force sensors implemented on early designs of ambidextrous fingers are implemented on the Ambidextrous Robot Hand as well. In case

grasping algorithms are successful, a future version of the Ambidextrous Hand may include force sensors and additional wires inside its mechanical architecture.

Three different algorithms are implemented to grasp objects with force feedback, which are PID control, bang-bang control and BSC. The implementation and the results obtained with each of these algorithms are going to be discussed. The originality of the grasping abilities of the Ambidextrous Hand and of the grasping algorithms are also going to be compared with the ones of other robot hands.

Force targets of 1 N are fixed to each sensor of each experiment. However, given that the object is put in contact with other points as the force sensors and that the weight of the fingers must be taken into account as well, the overall force applied to objects should overreach 10 N, which is why a force target of 12 N is fixed for the thumb.

Contrary to the pressure and angular sensors, which are connected to the PAMs and to the fingers' displacements, force sensors only cover some strategic points of the fingers. Therefore, in case objects get into contact with the robotic fingers at a point not covered by force sensors, the fingers carry on closing without any variations in the grasping algorithms. Thus, the grasping algorithms are combined with an NN used as a security system. The implementation of this NN is discussed in the report of N. Lesne [289]. With the implementation of the NN, the controllers do not only take the feedback of their own fingers into account, but the feedback of each finger. If the setpoint is reached for a force sensor whereas other sensors provide no feedback, the angular position is taken into account. A mechanism similar to the one illustrated in Figure 5.10 is then triggered. If the angular feedbacks of fingers show that the fingers are almost perpendicular to the palm, then the fingers do not touch the object and are brought back to a position close to vertical. On the contrary, if the fingers' angular feedbacks are close to the one of the finger that touches the object, then these fingers touch the object as well and the grasping algorithms are stopped.

Experiments are performed on empty Coca-Cola cans, to observe if the control algorithms cause any deformations to the objects.

The work introduced in this Section is based on the upgrade of the hardware developed in [289]. The algorithms discussed in the Sections 5.3.1, 5.3.2 and 5.3.3 have also been implemented in collaboration with [289].

5.3.1. Tactile feedback driven by PID control

The same principle that was used on early prototype in Section 3.4.3 is applied to the complete design of the Ambidextrous Robot Hand. However, because of the asymmetrical tendons routing, $u(t)$ needs to be calculated taking the new mechanical specifications into account. $u(t)$ is consequently divided into three different outputs for the three PAMs driving each finger.

5.3.1.1.   Implementation of the PID control

The three outputs of the PID controllers are $u_{pl}(t)$, $u_{mr}(t)$ and $u_{ml}(t)$, respectively attributed to the proximal left, medial right and medial left PAMs. The same notations are used for the gain constants. The adapted PID equation is defined as:

$$\begin{bmatrix} u_{pl}(t) \\ u_{mr}(t) \\ u_{ml}(t) \end{bmatrix} = \begin{bmatrix} K_{p_{pl}} & K_{i_{pl}} & K_d \\ K_{p_{mr}} & K_{i_{mr}} & K_d \\ K_{p_{ml}} & K_{i_{ml}} & K_d \end{bmatrix} \begin{bmatrix} e(t) \\ \int_0^t e(\tau)d\tau \\ \frac{d}{dt}e(t) \end{bmatrix} \tag{5.36}$$

Because of the fingers' architecture, some PAMs must contract slower than others to imitate a human behaviour when the fingers are tightening around an object. It mainly avoids having medial and distal phalanges totally close when the proximal phalange is bending. The proportional and integrative constant gains are consequently defined as:

$$\begin{bmatrix} K_{p_{ml}} \\ K_{i_{ml}} \end{bmatrix} = \begin{bmatrix} K_{p_{pl}}/3 \\ K_{i_{pl}}/3 \end{bmatrix} = \begin{bmatrix} -K_{p_{mr}} \\ -K_{i_{mr}} \end{bmatrix} \tag{5.37}$$

when the object is on the left side, whereas defined as:

$$\begin{bmatrix} K_{p_{mr}} \\ K_{i_{mr}} \end{bmatrix} = \begin{bmatrix} 0.4 * K_{p_{ml}} \\ 0.4 * K_{i_{ml}} \end{bmatrix} = \begin{bmatrix} -K_{p_{pl}} \\ -K_{i_{pl}} \end{bmatrix} \tag{5.38}$$

when the object is on the right side.

Identical derivative gain constants are used for the three different PAMs.

Using equation (5.36), PID control loops with identical gain constants are sent to the four fingers with a target of 1 N and an error margin of 0.05 N, whereas the thumb is assigned to a target of 12 N with an error margin of 0.5 N.

5.3.1.2.   *Results obtained with the PID control*

Data is collected every 0.05 sec while the grasping algorithm is running. The results of the experiment are shown in Figure 5.14. The feedback collected from the thumb is not included in the diagram as it stabilises itself at 12.23 N, which is a much higher value than the four other fingers. The feedback collected before 0.1 sec is not included either, as the fingers are not touching the object yet at 0.05 sec.

(a)
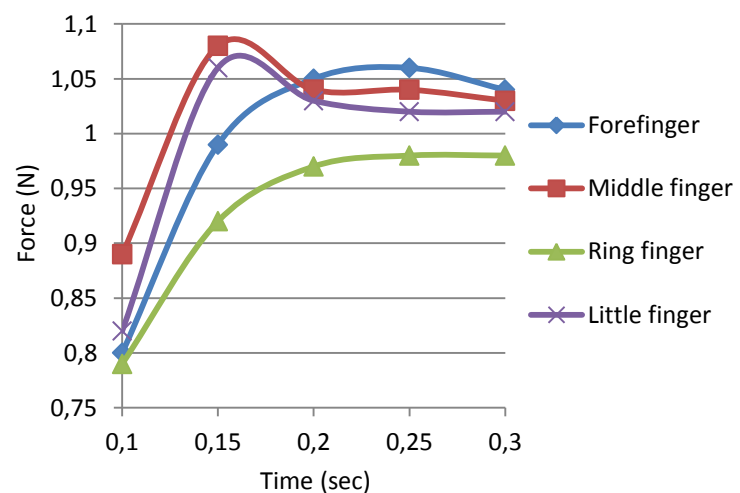
(b)

Figure 5.14: Ambidextrous Hand grasping a can with PID control and force feedback
(a) an image and (b) the force against time for the four fingers

Figure 5.14 (b) shows that the fingers start grasping the object at around 0.15 sec and that the grasping becomes more stable after 0.2 sec. Most of the fingers' force feedbacks have an overshoot but it never exceeds 10% of the value fixed as target and the force is automatically adjusted at the next collection. These small overshoots are explained because different parts of the fingers get into contact with the object before the object actually gets into contact with the force sensor. Consequently, the PAM's elasticity already makes the

fingers bending slower when the phalanges touches the object. As the can does not deformed with the fingers' pressure, it can be deduced that the grasping control is both fast and accurate when the Ambidextrous Hand is driven by PID loops.

5.3.1.3.   *Comparison with other grasping algorithms*

The mechanical features relative to the grasping of the Ambidextrous Hands and the results obtained with tactile feedback driven by PID control are compared with the ones of other robotic models in Table 5.7. Robot hands for which the grasping time depends on an HCI, such as data gloves or EMGs, as for [99], [143] or [123] are not taken into account in Table 5.7. The implementation of an HCI indeed requires a longer process time for the algorithms, making the control system different from the one described in Section 5.3.1.1. Half of the maximum overshoots (or errors) taken into account Table 5.7 are considered when the force target is fixed to 1 N ± 10%, which matches with the data discussed in Section 5.3.1.2. This is the case for the hands [63], [98] and [282], whereas the experiments realised with the hands [291] and [96] are done with a setpoint of 0.5 N, against a setpoint of 3 N for [292]. As the thumb of the Ambidextrous Hand is not opposable to the other fingers, the opposition of other robot hands' thumbs is also considered. With the exception of [290], each other robot hand summarised in Table 5.7 grabs objects with a thumb in an opposite position. Nevertheless, the mechanical architectures of the hands [117], [61], [98] and [101] do not allow the thumbs to line up with the palm and the other fingers. Their thumbs are therefore systematically opposite, without being opposable. The Ambidextrous Hand, the hand designed by S. Nishino et al. [96] and the TU Bionic Hand [290] are consequently the only models of Table 5.7 that have an anthropomorphic positioning of five fingers with only thirteen or fifteen DOFs, instead of a minimum of nineteen DOFs for the DLR Hand [281].

Grasping times usually do not exceed 0.25 sec for the models of Table 5.7 designed since 2012, as for [281], [94], [282] and the Ambidextrous Hand. The grasping algorithm implemented on the DLR Hand II [293], in 2012 as well, explores a totally different method as the object surface is firstly sampled, before proceeding to the investigations of the best grasping spots. These spots permit the fingers to grab the object in an anthropomorphic way, matching with the local curvature of the object. The algorithm is however longer to process, as it can take up to 30 sec to grab an object. Apart from this case, grasping times are much longer before 2012, as for the ITU Hand [117], which is driven by SMAs (that have the

slowest reaction speed among the artificial muscles introduced in Section 2.1.3) and which has a grasping time of 3.76 sec. The other examples are the hands engineered by S. Nishino et al. [96], D. Gunji et al. [61] and J.Y. Nagase et al. [98], for which the grasping times are respectively estimated to 1.0 sec, 0.6 sec and 0.9 sec. The grasping algorithm designed by J.Y. Nagase et al. [98] is both among the most accurate and the slowest engineered after 2010 in Table 5.7. As for the angular displacements discussed in Section 5.1.3, it is observed that fuzzy logic allows more precise but slower movements than the ones driven by PID and PD controls. It is also noticed that, contrary to the papers discussed in Section 5.1.3, PD control is implemented more often than PID control to grab objects. This is explained because the grasping time is usually reached in a shorter delay than the full rotation of fingers from open to close positions. Consequently, as observed in the transfer function of PID controllers shown in equation (5.36), the integrative term does not have time to become significant and can be removed from the PID controllers. Results obtained with algorithms different from fuzzy logic are accurate as well, as they do not exceed 10% of the setpoint for the models [63], [96] and the Ambidextrous Hand. The DEXMART Hand [282] uses a different system based on NN, the aim of which being to predict the force applied by the fingertips during the fingers' torque reconstruction.

Table 5.7: Comparison of grasping features between the Ambidextrous Hand and other models, when the Ambidextrous Hand's tactile feedback is driven by PID control

Robot hand	# fingers	Type of actuators	# DOFs	Grasping algorithm	Anthropomorphic positioning of fingers	Thumb opposite to other fingers during grasping	Grasping time (sec)	Max. overshoot or error (%)	Ambidexterity
Gifu Hand II [291], 2002	5	Motors	16	PID	✓	✓	0.55[ab]	16%[ab]	
High-speed hand [280], 2003	3	Motors	8	PD		✓	0.05[a]	N/A	
ITU Hand [117], 2004	2	SMAs	1[a]	N/A		✓	3.76	N/A	
I. Yamano and T. Maeno [63], 2005	5	SMAs	20	N/A	✓	✓	N/A	6%[a]	
L. Zollo et al. [54], 2007	3	Motors	10[a]	PD	✓	✓	N/A	N/A	
S. Nishino et al. [96], 2007	5	PAMs	13[a]	PID, Cascade	✓	✓	1.0[a]	6%[a]	
D. Gunji et al. [61], 2008	2	Motors	1	PD		✓	0.6[a]	N/A	
T. Yoshikawa [292], 2010	2	Motors	4[a]	PID		✓	0.55[a]	22%[a]	
J.Y. Nagase et al. [98], 2011	4	PAMs	N/A	Fuzzy logic	✓ [c]	✓	0.9[a]	9%[ad]	
DLR Hand II [293], 2012	4	Motors	16[a]	N/A	✓	✓	28.7	N/A	
DLR Hand [281], 2012	5	Motors	19	Cascade	✓	✓	0.1[a]	N/A	
Shadow Hand [94], 2013	5	PAMs	20	PID	✓	✓	0.15[a]	N/A	
Shadow Hand [62], 2013	5	Motors	20	PID	✓	✓	0.15[a]	N/A	
ACT Hand [66], 2013	5	Motors	23	N/A	✓	✓	N/A	N/A	
T. Nuchkrua et al. [101], 2013	3	PAMs	3	N/A		✓	N/A	N/A	
TU Bionic Hand [290], 2013	5	Motors	15	PID	✓		0.208	N/A	
DEXMART Hand [282], 2014	5	Motors	20	NN	✓	✓	0.25[a]	25%[ad]	
Ambidextrous Hand [41], 2014	5	PAMs	13	PID	✓		0.20	8%	✓

[a] Estimations are made from curves, pictures or videos of the robot hands
[b] Experiments do not concern grasping but contact tasks
[c] Only for grasping
[d] For a target of 1 N ± 10%, whereas the error can exceed 30% for lower force targets

In conclusion, the Ambidextrous Hand has a grasping time and a maximum overshoot close to the best ones obtained with other robot hands. It can therefore successively grab objects despite its limited number of DOFs, and it is the only robotic model that can grab objects with an ambidextrous behaviour, either as a left or a right hand, equally performing well.

5.3.2. Tactile feedback driven by bang-bang control

It was observed in [185] that a bang-bang controller was actuating a bipedal walking robot being cascaded with a PI controller. This Section aims at implementing a bang-bang controller on a robot hand actuated by PAMs for the first time. The bang-bang algorithm is cascaded with a proportional control that is used as an outer loop.

5.3.2.1.   Implementation of the bang-bang control

The bang-bang controller is implemented to make the fingers close around objects without taking any temporal parameters into account. The algorithm stops itself for each finger when the force target is reached and does not make the fingers go backward in case of overshoots. To compensate the absence of backward control, a further condition is implemented in addition to initial requirements. Indeed, as the force applied by the four fingers is controlled with less accuracy than with PID loops, the thumb must offset the possible excess of force to balance the grasping of the object. Therefore, a balancing equation is defined as:

$$F_{tmin} = W_o + \sum_{f=1}^{4} F_f \tag{5.39}$$

where F_{tmin} is the minimum force applied by the thumb, whereas F_f refers to the force applied by each of the four other fingers. W_o is an approximate weight of the object to be grab. It is negligible for light objects but needs to be defined for objects weighing more than 25 N. A more accurate mathematical model would also include the weight of the other fingers as $\sum_{f=1}^{4} W_f$, but F_{tmin} always fits with equation (5.39) for light objects. Moreover, as the summation of W_f is close to 7 N, it does not interfere either with heavier objects, which is why W_f is not included in (5.39). As for PID control investigated in section 5.3.1, the phalanges must close with appropriate speed's ratios to tighten around objects. Therefore, an approach similar to one of the methods used in [187] is implemented. The bang-bang controllers of the Ambidextrous Hand are driven by proportional controllers, for which the coefficients are the same as the ones used in section 5.3.1. A diagram of the bang-bang

control is shown in Figure 5.15, in which F_t is the force set as target and $F_f(t)$ is the force received from each sensor.
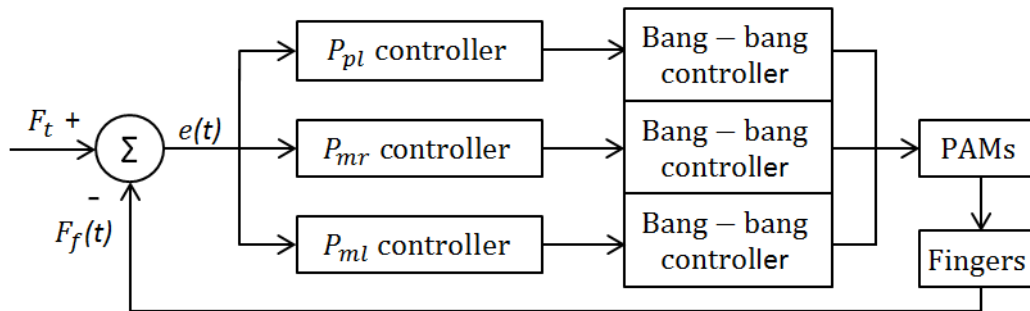
Figure 5.15: Bang-bang loops cascaded with proportional controllers

5.3.2.2.   *Results obtained with the bang-bang control*

The experimental settings are identical to the ones described in Section 5.3.1, where the Coca-Cola can is used to evaluate any deformation caused by grasping algorithms. The results obtained with the bang-bang controller are demonstrated in Figure 5.16. This time, it is observed in (a) that the can becomes deformed when it is grasped on the left hand side.
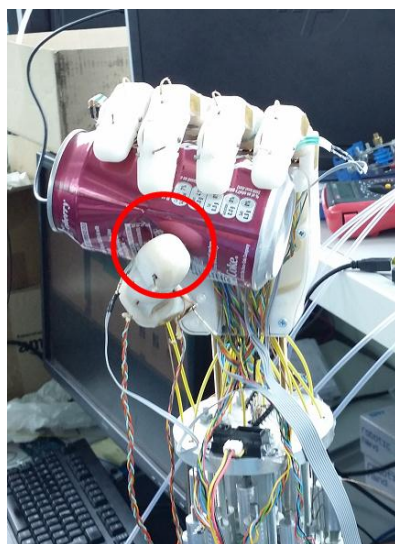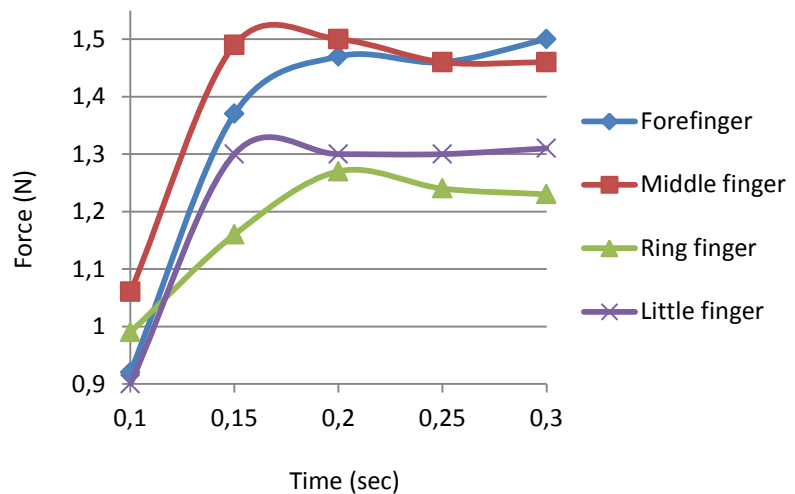
| (a) | (b) |

Figure 5.16: Ambidextrous Hand grasping a can with bang-bang control and force feedback (a) an image and (b) the force against time for the four fingers

Without the integrative and derivative gains, Figure 5.16 (b) shows that the fingers' speed barely varies when they start touching the object, as the scopes of the curves are much

higher as the ones obtained in Figure 5.14 (b), which makes the bang-bang controller faster than the PID loops. The bang-bang controllers also stop when the value of 1 N is overreached but, without predicting the approach to the setpoint, the process variables have huge overshoots. The overshoot is mainly visible for the middle finger, which overreaches the setpoint by more than 50%. Even though backward control is not implemented in the bang-bang controller, it is seen the force applied by some fingers decreases after 0.20 sec. This is due to the deformation of the can, which reduces the force applied on the fingers. It is also noticed that the force applied by some fingers increase after 0.25 sec, whereas the force was decreasing between 0.20 and 0.25 sec. This is explained because of the thumb's adduction that varies from 7.45 N to 15.30 N from 0.10 sec to 0.25 sec. Even though the fingers do not tighten anymore around the object at this point, the adduction of the thumb applies an opposite force that increases the forces collected by the sensors. The increase is mainly visible for the forefinger, which is the closest one from the thumb.

Contrary to PID loops, it is seen that the force applied by some fingers may not change between 0.15 sec and 0.20 sec, which indicates the grasping stability is reached faster with bang-bang controllers. The bang-bang controllers can consequently be applied for heavy objects, changing the setpoint of F_f defined in equation (5.39). Experiments showed that bang-bang control could be applied to plastic bottles, the same way as PID control in Section 5.2.1.

5.3.2.3.   *Comparison with other bang-bang controls*

The features relative to the bang-bang control implemented on the Ambidextrous Hands and the results obtained from it are compared with the ones of other bang-bang controls in Table 5.8. The bipedal walking robot engineered in Vrije Universiteit Brussel and discussed in [146], [185], [186] and [187] is the only project revealed in the literature review of Section 2.5.1.2 for which bang-bang control is implemented on a robotic structure driven by PAMs. Nevertheless, even though the hand designed by Z. Xu et al. [142] is actuated by air cylinders instead of PAMs, its architecture is much closer to the one of the Ambidextrous Hand, which is why it is included in Table 5.8 as well.

Table 5.8: Comparison of bang-bang controls' characteristics between the Ambidextrous Hand and other robotic models

Bang-bang control	Robotic structure	Type of actuators	Aim of the bang-bang control	Controller used as an outer loop	# DOFs	# actuators	Execution time (sec)	Error max. (%)	Ambidexterity
R. Van Ham et al. [146], 2003	Modular part of a leg	PAMs	Pressure control	PID	N/A	2	0.2[a]	N/A	
B. Vanderborght et al. [185], 2005	Two legs	PAMs	Generate a joint trajectory	PI	3	6	0.4[a]	4% for pressure[a] 0.27% for angle[a]	
B. Vanderborght et al. [186], 2005	Two legs	PAMs	Generate a joint trajectory	PID	3	6	0.2[a]	3% for pressure 4.5% for angle[a]	
B. Vanderborght et al. [187], 2006	Two legs	PAMs	Generate a joint trajectory	Delta-p	6	12	0.15[a]	17% for pressure[a] 17.5% for position[a]	✓
Z. Xu et al. [142], 2013	Index of a hand	Air cylinders	Evaluation of speed capabilities	None	2[b]	4[b]	0.33	N/A	
Ambidextrous Hand [41], 2014	Hand	PAMs	Force control	Proportional	9[b]	14[b]	0.15	53% for the force	✓

[a] Estimations are made from curves
[b] A number of DOFs and actuators are unused for the bang-bang control

Table 5.8 shows that bang-bang control is not usually implemented on complex structures, as the Ambidextrous Hand and the two legs discussed in [187] are the only architectures that exceed ten actuators. The Ambidextrous Hand is also the only robotic structure in Table 5.8 that has more than ten DOFs. The execution times are not very significant, given that the aims of the bang-bang controls are totally different from one project to another; it is nevertheless observed that the execution times never exceed 0.4 sec, as bang-bang controls aim at making a system switch from one state to another as fast as possible. The system proves its efficiency for the walking robot introduced in [146], [185], [186] and [187], but provides a huge overshoot of 53% when it is implemented on the Ambidextrous Hand.

Consequently, despite the originality of the bang-bang control to grab objects, its implementation on an ambidextrous device and its grasping time of 0.15 sec (25% shorter than the one obtained with the PID control), the bang-bang control is not accurate enough to control the fingertips' force of the Ambidextrous Hand.

5.3.3. Tactile feedback driven by BSC

BSC compares the system's evolution to stabilising functions. Derivative control is recursively applied until the fingers reach the conditions implemented in the control loops. As the literature review revealed no robot hands driven by BSC, this Section aims at validating the possibility to control such a mechanism using BSC. An exception can almost be found in [296], as the paper discusses a robot manipulator with 5 DOFs controlled by BSC but, in addition to not being a hand with 13 DOFs, the mechanical system is actuated by DC motors, for which the dynamics are totally different from PAMs.

5.3.3.1. Implementation of the BSC

The first step of the BSC consists in tracking the error $e_1(t)$ defined as:

$$\begin{bmatrix} e_1(t) \\ \dot{e}_1(t) \end{bmatrix} = \begin{bmatrix} F_t - F_f(t) \\ -\dot{F}_f(t) \end{bmatrix} \tag{5.40}$$

where F_t is the force put as target and $F_f(t)$ is the force received for each finger. The stability of this close loop system is then evaluated using a first Lyapunov function defined as:

$$V_1(e_1) = \frac{1}{2} e_1^2(t) < F_{gmin} \tag{5.41}$$

$$\dot{V}_1(e_1) = e_1(t) * \dot{e}_1(t) = -\dot{F}_f(t) * e_1(t) \tag{5.42}$$

The force provided by the hand is assumed not being strong enough as long as $e_1^2/2$ exceeds a minimum grasping force defined as F_{gmin}. In (5.42), it is noted that $\dot{e}_1(t) \neq 0$ as long as $F_f(t)$ keeps varying. Therefore, $\dot{V}_1(e_1)$ cannot be stabilised until the system stops moving. Thus, a stabilising function is introduced. This stabilising function is noted as a second error $e_2(t)$:

$$e_2(t) = k * \dot{e}_1(t) \qquad\qquad (5.43)$$

with k a constant > 1. $e_2(t)$ indirectly depends on speed, as the system cannot stabilised itself as long as the speed carries on varying. Consequently, both the speed of the system and $e_2(t)$ are equal to zero when one finger reaches a stable position, even if $F_f(t) \neq F_t$. k aims at increasing $\dot{e}_1(t)$ to anticipate the kinematic moment when $\dot{e}_1(t)$ becomes too low. In that case, the BSC must stop running as $F_f(t)$ is close to F_t. Both of the errors are considered in a second Lyapunov function:

$$V_2(e_1, e_2) = \frac{1}{2}(e_1^2(t) + e_2^2(t)) < F_s \qquad\qquad (5.44)$$

$$\dot{V}_2(e_1, e_2) = e_1(t) * \dot{e}_1(t) + e_2(t) * \dot{e}_2(t) \qquad\qquad (5.45)$$

where F_s defines a stable force applied on the object. This second step allows stabilising the system using derivative control. Using (5.43), (5.45), can be simplified as:

$$\dot{V}_2(e_1, e_2) = \dot{e}_1(t) * (e_1(t) + k\ddot{e}_1(t)) \qquad\qquad (5.46)$$

The whole BSC process is illustrated in Figure 5.17. According to the force feedback $F_f(t)$, the fingers' positions adapt themselves until the conditions of the Lyapunov functions $(V_1, \dot{V}_1)$ and $(V_2, \dot{V}_2)$ are reached.
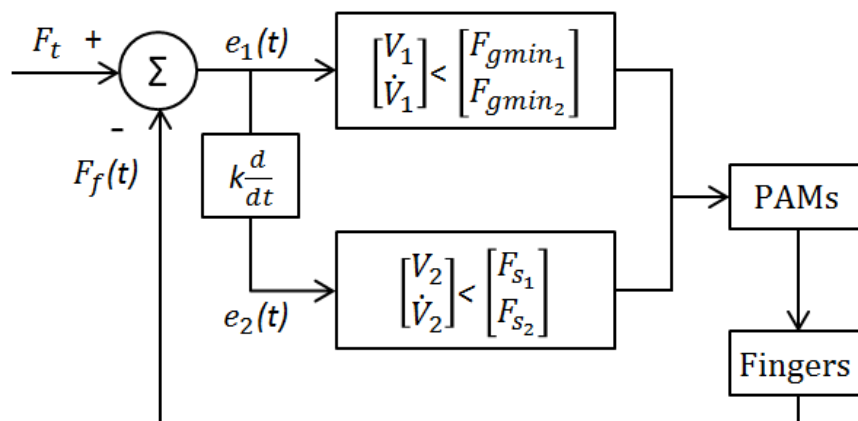
Figure 5.17: Diagram of the backstepping controller

5.3.3.2. *Results obtained with the BSC*

The experimental settings are identical to the ones described in Section 5.3.1, where a Coca-Cola can is used to evaluate any deformation caused by grasping algorithms. The results obtained with the BSC are demonstrated in Figure 5.18.
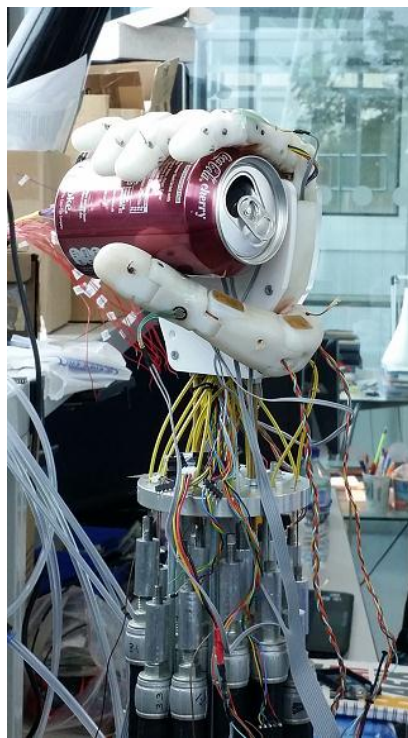
(a)
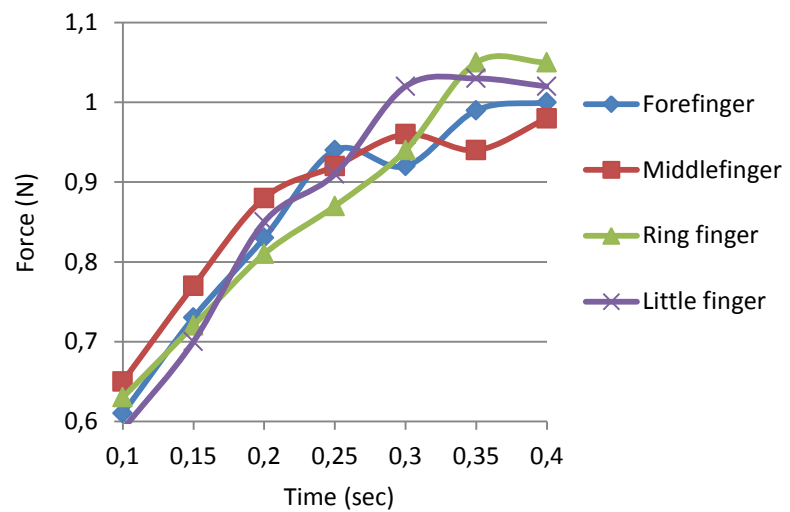
(b)

Figure 5.18: Ambidextrous Hand grabbing a can with BSC and force feedback (a) an image and (b) the force against time for the four fingers

Contrary to PID and bang-bang controllers, Figure 5.18 (b) shows that the fingers tighten much slower around objects using BSC. On another hand, the BSC also provides more flexibility than the two controllers previously experimented. This is explained because the target of the BSC is not only based on force feedback, but also on speed's stability. Even though the fingers provide enough force to grab the can at 0.30 sec, the system carries on moving until 0.40 sec. Therefore, it is also noticed that the BSC is longer to stabilise than PID and bang-bang controls. The force collected for the thumb at the end of the experiment is 13.10 N, which is a value close to the one obtained with the PID control. It can also be noted that the fingers' speed is slower using BSC, as none of the sensors collect more than 0.80 N after 0.15 sec. The higher speeds of the PID and bang-bang controllers are respectively explained because of the integrative term and the lack of derivative control.

5.3.3.3.   Comparison with other BSCs

The features relative to the BSC implemented on the Ambidextrous Hands and the results obtained from it are compared with the ones of other BSCs in Table 5.9. Some robotic structures actuated by motors are included in Table 5.9 as well, as their number of DOFs is closer to the one of the Ambidextrous Hand and some of their BSCs are related to force control. The maximum errors are also indicated, even though its meaning differs between the BSC of the Ambidextrous Hand and the other ones. Indeed, the errors obtained with the Ambidextrous Hand and the manipulators [294] and [295] are the only ones that can be defined as overshoots. In other cases, the BSC react as a SMC, the aim of which being to make its sliding phase closer to a variable referencial state. The maximum errors most often refer to positions, such as in [202], [296], [297], [299] or [197], but also to lengths, such as in [199] or [207], or to angles, such as in [294] or [298]. BSCs related to force control aim at defining a force trajectory in [300] or stabilising manipulators' trajectory in [295]. Thus, the BSC of the Ambidextrous Hand is the only one designed to control the force applied by a robotic structure instead of by an actuator and to grab objects.

Table 5.9: Comparison of BSCs' characteristics between the Ambidextrous Hand and other robotic models

BSC	Robotic structure	Type of actuators	Aim of the BSC	Algorithms to which it is combined	# DOFs	# actuators	Execution time (sec)	Error max. (in %)	Ambidexterity
C.-Y Su and Y. Stepanenko [294], 1997	Mani-pulator	Motors	Trajectory control	None	N/A	N/A	0.3[a]	10%[a]	
P. Carbonell et al. [199], 2001	N/A, single PAM	PAM	PAM's length control	None	N/A	1	2.4[a]	8%[a]	
P. Carbonell et al. [207], 2001	N/A, single PAM	PAM	PAM's length control	Fuzzy logic	N/A	1	7[a]	1%[a]	
D. Nganya-Kouya et al. [300], 2002	Mani-pulator	N/A	Force and position control	None	4	N/A	9[a]	N/A	
Lotfazar et al. [296], 2003	Mani-pulator	Motors	Trajectory control	None	5	5	2[a]	N/A	
S.-H. Wen [295], 2007	Mani-pulators	N/A	Force and position control	NN	N/A	N/A	1.9[ab]	9%[ab]	
H. Aschemann and D. Schindele [202], 2008	Parallel robot	PAMs	Position control	None	2	4	0.3[a]	4%[a]	
M.R. Soltanpour and M.M. Fateh [299], 2009	Mani-pulator	Motors	Trajectory control	SMC	2	N/A	7.6[ab]	<10^{-3}%[b]	
X. Liu and A. Liadis [298], 2012	Parallel robot	Motors	Position control	Fuzzy logic	2	2	N/A	N/A	
L. Qin et al. [297], 2014	Arm	N/A	Trajectory control	SMC	6	N/A	0.45[a]	2%[a]	
H. Aschemann and D. Schindele [197], 2014	Axis	PAMs	Position control	None	1	2	4[a]	1.4%[a]	
Ambidextrous Hand [41], 2014	Hand	PAMs	Force control	None	9[c]	14[c]	0.37	4%	✓

[a] Estimations are made from curves
[b] Results are obtained through a simulation
[c] Four DOFs and four actuators are unused for the BSC

As for bang-bang-controls and SMCs, Table 5.9 shows that BSCs are usually implemented on structures with less than five DOFs, such as manipulators, arms or parallel robots. The Ambidextrous Hand is the only robotic structure of Table 5.9 that has more than ten DOFs (even though the BSC is only implemented on nine of them), which is about the double of the manipulator [296] and the arm [297], which respectively have the second and

third higher number of DOFs of Table 5.9. Moreover, it is noticed that the number of DOFs does not exceed two when the other BSCs are implemented on structures driven by PAMs. The BSC of the Ambidextrous Hand has an execution time of about 0.37 sec, which is one of the shortest of Table 5.9, with [294] and [202], which both have execution times estimated to 0.3 sec, as well as [297], which has an execution time of 0.45 sec. However, the maximum error of 4% for the Ambidextrous Hand's BSC is much higher than the ones obtained with the practical results introduced in [207], [297] or [197]. The control algorithms introduced in [297] therefore appears to be ones of the most efficient of Table 5.9, as the arm has 6 DOFs and the BSC is both among the fastest and the most accurate. Nevertheless, the BSC of the Ambidextrous Hand is the only one that is implemented on an ambidextrous structure and which is used to grab objects.

In conclusion, the implementation of the BSC on the Ambidextrous Hand is quite successful, as the obtained results are among the best of Table 5.9. Nevertheless, its grasping time of 0.37 sec is 85% slower than the grasping time obtained with PID control in Section 5.3.1, and also much slower than the grasping times of most of robot hands summarised in Table 5.7, such as [280], [281], [94] or [282]. Consequently, the BSC is not the best option to grab objects with the Ambidextrous Hand.

5.4.   Comparison of the four algorithms relative to force control

The different behaviours observed for the algorithm of Section 5.2.2 and the three algorithms of Section 5.3 are summarised in Table 5.10. Because of its implementation, the SMC differs to the three other algorithms on a number of points. First, the algorithms to which the SMC is combined do not run in parallel but in different times, the PPSC making the transition between the SMC and the two PID controls introduced in Section 5.1. Secondly, the percentage of overshoot is not applicable for the SMC, as, because of the way the SMC is implemented on the Ambidextrous Hand, its aim is precisely to have an overshoot (or to cross the sliding surface) to grab objects (its high sensibility is still proved by the experiments of Section 5.2.2.2). Finally, the grasping and settling times are the same for the SMC. The grasping time represents the time at which the object is grabbed, whereas the settling time represents the time at which the algorithms stop running and at which the fingers stop adjusting their positions. Thus, in case of the SMC, the grasping time and the settling

time are the same because, as for bang-bang control, no backward control is implemented. However, the grasping and settling times are different for the bang-bang control. Indeed, because of the bang-bang control's low sensitivity, the force applied by the fingertips carries on increasing even after the object is grabbed.

Table 5.10: Comparison between the four algorithms relative to force control

Grasping algorithms	Algorithms to which it is combined	Averaged rising time (sec)	Averaged % of overshoot	Averaged # of oscillations	Averaged grasping time (sec)	Averaged settling time (sec)
SMC	PID, PPSC	0.20	N/A	0	0.23	0.23
PID	NN	0.16	5.3%	0	0.20	0.25
Bang-bang	Proportional, NN	0.10	40%	0	0.15	0.20
BSC	NN	0.29	2.3%	0	0.37	0.39

The best performances are reached with SMC and PID control, as they are both among the fastest and the most accurate ones of Table 5.10.

Bang-bang control is the fastest algorithm but it is also the less efficient one. It is indeed not smooth enough to adapt itself to the shape of the objects and can crush them. As introduced in section 2.5.1.2, the shooting function of the bang-bang controller is usually regularised by additional controllers, which is why it is cascaded in [185] and [187]. However, bang-bang control can be used to grab heavy object. The higher is the PAMs' pressure, the slower the PAMs contract, which is why their elasticity automatically opposes itself to the shooting function effect in that case.

BSC may be the most accurate algorithm, but also the slowest one. As for PID control, BSC permits the fingers to adapt to the shape of objects with backward movements. Nevertheless, because of proportional and integrative controls, PID loops have the advantages to make the fingers move faster, which is why Table 5.2 and Table 5.7 revealed that a high number of robotic hands are driven by PID controllers. The combination of PID control with SMC is also the reason why the rising time is reached so fast with SMC. As for conventional SMC, BSC depends on derivative and double derivative controls. This is the reason why the grasping time is much higher with the BSC, as this one is not combined with proportional or integrative controls. Therefore, it takes almost 0.40 sec for the fingers to stabilise themselves with BSC, against 0.23 sec for SMC, 0.25 sec for PID control and 0.20 sec for bang-bang control. Indeed, as for SMC, the main advantage of BSC is its ability to

regulate nonlinear actuators. This is the reason why these two algorithms receive feedbacks from pressure or position sensors, as in [199], [202], [102], [203] or [197]. Nevertheless, in the case considered in Section 5.3, the feedback is received from force sensors directly implemented on the mechanical structure instead of the actuators themselves, as in Section 5.2.

The advantages and the inconveniences of the Ambidextrous Hand's SMC and PID control are summarised in Table 5.11. The main points concern the price of sensors, already discussed in Section 5.3, and the differences of implementation. It is observed in general that SMC is easier to implement from a mechanical point of view, whereas PID is easier to implement from an algorithmic point of view. Pressure transducers are indeed implemented in the pneumatic interface, whereas force sensors have to be implemented inside the mechanical structure of the hand. On another hand, the implementation and the calibration of grasping algorithms receiving feedback from force sensors is indeed much faster than the ones receiving feedback from pressure transducers, as the hysteresis of PAMs does not need to be taken into account with force sensors.

Table 5.11: Advantages and inconveniences of SMC and PID control

Grasping algorithms	Advantages	Inconveniences
SMC (Section 5.2.2)	-Eases the mechanical architecture of the hand (additional wires do not need to be routed inside) -Eventual repairs or replacements are easy (sensors and wires are directly accessible) -Objects can be detected at any points of the finger -Totally unique use of the algorithm	-Pressure transducers are more expensive (about six times the price of force sensors) -The pneumatic and electronic interfaces are bulkier -Can take up to 3 hrs to be calibrated -Backward control is not included in the algorithm (but can be implemented separately) -Is about 15% slower
PID control (Section 5.3.1)	-Force sensors are cheaper (about one sixth of the price of pressure transducers) -The pneumatic and electronic interfaces are smaller -Can be calibrated in less than 10 min -Backward control is directly included in the algorithm -Is about 15% faster	-Complicates the mechanical architecture of the hand (additional wires must be routed inside) -Eventual repairs or replacements are made difficult (sensors and wires cannot be accessed without opening the mechanical structure of the hand) -Objects must be in contact with the force sensors -Very common use of the algorithm

Despite the differences between the two algorithms, Table 5.11 shows that both of them can be implemented and used in future stages of the project.

The right and left behaviours of the Ambidextrous Hand can also be combined to grab objects in atypical positions, as shown in Figure 5.19. As for the ambidextrous behaviours illustrated in Figure 5.4 (c) or (d), such gestures cannot be reached by human hands. The Ambidextrous Hand can therefore be considered as an artistic project as it illustrates an epistemological rupture, which is a common purpose of contemporary arts [6].
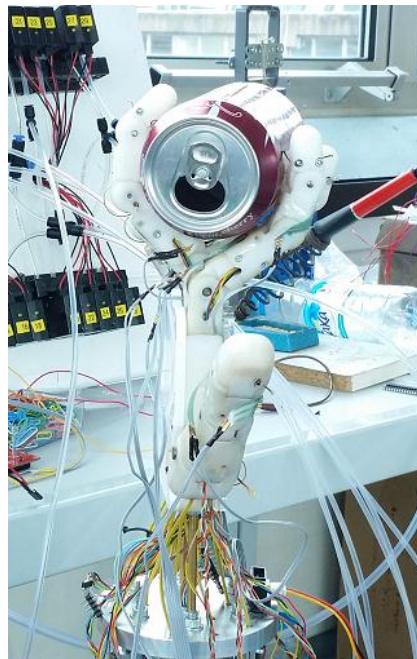
Figure 5.19: Ambidextrous Hand grabbing a can combining left and right behaviours

5.5. Chapter summary

This Chapter has introduced a number of control algorithms specifically adapted to the Ambidextrous Robot Hand.

First, the angular displacement of the ambidextrous finger was controlled using a PPSC switching between two types of PID controllers, the first being tuned with conventional gain constants and the second one with dynamic coefficients. The results revealed an accuracy and an angular speed close to the ones of other robotic models, but with an ambidextrous behaviour.

Secondly, the grasping abilities of the Ambidextrous Hand were considered connecting a SMC to pressure and angular feedbacks. It allowed controlling the force provided by the ambidextrous fingers without any force sensors and grabbing objects. No SMCs have been used in a similar way in the past.

As the pressure transducers were too expensive to be implemented both on the right side and on the left side on the hand, the third part of this chapter consisted in investigating other grasping algorithms receiving feedback from force sensors. Three algorithms, which are PID, bang-bang and BS controls were analysed on this point. A NN was combined to these grasping algorithms as a safety mechanism, in case objects are in contact with parts of the fingers not covered with sensors, the implementation of which being explained in [289]. Despite the originality of bang-bang and BS controls on a robot hand, the best results were obtained with PID control, commonly used in robotics. It permitted a fast and accurate grasping of objects, as for other robotic models, whereas bang-bang control was inaccurate and BSC was too slow.

The four grasping algorithms were compared to each others in the final part of this Chapter. SM and PID controls revealed similar results, showing that the grasping abilities of the Ambidextrous Hand can be achieved both with pressure transducers or force sensors.

Chapter 6: Conclusion

This thesis has covered the development of the Ambidextrous Robot Hand engineered in Brunel University, from its early prototypes designs to advanced control algorithms. The three main novel pieces of work introduced in this thesis are the unique ambidextrous design for a robot hand discussed in Chapter 4, control algorithms specific to the mechanical structure of the robot hand described in Chapter 5 and the online remote control access introduced in Chapter 3.

Initially, the theoretical knowledge necessary to start the project was introduced in Chapter 2. The Chapter included mechanical designs of robot hands and discussed the differences specific to the different types of actuators. It was observed that PAMs, the actuators that are implemented on the Ambidextrous Hand, have an excellent ratio between strength and weight, a short reaction speed and add flexibility to robotic systems. However, the non-linearity existing between the air pressure and the force they provide complicates the design of control algorithms. Their implementation also implies a number of PAMs often twice higher than the number of DOFs, whereas some other actuators, such as motors or SMAs, permit to actuate one DOF each.

As robot hands controlled by PAMs are not numerous, other structures controlled by PAMs, such as arms or legs, were also investigated. Thus, their control algorithms could be explored as well. It was revealed that PID controllers were widely used to drive robotic systems. It was also observed that nonlinear algorithms, the main ones being SMC and BSC, are often implemented on robotic arms, axes or parallel robots, but have never been implemented on hands driven by PAMs. Additionally, IA-based algorithms, and mainly NNs, are often combined with feedback or nonlinear algorithms to control robotic structures.

Chapter 3 discussed the feasibility study of the project. The pneumatic and electronic interfaces were described before designing prototypes of a number of ambidextrous fingers made of Meccanos. The different behaviours of these prototypes were analysed and improved until reaching an ambidextrous range, almost twice higher than the ones of other robotic fingers. The final prototype had two DOFs (flexion/extension of the proximal phalange and flexion/extension of the medial and distal phalanges, for which the movement is coupled) and was driven by four PAMs. A feasibility study about control theory was also presented. A

conventional parallel form of PID controllers was used to control both the angular motion and the force applied by the best prototype of ambidextrous fingers. The implementation of PID loops was successful in both cases. The robotic system was then connected to a unique remote control platform, discussed in [31]. The RCI is accessible from the website of the project, based on TCP/IP, and provides a streaming video as feedback.

Chapter 4 introduced the progress of the project achieved between the actuation of a single finger made of Meccanos and the actuation of a whole ambidextrous robot hand made of 3D printed pieces. The discussion mainly concerned the choice and the calibration of sensors, the design of a testbench and the upgrades of the electronic and pneumatic interfaces, as the upgrade of the mechanical architecture of the robot hand is described in [254]. The testbench was designed to test more advanced prototypes of ambidextrous fingers. Contrary to the tests performed in Chapter 3, the pressure of PAMs and the force they provide are collected when the prototypes are moving. The testing revealed that pressure feedback was more reliable than PAMs' force feedback to work in coordination with angular displacement. Therefore, the holding structure of the robot hand did not need to incorporate load cells, which simplified the mechanical architecture of the forearm. Based on testing's observations, the best prototypes were chosen to achieve an ambidextrous hand of thirteen DOFs actuated by eighteen PAMs. In addition to its ambidexterity and its wide range, the design is made even more original by an asymmetrical tendon routing, allowing controlling the flexion/extension of each finger (except the thumb) with three PAMs instead of four. Because of this reduction of PAMs, the Ambidextrous Robot Hand has a ratio between its number of DOFs and its number of actuators higher than the one of a number of robot hands driven by PAMs.

Chapter 5 described the algorithms engineered to control the Ambidextrous Robot Hand and that are implemented on the hardware system discussed in [255]. The control algorithms must take the ambidextrous range, the asymmetrical tendon routing and the nonlinearity of PAMs into account. PID controllers similar to the ones engineered in Chapter 3 could control the global angular displacement of fingers, but gain constants needed to be turned into dynamic coefficients when the finger was reaching a position close to vertical. A PPSC was therefore designed to switch the gain constants of the PID controllers to constant or to dynamic coefficients according to the fingers' position. The combination of PID control and PPSC was thus achieved for the first time on a robot hand. Tests revealed that, in addition to the ambidextrous behaviour, the angular accuracy and the angular speed are

higher than the ones obtained with many other robot hands, and among the very best ones for robotic structures driven by PAMs or with asymmetrical tendon routings.

Different force controls were also investigated. The first one consisted in an SMC controlling the force applied by the fingers according to pressure and angular feedbacks. The SMC was designed taking the PAMs' hysteretic behaviour and the side of the hand into account. It was revealed that the Ambidextrous Hand could grab objects with accuracy, despite the limited number of DOFs of its thumb. It was also the first time an SMC was designed to grab objects and to control the force provided by a robotic structure without any force feedbacks, by crossing the sliding surface defined by the algorithm. Next grasping algorithms aimed at reaching the same results from fingers' force feedback. Three algorithms were designed for this purpose, in collaboration with [289]: PID control, bang-bang control cascaded with a proportional controller as an outer loop and BSC. Each of the control algorithms was adapted to the nonlinear tendon routing of the Ambidextrous Hand and combined with a NN that was taking the force feedback of other fingers into account, in case objects would not be in contact with force sensors. The implementations of a bang-bang control and a BSC in such a context were totally unique, but none of them reached the expected results, as the bang-bang control was not accurate enough and BSC was too slow. Best results were therefore achieved with conventional PID controllers, for which the grasping force was among the most accurate and the fastest among the robot hands, but achievable both on left and on right sides. The results obtained with PID control driven by force feedback were very close to the ones obtained with the SMC driven by pressure and angular feedbacks. The main differences concern the implementations and the price of sensors. In the first case, PID controllers permit a simpler algorithmic implementation and cheaper sensors, but complicate the mechanical architecture of the hand as additional wires must be routed inside. In the second case, the calibration of the SMC is much longer and the sensors are much more expensive, but the control algorithm is much more original and additional wires do not need to be routed inside the mechanical architecture of the hand. Both solutions are possible for next stages of the project.

6.1.   Recommendations for further study

The following recommendations are put forward for further study of the remote-controlled Ambidextrous Hand Project.

Two observations concern the choice of material. Some was chosen before the design of the Ambidextrous Hand and, consequently, does not exactly match with its characteristics.

The first of these observations concern the length of PAMs. Indeed, the Ambidextrous Hand's PAMs are 300 mm long and can contract up to 8 bars, but the pressure never overreaches 4 bars, as such a pressure is enough to reach the extreme ranges of the fingers or to grab objects. Shorter PAMs can consequently actuate the robotic structure. Shorter PAMs would inflate faster, and therefore increase the movement's speed of the fingers.

In case the SMC would be implemented again on shorter PAMs, the inequations that trigger the SMC would need to be modified as a consequence. The behaviour of the fingers' angles against PAMs' pressure would need to be observed again and a linear function would not be applicable any more. Instead of, a rational function, or the sum of a linear function and an exponential function with a power variable smaller than one can certainly be used to hug the nonlinear behaviour of PAMs.

Secondly, the pneumatic circuit is currently connected to the air compressor with a hose tail barb of an ID of 4 mm. Hose tail barb with an ID of 6 mm or 8 mm, combined with the adequate pneumatic equipment, would also permit increasing the speed of the system.

More interactions could also be possible connecting the robot hand to devices such as data gloves, or to the HGR and EMG interfaces which are currently under development. HGR does not require any hardware from the side of the user and would therefore be compatible with the Ambidextrous Hand's website's RCI, contrary to EMG that requires electrodes and electronic interfaces. Thus, the client developed on Qt4 discussed in Chapter 3 would be compatible and useful for the EMG interfaces.

Concerning the mechanical behaviour, the grasping abilities would be more anthropomorphic if the thumb had at least four DOFs, one of them permitting opposable movements. Additional wires would also need to be routed inside the mechanical architecture for further experiments involving force sensors.

Finally, the possibilities of movements could be increased if the Ambidextrous Hand were connected to a wrist and to an ambidextrous arm. Therefore, mechanical parameters should be investigated, especially to choose the dimensions of the PAMs driving the arm. The electronic and pneumatic interfaces would also need to be upgraded as a consequence. Fixing these interfaces close to the elbow's level would shorten the length of the pneumatic tubes connecting the solenoid valves to the PAMs and thus, increase the speed of the system.

The coordination of movements between the hand and the arm can possibly be achieved using the same kind of algorithms that coordinate the movements of fingers. Feedback or nonlinear algorithms can therefore be combined with NNs to control the parallel movements of such a structure.

Bibliography

[1] Plato. (~390 BCE) "Hippias Major".

[2] Aristotle. (~335 BCE) "Poetics".

[3] I. Kant. (1790) "Critique of Judgement", 235 p.

[4] E.H. Gombrich. (1950) "The Story of Art". Phaidon, 481 p.

[5] L. N. Tolstoy. (1897) "What is Art?", 360 p.

[6] N. Heinich. (2005) "Etre artiste". Klincksieck, 128 p, in French.

[7] Stelarc. (2010) "Excess and Indifference: Alternate Body Architectures", Hazel Gardiner and Charlie Gere edn, *Art Practice in a Digital Culture*, pp. 93-116.

[8] S. Carter. (2011) "The emergence of art-science", *BMJ,* vol. 343, pp. 1-2.

[9] N. Hall. (2013) "Merging Science and Art: The Bigger Picture", *The STEAM Journal,* vol. 1, no. 1, pp. 1-9.

[10]   N. Sellars. (2012) "The optics of anatomy and light: a studio-based investigation of the construction of anatomical images", PhD thesis, Monash University, 186 p.

[11]   C.D. Murray, S. Pettifer, T. Howard, E. Patchick, F. Caillette and J. Murray. (2010) "Virtual Solutions to Phantom Problems: Using Immersive Virtual Reality to Treat Phantom Limb Pain", in Craig Murray (ed.) *Amputation, Prosthesis Use, and Phantom Limb Pain*, pp. 175-196.

[12]   D.V. Buonomano and M.M. Merzenich. (1998) "Cortical plasticity: from synapses to maps", *Annual review of Neuroscience*, vol. 21, pp. 149-186.

[13]   G.F. Wittenberg. (2010) "Experience, Cortical Remapping, and Recovery in Brain Disease", *Neurobiology of Disease*, vol. 37, no. 2, pp. 252-258.

[14]   H. Flor, M. Diers, and J. Andoh. (2013) "The neural basis of phantom limb pain", *Trends in Cognitive Sciences*, vol. 17, no. 7, pp. 307-308.

[15]   H. Flor, T. Elbert, S. Knecht, C. Wienbruch, C. Pantev, N. Birbaumers, W. Larbig, and E. Taub. (1995) "Phantom-limb pain as a perceptual correlate of cortical reorganization following arm amputation", *Nature*, vol. 375, no. 6531, pp. 482-484.

[16]   H. Flor. (2003) "Cortical Reorganisation and Chronic Pain: Implications for Rehabilitation", *Journal of Rehabilitation Medicine*, vol. 41, pp. 66-72.

[17]   R. Moucha and M.P. Kilgard. (2006) "Cortical plasticity and rehabilitation", *Progress in Brain Research*, vol. 157, pp. 111-122.

[18]   B.D. Darnall. (2009) "Self-Delivered Home-Based Mirror Therapy for Lower Limb Phantom Pain", *American Journal of Physical Medicine & Rehabilitation,* vol. 88, pp. 78-81.

[19]   V.S. Ramachandran. (2005) "Plasticity and functional recovery in neurology", *Clinical Medicine,* vol. 5, no. 4, pp. 368-73.

[20]   B. Rosén and G. Lundborg. (2005) "Training with a mirror in rehabilitation of the hand", *Scandinavian Journal of Plastic and Reconstructive Surgery and Hand Surgery*, vol. 39, no. 2, pp. 104-108.

[21]   M.E. Michielsen, R.W. Selles, J.N. van der Geest, M. Eckhardt, G. Yavuzer, H.J. Stam, M. Smits, G.M. Ribbers, and J.B. Bussman. (2011) "Motor Recovery and Cortical Reorganization After Mirror Therapy in Chronic Stroke Patients: a Phase II Randomized Controlled Trial", *Neurorehabilitation and Neural Respair*, vol. 25, no. 3, pp. 223-233.

[22]   S.J. Blakemore, D.M. Wolpert, and C.D. Frith. (2002) "Abnormalities in the awareness of action", *Trends in Cognitive Sciences,* vol. 6, no. 6, pp. 237-242.

[23]   C.D. Murray, E. Patchick, S. Pettifer, F. Caillette, and T. Howard. (2006) "Immersive Virtual Reality as a Rehabilitative Technology for Phantom Limb Experience: A Protocol", *CyberPsychology and Behavior,* vol. 9, no. 2, pp. 167-170.

[24]   M. Ortiz-Catalan, N. Sander, M.B. Kristoffersen, B. Håkansson, and R. Brånemark. (2014) "Treatment of phantom limb pain (PLP) based on augmented reality and gaming controlled by myoelectric pattern recognition: a case study of a chronic PLP patient", *Frontiers in Neuroscience*, vol. 8, no. 24, pp. 1-7.

[25]   J. Cole, S. Crowle, G. Austwick, and D.H. Slater. (2009) "Exploratory findings with virtual reality for phantom limb pain; from stump motion to agency and analgesia", *Disability and Rehabilitation*, vol. 31, no. 10, pp. 846-854.

[26]   T. Caires and M. Prywata. (2011) *The Artificial Muscle-Operated (AMO) Arm.* Available at: http://www.robaid.com/bionics/brain-controlled-artificial-muscle-operated-amo-arm.htm. Last access: 2015.

[27]   Y. Matsuoka, P. Afshar, and M. Oh. (2006) "On the design of robotic hands for brain–machine interface", *Neurosurg Focus 20,* vol. 20, pp. 1-9.

[28]   X. Jiang, C. Xiong, R. Sun, and Y. Xiong. (2010) "Characteristics of the Robotic Arm of a 9-DoF Upper Limb Rehabilitation Robot Powered by Pneumatic Muscles", *ICIRA 2010,* vol. LNAI 6425, pp. 463-474.

[29]   Z. Li. (2003) "Using robotic hand technology for the rehabilitation of recovering stroke patients with loss of hand power", Master of Science thesis, North Carolina State University.

[30]   T'nB Intelligent accessories. "PIXY WEBCAM 350K". Available at: http://www.t-nb.com/media/documents/prodsheets/PIXY350_FP_EN.pdf. Last access: 2015.

[31]   A. Dilly. (2012) "Embedded Webcam and Hand gesture recognition for Robotic Hand Remote Control", report.

[32]   M. Honoré. (2013) "Ambidextrous robot hand: Electromyography", report.

[33]   imaJination. Available at: http://imajination.in/. Last access: 2015.

[34]   Logitech. "HD Webcam C270". Available at: http://www.logitech.com/en-hk/product/hd-webcam-c270. Last access: 2015.

[35]   Science Museum "Science Museum Robotic Hand". Available at: http://www.amazon.co.uk/Great-Gizmos-GG4160SM-Science-Robotic/dp/B004V3C47Y. Last access: 2015.

[36]   B. Tondu. (2007) "Artificial Muscles for Humanoid Robots", Humanoid Robots, Human-like Machines, ed. Matthias Hackel, pp. 89-123.

[37]   E. Akyürek, T. Kalganova, M. Mukhtar, L. Steele, M. Simko, A. Nimmo, L. Kavanagh, L. Paramonov, A. Huynh, and Stelarc. "A Novel Design of Low Cost 3D Printed Ambidextrous Finger Designed for an Ambidextrous Robotic Hand", submitted.

[38]   E. Akyürek, T. Kalganova, M. Mukhtar, L. Paramonov, L. Steele, M. Simko, L. Kavanagh, A. Nimmo, A. Huynh, and Stelarc "Design and Development of Low Cost 3D Printed Ambidextrous Robotic Hand Driven by Pneumatic Muscles", *International Journal of Engineering and Technical Research (IJETR),* vol. 2, no. 10, pp. 179-188.

[39]   E. Akyürek, A. Dilly, F. Jourdan, Z. Liu, S. Chattoraj, I. Berruezo Juandeaburre, M. Heinrich, L. Paramonov, P. Turner, Stelarc, and T. Kalganova. (2013) "Remote-

Controlled Ambidextrous Robot Hand Concept", *Journal of Computer Technology and Application,* vol. 4, no. 4, pp. 569-574.

[40]   E. Akyürek, A. Huynh, and T. Kalganova. (2014) "Control of an Asymmetrical Design of a Pneumatically Actuated Ambidextrous Robot Hand", *International Journal of Electrical, Electronics, Communication, Energy Science and Engineering, vol.* 8, no. 5, pp. 990-995.

[41]   M. Mukhtar, E. Akyürek, N. Lesne, and T. Kalganova. "Comparison of Grasping Algorithms Implemented on an Ambidextrous Robot Hand", submitted.

[42]   A.M. Dollar and R.D. Howe. (2007) "The SDM Hand as a Prosthetic Terminal Device: A Feasibility Study", *Proc. IEEE International Conference on Rehabilitation Robotics*, pp. 978-983.

[43]   M. Stark (2011). "The Natural Dexterous Hand". Available at: http://www.swisswuff.ch/tech/?p=427. Last access: 2015.

[44]   M.S. Johannes, J.D. Bigelow, J.M. Burck, S.D. Harshbarger, M.V. Kozlowski and T. Van Doren. (2011) "An overview of the developmental process for the modular prosthetic limb", *Johns Hopkins APL Tech. Dig.,* vol. 30, no. 3, pp. 207-216.

[45]   RSLSteeper. (2012) "Bebionic3". Available at: http://bebionic.com/the_hand/features. Last access: 2015.

[46]   Touch Bionics. (2014) "i-limb ultra revolution". Available at: http://www.touchbionics.com/products/active-prostheses/i-limb-ultra. Last access: 2015.

[47]   A. Saenz (Singularity University). (2010) "How Much is the Newest Advanced Artificial Hand? $11,000 USD (video)". Available at: http://singularityhub.com/2010/06/30/how-much-is-the-newest-advanced-artificial-hand-11000-usd-video/. Last access: 2015.

[48]   C.S. Lovchik and M.A. Diftler, (1999) "The Robonaut Hand: A Dexterous Robot Hand For Space", *Proc. IEEE International Conference on Robotics & Automation,* vol. 2, pp. 907-912.

[49]   T. Mouri, H. Kawasaki, K. Yoshikawa, J. Takai, and S. Ito. (2002) "Anthropomorphic Robot Hand: Gifu Hand III", *Proc. of Int. Conf. ICCAS*, pp. 1288-1293.

[50]   S. Kawamura, H. Kino, and C. Won. (2000) "High-speed manipulation by using wire-driven robots", *Robotica,* vol. 18, pp. 13-21.

[51]   T. Hasegawa, K. Murakami, and T. Matsuoka. (1999) "Grasp planning for precision manipulation by multifingered robotic hand", *1999 IEEE International Conference on Systems, Man, and Cybernetics, 1999. IEEE SMC '99 Conference Proceedings,* vol. 6, pp. 762-767.

[52]   H. Hu, J. Li, Z. Xie, B. Wang, H. Liu, and G. Hirzinger. (2005) "A robot arm/hand teleoperation system with telepresence and shared control", *Proceeding of the 2005 IEEE/ASME International Conference on Advanced Intelligent Mechatronic*, pp. 1312-1317.

[53]   M. Ceccarelli, N.E. Nava Rodriguez, and G. Carbone (2006). "Design and tests of a three finger hand with 1-DOF articulated fingers", *Robotica,* vol. 24, pp. 183-196.

[54]   L. Zollo, S. Roccella, E. Guglielmelli, M.C. Carrozza, and P. Dario. (2007) "Biomechatronic Design and Control of an Anthropomorphic Artificial Hand for Prosthetic and Robotic Applications", *IEEE/ASME Transactions on Mechatronics, vol.*12, no. 4, pp. 418-429.

[55]   Meka   Robotics   (2009).   "H2   Compliant   Hand".   Available   at: http://www.hizook.com/blog/2009/10/18/meka-robotics-humanoid-torso-and-anthropomorphic-hands. Last access: 2015.

[56]   G. ElKoura and K. Singh. (2003) "Handrix: Animating the Human Hand", *Proceedings of the 2003 ACM SIGGRAPH/Eurographics symposium on Computer animation,* pp. 110-119.

[57]   P.J. Kyberd, C. Light, P.H. Chappell, J.M. Nightingale, D. Whatley, and M. Evans. (2001) "The design of anthropomorphic prosthetic hands: A study of the Southampton Hand", *Robotica,* vol. 19, pp. 593-600.

[58]   N. Fukaya, S. Toyama, T. Asfour and R. Dillmann. (2000) "Design of the TUAT/Karlsruhe Humanoid Hand", *IEEE/RSJ International Conference on Intelligent Robots and Systems (IROS 2000),* vol. 3, pp. 1754-1759.

[59]   G. Stellin, C. Cipriani, F. Zaccone, M.C. Carrozza, C. Laschi and P. Dario. (2008) "Design of an anthropomorphic dexterous hand for a 2-years-old humanoid : ongoing work", *Proceedings of RoManSy*, pp. 1-8.

[60]   Ishikawa Watanabe Laboratory. (2009) "High-speed robot hand". Available at: http://www.k2.t.u-tokyo.ac.jp/fusion/HighspeedHand/. Last access: 2015.

[61]   D. Gunji, Y. Mizoguchi, S. Teshigawara, A. Ming, A. Namiki, M. Ishikawaand and Makoto Shimojo. (2008) "Grasping Force Control of Multi-Fingered Robot Hand based on Slip Detection Using Tactile Sensor", *IEEE International Conference on Robotics and Automation (ICRA)*, pp. 2605-2610.

[62]   Shadow Robot Company Ltd. (2013) "Shadow Dexterous Hand E1 Series (E1M3R, E1M3L,   E1P1R,   E1P1L)".   Available   at: http://www.shadowrobot.com/products/dexterous-hand/. Last access: 2015.

[63]   I. Yamano and T. Maeno. (2005) "Five-fingered Robot Hand using Ultrasonic Motors and Elastic Elements", *Proceeding of the 2005 International Conference on Robotics and Automation*, pp. 2673-2678.

[64]   C. Chivu, C. Chivu and C. Georgescu. (2008) "Design and fuzzy control of hand prosthesis or anthropomorphic robotic hand", *Journal WSEAS Transactions on Systems and Control,* vol. 3, no. 5, pp. 333-342.

[65]   F. Ficuciello, G. Palli, C. Melchiorri, B. Siciliano. (2013) "Mapping Grasps from the Human Hand to the DEXMART Hand by Means of Postural Synergies and Vision", *Experimental Robotics,* vol. 88, pp. 515-529.

[66]   A.D. Deshpande, Z. Xu, M.J. Vande Weghe, B.H. Brown, J. Ko, L.Y. Chang, D.D. Wilkinson, S.M. Bidic, and Y. Matsuoka. (2013) "Mechanisms of the Anatomically Correct Testbed (ACT) Hand", *IEEE/ASME Transactions on Mechatronics,* vol.18, pp. 238-250.

[67]   M. Grebenstein, A. Albu-Schäffer, T. Bahls, M. Chalon, O. Eiberger, W. Friedl, R. Gruber, U. Hagn, R. Haslinger, H. Höppner, S. Jörg, M. Nickl, A. Nothhelfer, F. Petit, B. Pleintinger, J. Reil, N. Seitz, T. Wimböck, S. Wolf, T. Wüsthoff, and G. Hirzinger. (2011) "The DLR Hand Arm System", *IEEE International Conference on Robotics and Automation (ICRA)*, pp. 3175-3182.

[68]   C.H. Kuo and C.T. Chen (2010) "Development of Tendon Based Dexterous Robot Hand", *Advances in Robot Manipulators*, pp. 255-266.

[69]   Prensilia   Srl   (2010)   "The   EH1   Milano   Hand".   Available   at: http://www.prensilia.com/index.php?q=en/node/41. Last access: 2015.

[70]   Elumotion Ltd (2010) "Elu2 hand". Available at: http://www.elumotion.com/Elu2-hand.htm. Last access: 2015.

[71]   S. Takamuku, G. Gómez, K. Hosoda and R. Pfeifer. (2007) "Haptic discrimination of material properties by a robotic hand", *IEEE 6th International Conference on Development and Learning, 2007. ICDL 2007*, pp. 1-6.

[72]   R. Mahmoud, A. Ueno, and S. Tatsumi. (2011) "An assistive tele-operated anthropomorphic robot hand: Osaka City University Hand II", *2011 6th ACM/IEEE International Conference on Human-Robot Interaction (HRI)*, pp. 85-92.

[73]   L. Xiao, Y. Yunyue, Z. Zhuo. (2007) "Study of the Linear Hall-Effect Sensors Mounting Position for PMLSM", *2nd IEEE Conference on Industrial Electronics and Applications, 2007. ICIEA 2007*, pp. 1175-1178.

[74]   Shadow Robot Company Ltd. (2013) "Shadow Dexterous Hand E1M3R, E1M3L". Available at: http://www.shadowrobot.com/products/dexterous-hand/. Last access: 2015.

[75]   Barret Technology Inc. (2009) "WAM specifications". Available at: http://www.barrett.com/robot/products-arm-specifications.htm. Last access: 2015.

[76]   H. Kawasaki, H. Shimomura and Y. Shimizu. (2001) "Educational-industrial complex development of an anthropomorphic robot hand 'Gifu hand'", *Advanced Robotics,* vol. 15, no. 3, pp. 357-363.

[77]   F. Daerden and D. Lefeber. (2002) "Pneumatic Artificial Muscles: actuators for robotics and automation", *European Journal of Mechanical and Environmental Engineering,* vol. 47, no. 1, pp. 11-21.

[78]   B.K.S. Woods, C.S. Kothera, and N.M. Wereley. (2014) "Whirl Testing of a Pneumatic Artificial Muscle Actuation System for a Full-Scale Active Rotor", *Journal of the American Helicopter Society*, vol. 59, no. 2, pp. 1-11.

[79]   Y. Bar-Cohen and S. Leary. (2000) "Electroactive Polymers as Artificial Muscles Changing Robotics Paradigms", *National Space and Missile Materials Symposium,* pp. 1-7.

[80]   Shadow Robot Company. (2011) "Shadow 30mm Air Muscle - Specification", Specification edn. Available at: http://www.shadowrobot.com/wp-content/uploads/2012/11/datasheet_30mm_sam.pdf. Last access: 2015.

[81]   Festo   (2008)   "Fluidic   Muscle   DMSP/MAS".   Available   at:
        https://www.festo.com/rep/en_corp/assets/pdf/info_501_en.pdf. Last access: 2015.

[82]   Y.T. Tadesse. (2009) "Creating Human-Like Facial Expressions Utilizing Artificial
        Muscles and Skin", PhD thesis, Virginia Polytechnic Institute and State University.

[83]   K.J. Kim and S. Tadokoro. (2007) "Electroactive Polymers for Robotic Applications",
        in Springer (ed.), 287 p.

[84]   N. Saga, T. Nakamura and K. Yaegashi. (2007) "Mathematical Model of Pneumatic
        Artificial Muscle Reinforced by Straight Fibers", *Journal of Intelligent Material Systems
        and Structures,* vol. 2, no. 6, pp. 175-180.

[85]   N. Tsujiuchi, T. Koizumi, S. Nishino, H. Komatsubara, T. Kudawara and Masanori
        Hirano. (2008) "Development of Pneumatic Robot Hand and Construction of Master-
        Slave System", *Journal of System Design and Dynamics,* vol. 2, no. 6, pp. 1306-1315.

[86]   E. Kelasidi, G. Andrikopoulos, G. Nikolakopoulos and S. Manesis. (2012) "A Survey
        on Pneumatic Muscle Actuators Modeling", *Journal of Energy and Power Engineering,*
        6, pp. 1442-1452.

[87]   Z. Varga and M. Moučka. (2009) "Mechanics of pneumatic artificial muscle",
        Journal of applied science in the thermodynamics and fluid mechanics, vol. 3, no. 2, pp.
        1-6.

[88]   C. Hartmann, J. Boedecker, O. Obst, S. Ikemoto and M. Asada. (2012) "Real-Time
        Inverse Dynamics Learning for Musculoskeletal Robots based on Echo State Gaussian
        Process Regression", *Robotics : Science & Systems,* pp. 113-120.

[89]   T. Noritsugu, T. Yoshio and I. Kazutoshi. (1999) "Improvement of control
        performance of pneumatic rubber artificial muscle manipulator by using
        electrorheological fluid damper", *1999 IEEE International Conference on Systems, Man,
        and Cybernetics, 1999. IEEE SMC '99 Conference Proceedings,* vol. 4, pp. 788-793.

[90]   Y. Honda, F. Miyazaki and A. Nishikawa. (2010) "Control of pneumatic five-fingered
        robot hand using antagonistic muscle ratio and antagonistic muscle activity", *Proc. 3rd
        IEEE RAS & EMBS International Conference on Biomedical Robotics and
        Biomechatronics*, pp. 337-342.

[91]   N.G. Tsagarakis and D.G. Caldwell (2003) "Development and Control of a 'Soft-Actuated' Exoskeleton for Use in Physiotherapy and Training", *Autonomous Robots,* vol. 15, no. 1, pp. 21-33.

[92]   Y.K. Lee and I. Shimoyama. (1999) "A skeletal framework artificial hand actuated by pneumatic artificial muscles", *Proceedings 1999 IEEE International Conference on Robotics and Automation, 1999,* vol. 2, pp. 926-931.

[93]   Shadow Robot Company. (2005) "Design of a Dextrous Hand for advanced CLAWAR applications". Available at : http://www.shadowrobot.com/downloads/dextrous_hand_final.pdf. Last access: 2015.

[94]   Shadow Robot Company Ltd. (2013) "*Shadow Dexterous Hand E1P1R, E1P1L*". Available at: http://www.shadowrobot.com/products/dexterous-hand/. Last access: 2015.

[95]   P. Scarfe, E. Lindsay. (2006) "Air Muscle Actuated Low Cost Humanoid Hand", *International Journal of Advanced Robotic Systems,* vol. 3, no. 1, pp. 139-146.

[96]   S. Nishino, N. Tsujiuchi, T. Koizumi, H. Komatsubara, T. Kudawara, M. Shimizu. (2007) "Development of Robot Hand with Pneumatic Actuator and Construct of Master-Slave System", *Proceedings of the 29th Annual International Conference of the IEEE EMBS,* pp. 3027-3030.

[97]   G. Huang. (2010) "Festo's Extraordinary Robots That Mimic Biology II: Bionic Learning network". Available at: https://www.youtube.com/watch?v=NNNfn7ac-rY. Last access: 2015.

[98]   J.Y. Nagase, N. Saga, T. Satoh and K. Suzumori. (2011) "Development and Control of a Multifingered Robotic Hand Using a Pneumatic Tendon-Driven Actuator", *Journal of Intelligent Material Systems and Structures,* vol.23, no.3, pp. 345-352.

[99]   C.Y. Lau and A. Chai (2012) "The Development of a Low Cost Pneumatic Air Muscle Actuated Anthropomorphic Robotic Hand", *International Symposium on Robotics and Intelligent Sensors 2012 (IRIS 2012),* vol. 41, pp. 737-742.

[100]   A. Uribe, E. Diaz and H. Leon. (2012) "Human Anthropomorphic Gripper as an Automation Tool", *12th International Conference on Control, Automation and Systems (ICCAS), 2012*, pp. 739-744.

[101]   T. Nuchkrua, T. Leephakpreeda and T. Mekarporn. (2013) "Development of Robot Hand with Pneumatic Artificial Muscle for Rehabilitation Application", *2013 IEEE 7th*

International Conference on Nano/Molecular Medicine and Engineering (NANOMED), pp. 55-58.

[102]   S. Boudoua, F. Hamerlain and M. Hamerlain. (2010) "Neuro Sliding Mode Based Chatter Free Control for an Artificial Muscles Robot Arm", *International Joint Conference on Neural Networks (IJCNN)*, pp. 1-7.

[103]   I. Boblan, R. Bannasch, H. Schwenk, F. Prietzel, L. Miertsch and A. Schulz. (2004) "A Human-Like Robot Hand and Arm with Fluidic Muscles: Biologically Inspired Construction and Functionality", *Embodied Artificial Intelligence,* vol. 3139, pp. 160-179.

[104]   P. Pomiers. (2003) "Modular Robot Arm Based on Pneumatic Artificial Rubber Muscles (PARM)", *Proceedings of the 6th International Conference on Climbing and Walking Robots and the Support Technologies for Mobile Machines*, pp. 879-886.

[105]   L. Chikh, P. Poignet, F. Pierrot and M. Michelin (2010) "A predictive robust cascade position-torque control strategy for Pneumatic Artificial Muscles", *American Control Conference (ACC), 2010*, pp. 6022-6029.

[106]   P.Y. Chua, M. Bezdicek, S. Davis, D.G. Caldwell, J.O. Gray. (2006) "Tele-Operated High Speed Anthropomorphic Dextrous Hands with Object Shape and Texture Identification", *2006 IEEE/RSJ International Conference on Intelligent Robots and Systems,* pp. 4018-4023.

[107]   J. Yufei, L.C. Yik, A. Chai. (2012) "PAM Robotic Hand - Swinburne University of Technology". Available at: https://www.youtube.com/watch?v=I9vWDPVMICI. Last access: 2015.

[108]   Y. Bellouard. (2008) "Shape memory alloys for microsystems: A review from a material research perspective", *Materials Science and Engineering: A*, vol. 481-482, pp. 582-589.

[109]   S. Dilibal, E. Guner, and N. Akturk. (2002) "Three-finger SMA robot hand and its practical analysis", *Robotica,* vol. 20, no. 2, pp. 175-180.

[110]   M.J. Mosley and C. Mavroidis. (2001) "Experimental Non-Linear Dynamics of a Shape Memory Alloy Wire Bundle Actuator", *Journal of Dynamic systems, Measurement, and Control*, vol. 123, no. 1, pp. 103-112.

[111] M.J. Mosley, C. Mavroidis and C. Pfeiffer (2002). "Design And Dynamics Of A Shape Memory Alloy Wire Bundle Actuator", *Proceedings Of the ANS, 8th Topical Meeting on Robotics and remote Systems,* pp. 1-14.

[112] K.J. De Laurentis, C. Pfeiffer, and C. Mavroidis. (2000) "Development of a shape memory alloy actuated hand", *Proceedings of the 7th International Conference on New Actuators*, pp.281-284.

[113] K.J. De Laurentis and C. Mavroidis. (2004) "Rapid fabrication of a non-assembly robotic hand with embedded components", *Assembly automation,* vol. 24, no. 4, pp. 394-405.

[114] V. Bundhoo, E. Haslam, B. Birch, and E.J. Park. (2009). "A shape memory alloy-based tendon-driven actuation system for biomimetic artificial fingers, part I: design and evaluation", *Robotica,* vol. 27, no. 1, pp. 131-146.

[115] S. Dilibal, E. Guner, and N. Akturk. (2002) "Three-finger SMA robot hand and its practical analysis", *Robotica,* vol. 20, no. 2, pp. 175-180.

[116] K. Yang and C.L. Gu. (2002) "A novel robot hand with embedded shape memory alloy actuators", *Proceedings of the Institution of Mechanical Engineers, Part C: Journal of Mechanical Engineering Science,* vol. 216, no. 7, pp. 737-745.

[117] S. Dilibal, R.M. Tabanli, and A. Dikicioglu. (2004) "Development of shape memory actuated ITU Robot Hand and its mine clearance compatibility", *Journal of Materials Processing Technologies,* vol. 155-156, pp. 1390-1394.

[118] K.J. Cho and H. Hasada. (2005) "Multi-axis SMA actuator array for driving anthropomorphic robot hand", *Proceedings of the 2005 IEEE International Conference on Robotics and Automation,* pp. 1356 -1361.

[119] K.J. Cho, J. Rosmarin, and H. Asada. (2007) "SBC Hand: A Lightweight Robotic Hand with an SMA Actuator Array implementing C-segmentation", *2007 IEEE International Conference on Robotics and Automation,* pp. 921-926.

[120] K. Andrianesis and A. Tses. (2008) "Design of an Anthropomorphic Prosthetic Hand Driven by Shape Memory Alloy Actuators", *2nd IEEE RAS & EMBS International Conference on Biomedical Robotics and Biomechatronics, 2008. BioRob 2008,* pp. 517-522.

[121] S. Matsubara, S. Okamoto, and J.H. Lee (2012). "Prosthetic Hand Using Shape Memory Alloy Type Artificial Muscle", *Proceedings of the International MultiConference of Engineers and Computer Scientists 2012,* vol. 2, pp. 773-778.

[122] J.H. Lee, S. Okamoto, and S. Matsubara. (2012) "Development of Multi-Fingered Prosthetic Hand Using Shape Memory Alloy Type Artificial Muscle", *Computer Technology and Application,* vol. 3, pp. 773-778.

[123] T. Maeno and T. Hino. (2006) "Miniature five-fingered robot hand driven by shape memory alloy actuators", *Proceedings of the 12th IASTED International Conference Robotics and Applications,* pp. 174-179.

[124] M. Terauchi, K. Zenba, A. Shimada, and M. Fujita. (2006) "Controller Design on the Fingerspelling Robot Hand using Shape Memory Alloy", *International Joint Conference SICE-ICASE,* pp. 3480-3483.

[125] J.B. Rosmarin and H.H. Asada. (2008) "Synergistic Design of a Humanoid Hand with Hybrid DC Motor − SMA Array Actuators Embedded in the Palm", *2008 IEEE International Conference on Robotics and Automation, ICRA 2008,* pp. 773-778.

[126] Y. Bar-Cohen, T. Xue, M. Shahinpoor, J. Simpson, and J. Smith. (1998) "Flexible, Low-mass Robotic Arm Actuated by Electroactive Polymers and Operated Equivalently to Human Arm and Hand", *Robotics 98: The 3rd Conference and Exposition/Demonstration on Robotics for Challenging Environments*, pp.15-21.

[127] D. Bhattacharyya, T. Schäfer, S.R. Wickramasinghe, and S. Daunert. (2013) "Responsive Membranes and Materials". Wiley, 432 p.

[128] D. Hanson, R. Bergs, Y. Tadesse, V. White, and S. Priya. (2006) "Enhancement of EAP actuated facial expressions by designed chamber geometry in elastomers", *Proc. SPIE 6168, Smart Structures and Materials 2006: Electroactive Polymer Actuators and Devices (EAPAD)*, vol. 6168, pp.1-9.

[129] Y. Tadesse, D. Moore, N. Thayer, and S. Priya. (2009) "Silicone based artificial skin for humanoid facial expressions", *Proc. SPIE 7287, Electroactive Polymer Actuators and Devices (EAPAD) 2009*, vol. 7287, pp.1-10.

[130] J.W. Kwak, H.J. Chi, K.M. Jung, J.C. Koo, J.W. Jeon, Y. Lee, J. Nam, Y. Ryew, and H.R. Choi. (2005) "A face robot actuated with artificial muscle based on dielectric elastomer", *Journal of Mechanical Science and Technology*, vol. 19, no. 2, pp. 578-588.

[131] C. Laschi, B. Mazzolai, V. Mattoli, M. Cianchetti, and P. Dario. (2009) "Design and Development of a Soft Actuator for a Robot Inspired by the Octopus Arm", *Experimental Robotics Springer Tracts in Advanced Robotics*, vol. 54, no. 2, pp. 25-33.

[132] Y. Bar-Cohen. (2005) "Biomimetics—using nature to inspire human innovation", *Bioinspiration & Biometics*, vol. 1, no. 1, pp. 1-12.

[133] G. Kovacs, P. Lochmatter, and M. Wissler. (2007) "An arm wrestling robot driven by dielectric elastomer actuators", *Smart Materials and Structures*, vol. 16, no. 2, pp. 578-588.

[134] EAMEX Corporation. "EAP material and product manufacturers". Available at: http://ndeaa.jpl.nasa.gov/nasa-nde/lommas/eap/EAP-material-n-products.htm.   Last access: 2015.

[135] DrBarCohen.   (2011)   "hand.mov".   Available   at: https://www.youtube.com/watch?v=s9ccqzABPu0. Last access: 2015.

[136] C. Juan, M. Jungong, and W. Qiang. (2008) "Fault Mechanism Analysis and Accelerate Life Testing for Pneumatic Cylinders", *6th International Conference on Industrial Informatics, 2008. INDIN 2008,* pp. 1694-1699.

[137] K. Watanabe, H. Nagayasu, N. Kawakami, an S. Tachi. (2008) "Mechanical Compliance Control System for A Pneumatic Robot Arm", *2008 SICE Annual Conference,* pp. 2789-2794.

[138] K. Hoshino and W.D.G. Krishantha. (2007) "Calligraphic motion by humanoid robot arm using air cylinder actuators as endoskeletons", *ICM2007 4th IEEE International Conference on Mechatronics,* pp. 1-6.

[139] S.C. Jacobsen, E.K. Iversen, D.F. Knutti, R.T. Johnson, and K.B. Biggers. (1986) "Design of the Utah/M.I.T. Dextrous Hand", *1986 Proceedings IEEE International Conference on Robotics and Automation,* vol. 3, pp. 1520-1532.

[140] D.D. Wilkinson, M. Vande Weghe, Y. Matsuoka. (2003) "An Extensor Mechanism for an Anatomical Robotic Hand", *Proc. IEEE International Conference on Robotics and Automation,* vol. 1, pp. 238-243.

[141] S. Takamuku, A. Fukuda and K. Hosoda. (2008) "Repetitive grasping with anthropomorphic skin-covered hand enables robust haptic recognition", *IEEE/RSJ*

International Conference on Intelligent Robots and Systems, 2008. IROS 2008, pp. 3212-3217.

[142] Z. Xu, V. Kumar, and E. Todorov. (2013) "A Low-Cost and Modular, 20-DOF Anthropomorphic Robotic Hand: Design, Actuation and Modeling", *13th IEEE-RAS International Conference on Humanoid Robots (Humanoids),* pp. 378-375.

[143] Festo. (2012) "Exo-hand". Available at: http://www.festo.com/cms/en_corp/12713.htm. Last access: 2015.

[144] T. Akagi, S. Dohta, F. Zhao, and T. Fujikawa. (2011) "Development and Attitude Control of Flexible Robot Arm Using Flexible Pneumatic Cylinder with Simple Structure", *International Journal of Automation Technology,* vol. 5, no. 4, pp. 621-628.

[145] L. Di Jasio, T. Wilmshurst, D. Ibrahim, J. Morton, M.P. Bates, J. Smith, D.W. Smith, an Chuck Hellebuyck. (2007) "PIC Microcontrollers: Know It All (Newnes Know It All)". Newnes, 928 p.

[146] R. Van Ham, B. Verrelst, F. Daerden, and D. Lefeber (2003) "Pressure Control with On-Off Valves of Pleated Pneumatic Artificial Muscles in a Modular One-Dimensional Rotational Joint", *International Conference on Humanoid Robots,* pp. 761-768.

[147] Futurlec *"PIC18F458 Controller".* Available at: http://www.futurlec.com/PIC18F458_Controller.shtml. Last access: 2015.

[148] T. Kato, T. Higashi, and K. Shimizu. (2010) "Teleoperation of a Robot Arm System Using Pneumatic Artificial Rubber Muscles: Teleoperation over the Internet Using UDP and a Web Camera", *2010 International Conference on Broadband, Wireless Computing, Communication and Applications (BWCCA)*, pp. 714-718.

[149] Arduino "Arduino Uno". Available at: http://arduino.cc/en/Main/ArduinoBoardUno. Last access: 2015.

[150] Arduino "Arduino Mega 2560". Available at: http://arduino.cc/en/Main/ArduinoBoardMega2560. Last access: 2015.

[151] Arduino "Arduino Ethernet". Available at: http://arduino.cc/en/Main/ArduinoBoardEthernet. Last access: 2015.

[152] Society of robots "Axon". Available at: http://www.societyofrobots.com/axon/.

[153] Elexol "Ether IO24 R". Available at: https://www.elexol.com/IO_Modules/Ether_IO_24.php. Last access: 2015.

[154] Elexol "Ether IO72 TCP". Available at: http://www.elexol.com/IO_Modules/Ether_IO72_TCP.php. Last access: 2015.

[155] Würz elektronik "Microcontroller Module ec555 with MPC555 Chip". Available at: http://www.wuerz-elektronik.com/mpc555.html. Last access: 2015.

[156] Pololu *Orangutan* "SVP-1284". Available at: http://www.pololu.com/product/1325/. Last access: 2015.

[157] Olimex Ltd (2011) "PIC32-PINGUINO" *development board Users Manual*. Available at: http://www.adafruit.com/products/469#description-anchor. Last access: 2015.

[158] Pololu (2011) "Pololu Micro Serial Servo Controller (assembled)". Available at: http://www.pololu.com/product/207. Last access: 2015.

[159] Elexol "USBIO24 DIP R". Available at: http://www.elexol.com/IO_Modules/USB_IO_Dip.php. Last access: 2015.

[160] G.S. Gupta, S.C. Mukhopadhyay, and M. Finnie. (2009) "WiFi-based control of a robotic arm with remote vision", *Instrumentation and Measurement Technology Conference, 2009. I2MTC '09. IEEE*, pp. 557-562.

[161] S.S. Yeh, C.C. Hsu, T.C. Shih, J.P. Hsiao, and P.L. Hsu (2008) "Remote control realization of distributed rescue robots via the wireless network", *SICE Annual Conference, 2008,* pp. 2928-2932.

[162] H. Rissanen, J. Mahonen, K. Haataja, M. Johansson, J. Mielikainen, and P. Toivanen. (2009) "Designing and implementing an intelligent Bluetooth-enabled robot car", *IFIP International Conference on Wireless and Optical Communications Networks, 2009. WOCN '0*, pp. 1-6.

[163] Z. Zhang. (2012) "The Internet remote robot with Skype webcam", *2012 International Conference on System Science and Engineering (ICSSE)*, pp. 117-119.

[164] G. Paravati, B. Pralio, A. Sanna, and F. Lamberti. (2011) "A Reconfigurable Multi-Touch Remote Control System for Teleoperated Robots", *2011 IEEE International Conference on Consumer Electronics (ICCE)*, pp. 153-154.

[165]   K.C. Wickramatunge and T. Leephakpreeda. (2009) "Study on mechanical behaviors of pneumatic artificial muscle", *International Journal of Engineering Science,* vol. 48, pp. 188-198.

[166]   K. Kawashima, T. Sasaki, A. Ohkubo, T. Miyata, and T. Kagawa. (2004) "Application of robot arm using fiber knitted type pneumatic artificial rubber muscles", *2004 IEEE International Conference on Robotics and Automation, 2004. Proceedings. ICRA '04*, vol. 5, pp. 4937-4942.

[167]   S. Laksanacharoen. (2004) "Artificial Muscle Construction Using Natural Rubber Latex in Thailand", *The 3rd Thailand and Material Science and Technology Conference*, pp. 1-3.

[168]   B. Verrelst, F. Daerden, D. Lefeber, R. Van Ham, and T. Fabri. (2000) "Introducing Pleated Pneumatic Artificial Muscles for the Actuation of Legged Robots : a One-dimensional Set-up", *CLAWAR 2000: Third International Conference*, pp. 583-590.

[169]   B. Vanderborght, B. Verrelst, R. Van Ham, J. Naudet, J. Vermeulen, D. Lefeber, and F. Daerden. (2004) "LUCY, a Bipedal Walking Robot with Pneumatic Artificial Muscles", *IEEE Conference on Mechatronics and Robotics,* pp. 106-114.

[170]   K.S. Aschenbeck, N.I. Kern, R.J. Bachmann, and R.D. Quinn. (2006) "Design of a Quadruped Robot Driven by Air Muscles", *The First IEEE/RAS-EMBS International Conference on Biomedical Robotics and Biomechatronics, 2006. BioRob 2006*, pp. 875-880.

[171]   Y. Yamada, S. Nishikawa, K. Shida, and Y. Kuniyoshi. (2011) "Pneumatically-driven Quadruped Robot PIGORASS". Available at: http://www.plasticpals.com/?p=30286. Last access: 2015.

[172]   K. Xing, J. Huang, Q. Xu, and Y. Wang. (2009) "Design of a wearable rehabilitation robotic hand actuated by pneumatic artificial muscles", *7th Asian Control Conference, 2009. ASCC 2009*, pp. 740-744.

[173]   T. Noritsugu, M. Takaiwa, and D. Sasaki. (2008) "Power Assist Wear Driven with Pneumatic Rubber Artificial Muscles", *15th International conference on Mechatronics and Machine Vision in Practise*, pp. 109-118.

[174] T. Noritsugu, M. Takaiwa, and D. Sasaki. (2009) "Development of Power Assist Wear Using Pneumatic Rubber Artificial Muscles", *Journal of Robotics and Mechatronics,* vol. 21, no. 5, pp. 607-608.

[175] A.D. Deshpande, J. Ko, D. Fox, and Y. Matsuoka. (2009) "Anatomically Correct Testbed Hand Control: Muscle and Joint Control Strategies", *IEEE International Conference on Robotics and Automation*, pp. 4416-4422.

[176] N. Tsujiuchi, T. Koizumi, H. Kan, H. Takeda, T. Kudawara, and M. Hirano. (2009) "Modeling and control of a joint driven by pneumatic actuator", *Industrial Electronics, 2009. IECON '09. 35th Annual Conference of IEEE*, pp. 2271-2276.

[177] Y. Honda, F. Miyazaki, and A. Nishikawa. (2010) "Angle control of pneumatically-driven musculoskeletal model using antagonistic muscle ratio and antagonistic muscle activity", *2010 IEEE International Conference on Robotics and Biomimetics (ROBIO)*, pp. 1722-1727.

[178] Y. Honda, F. Miyazaki, and A. Nishikawa. (2012) "Angle Control of a Pneumatically Driven Musculoskeletal Model Based on Coordination of Agonist-Antagonist Muscle", *Journal of Mechanics Engineering and Automations (ROBIO)*, vol. 2, pp. 709-719.

[179] K.K. Ahn and H.P.H. Anh. (2006) "Design & Implementation an Adaptive Takagi-Sugeno Fuzzy Neural Networks Controller for the 2-Links Pneumatic Artificial Muscle (PAM) Manipulator using in Elbow Rehabilitation", *First International Conference on Communications and Electronics, 2006. ICCE '06*, pp. 356-361.

[180] J. Wu, J. Huang, Y. Wang, and K. Xing. (2010) "RLS-ESN based PID control for rehabilitation robotic arms driven by PM-TS actuators", *The 2010 International Conference on Modelling, Identification and Control (ICMIC)*, pp. 511-516.

[181] T. Yanbing and W. Xiaoxin. (2010) "Parameter self-tuning of PID in pneumatic artificial muscle joint based on PSO algorithm", *2010 29th Chinese Control Conference (CCC)*, pp. 3205-3208, in Chinese.

[182] H.P.H. Anh and K.K. Ahn. (2011) "Hybrid control of a pneumatic artificial muscle (PAM) robot arm using an inverse NARX fuzzy model", *Journal Engineering Applications of Artificial Intelligence,* vol. 24, no. 4, pp. 697-716.

[183] J. Wu, J. Huang, Y. Wang, K. Xing and Q. Xu. (2009) "Fuzzy PID control of a wearable rehabilitation robotic hand driven by pneumatic muscles", *International*

Symposium on Micro-NanoMechatronics and Human Science, 2009. MHS 2009, pp. 408-413.

[184]   G. Andrikopoulos, G. Nikolakopoulos and S. Manesis. (2014) "Advanced Non-linear PID Based Antagonistic Control for Pneumatic Muscle Actuators", *IEEE Transactions on Industrial Electronics,* vol. 61, no. 99, pp. 1-12.

[185]   B. Vanderborght, B. Verrelst, R. Van Ham, J. Vermeulen and D. Lefeber. (2005) "Dynamic Control of a Bipedal Walking Robot actuated with Pneumatic Artificial Muscles", *Proceedings of the 2005 IEEE International Conference on Robotics and Automation, 2005. ICRA 2005*, pp. 1-6.

[186]   B. Vanderborght, B. Verrelst, R. Van Ham, M. Van Damme and D. Lefeber (2005) "A pneumatic biped: experimental walking results and compliance adaptation experiments", *2005 5th IEEE-RAS International Conference on Humanoid Robots*, pp. 44-49.

[187]   B. Vanderborght, B. Verrelst, R. Van Ham, M. Van Damme, P. Beyl and D. Lefeber. (2006) "Torque and compliance control of the pneumatic artificial muscles in the biped "Lucy"", *Proceedings 2006 IEEE International Conference on Robotics and Automation, 2006. ICRA 2006*, pp. 842-847.

[188]   C. Silva and E. Trélat. (2010) "Smooth Regularization of Bang-Bang Optimal Control Problems", *IEEE Transactions on Automatic Control,* vol. 55, no. 11, pp. 2488-2499.

[189]   B. Bonnard, J.B. Caillau, and E. Trélat (2007) "Second order optimality conditions in the smooth case and applications in optimal control", *ESAIM: Control, Optimisation and Calculus of Variations, vol.* 13, no. 2, pp. 207-236.

[190]   F. Nagi, L. Perumal, J. Nagi. (2009) "A new integrated fuzzy bang–bang relay control system", *Mechatronics, vol.* 19, no. 5, pp. 748-760.

[191]   H. Shibasaki, H. Ogawa, R. Tanaka and Y. Ishida. (2013) "High speed activation and stopping control system using the bang-bang control for a DC motor", *2013 IEEE International Symposium on Industrial Electronics (ISIE)*, pp. 1-6.

[192]   A. Hildebrandt, O. Sawodny, R. Neumann and A. Hartmann. (2005) "A Cascaded Tracking Control Concept for Pneumatic Muscle Actuators", *Proceedings of the 2005 American Control Conference, 2005,* vol. 1, pp. 680-685.

[193]   S.V. Krichel, O. Sawodny and A. Hildebrant. (2010) "Tracking control of a pneumatic muscle actuator using one servovalve", *2010 American Control Conference (ACC)*, pp. 4385-4390.

[194]   T.V. Minh, T. Tjahjowidodo, H. Ramon and H. Van Brussel. (2010) "Cascade position control of a single pneumatic artificial muscle–mass system with hysteresis compensation", *Mechatronics,* vol. 20, no. 3, pp. 402-414.

[195]   H. Aschemann and E.P. Hofer. (2006) "Nonlinear Trajectory Control of a High-Speed Linear Axis Driven by Pneumatic Muscle Actuators", *IECON 2006 - 32nd Annual Conference on IEEE Industrial Electronics*, pp. 3857-3862.

[196]   D. Schindele and H. Aschemann. (2010) "Trajectory tracking of a pneumatically driven parallel robot using higher-order SMC", *15th International Conference on Methods and Models in Automation and Robotics (MMAR)*, pp. 387-392.

[197]   H. Aschemann and D. Schindele. (2014) "Comparison of Model-Based Approaches to the Compensation of Hysteresis in the Force Characteristic of Pneumatic Muscles", *IEEE Transactions on Industrial Electronics,* vol. 61, no. 7, pp. 3620-3629.

[198]   A. Bierbaum, J. Schill, T. Asfour and R. Dillmann. (2009) "Force Position Control for a Pneumatic Anthropomorphic Hand", *IEEE-RAS International Conference on Humanoid Robots*, pp. 21-27.

[199]   P. Carbonell, Z.P. Jiang, and D.W. Repperger. (2001) "Nonlinear control of a pneumatic muscle actuator: backstepping vs. sliding-mode", *Proceedings of the 2001 IEEE International Conference on Control Applications, 2001. (CCA '01)*, pp. 167-172.

[200]   M. Van Damme, B. Vanderborght, R. Van Ham, B. Verrelst, F. Daerden, D. Lefeber (2007) "Proxy-Based Sliding Mode Control of a Manipulator Actuated by Pleated Pneumatic Artificial Muscles", *2007 IEEE International Conference on Robotics and Automation*, pp. 4355-4360.

[201]   H. Aschemann and D. Schindele. (2008) "Sliding-Mode Control of a High-Speed Linear Axis Driven by Pneumatic Muscle Actuators", *IEEE Transactions on Industrial Electronics,* vol. 55, no. 11, pp. 3855-3864.

[202]   H. Aschemann and D. Schindele. (2008) "Nonlinear Model-Based Control of a Parallel Robot Driven by Pneumatic Muscle Actuators", in Harald Aschemann (ed.) *New approaches in Automation and Robotics.* I-Tech Education and Publishing, pp. 25-41.

[203]   K. Braikia, B. Tondu and P. Acco (2010) "Practical design of real time VSS applied for flexibal robot", *2010 11th International Workshop on Variable Structure Systems (VSS)*, pp. 376-382.

[204]   A. Rezoug, M. Hamerlain and M. Tadjine. (2012) "Adaptive RBFNN type-2 fuzzy sliding mode controller for robot arm with pneumatic muscles", *2012 IEEE International Conference on Robotics and Biomimetics (ROBIO)*, pp. 1287-1292.

[205]   M. Chettouh, R. Toumi, and M. Hamerlain. (2008) "High-Order Sliding Modes for a Robot Driven by Pneumatic Artificial Rubber Muscles", *Advanced Robotics,* vol. 1, no. 22, pp. 689-704.

[206]   Z. Tong, Z. Ling, and W. Tao. (2011) "New Sliding Mode Control for Pneumatic Muscle Actuator Joint Model via Delta Operator Approach", *Third International Conference on Measuring Technology and Mechatronics Automation (ICMTMA),* vol.2, pp. 686-689.

[207]   P. Carbonell, Z.P. Jiang, and D.W. Repperger. (2001) "A fuzzy backstepping controller for a pneumatic muscle actuator system", *Proceedings of the 2001 IEEE International Symposium on Intelligent Control, 2001. (ISIC '01)*, pp. 353-358.

[208]   S. Tian, G. Ding, D. Yan, L. Lin, and M. Shi (2004) "Nonlinear Controlling of Artificial Muscle System with Neural Networks", *IEEE International Conference on Robotics and Biomimetics, 2004. ROBIO 2004*, pp. 56-59.

[209]   P.K. Jamwal and S.Q. Xie. (2012) "Artificial Neural Network based dynamic modelling of indigenous pneumatic muscle actuators", *2012 IEEE/ASME International Conference on Mechatronics and Embedded Systems and Applications (MESA)*, pp. 190-195.

[210]   T. Kosaki and M. Sano. (2011) "Control of a Parallel Manipulator Driven by Pneumatic Muscle Actuators Based on a Hysteresis Model", *Journal of Environment and Engineering,* vol. 6, no. 2, pp. 316-327.

[211]   K.K. Ahn and N.H.T. Chau. (2007) "Intelligent Phase Plane Switching Control of a Pneumatic Muscle Robot Arm with Magneto-Rheological Brake", *Journal of Mechanical Science and Technology,* vol. 21, no. 8, pp. 1196-1206.

[212] T.D.C. Thanh and K.K. Ahn. (2006) "Intelligent phase plane switching control of pneumatic artificial muscle manipulators with magneto-rheological brake", *Mechatronics,* vol. 16, no. 2, pp. 85-95.

[213] H.P.H. Anh, N.H. Phuc. (2010) "Inverse Neural MIMO NARX Model Identification of Nonlinear System Optimized with PSO", *Fifth IEEE International Symposium on Electronic Design, Test and Application, 2010. DELTA '10*, pp. 144-149.

[214] M.E.H. Pedersen and A.J. Chippereld. (2010) "Simplifying particle swarm optimization", *Applied Soft Computing,* vol. 10, no. 2, pp. 618-628.

[215] M. Mitchell. (1996) "An Introduction to Genetic Algorithms", MIT Press, 162 p.

[216] K.K. Ahn and H. P. H. Anh. (2006) "System Modeling and Identification the Two-Link Pneumatic Artificial Muscle (PAM) Manipulator Optimized with Genetic Algorithms", *International Joint Conference SICE-ICASE, 2006*, pp. 4744-4749.

[217] K.K. Ahn and H.P.H. Anh. (2007) "System Modeling Identification and Control of the Two-Link Pneumatic Artificial Muscle Manipulator Optimized with Genetic Algorithms", *IEEE International Conference on Control and Automation, 2007. ICCA 2007*, pp. 501-506.

[218] K.K. Ahn and H.P.H. Anh. (2007) "System Identification and Self-Tuning Pole Placement Control of the Two-Axes Pneumatic Artificial Muscle Manipulator Optimized by Genetic Algorithm", *International Conference on Mechatronics and Automation, 2007. ICMA 2007*, pp. 2604-2609.

[219] H.P.H. Anh, K.K. Ahn and Y.J. Il. (2008) "Identification of the 2-Axes Pneumatic Artificial Muscle (PAM) Robot Arm Using Double NARX Fuzzy Model and Genetic Algorithm", *International Conference on Smart Manufacturing Application, 2008. ICSMA 2008*, pp. 84-89.

[220] M.K. Chang, P.L. Yen and T.H. Yua. (2006) "Angle Control of a one-Dimension Pneumatic Muscle Arm using Self-Organizing Fuzzy Control", *IEEE International Conference on Systems, Man and Cybernetics, 2006. SMC '06,* vol. 5, pp. 3834-3838.

[221] X. Zhu, G. Tao, B. Yao, and J. Cao. (2008) "Adaptive Robust Posture Control of Parallel Manipulator Driven by Pneumatic Muscles with Redundancy", *American Control Conference, 2007. ACC '07,* vol. 13, no. 4, pp. 441-450.

[222] G. Tao, X. Zhu, B. Yao and J. Cao. (2007) "Adaptive Robust Posture Control of a Pneumatic Muscles Driven Parallel Manipulator with Redundancy", *Proceedings of the 2007 American Control Conference*, pp. 3408-3413.

[223] Harder & Steenbeck Airbrush. (2005) "Instruction manual for compressors Eurotec 20A / 30A / 50A". Available at: http://www.obeeliks.com/Manuals/Instruction%20manual%20EUROTEC%2020A%2030 A%2050A.pdf. Last access: 2015.

[224] J. Murillo, M. Doumit and N. Baddour. (2014) "Validation of Pneumatic Artificial Muscle for Powered Transfemoral Prostheses", *Proceedings of the Canadian Medical and Biological Engineering Society Conference,* pp. 1-5.

[225] Mead Fluid Dynamics. (2004) "Control Valves". Available at: http://mead-usa.com/products/media/isonic_vi_v4.pdfhttp://www.obeeliks.com/Manuals/Instruction manual EUROTEC 20A 30A 50A.pdf. Last access: 2015.

[226] Shadow Robot Company Ltd "Shadow Pneumatic Control Unit – Manual".

[227] Microship. (2009) "PIC18F2480/2580/4480/4580 Data Sheet". Available at: http://ww1.microchip.com/downloads/en/DeviceDoc/39637d.pdfhttp://piklab.sourceforge .net/. Last access: 2015.

[228] Sourceforge "Piklab - IDE for PIC microcontrollers". Available at: http://piklab.sourceforge.net/. Last access: 2015.

[229] Sourceforge "SDCC - Small Device C Compiler". Available at: http://sdcc.sourceforge.net/. Last access: 2015.

[230] A. Mohd Zaid, M. Atif Yaqub, M. Rizal Arshad and M.S. Wahab. (2011) "UTHM Hand: Mechanics Behind The Dexterous Anthropomorphic Hand", *World Academy of Science, Engineering and Technology,* vol. 50, pp. 150-154.

[231] e-hand.com "Normal Range of Motion Reference Values". Available at: http://www.eatonhand.com/nor/nor002.htm. Last access: 2015.

[232] L. Biagotti, F. Lotti, C. Melchiorri and G. Vassura. (2003) "Mechatronic Design of Innovative Fingers for Anthropomorphic Robot Hands", *Proc. IEEE International Conference on Robotics and Automation,* vol. 3, pp. 3187-3192.

[233]   F. Lotti and G. Vassura. (2002) "A novel approach to mechanical design of articulated fingers for robotic hands", *IEEE/RSJ International Conference on Intelligent Robots and Systems, 2002. IEEE/RSJ International Conference on,* vol. 2, pp. 1687-1692.

[234]   I. Berruezo Juandeaburre. (2011) "Pneumatic rubber muscle technology from Shadow Robot company", report.

[235]   S. Chattoraj. (2012) "Shadow robot project", report.

[236]   K.K. Ahn and T.D.C. Thanh. (2004) "Improvement of the Control Performance of Pneumatic Artificial Muscle Manipulators Using an Intelligent Switching Control Method", *KSME International Journal,* vol. 18, no. 8, pp. 1388-1400.

[237]   K.H. Ang, G. Chong and L. Yun. (2005) "PID Control System Analysis, Design, and Technology", *IEEE Transactions on control systems technology,* vol. 13, no. 4, pp. 559-576.

[238]   K.J. Aström and T. Hägglund. (1995) "PID Controllers: Theory, Design and Tuning". 2nd Revised Edition edn. ISA, 343 p.

[239]   G.J. Silva, G.J. Silva, A. Datta. (2005) "PID Controllers for Time-Delay Systems". Birkhaüser, 400 p.

[240]   F. Haugen. (2004) "PID Control". Tapir Academic Press, 293 p.

[241]   M.Y. Hassan and G. Kothapalli. (2010) "Comparison between Neural Network Based PI and PID Controllers", *International Conference on Systems Signals and Devices (SSD),* vol. 7, pp. 1-6.

[242]   X. Ancheng, Z. Jian, C. Jinmei and B. Tianshu. (2012) "A New Method to Coordinate the PI Controllers' Parameters of Doubly-fed Induction Generator", *Chinese Control Conference (CCC),* vol. 31, pp. 6776-6780.

[243]   A.V. Sant, K.R. Rajagopal and N.K. Sheth. (2011) "Permanent Magnet Synchronous Motor Drive Using Hybrid PI Speed Controller With Inherent and Noninherent Switching Functions", *IEEE Transactions on magnetics,* vol. 47, no. 10, pp. 4088-4091.

[244]   W. Tang, G. Chen, R. Lu. (2001) "A modified fuzzy PI controller for a exible-joint robot arm with uncertainties", *Fuzzy Sets and Systems,* vol. 118, no. 1, pp. 109-119.

[245]   B. Kristiansson and B. Lennartson. (2006) "Robust Tuning of PI and PID Controllers", *IEEE Control Systems,* vol. 26, no. 1, pp. 55-69.

[246]   Alpha. (2009) "Potentiometers RV120F-20-15F-SERIES". Available at: http://www.mouser.com/catalog/specsheets/TW-700151.pdf. Last access: 2015.

[247]   Phidgets. (2010) "Product Manual 1131 – Thin Force Sensor". Available at: http://www.phidgets.com/products.php?product_id=1131. Last access: 2015.

[248]   Interlink Electronics. "FSR Force Sensing Resistor Integration Guide and Evaluation Parts Catalog". Available at: https://www.sparkfun.com/datasheets/Sensors/Pressure/fsrguide.pdf. Last access: 2015.

[249]   Nokia "Qt4". Available at: http://qt.nokia.com/. Last access: 2015.

[250]   Z. Liu. (2012) "Remote Control for Robotic Hand", report.

[251]   F. Jourdan. (2012) "Ambidextrous Robot Hand with an embedded camera", report.

[252]   M. Heinrich. (2012) "Development of a robot hand's multimedia applications", report.

[253]   C. Borst, M. Fischer, S. Haidacher, H. Liu, and G. Hirzinger. (2003) "DLR Hand II: Experiments and Experiences with an Anthropomorphic Hand", *Proceedings of the 2003 IEEE International Conference on Robotics & Automation, 2003*, vol. 1, pp. 702-707.

[254]   A. Nimmo, L. Kavanagh, L. Steele, M. Simko. (2013) "Design and Manufacture of Anthropomorphic, Ambidextrous, Air Muscle Actuated Robotic Hand", dissertation.

[255]   A. Huynh. (2013) "Controlling a Pneumatically Actuated, Ambidextrous Robot Hand", report.

[256]   Coventry Scale Company. "TSA Alloy Steel S Type Load Cells". Available at: http://www.coventryscale.co.uk/product_info.php?ID=5896http://qt.nokia.com/. Last access: 2015.

[257]   Procter & Chester Measurements. "615 & 616 - Bi-Directional S-Type Load Cells". Available at: http://www.pcm-uk.com/loadcell-bd-st-615.htmlhttp://qt.nokia.com/. Last access: 2015.

[258]   Phidgets. "3134 - Micro Load Cell (0-20kg) - CZL635". Available at: http://www.phidgets.com/products.php?product_id=3134. Last access: 2015.

[259]   Phidgets. "3135 - Micro Load Cell (0-50kg) - CZL635". Available at: http://www.phidgets.com/products.php?product_id=3135. Last access: 2015.

[260] Phidgets. "3132 - Micro Load Cell (0-780g) - CZL616C". Available at: http://www.phidgets.com/products.php?product_id=3132. Last access: 2015.

[261] Freescale Semiconductor Inc. "Integrated Silicon Pressure Sensor On-Chip Signal Conditioned, Temperature Compensated and Calibrated". Available at: http://cache.freescale.com/files/sensors/doc/data_sheet/MPX5700.pdf. Last access: 2015.

[262] Honeywell. "TruStability® Silicon Pressure Sensors: HSC Series-High Accuracy". Available at: http://www.farnell.com/datasheets/1676942.pdf. Last access: 2015.

[263] Honeywell. "Basic Board Mount Pressure Sensors". Available at: http://www.farnell.com/datasheets/1795774.pdf. Last access: 2015.

[264] Honeywell. "TruStability® Board Mount Pressure Sensors: NSC Series-Uncompensated/Unamplified". Available at: http://www.farnell.com/datasheets/1499905.pdf. Last access: 2015.

[265] Honeywell. "40PC Pressure Sensors Miniature Signal Conditioned". Available at: http://datasheet.octopart.com/40PC150G2A-Honeywell-datasheet-10224970.pdf. Last access: 2015.

[266] S3i Group. "8mm Hook-Eye Open Body Turnbuckle – Affodable Stainless Stell Tensioner". Available at: https://www.s3i.co.uk/8mm-Hook-Eye-Open-Turnbuckle.html. Last access: 2015.

[267] Telemanique. "xy2cz404 turnbuckle M8 – for XY2C". Available at: http://docs-europe.electrocomponents.com/webdocs/129c/0900766b8129cb9e.pdf. Last access: 2015.

[268] Telemanique. "xy2cz402 turnbuckle M6 – for XY2C". Available at: http://docs-europe.electrocomponents.com/webdocs/129c/0900766b8129cb8a.pdf. Last access: 2015.

[269] One Stop DIY. "Turnbuckle Wire Strainer Tensioner Hook–eye bzp zinc plated 6mm". Available at: http://www.amazon.co.uk/TURNBUCKLE-WIRE-STRAINER-TENSIONER-HOOK/dp/B007LKYTPO. Last access: 2015.

[270] S3i Group. "Eye – Eye Lifting Turnbuckle". Available at: https://www.s3i.co.uk/eye-eye-lifting-turnbuckle.php. Last access: 2015.

[271] A. Cavallo, G. De Maria, C. Natale, S. Pirozzi. (2010) "Minimally invasive force sensing for tendon-driven robots", *Cutting Edge Robotics 2010,* pp.379-394.

[272] STMicroelectronics. (1998) "LF155-LF255-LF355 LF156-LF256-LF356 LF157-LF257-LF357 Wide Bandwith single J-fet Operational Amplifier". Available at: http://www.digchip.com/datasheets/parts/datasheet/456/LF155-LF255-LF355.php. Last access: 2015.

[273] Texas Instruments. (2014) "ULN2803A Darlington Transistor Arrays". Available at: http://www.ti.com/lit/ds/symlink/uln2803a.pdf. Last access: 2015.

[274] Legris. "PTFE Tube". Available at: http://uk.rs-online.com/web/p/coil-tubing-without-connectors/3985566/. Last access: 2015.

[275] Norgren. "Air Reservoirs M163 & M/164". Available at: http://docs-europe.electrocomponents.com/webdocs/0092/0900766b80092492.pdf. Last access: 2015.

[276] Werther International. "Sil-Air 15". Available at: http://www.werthercompressors.com/prodotto/silair_silair15.pdf. Last access: 2015.

[277] Werther International. "Sil-Air 30/12". Available at: http://www.werthercompressors.com/prodotto/silair_silair30-12.pdf. Last access: 2015.

[278] Werther International. "Sil-Air 15 D, Sil-Air 30 D". Available at: http://www.werthercompressors.com/prodotto/silair_silair15D.pdf. Last access: 2015.

[279] Werther International. "Sil-Air 50 D". Available at: http://www.werthercompressors.com/prodotto/silair_silair50D.pdf. Last access: 2015.

[280] A. Namiki, Y. Imai, M. Ishikawa, and M. Kaneko. (2003) "Development of a high-speed multifingered hand system and its application to catching", Proceedings of the 2003 *IEEE/RSJ International Conference on Intelligent Robots and Systems, 2003. (IROS 2003),* vol. 3, pp. 2666-2671.

[281] M. Grebenstein, M. Chalon, W. Friedl, S. Haddadin, T. Wimböck, G. Hirzinger, and R. Siegwart. (2012) "The hand of the DLR Hand Arm System: Designed for interaction", *The International Journal of Robotics Research,* vol. 31, no. 13 pp. 1531-1555.

[282] G. Palli, C. Melchiorri, G. Vassura, U. Scarcia, L. Moriello, G. Berselli, A. Cavallo, G. De Maria, C. Natale, S. Pirozzi, C. May, F. Ficuciello, and B. Siciliano. (2014) "The DEXMART hand: Mechatronic design and experimental evaluation of synergy-based control for human-like grasping", *The International Journal of Robotics Research,* vol. 33, no. 5 pp. 799-824.

212

[283]   E. Akyürek, M. Mukhtar, A. Huynh, L. Steele, M. Simko, L. Kavanagh, A. Nimmo, T. Kalganova, L. Paramonov, and Stelarc. (2013) *Ambidextrous Robot Hand - Brunel University London*. Available at: https://www.youtube.com/watch?v=lFH5fcpn5xU. Last access: 2015.

[284]   Y. Shtessel, C. Edwards, L. Fridman, and A. Levant. (2014) "Introduction : Intuitive Theory of Sliding Mode Control", in Birkhäuser (ed.) *Sliding Mode Control and Observation*, pp. 1-42.

[285]   K.D. Young, V.I. Utkin, and Ü. Özgüner. (1999) "A Control Engineer's Guide to Sliding Mode Control", *IEEE Transactions on Control Systems Technology,* vol. 7, no. 3, pp. 328-342.

[286]   J. Jalani, N. Mahyuddin, G. Herrmann, and C. Melhuish. (2013) "Active Robot Hand Compliance using Operational Space and Integral Sliding Mode Control", *2013 IEEE/ASME International Conference on Advanced Intelligent Mechatronics (AIM)*, pp. 1749-1754.

[287]   E.D. Engeberg and S.G. Meek. (2009) "Backstepping and Sliding Mode Control Hybridized for a Prosthetic Hand", *IEEE Transactions on Neural Systems and Rehabilitation Engineering,* vol. 17, no. 1, pp. 70-79.

[288]   Brunel University. (2014) "Ambidextrous Robot Hand - Brunel University London". Available   at: https://www.youtube.com/watch?v=DUGEkK_WsbI&list=UUEeI6yVSqlChchZNHTW9 NSw. Last access: 2015.

[289]   N. Lesne. (2014) "Ambidextrous Robot Hand Controlled By Air Muscles", report.

[290]   N.M. Kakoty and S.M. Hazarika. (2013) "Local Hand Control for Tezpur University Bionic Hand Grasping", *Air'13: Proceedings of Conference on Advances in Robotics*, pp 1-7.

[291]   H. Kawasaki, T. Komatsu, and K. Uchiyama. (2002) "Dexterous Anthropomorphic Robot Hand With Distributed Tactile Sensor: Gifu Hand II", *IEEE/ASME Transactions on Mechatronics*, vol. 7, no. 3, pp. 296-303.

[292]   T. Yoshikawa. (2010) "Multifingered robot hands: Control for grasping and manipulation", *Annual Reviews in Control,* vol. 34, no. 2, pp. 199-208.

[293] M.A. Roa, M.J. Argus, D. Leidner, C. Borst, and G. Hirzinger. (2012) "Power Grasp Planning for Anthropomorphic Robot Hands", *IEEE International Conference on Robotics and Automation (ICRA)*, pp. 563-569.

[294] C.-Y. Su and Y. Stepanenko. (1997) "Backstepping-Based Hybrid Adaptive Control of Robot Manipulators Incorporating Actuator Dynamics", *International Journal of Adaptive Control and Signal Processing,* vol. 11, no. 4, pp. 141-153.

[295] S.-H. Wen and B. Mao. (2007) "Hybrid Force and Position Control of Robotic Manipulators Using Passivity Backstepping Neural Networks", *Advances in Neural Networks – ISNN 2007,* vol. 4491, pp. 863-870.

[296] A. Lotfazar, M. Eghtesad, and M. Mohseni. (2003) "Integrator Backstepping Control of a 5 DOF Robot Manipulator with Cascaded Dynamics", *IJE Transactions B: Applications,* vol. 16, no. 4, pp. 373-383.

[297] L. Qin, F. Liu, and L. Liang. (2014) "The Application of Adaptive Backstepping Sliding Mode for Hybrid Humanoid Robot Arm Trajectory Tracking Control", *Advances in Mechanical Engineering,* vol. 6, no. 307985, pp. 1-9.

[298] X. Liu and A. Liadis. (2012) "Fuzzy Adaptive Backstepping Control of a Two Degree of Freedom Parallel Robot", *International Robotics and Applications,* vol. 7506, pp. 601-610.

[299] M.R. Soltanpour and M.M. Fateh. (2009) "Sliding Mode Robust Control of Robot Manipulator in the Task Space by Support of Feedback Linearization and BackStepping Control", *World Applied Sciences Journal,* vol. 6, no. 1, pp. 70-76.

[300] D. Nganya-Kouya, M. Saad, and L. Lamarche. (2014) "Backstepping adaptive hybrid force/position control for robotic manipulators", *Proccedings of the 2002 American Control Conference,* vol. 6, pp. 4595-4600.